

ulm university universität

uulm

“Development and optimization of bibenzimidazole transition metal chromophores for luminescent ion sensing and photocatalysis”

Dissertation zur Erlangung des Doktorgrades Dr.rer.nat.
der Fakultät für Naturwissenschaften der Universität Ulm

vorgelegt von
M. Sc. Chem.-oec. Sebastian Andreas Rommel,
geboren am 10.06.1987 in Augsburg

2016

Amtierender Dekan: Prof. Dr. Peter Dürre

Erstgutachter: Prof. Dr. Sven Rau
Zweitgutachter: Prof. Dr. Carsten Streb

Tag der öffentlichen Verteidigung: 05.10.2016

This thesis is based on the following publications. They form the basis of chapter "3. Investigated systems", and are reprinted in chapter "6. Publications" with the permission of the respective publisher.

1 „Sebastian A. Rommel, Dieter Sorsche, Nils Rockstroh, Frank W. Heinemann, Joachim Kübel, Maria Wächtler, Benjamin Dietzek and Sven Rau, *Eur. J. Inorg. Chem*., **2015**, 3730 – 3734."
With permission of the publisher John Wiley and Sons. (License Number: 3910161485883).

2 "Sebastian A. Rommel, Dieter Sorsche, Apoorva Dixit and Sven Rau, *Eur. J. Inorg. Chem*., **2016**, 40 – 48."
With permission of the publisher John Wiley and Sons. (License Number: 3910180027115).

3 „Sebastian A. Rommel, Dieter Sorsche and Sven Rau, *Dalton Trans*, **2016**, *45*, 74 –77." Reproduced by permission of The Royal Society of Chemistry.

4 „Dieter Sorsche, Sebastian A. Rommel and Sven Rau, *Eur. J. Inorg. Chem.* **2016**, 1503-1513.*"*
With permission of the publisher John Wiley and Sons (License Number: 3910180469196).

5 „Sebastian A. Rommel, Dieter Sorsche, Stefanie Schönweiz, Joachim Kübel, Nils Rockstroh, Benjamin Dietzek, Carsten Streb and Sven Rau, *Journal of Organomet. Chem.* **2016**, accepted manuscript"
With permission of the publisher Elsevier Limited The Boulevard, Langford Lane , Kidlington, Oxford, OX5 1GB, UK. (License Number: 3912400498568)

Dedicated to my family

Abstract

The recognition and fixation of highly reactive systems by binding within defined spatial geometries is a fundamental principle of the enlivened nature. In the last four decades this biologically tenet was transferred to artificial systems and the yet emergent area of supramolecular chemistry developed to a driving force. The latter defined itself “over and above the molecule”, that is the chemistry of tailored intermolecular interactions. Thereby, not only the interplay of molecules, but also that of characteristic molecule entities – with its inherent features – is defined as “supramolecular”.[1,2]

The stunning development of this research area is inseparably related to the increasing knowledge of preparative methods for the synthesis and characterization of complex host-guest structures.[3] Accessible and comprehensively investigated supramolecular host-compounds of today range from “classic” crown ethers[4] over calixarenes[5] and imines[6–11] to photosensible hosts.[1,12,13] The mentioned compound classes bear a receptor function for second-sphere interaction with substrates, and hence enable the selective coordination of anionic, cationic and neutral guests. These features provide the basis for the development of the research area of artificial molecular recognition.

Especially, transition metal chromophores based on polypyridyl ruthenium(II), osmium(II) or iridium(III) complexes have become fundamental building blocks in numerous molecular optical sensors.[14–18] This is mainly due to the outstanding photophysical properties, i.e. broad light absorption and emission features across the visible regime of the light spectrum. Furthermore, the complexes are featured with long-lived triplet metal-to-ligand charge transfer (^{3}MLCT) states.[14,19–27]

The focal point of this work was the synthesis and characterization of luminescent complex compounds for the usage as supramolecular sensors and for application in the heterogeneous light-induced water reduction. Along these lines, the principal chromophore scaffolds investigated in this thesis are primarily derivatives of bis(2-phenylpyridine) iridium(III) α-diimine and in the second instance bis(2,2’-bipyridine) ruthenium(II) α-diimine.

In the first part of the thesis the iridium(III) model complex of 5,5’,6,6’-tetramethyl-2,2’-bibenzimidazole and its homodinuclear complex bearing a simple unsubstituted bibenzimidazole motif are introduced. The structure-property relations of the iridium(III) bibenzimidazole complex are discussed and compared to related ruthenium(II) complexes. Especially the acid-base chemistry is outstanding with a strongly luminescent character in all protonation states of the complex. This feature is of pivotal importance for this and further studies, as it could provide a spectroscopic tool for direct observation of proton release of these molecules.

Inspired by the special features of the iridium(III) model complex, the interaction of the latter with basic anions was investigated. Hydrogen bond donor features of the iridium(III) complex were experimentally verified and implications for luminescent sensing could be drawn.

In a second step the present supramolecular sensor strategy was optimized using the intermolecular quencher 3,5-dinitrobenzoate (DNBA). Strong H-bond supported ion pair bonding with the electron accepting dinitro-benzoate anion switches the luminescence “off”. The luminescence of the sensor system is switched back “on” when benzoate is replaced by competing H-bonded small anions, therefore leading to enhanced sensitivity of the sensor system. Additionally, to the best of my knowledge, the presented system exceeds all ruthenium(II) biimidazole-type sensors known in literature so far, regarding an increase in luminescence intensity of e.g. 450 % for chloride and as the change in the luminescence intensity can easily be followed with the naked eye.

For ruthenium(II) complexes, pioneering work was performed by Ye and co-workers who presented a number of Ru(II) imidazole-like complexes acting as promising anion sensors, however limited by small selectivity and sensitivity. In order to improve the literature known ruthenium(II) based sensors, sterically demanding substituents were introduced in the ligand framework of the bibenzimidazole. Thereby, the secondary binding site of the complexes are spatially confined which leads to a functional dimming of the emission intensity. Subsequently, the recognition properties towards small anions of the complexes could be directed selectively, accompanied by a significant enhancement in luminescence sensitivity.

In a conclusive project, the heterodinuclear bibenzimidazole bridged iridium(III)/ ruthenium(II) complex **Ir-BBI-Ru** was synthesized to investigate the synergy effects of the sole chromophore units tested before. The comprehensive investigation of the basic properties of the complex and its applicability as photosensitizer in the light-induced hydrogen production are presented.

Table of contents

1 Introduction 1

1.1 General introduction 1

1.2 Theoretical fundamentals and state of research 3

1.2.1 Chemistry of Iridium(III) complexes 3

1.2.2 State of research 7

2 Structure of the thesis 34

3 Investigated systems 37

3.1 Second sphere chemistry of an iridium(III) chromophore 37

3.1.1 Synthesis, characterization and acid-base chemistry of a luminescent iridium(III) bibenzimidazole system and its homodinuclear analogon 37

3.1.2 Interaction of an iridium(III)bibenzimidazole complex with different anions: implications for luminescent sensing 43

3.1.3 Supramolecular H-bond driven light switch 48

3.2 Improvement of an anion sensing strategy for ruthenium(II) complexes through sterically confined 2,2'-bibenzimidazole-type ligands 54

3.3 Photochemical application of a heterodinuclear bibenz-imidazole bridged iridium(III)/ruthenium(II) complex 60

4 Summary and outlook 66

5 References 73

6 Publications 78

7 Curriculum vitae 196

8 Publications and conference contributions 197

8.1 Publications in peer reviewed journals 197

8.2 Conference proceedings 197

8.2.1 Poster contributions 197

8.2.2 Travel grants 198

9 Abbreviations 199

10 Acknowledgements 201

11 Declaration of honesty in academic work 202

1 Introduction

1.1 General introduction

Luminescent transition-metal complexes are tempting for their utilisation in diverse applications, such as OLED-, bioanalytical- and sensor- applications as well as in the field of photocatalytic water splitting.[28–32] Thereby, the effectiveness of a complex in a specific role is determined by their excited-state properties which can be manipulated by synthetic modifications at the ligands. At an early stage, work in this field focused mainly on tris-diimine ruthenium(II) complexes, such as $[Ru(bpy)_3]^{2+}$ (bpy = 2,2'-bipyridine). However, these compounds offer limited colour tuning capability due to thermal population of a nonemissive metal-centered (^{3}MC) state.[28,33] Iridium(III) complexes, on the other hand, offer broader tuning possibilities due to their increased ligand-field stabilization energy, and thus less thermally accessible ^{3}MC states.[28] Furthermore, with strong-field ligands the split-up of the d-orbitals can be further enhanced. As a result, bis-cyclometalated iridium(III) complexes have displaced ruthenium(II) compounds at the forefront of many photochemical and photophysical investigations.[28,34–38] These days iridium(III) complexes are considered to be most promising as they exhibit (1) high phosphorescence quantum efficiency (2) good photo-and thermal stabilities (3) relatively short phosphorescence lifetimes (4) facile colour tuning through ligand structure control and (5) large cross-section for the exciton formation.[39,40] These characteristic features were attributed to the efficient spin-orbit coupling provided by the iridium metal as well as the strong structural and electronic interactions between the Ir metal and the ligands.

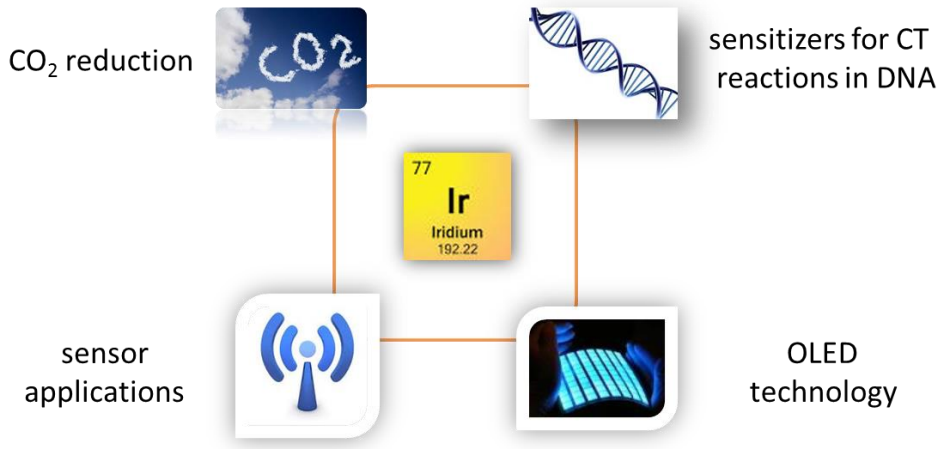

Figure 1: Schematic depiction of the application fields of iridium(III) complexes.

The aforementioned synthetic versatility, accompanied by the reversible electrochemistry and the robust nature of iridium(III) complexes render the latter appealing materials for a range of applications.[28] Above all, the most important prognosticated usage of iridium(III) complexes is electrophosphorescence including light-emitting electrochemical cells (LECs)[41–43] and organic light-emitting devices (OLEDs).[44,45] This applicability is based on the aforementioned special characteristics of iridium(III) compounds, which allow both nearly 100% internal device quantum efficiency and versatile colour tuning through variation in the ligand structure.[39] Furthermore, facile generation of triplet states then allows applications as sensitizers for charge-transfer reactions in DNA[46–48], as photocatalysts for CO_2 reduction[49,50] and as encouraging supramolecular sensors (see Figure 1).[51–53]

Among the various promising application fields of iridium(III) complexes the recognition and sensing of ions, and especially of anions is a fundamental topic in the research area of supramolecular chemistry. This can be contributed to the important parts played by anions in different clinical, biological and chemical processes.[54,55] Since 1997 a continuous increase in the published items regarding sensor applications based on iridium(III) could be observed, accompanied by a linear surge of citations (see Figure 2).[56]

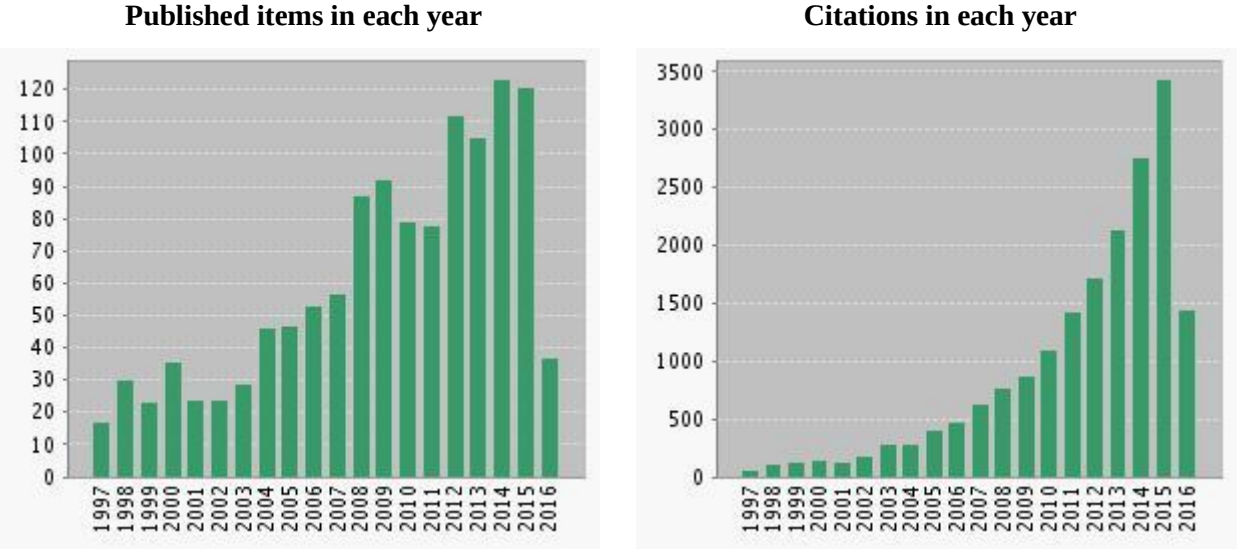

Figure 2: Left: items published in each year (search for “iridium“ and “sensor“ in “Web of Science”); right: citations in each year.[56]

The fluoride anion for example is known for its significance in the prevention of tooth decay. Furthermore, it has also been intensively explored as a treatment for osteoporosis.[57] In addition, anions like acetate or phosphate are critical components of various metabolic processes. Consequently, designing new phosphorescent metal complex sensors for ions is of great importance and has hence gained much attention in the field of supramolecular sensor chemistry.[16–18,57,58] The following chapters cover the theoretical fundamentals of iridium(III) based chemistry and the state of research in the field of luminescent sensing with biimidazole complexes.

1.2 Theoretical fundamentals and state of research

1.2.1 Chemistry of Iridium(III) complexes

1.2.1.1 History and synthesis of cyclometalated Iridium(III) complexes

Amongst the pioneers in the study of the coordination chemistry and properties of iridium(III) complexes were undeniable the groups of Demas, Williams and Watts. Initial work focused on the model complex $[Ir(bpy)_3]^{3+}$ (bpy = 2,2'-bipyridine) and the related aquo complexes of the form $[(bpy)_2\text{-}IrCl_n(H_2O)_{(2-n)}]^{3-n}$.[59–65] In 1974, the first example of what is probably the most common precursor for accessing heteroleptic iridium(III) complexes that have the general form $[\{(C\text{^}N)_2Ir(\mu\text{-}Cl)\}_2]$ (C^N = cyclometalating ligand) was presented by Nonoyama.[66] This discovery gave birth to a new family of *ortho*-metalated complexes, with the most important member of the general form $[(C\text{^}N)_2Ir(N\text{^}N)]^+$. Its archetypical example $[(ppy)_2Ir(bpy)]^+$.was first reported by King and Watts in 1987.[37,67]

The well-established synthesis of cationic heteroleptic iridium(III) complexes proceeds according to Scheme 1. This strategy, elucidated by Nonoyama in 1974, involves the reaction of two equivalents of the **C^N** ligand with the metal compound $IrCl_3 \cdot nH_2O$ to form the neutral dinuclear iridium(III) intermediate $[\{(C\text{^}N)_2Ir(\mu\text{-}Cl)\}_2]$, followed by decomposition upon reaction with a **L^X** ancillary ligand.[59,66]

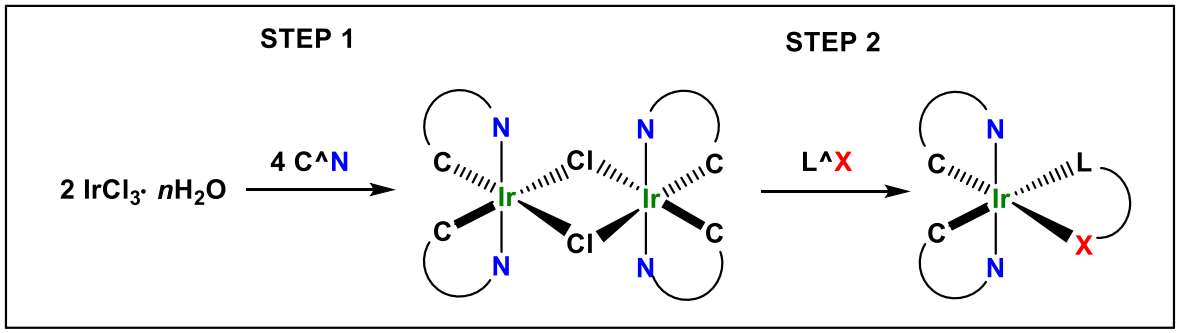

Scheme 1: Main synthetic strategy used for the synthesis of cationic heteroleptic iridium(III) complexes presented by Nonoyama et al..[66]

In general, the reaction is temperature controlled so that the position of the two nitrogen atoms of the **C^N** ligand are orientated mutually in a *trans* configuration. The solvents most frequently used are high boiling alcohols such as $2\text{-}EtOCH_2OH$ to facilitate solubilization, however, milder conditions for dimer cleavage that involve e.g. dichloromethane and methanol also proved to be suitable.[59]

1.2.1.2 The photophysics of cyclometallated bis(phenylpyridine) iridium(III) diimine complexes

The general photophysical features of bis(phenylpyridine) iridium(III) diimine complexes could be explained with the simple model of bis(2-phenylpyridine) (2,2'-bipyridine) iridium(III) (**Ir-bpy**).[68] The

latter is isostructural and isoelectronic with the model compound $Ru(bpy)_3^{2+}$. The general structure of **Ir-bpy** includes one d^6 core Ir atom, coordinated by two monoanionic (C^N) and one neutral (N^N) bidentate σ donor/π acceptor ligand.[39,69] The most popular C^N ligand generally is 2-phenylpyridine (**ppy**) which is called a cyclometalating ligand, whereas other ligands, for example 2,2'-bipyridine (N^N), are named ancillary ligands. In iridium(III) complexes the d orbitals split into two sets of degenerated orbitals, t_{2g} and e_g, which are separated by an energy gap Δ_0. The different photophysical characteristics of iridium(III) compared to their ruthenium(II) analogues are a result of the higher oxidation state of Ir^{III}, the size of its 5d orbitals, and the high ligand-field splitting energy (LFSE) due to the presence of two cyclometalating C^N ligands – factors that affect the magnitude of Δ_0.[59] The strong σ donor and covalent character of the Ir-C_{C^N} bond hence is known to render metal-to-ligand (MLCT) and ligand-to-ligand charge-transfer (LLCT) transitions. Both of them are much more energetically accessible than undesired metal-centered (MC) ones, which outlines a distinctive electronic feature for iridium complexes relative to those of ruthenium.[70,71]

The crystal structure of **Ir-bpy** was recently reported by Bolink et al..[72] Herein the iridium adopts a pseudo-octahedral geometry with the two nitrogen atoms of the 2-phenylpyridine ligands in a mutually *trans* position. The Ir-C bond between the Ir(III) metal and the ppy-based ligands is known to be very strong and comparable to a covalent bond. Hence, the structure of the complex is characterized as a multiply bonded and compact framework, that brings both good thermal stability and extensive electronic interactions between the d-orbital of the iridium core and π orbital of the ligands.[39]

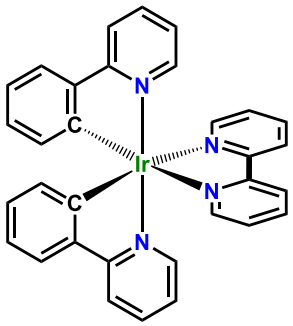

Scheme 2: Depiction of bis (2-phenyl-pyridine)(2,2'-bi-pyridine) iridium(III) (**Ir-bpy**).[68]

As can be seen in Figure 3 the visible light absorption of **Ir-ppy** is comparatively poor as characterized by high-energy absorption bands between 200 and 300 nm and a precipitously drop-off at lower energies. In general, for most cationic iridium(III) complexes, including **Ir-ppy**, the absorption band that corresponds to the HOMO→LUMO transition is poorly absorptive; a result of poor spatial overlap between the electron densities of the two molecular orbitals, and contains mixed MLCT-LC character.

The high-energy absorptions were assigned to spin-allowed $^1\pi$- π^* ligand-centered (^{1}LC) from both the ppy and bpy ligands. The nature of the absorption bands between 300 and 450 nm is most likely best described as an admixture of spin-allowed charge-transfer (^{1}CT) transitions including both dπ→ π^*_{bpy}

metal-to-ligand (^{1}MLCT) and $\pi_{ppy} \rightarrow \pi^*_{bpy}$ ligand-to-ligand (^{1}LLCT) processes.[59] Furthermore, very low intensity bands around 450 nm were assigned to normally spin-forbidden triplet transitions (^{3}MLCT and ^{3}LLCT).

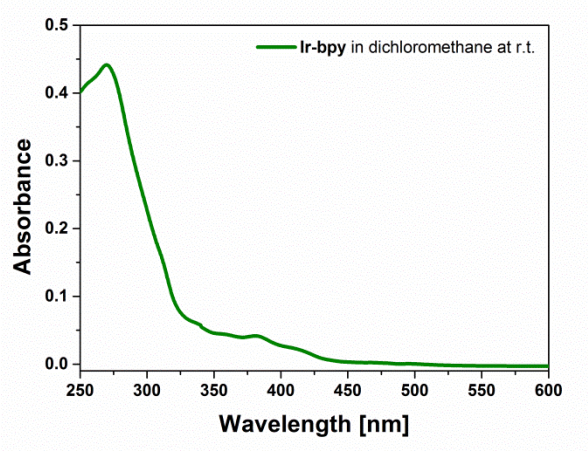

Figure 3: UV/vis spectrum of **Ir-bpy** in dichloromethane (c = 5 E^{-6} M).

Direct electronic transitions between singlet and triplet states are accessible due to the large spin-orbit coupling of iridium. In fact, iridium possesses the largest spin orbit coupling constant with ξ = 3909 cm^{-1} among the d-block elements (for reference: ξ = 431 cm^{-1} (Fe), ξ = 1042 cm^{-1} (Ru), ξ = 3381 cm^{-1} (Os)).[59] Similar to many phosphorescent and fluorescent chromophores, multiple optical excitation paths are available in the iridium(III) complex. At least four transitions have to be considered, that is singlet and triplet metal-to-ligand charge-transfer transitions (^{1}MLCT and ^{3}MLCT) and singlet and triplet ligand-centered transitions (^{1}LC and ^{3}LC).[39,59]

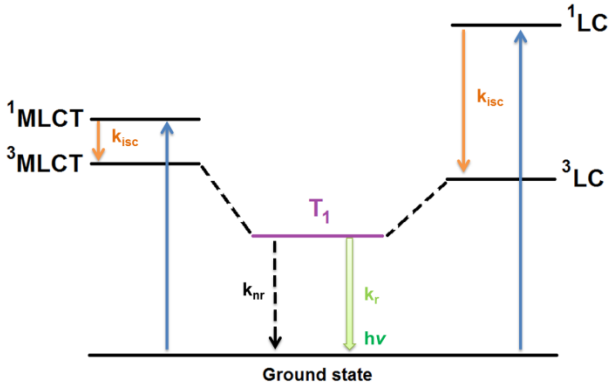

Scheme 3: The energetic closeness and degree of overlap between triplet LC and MLCT states results in the formation of a mixed lowest excited state (T_1). The excited molecule relaxes to the ground state through radiative (k_r) and nonradiative (k_{nr}) pathways. [28]

Strong spin-orbit coupling from the iridium(III) center facilitates intersystem crossing to energetically similar triplet states and hence enables the formation of an emissive, mixed triplet excited state [T_1].[28] Vast efforts have been made to clarify the nature of the excited state as well as the structural factores by

which it can be controlled and ,accordingly, emission of bis-cyclometalated iridium(III) complexes results most likely from a mixed MLCT-LC character.[28,59,73]

1.2.2 State of research

Recent advances in luminescent sensing with biimidazole complexes

Sebastian A. Rommel[a], Dieter Sorsche[a] and Sven Rau[a]*

Institute for Inorganic Chemistry I, Ulm University, Albert-Einstein-Allee 11, 89081 Ulm, Germany
E-mail: sven.rau@uni-ulm.de, http://www.uni-ulm.de/nawi/nawi-anorg1

Abstract

Luminescent supramolecular metal complexes have attracted great attention over the last decades. Especially, transition metal compounds have come into focus for luminescent sensing applications in recent years due to their promising spectroscopic and luminescent properties. In this contribution we discuss the development potential of the recognition and sensing features of a selection of luminescent complexes of ruthenium(II), iridium(III), osmium(II) and cobalt(III). The sensor application will be enabled over biimidazol ligand scaffolds. At the beginning we will outline the universal photophysical properties of complex bound imidazoles, because of the significant importance for the recognition process of ions. In the second part we will elaborate on the development of the ruthenium(II), iridium(III), osmium(II) and cobalt(III) based colorimetric anions sensors. Thereby the different transition metals were considered individually and the respective development trend within this group demonstrated.To finalize we present the selected example of a ruthenium(II) based cation sensor and its importance for ongoing research effort.

Introduction

Transition metal chromophores based on polypyridyl ruthenium(II), osmium(II) or iridium(III) complexes have become fundamental building blocks in numerous technological applications such as artificial photosynthesis and photocatalysis, in the development of DNA-targeting drugs and in application as molecular optical sensors. This is mainly due to outstanding photophysical properties, i.e. broad light absorption and emission features across the visible regime of the light spectrum, and related long-lived triplet metal-to-ligand charge transfer (^{3}MLCT) states.[1–10] Within its lifetime interactions with the surrounding matrix and other molecular species therein may alter the excited-state of the chromophore in a characteristic way, hence leading to an optical output that can be read as a local probe. The recognition and sensing of selective anions is a fundamental topic in the research area of supramolecular chemistry because of the important roles played by anions in different clinical, biological and chemical processes. [11,12] The fluoride anion for example has been intensively explored as a treatment for osteoporosis.[13] Additional, anions like acetate or phosphate are critical components of various metabolic processes. Consequently, designing new phosphorescent metal complex sensors for ions is of great importance, and has therefore gained much attention in the field of luminescent sensing and supramolecular chemistry.[13–17]

The basic design principle of a molecular sensor comprises the combination of a photoactive chromophore unit with a supramolecular binding site for the ideally selective interaction with a distinct target. Close spatial proximity or electronic coupling between both components assures perturbation of the photophysical properties of the chromophore upon substrate binding. It has been shown that recognition of anions occurs efficiently *via* hydrogen bonding interactions that can be followed by a change in the spectral responses of the signalling subunit.[18–26] In this regard, imidazole-type ligands have attracted increasing attention. The imidazole ring is ubiquitous in nature and the imidazole functionality hence plays critical roles in the human body, notably as histidine and

histamine.[27] Many applications of imidazole-type structures revolve around its ability to bond metals coordinatively *via* the imine part of the five-membered ring, and its ability to establish hydrogen bonds with negatively polarized binding sites in the molecular scaffold of drugs, proteins or simple anions.[12,14–16,28–31] It should further be mentioned that one of the most common ligands at the active sites of metalloproteins is the imidazole ring of histidine residues.[27,28]

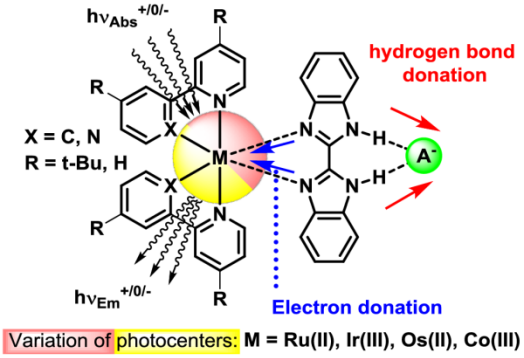

Scheme 1: Schematic representation of the interaction of anions with the NH function of complexes of Ru(II), Ir(III), Os(II) and Co(III).

The fused structure of 2,2'-biimidazole (Biim) and 2,2'-bibenzimidazole (BBI) has long been recognized as suitable ligands for transition metal complexes due to the chelating α-diimine ligand sphere (see Scheme 1). Complexation of bibenzimidazoles with metal centers has several fundamental consequences for anion binding *via* hydrogen bonds. For the manifold of transition metal complexes reported which undergo chelating binding of BBI or Biim ligands, the two corresponding amine functions were shown to adopt a peripheral *cis* orientation. On the one hand, due to the decreased bite angle of the unbound bibenzimidazole (36°) as compared for example to 2,2'-bipyridine (60°) bending of the bibenzimidazole about the diamine ligand scaffold is observed. The corresponding bite angle adopted by the diamine is subsequently widened due to the rigidity of the imidazole five-membered ring.

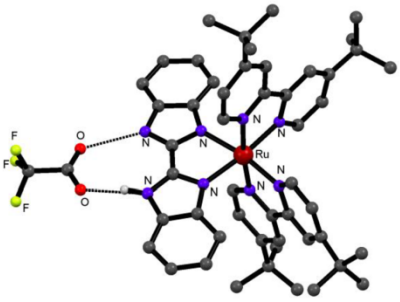

Figure 1: Molecular structure of the hydrogen bond network of a Ru(II) bibenzimidazole complex and trifluoroacetate. Reproduced from CCDC182296 according to ref. [33].

The manifold of solid-structures of Biim and BBI complexes reported in recent years suggests that binding of multiple or two-atomic hydrogen bond acceptors such as acetate is favoured as a

consequence of the widened hydrogen bond donor geometry. Various molecular structures are known where interesting hydrogen bond architectures are formed.[33–40] One example is the hydrogen bond network gained of the reaction of a ruthenium(II) bibenzimidazole complex with trifluoroacetic acid in Figure 1. Another detailed hydrogen bond architecture was reported by Walther et al. where the Ru(II) bibenzimidazole complexes are interconnected *via* their N–H functions by a complicated network involving (i) water molecules serving as hydrogen bond acceptors for N–H and O–H donors and (ii) triflate molecules serving as hydrogen bond acceptors for O–H hydrogen bond donors from water molecules connected to different ruthenium complexes (see Figure 2).

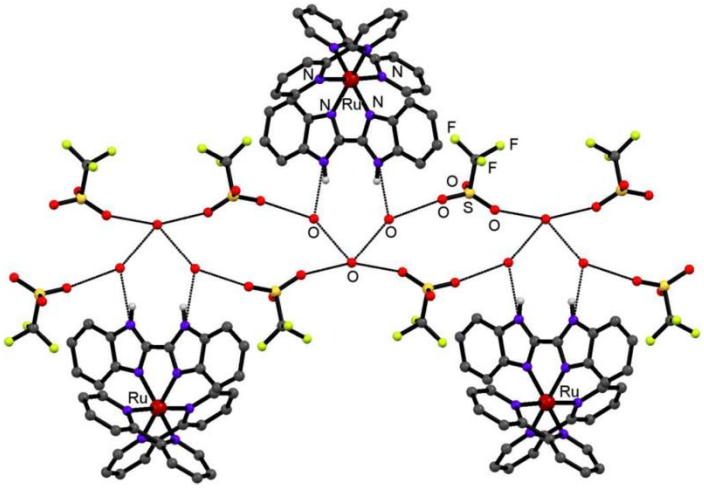

Figure 2: Hydrogen bonding network of $[Ru(H_2bibzim)(bpy)_2][CF_3\text{-}SO_3]_2\cdot 3H_2O$ in the solid state. Reproduced from CCDC152514 according to ref. [35].

Further, interactions between the NH function of the bibenzimidazole with molecular metal oxides, i.e. polyoxometalate were observed. In the crystal packing of the molecular structure in Figure 3, the diprotonated tetramethyl bibenzimidazole ligand forms two hydrogen-bonded interactions with a molybdate cluster, resulting in the observation of two short N–H···O–Mo interactions.

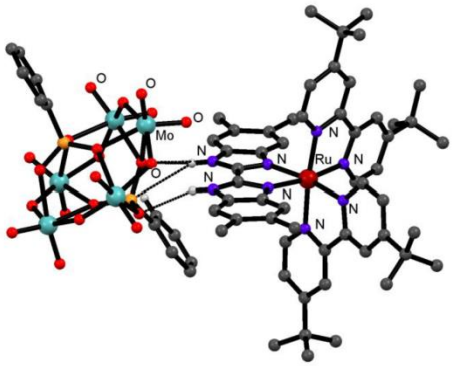

Figure 3: Ball-and-stick representation of the hydrogen-bonded aggregate between a Ru(II) photosensitizer and a molybdate cluster. Reproduced from CCDC 823884 according to ref. [41].

On the other hand, the strength of a hydrogen bond interaction and, in particular, the limit in contrast to simple protolysis is determined by the relative acid strength of both binding partners as characterized by the respective pK_a values. Lewis basicity of the diimine and Brønsted acidity of the diamine are strongly coupled due to electronic coupling within the six electron π-system of imidazole. That is, upon binding to a metal center acidity of the amine is increased and depends strongly on the oxidation state of the former.[11,29–31] *Vice versa* deprotonation of the peripheral diamine functions have been shown to significantly alter the ligand field of the coordinated metal as reflected by major changes of the respective electronic transitions. This general interplay of cation-anion coordination events has been recognized as potential tools for anion sensing in recent years. Comprehensive general reviews on the anion recognition and sensing by transition-metal complexes with polarized N-H recognition motifs, or generally imidazolium receptors for the recognition of anions have been reported elsewhere.[13,27,32,33] The present review highlights the recent development of transition-metal biimidazole and bibenzimidazole receptors for the recognition of various anions and cations. It is focussed in particular on the photophysical responses upon ion binding generated by polypyridyl ruthenium(II), iridium(III), osmium(II) and cobalt(III) fragment chromophores developed in the last decade.

1. Acid-Base-Chemistry of transition metal bi(benz)imidazole complexes

The application of 2,2‘-biimidazole and its derivatives (including 2,2‘-bibenzimidazoles and derivatives thereof) for anion sensing is advantageous due to the presence of a peripheral ortho-diamine hydrogen bond donor functionality. Metal coordination has two important consequences for the properties of this donor. That is (i) due to the five-membered ring geometry the 2,2‘-biimidazole is distorted when bound to a metal ion in order to decrease the bite angle. The peripheral amine diamine geometry is hence widened and as a consequence, a number of solid-state structural data have let to the suggestion that this geometry may favor interactions with multiple hydrogen bond acceptors. Examples cover both combined interaction with a halide and water or interaction with molecular acceptors such as hydrogen sulphate, dihydrogen phosphate, and acetate. [33,35,39,40,45–49] (ii) Due to delocalization of the π-electron system corresponding to the imidazole unit, electron density donation towards a metal center increases the acidity of the amine functions and hence shifts the pH value range for hydrogen bonding. This complementary interaction between Lewis basicity of the diimine and Brønsted acidity of the diamine naturally leads to increased sensitivity of the ligand field of a coordinated metal ion with the protonation state of the complex.

In the early 1980s Haga and co-workers have hence investigated the protonation dependence of the photophysical properties of a bis(2,2‘-bipyridine) ruthenium (2,2‘-bibenzimidazole) complex.[38,50] As one would expect, deprotonation of the 2,2‘ bibenzimidazole increases its σ-donor strength towards the metal ion and hence decreases the HOMO/LUMO gap. This has been characterized by a bathochromic shift of the MLCT absorption with the respective maxima shifted from λ_{max} = 463 nm to λ_{max} = 507 upon single deprotonation and a subsequent shift to λ_{max} = 551 nm upon second deprotonation. This general behaviour has been established for a number of related 2,2‘-biimidazole ruthenium(II) derivatives, whereas it should be noted that naturally, different pKa values have been determined mainly based on the ligand structure.[38–40,45–47,49–51]

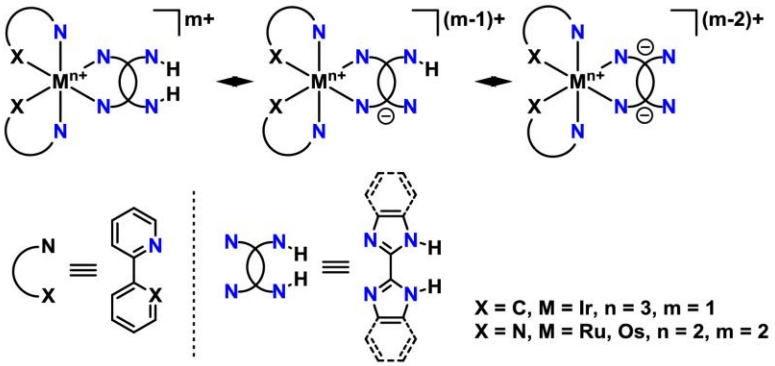

Figure 4.: Acid-base properties of selected transition metal bisimidazoles.

The three different protonation states can clearly be discriminated and the latter can selectively be adjusted with the pH value. Another significant feature of Ru(II) complexes is the change of the emission intensity upon deprotonation. A decrease of the emission intensities of $[Ru(bpy)_2L]^{2+}$ (L= Biim, BBI) together with a slight red shift is observed with increasing the pH value. After the second deprotonation step the luminescence of the complex is nearly completely lost.[34,35,37–39] The absorbance behaviour has been similarly observed for the related osmium(II) complexes, whereas only a minor response of the direct ^{3}MLCT excitation band around 600 nm has been noted.[52] It was further reported that for both ruthenium(II) and osmium(II) complexes a cathodic shift of the metal related M^{2+}/M^{3+} oxidation was observed which is in agreement with an increased electron density due to increased σ-donation from the ligand.[54]

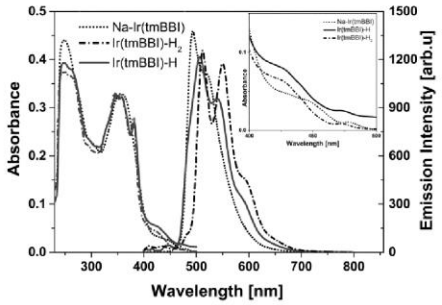

Figure 5. UV/Vis and emission spectra of Ir(tmBBI)-H_x (x =0, 1, 2) in chloroform. The different protonation states were observed in pure chloroform for Na-Ir(tmBBI) (dotted), upon the addition of aqueous HCl (for Ir(tmBBI)-H, solid line), and upon the addition of aqueous HPF_6 (for Ir(tmBBI)-H_2, dash-dot). Reproduced from reference [37] with permission of the publisher John Wiley and Sons.

In recent years, the group of Wenger and Rau reported the synthesis of 2,2‘ biimidazole and 2,2‘ bibenzimidazole complexes of the bis(2-phenylpyridine) iridium(III) chromophore. Groundwork on the pH value dependency of the photophysics of these new near-UV absorbing complexes has been reported.[37,55] In general BBI and Biim complexes of iridium(III) have been proven to be good emitters. The recently reported iridium(III)bibenzimidazole was shown to remain luminescent in all three protonation states of the ligand, which in principal would provide luminescence as probe channel for

intermolecular interactions utilizing H-bond interaction and hence enable sensing in different pH value regimes as compared to ruthenium(II) analogues.[40–42]

In the following, we will focus on the anion recognition features of especially ruthenium(II) and iridium(III) based imidazole type sensors.

2. Sensors for small anions

2.1 Ruthenium(II) based complexes with anion recognition features

Ruthenium(II) complexes coordinated to imidazoles and especially to bi(benz)imidazole ligands have been used as anion receptors since 2005.[43] In general, the stability of these complexes and their redox and chromogenic properties make them suitable candidates for molecular recognition.[27] Coordination of transition metals to the nitrogen atoms in these ligands enhances the acidity of the NH groups and enables them to establish complementary hydrogen bonds with suitable anions. The introduction of the phenylene moieties in bibenzimidazole as compared to biimidazole has been shown to increase the acidity of the amine functions (*vide supra*). Compared to the free biimidazole (pk_a = 11.5), the pK_a values of their corresponding Ru(II) complexes are significant lower, which in turn enhances their potential to function as receptors for anion recognition through hydrogen bonding in solution. The pK_a values principally depend on the charge of the metal core and the structure of the co-ligands.

The solution properties of metal biimidazole complexes as anion receptors were firstly investigated by McPartlin et al..[57] They utilized the η^6-para-isopropylmethylbenzene scaffold to construct the Ru(II) biimidazole complex **1** for anion sensing. **1** has been found to establish strong, non-selective interactions with several simple inorganic anions such as bromide, nitrate, hydrogensulfate, iodide or perrhenate (Figure 6).[43] Anion recognition was demonstrated *via* IR spectroscopy, where a shift of about 100 cm^{-1} in the affected NH signal was observed indicative for strong N-H···X interactions. Anion sensing studies were performed by means of ^{1}H-NMR titrations with the respective anions, both in acetonitrile and the more competitive dimethylsulfoxide. Binding constants are in the range of 1100 for I^- to 6000 for HSO_4^- in acetonitrile, determined via ^{1}H-NMR titration (see also Table 2).

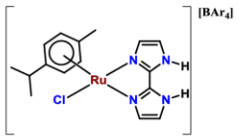

1

Figure 6.: Ru(II)-biimidazole receptor **1** reported by McPartlin et al..[57]

Interestingly, the results showed that complementarity in shape between host and guest favors the anion binding capacity for Y-shaped acceptors like nitrate (see Figure 7).

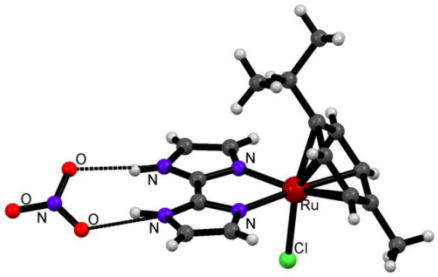

Figure 7: View of the crystalline structure of the**1**·[NO_3] adduct. Reproduced from CCDC 279202 according to ref. [57].

This is reflected by binding constants of NO_3^- ions in the same order as compared to e.g. chloride and bromide, although the latter are more basic. It has been stated that the better matching of the structure of host and guest could partly compensate for the higher basicity.

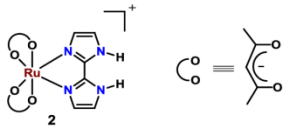

Figure 8.: Ru(III) biimidazole receptor **2** reported by Lahiri et al.. [58]

However, for a ruthenium(II) complex with 2,2'biimidazole-like ligand visible-light-induced photooxidation by singlet oxygen was presented recently by Ye and coworkers.[59] As can be seen in Scheme 2 the Ru(II) biimidazole complex **Ru-1** is converted to the unexpected products **Ru-1a** and **Ru-1b** when being exposed to oxygen atmosphere under irradiation with household light.

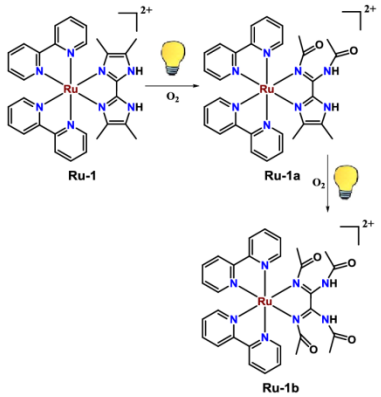

Scheme 2: Visible-light-induced photooxidation of ruthenium(II) complex **Ru-1** with 2,2'-biimidazole-like ligand by singlet oxygen presented by Ye et al..[59]

The conversion process was characterized as solvent and concentration dependent. **Ru-1a** should be an intermediate during the photoreaction and be stable in the solid state as well as in acetonitrile solution with high concentration. However, the intermediate can be further converted into **Ru-1b** in methanol or dilute acetonitrile solution. In each ring opening reaction of one of the imidazole rings is

cleaved and two new acetyl groups are formed. Therefore, upon handling ruthenium(II) biimidazole complexes one should be sensible of the possibility of photooxidation by singlet oxygen.

The structurally related paramagnetic biimidazole ruthenium(II) complex **2**[58] incorporating the electron rich σ-donating acetylacetonate ($acac^-$) ligand was presented by Lahiri et al.. The group focussed on the colorimetric recognition and on the absorbance changes made upon interaction of **2** with Cl^-, Br^-, I^-, HSO_4^-, $H_2PO_4^-$, OAc^- and F. However unless to fluoride, acetate and $H_2PO_4^-$ only weak hydrogen bonding interaction with the remaining ions in the solution state were observed, resulting in a steady colour and correspondingly only negligible changes in the UV/vis spectra. Stronger effects in terms of proton abstraction were observed in the presence of the more basic anions $H_2PO_4^-$, OAc^- and F^-. Similar to hydroxide ions, fluoride and acetate ions deprotonate **2** once at a 1:1 ratio, whereas for $H_2PO_4^-$ an excess of anion (1:4) is needed. Initial hydrogen bonding between the N–H protons of **2** and the strongly basic anions was suggested, which subsequently facilitates the transfer of a N–H proton to the anions. The stronger hydrogen bonding between **2** and OAc^- in relation to HSO_4^- or $H_2PO_4^-$ was attributed by the authors to the difference in pK_{a1} values of 4.75, 1.89, 1.43 for HOAc, H_2SO_4 and H_3PO_4, respectively.[44,45] Finally, binding constants *via* nonlinear curve fitting procedure of absorbance titration experiments were determined (OAc^-: log K = 5.92; F^-: log K = 4.7). Interestingly, only excess fluoride was shown to deprotonate the complex twofold, whereas for acetate the formation of strong hydrogen bonding between **2** and the acetate anion after the first deprotonation step was observed leading to no further deprotonation. This was further confirmed by the high binding constant between OAc^- and **2**. The authors suggest the stable hydrogen bond formation in Scheme 3 between the monodeprotonated **2** and the acetate anion, thus suppressing the second NH abstraction of **2**.

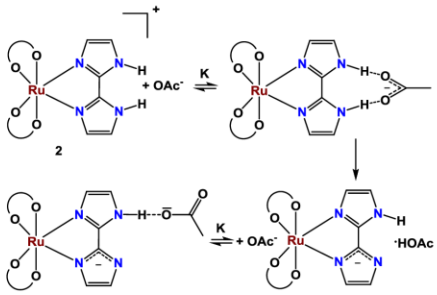

Scheme 3: Stable hydrogen bond formation of **2** and acetate anion.[58]

Based on the optical properties of the Ru(II)-bipyridine moiety and the biimidazole unit as an anion receptor, Ye et al. have described **3** and four related metalloreceptors (**4**, **5**, **6, 7**)[46–50] based on this framework. The studies clearly indicate that the absorption, emission and redox potential of the Ru(II) complexes **3**-**7** depend on the protonation state of the biimidazole-type ligands.[27,48] The authors defined the following three factors to determine the efficiency of hydrogen bonding: (i) the acidity of the metalloreceptor, (ii) the basicity of the anions, and (iii) the strength and number of hydrogen bonds.[27,48]

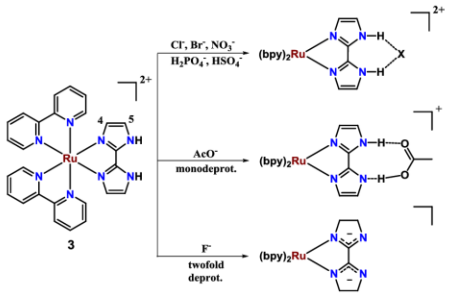

Scheme 4.: Ruthenium(II) biimidazole complex **3** as anion sensor reported by Ye et al..[39]

The anion interaction with complexes **3**-**6** was monitored *via* UV/vis, emission and ^{1}H-NMR spectroscopic titrations, electrochemical measurements, and ESI-MS measurements. However, as **6** is non-luminescent it was focused on the changes in the UV/vis spectrum. The study reports that, depending on the anions, **3**-**6** are appropriate receptors with varying degrees for ions *via* formation of N-H···X hydrogen bonding, or one- or twofold deprotonation, respectively. It was stated, that the characteristics of the interaction between the anions and the metalloreceptors **3**-**6** depend on the acidity of the N-H protons in the given receptor and the basicity of the receptor. In the present case, the N-H protons in complexes **3**-**6** display strong acidity, with pk_{a1} values of 7.2 (**3**), 5.75 (**4**), 6.21 (**5**) and 3.62 (**6**) (see Table 1). For complexes **3** and **4** Haga has already published similar values for the acidity of the complexes in 1983.[62] These are obviously determined by the structure of the biimidazole ligand and the electronic situation of the respective bibenzimidazole ligand. The +I effect in **5** leads to a less acidic NH function, whereas the –M effect induced by the nitro functions in **6** leads to a significant acidification of the complex.

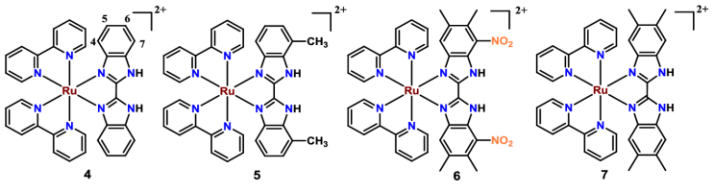

Figure 9.: Ruthenium(II) bibenzimidazole complexes **4**,**5**, **6** and **7** investigated by Ye et al..[40,45–47]

Table 1.: Relevant data for complexes **2**-**6**.

complex	pk_a		Deprotonation (equiv.)				Log (K)[b]	
	pk_{a1}	pk_{a2}	F^-		OAc^-		F^-	OAc^-
2	6.8[a]	11[a]	1	7	1	---	n.d.	n.d.
3	7.2[b]	12.1[b]	1	8	1	---	5.29	5.44
4	5.74[b]	10.51[b]	1	3	1	2	5.28	5.06/ 5.79
5	6.21[b]	10.79[b]	1	4	1	8	n.d.	n.d.
6	3.62[b]	n.d.	1	2	1	2	n.d.	n.d.

[a] $MeOH/H_20$ (1:9), [b] ACN/H_2O (2:3) and 0.1 $mol{\cdot}dm^{-3}$ H_2SO_4, n.d. = not determined; [b] equilibrium constants

In detail, first reports by Ye and co-workers employed the bis(2,2'-bipyridine) ruthenium(II) (2,2'-biimidazole) dication **3** as optical sensor for chloride, bromide, iodide, nitrate, hydrogen sulfate, dihydrogen phosphate, and acetate.[39] The sensor experiments were performed with the hexafluorophosphate salt of the complex and tetrabutylammonium salts of the anions in acetonitrile solution. With respect to the electronic absorption spectra it was stated that colorimetric sensing of the weakly basic anions chloride, bromide, iodide, nitrate, and hydrogen sulfate could not be achieved as the predominant visible light absorption features were unaffected by the presence of these ions. For the slightly more basic anion dihydrogen phosphate only a weak bathochromic shift was observed, whereas acetate and fluoride induced more prominent changes, corresponding to a onefold or twofold deprotonation of the complex, respectively (see Figure 10). According to titration experiments with the respective anion, fluoride, acetate and dihydrogen phosphate were discussed in more detail and equilibrium constants were calculated.

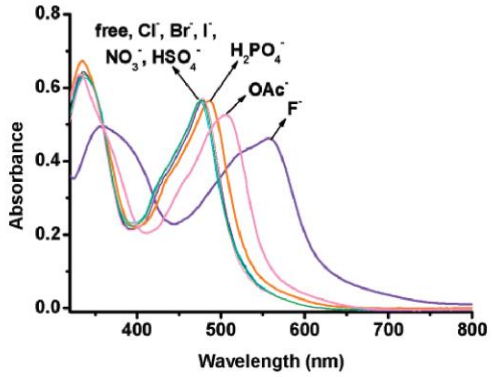

Figure 10: UV-vis spectra of **3** in MeCN solution (5×10^{-5} M, black) and the addition of 1 equiv of the respective anions. Reprinted with permission from Y. Cui, H.-J. Mo, J.-C. Chen, Y.-L. Niu, Y.-R. Zhong, K.-C. Zheng and B.-H. Ye, *Inorg. Chem.*, **2007**, 46, 6427–6436. Copyright 2016 American Chemical Society."[39]

Although theoretical calculations *via* a non-linear curve-fitting procedure were performed in order to support a 1:1 receptor ion binding, subsequent studies drew a reasonable doubt on the validity of this model (see further below). Additionally, ^{1}H-NMR spectroscopy has additionally been employed in order to characterize the interaction with the respective ions. For the strongly basic fluoride and acetate a characteristic shift of the related signals was observed in the spectra, indicating a deprotonation process. However, for the basic anions a shift of the N-H proton was notably which was not observed in dmso-d^6. Unfortunately hydrogen bonds with the weakly basic ions were not reported in this paper. However, in a following paper[40] the complex-anion interaction by means of hydrogen bonding events could be investigated for **3** by the shift of the typical NH signal located in the lowfield (11 ppm – 12.4 ppm) in deuterated acetonitrile. Binding constants between 3300 to 5700 were obtained, which are though comparable to those of **1** in McPartlins work.[57] Obviously, the more competitive solvent dimethylsulfoxide prevents a complex-anion interaction and makes aware that the solvent has a strong influence on the recognition features of complexes. Additionally, Ye et al. performed fluorescence titrations of **3** with anions. The strong basic anions confirm the deprotonation process, as in all cases the luminescence is nearly completely quenched. However, a complete different feature is obtained with the less basic anions. An interaction of the latter with **3** was only visible with Cl^- and HSO_4^- in solution with a slight decrease in the fluorescence intensities, whereas no interaction takes place with the weaker basic anions.

In a subsequent study Ye and co-workers further employed the bis(2,2'-bipyridine) ruthenium (2,2'-bibenzimidazole) dication **4**.[40] Again only a nearly negligible response to the interaction with the weakly basic anions chloride, bromide, iodide, nitrate, and hydrogen sulfate was observed by a slight increase of the MLCT absorption intensity. However, upon addition of the basic anions fluoride and acetate a gradual bathochromic shift of the absorption was reported for which initial hydrogen bonding was postulated accompanied by an ongoing N-H abstraction. This deprotonation can be followed easily with the naked eye by a change from a yellowish to a violet solution (see Figure 11).

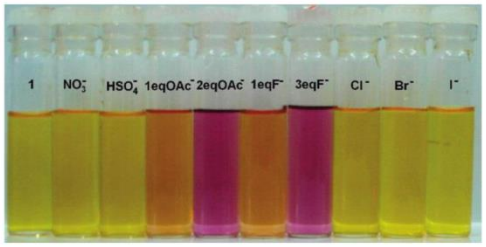

Figure 11: Color changes observed for **4** (8×10^{-5} M) in MeCN solution and in the presence of the corresponding anions as TBA salts. Reprinted with permission from Y. Cui, Y.-L. Niu, M.-L. Cao, K. Wang, H.-J. Mo, Y.-R. Zhong and B.-H. Ye, *Inorg. Chem.*, **2008**, 47, 5616–5624. Copyright 2016 American Chemical Society.[40]

This was supported by two single-crystal solid-state structures of the acetate and the trichloroacetate adducts, both showing the respective anion being bound to the complexes *via* complementary hydrogen bonds (see Figure 12).

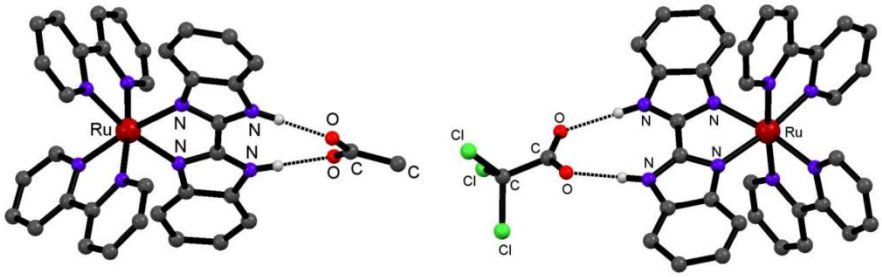

Figure 12: Molecular structure of complex **4** with acetate (left) and trichloroacetate (right). Reproduced from CCDC 649643 and CCDC649645 according to ref [40].

However, the authors stated that in solution the observed spectroscopic changes and the characteristic shifts in the ^{1}H-NMR spectra match the ones observed upon addition of sodium hydroxide, which generally supports the assumption that deprotonation is predominant over hydrogen bonding in solution. Later on, for complexes **3**, **4**, **5** and **7** Ye and coworkers employed two alternative strategies for the investigation of the related hydrogen bonded biimidazole – acetate hydrogen bond complex, that is (i) the addition of excess acetic acid in order to suppress deprotonation and subsequent addition of acetate, and (ii) addition of acetic acid to the mono-deprotonated complex.[45,63] Both methods revealed a new species with a MLCT absorption maximum at $\lambda = 491$ nm which had not been seen before and could be assigned to a hydrogen bonded complex-acetate adduct.[45] Moreover, electrochemical measurement was also employed to prove the

hydrogen bonded adduct. Addition of 400 equiv. of HOAc to **7** did not change the oxidation potential of the $Ru^{2+/3+}$ couple. However, when 1 equiv. of OAc^- was added to the above solution of **7**, a significant negative shift was observed on the oxidation wave. These results deviate significantly from the previously postulated ones, which casts reasonable doubt on the validity of the model of calculating equilibrium constants when a predominant deprotonation process is included. Additionally, the anion recognition features of **4** were investigated by ^{1}H-NMR titrations. Notably, Ye and coworkers observed no N-H signal when Cl^-, Br^-, I^- and NO_3^- anions were added to a solution of **4** in acetonitrile, except for HSO_4^-, where a considerable binding constant of 11209 (± 307) M^{-1} could be calculated. This nature was ascribed to the stronger electron donating nature and basicity of the HSO_4^- ion and hence would facilitate the selectivity of **4** toward HSO_4^-. However, the HSO_4^- anion has to be regarded with special care. Recently, our group reported that the reaction between Ru(II) complexes containing different biimidazole-type ligands with the sulfate dianion show a strong correlation between the substituents at the biimidazole core and the solubility of the product. In this study we could show that bibenzimidazole containing complexes precipitate from aqueous solution under presence of sulfate dianions, whereas the Ru(II) complexes containing unsubstituted biimidazole stay in solution. Further, a solid-state structure of a bibenzimidazole containing complex was presented that showed strong hydrogen bonds between the secondary amine function of the bibenzimidazole and the oxygen functionalities of the sulfate (see Figure 13), thus contributing to this unexpected behavior. [64] According to this, the exclusive hydrogen bonding event between **4** and the HSO_4^- anion, detectable in the ^{1}H-NMR titration experiments, is not unexpected.

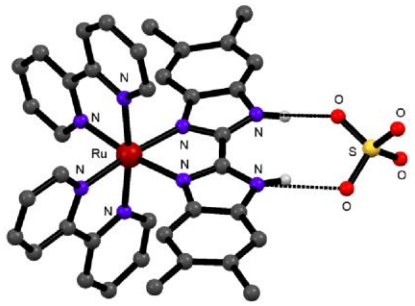

Figure 13: Solid-state molecular structure of the $[Ru(bpy)_2(tmbibzimH_2)](SO_4)$ complex presented by Rau et al.. Reproduced from CCDC759064 according to ref [64].

For both the 2,2'-biimidazole **3** and 2,2'-bibenzimdazole complex **4** Ye and co-workers reported that the ^{3}MLCT emission was quenched upon addition of the basic anions, which is in agreement with the luminescence quenching observed upon deprotonation with a strong base. Regarding the weakly basic anions, **4** only would give a response to HSO_4^- with an increase of emission intensity of about 40 %. Ye et al. claim, that the unstable N-H bond would make the interaction between **4** and Cl^-, Br^-, I^-, NO_3^- negligible, while the electron donating nature of HSO_4^- would allow the formation of hydrogen bonds with the N-H groups. Additionally, complex **4** was shown to exhibit distinguishable responses to the carboxylic acids $CCl_3CO_2^-$ and $CF_3CO_2^-$. Whereas $CF_3CO_2^-$ deprotonates **4** twice, $CCl_3CO_2^-$ induces only a mono-deprotonation. This was attributed to the stable formation of twofold hydrogen bonds between the monodeprotonated **4** and the $CCl_3CO_2^-$ anion and the geometrically matching of donor and acceptor, forming complementary linear "Y-type" hydrogen bonds.[61] Further, it was stated that

proton transfer is not only determined by the basicity of the anion but is also related to the strength of hydrogen bonding interaction.[61]

In additional studies Ye and coworkers claimed, that a moderate pka value is the key to control the binding affinity toward anions. Along these lines, a further development of the approach was reported through introducing either two methyl groups or nitro groups adjacent to the amine functions, that is in the 4,4'-positions of the 2,2'-bibenzimidazole. [46,47] They stated that the additional groups at the 4,4' position can open a small pocket to modulate the interaction of the N-H binding site with the anions and enhance the binding affinity. Therefore they introduced complex **5** and **6**.[46,47]

Table 2.: Binding constants of 1, 3, 4, 5 and 6 with anions *via* ^{1}H NMR titrations in ACN (Fitted to a 1:1 binding model).[46,47,57]

	K (M^{-1})				
	1	**3**	**4**	**5**	**6**
Anion					
Cl^-	n.c	5700 ±259[a]	n.c.	20396[a] ±1309 5.31[b] ±0.05	21053[a]
Br^-	4527[a] ±841	3682 ±245[a]	n.c.	18113[a] ±714 5.24[b] ±0.07	17767[a]
I^-	1114[a] ±207	3327 ±108[a]	n.c.	18682[a] ±747 5.21[b] ±0.04	4472[a]
NO_3^-	4828[a] ±587	4609 ±166[a]	n.c.	20988[a] ±886 5.18[b] ±0.04	n.c.
HSO_4^-	5920[a] ±370	4334 ±356[a]	11209[a] ±307 5.16[b] ±0.06	17146 ±857[a] 5.20[b] ±0.05	n.c.

[a] calculated *via* an absorption titration; [b] calculated *via* emission titration; n.c. = no chemical shift change of N-H function in the emission spectrum.

The basic features of the two newly complexes were quite similar to the aforementioned ones as addition of strongly basic anions caused a stepwise N-H abstraction of the respective complexes, whereas the colorimetric response towards weakly basic ions was negligible with almost no changes in the MLCT region of the UVvis spectrum. However, the characteristic N-H proton signal at the low-field of the ^{1}H-NMR spectra clearly indicated that indeed hydrogen bonds would be established, expressed by a significant shift of the proton signal. In pure acetonitrile solutions the N-H signal of the pristine complex would not appear, but emerge in the presence of the weakly basic anions chloride, bromide iodide, nitrate, and hydrogen sulfate at varying positions. The nitro-groups of **6** were shown to partake and potentially assist the hydrogen bond framework as shown by a single crystal solid-state structure obtained from the respective chloride salt. However, a major

disadvantage of sensor **6** is the complete loss of luminescence, which has been previously reported for related complexes.[36] The methyl substitution in **5** resulted in a strongly luminescent complex. A luminescence increase between 20-40% was reported upon hydrogen bonding of weakly basic anions for this complex. Most significantly, the emission increase in the presence of chloride, bromide, and iodide was observed exclusively with the dimethylated complex in contrast to either the unsubstituted 2,2'-biimidazole **3** or 2,2'-bibenzimidazole **4** complexes, where only for HSO_4^- a response was present. Herewith an important indication was given that the spatial restriction of the binding site through substitution was a successful strategy in order to use ruthenium(II)2,2'-bibenzimidazole complexes as sensors for weakly basic anions through luminescence. Further, binding constants of **5** via ^{1}H-NMR titration experiments were calculated and found to be in the range of 17000 to 21000. These are larger than those observed for **3**, with binding constants between 3300 to 5700, which are though comparable to those of **1** in McPartlins work.[43] The pk_a value of **5** is 1 pk_a unit lower than for **3**, indicating stronger acidity of the N-H protons, justifying the 4 to 5-fold increase of the binding constants. Although the methyl groups may not participate in the hydrogen bonding formation with the weak basic anions, the risen binding constants confirm the effect of the substitution. Complex **6**[47] which is featured with two nitro groups in the 4,4' position displays an open pocket that is smaller than that in receptor **5**.[47,49] The strong electron withdrawing nature of the nitro groups renders the imidazole N-H fragments highly acidic with a pk_a value of 3.62. The stronger N-H acidity, together with the small pocket of **6** hence induces a stronger binding towards Cl^- and Br^-, and a weaker to I^- with binding constants ranging from 4400 to 21000. Further, through the reduced binding space of **6** and the weaker basicity and larger size of the anions, NO_3^- and HSO_4^- are shut out.

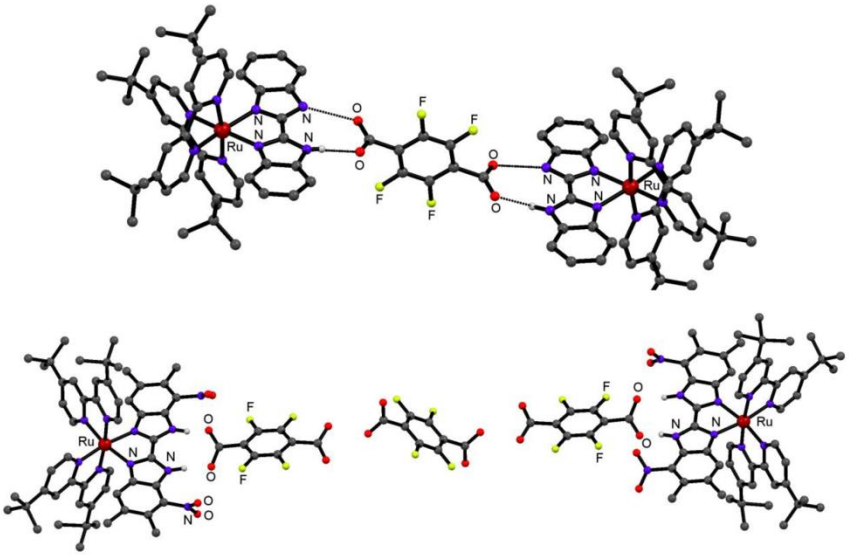

Figure 14: Above: H-bond network of ruthenium(II) bibenzimidazoles with tetrafluoro terephthalate; below: H-bond network of nitro-functionalized bibenzimidazole ruthenium(II) complexes with tetrafluoro terephthalate. Reproduced from CCDC182297 according to ref. [33] and CCDC631075 according to ref. [36].

On the basis of the observation that manipulations of the 4,4'-positions are of particular interest as they can define a pincer-like pocket around the hydrogen bond moiety,[37,49] Walther and coworkers established synthetic procedures to introduce a variety of substituents at this position.[36]

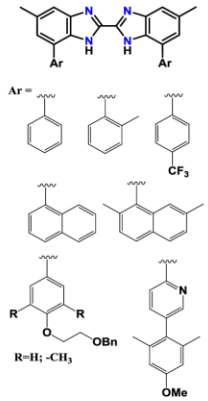

Figure 15: 4,4'-bisaryl-bibenzimidazole structures obtained by Siegel et al..[65,66]

Interestingly, introduction of nitro-functionalities at the 4,4'-position resulted in the surprising formation of complicated 2:3 H-bond adducts with tetrafluoro terephthalate. The unsubstituted ruthenium bibenzimidazole complex only forms a 2:1 adduct (see Figure 14).[33] Further, Siegel and coworkers established a highly interesting synthetic access towards bibenzimidazoles as organic supramolecular building blocks (see Figure 15). The synthetic access to 4,4'-disubstituted complexes with aryl substituents is very intriguing as it would allow vast control over the envisaged binding pocket.[65,66]

Our group introduced the three ruthenium(II) bibenzimidazole complexes **8**, **9**, and **10**. Complex **9** and **10** contain the structurally confined ligand 4,4'-di(p-anisyl)-2,2-bibenzimidazole. With introducing these aromatic substituents a direct spatial influence on the H-bond pocket was envisaged with the anisyl substituents entwining the *cis*-diamine.[37] *Via* ^{1}H-NMR spectroscopy it was shown that in **9** the anisyl rings are free to rotate around the C(benzimidazol)-C(anisyl) axis at room temperature, whereas a rigid C_2 symmetry, where rotation of the dimethylanisyl moiety is sterically hindered, is observed for **10**. The investigations strongly suggested that **10** could provide a more defined pincer geometry as compared to **9**, which is more flexible.

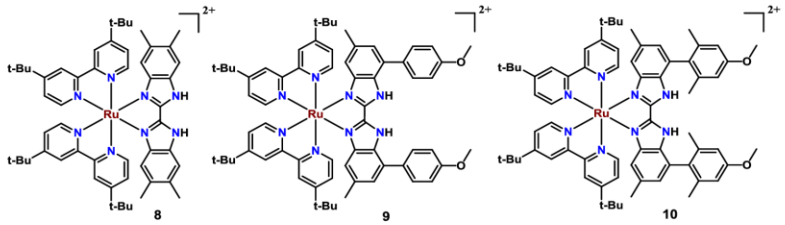

Figure 16.: 4,4' disubstituted bibenzimidazole Ruthenium(II) complexes reported by Rau et al..[49]

Via UV/Vis-, fluorescence and ^{1}H-NMR measurements the interaction of the halides F^-, Cl^-, Br^- and I^- with complexes **8**-**10** were investigated. Fluorescence studies showed that anisyl substitution leads to a "dimming effect" as a significant decrease of the emission intensity of **9** and **10** compared to **8** occurs. The dimming effect was however reversed upon hydrogen bonding between the complexes and weakly basic halides, leading to measurable anion sensitivity in terms of signal enhancement. As expected, fluorescence and absorption titration spectra of **8-10** with fluoride match with the behaviour observed upon deprotonation with TBAOH, therefore the interaction between the investigated complexes and fluoride could be best described as a subsequent N-H abstraction. The absorption spectra of **8** showed virtually no response to Cl^-, Br^- and I^- titration experiments in the MLCT region, whereas **9** and **10** revealed a sensitive response to the addition of chloride and bromide, i.e. a slight broadening and decrease in absorptivity of the MLCT absorptions bands. As only negligible changes by means of absorption and emission responses were obtained for **8**, the latter could not be seen as a suitable colorimetric sensor molecule for the detection of weakly basic halides. However, the weak sensor capabilities of **8** came not as a surprise, as complex **4** presented by Ye et al. showed only weak sensor capabilities, too.

In contrast to **8**, chloride and bromide induce a significant increase in luminescence intensity, i.e. an increase of 303 % of the initial value of **9** by adding 1 equiv. of chloride, or 279 % in the presence of bromide. A likewise effect, was obtained for **10**, with an increase of about 244 % when treated with chloride, and 193 % when treated with bromide. Iodide, however, was proved to induce only a negligible effect on the luminescence intensity and was therefore successfully excluded through the straitened pincer-like sensor entity. Binding constants *via* emission titration experiments were calculated for the respective anions with values in the range of log(5.13) up to log(6.26) (see Table 3), therefore demonstrating the strong interaction of the anions with the respective complexes. A similar trend was observed within ^{1}H-NMR titrations, where the spectra for **8**-**10** exhibit a deshielding of the acidic protons, indicative for hydrogen bonding with chloride and bromide. With iodide the respective signal could only be observed for **10**, whereas it disappeared in the spectra of **8** and **9**, leading to the assumption that a stabilization of the hydrogen bonding event takes place within the small pocket of **10**.

Table 3.: Luminescence increase of **8**,**9** and **10** and binding constants determined *via* emission titration.

		luminescence increase[a]	log(K_a[b])
8	Cl^-	103 %	---
	Br^-	103 %	5.13 ±16 %
	I^-	97 %	---
9	Cl^-	303 %	6.26 ±25%
	Br^-	279 %	5.63 ±7%
	I^-	111 %	---
10	Cl^-	244 %	5.82 ±14%
	Br^-	193 %	5.63 ±15%
	I^-	106 %	---

Additionally, it has to be emphasized that both **9** and **10** eventually outperform all yet reported ruthenium(II) bisimidazole complexes significantly in terms of luminescence intensity upon addition of the respective anion, which leads to a remarkably higher sensitivity as compared to **8**. Within this row of ruthenium(II) complexes for anion recognition applications, it has been demonstrated that due to the functional dimming, which has been introduced through the attachment of the phenylene rings, a significant enhancement in luminescence sensitivity has been achieved. This enhanced sensitivity and selectivity for weak-basic anions, especially among the halides, is to the best of our knowledge exceptional in the field of complex bound imidazole sensors.

2.2 Iridium(III) based complexes with anion recognition features

To the best of our knowledge, most of the investigated systems, especially those reported in this review, need inert conditions to operate properly.[39,40,45,47,49,58,67,68] This limits their applicability in the field of sensor chemistry and the necessity to develop systems that work under aerobic conditions is therefore evident. As the emission intensity of iridium(III) complexes is known not to be quenched *via* atmospheric oxygen, these complexes are more qualified to fulfill their task under aerobic atmosphere conditions.

Wenger et al. could show for the first time, that proton delocalization by means of hydrogen bonding interactions with an iridium(III) biimidazole complex can be monitored directly by optical spectroscopy due to the close proximity of the acidic N-H protons to the metal center.[40,54] Their group presented fundamental work on the photoacidic behaviour and photochemistry of the bis(phenylpyridine)iridium(III) biimidazole complex **11.** They focussed on proton coupled electron transfer (PCET) events. It was stated that the complex forms hydrogen-bonded 1:1 adducts with benzoate anions and is not deprotonated when an excess of benzoate anions is added. Salt bridges of **11** with 3,5-dinitrobenzoate (dnb^-) were observed in the crystal structure and it was shown, that the luminescence intensity decreases about 80 % compared to the pristine **11**, which was interpreted as oxidative quenching of the MLCT/IL state.[40,54]

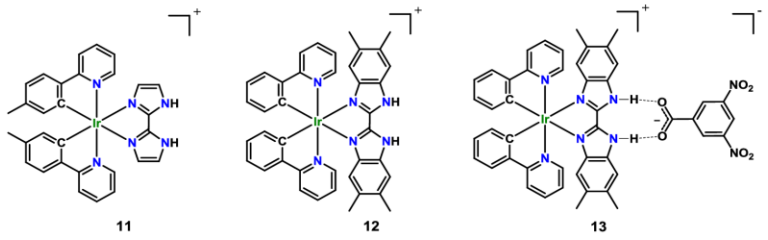

Figure 17.: Iridium(III) bi(benz)imidazole complexes for luminescent sensing reported by Wenger and Rau et al..[48,56,70]

Inspired by the precedent work, our group investigated the features of the iridium(III) bibenzimidazole complex **12** to serve as an anion sensor. We could show that **12** is luminescent in all of its three protonation states, and the respective protonation states could be distinguished selectively in the emission spectrum.[42] In principle, this feature provides an effective spectroscopic handle for the direct observation of a proton release and a possibility to observe interactions of the complex with various anions by means of hydrogen bonding events.

To investigate the sensor functionality of **12**, we considered the interaction of the complex with the basic anions F^-, OAc^-, $H_2PO_4^-$, and the weaker basic anions Cl^-, Br^-, I^-, and HSO_4^-. Interaction of **12** with the latter ions was screened by means of ^1H NMR and emission spectroscopy. The second sphere interactions of **12** with these anions resulted in only marginal changes in the absorption spectrum. Systematic studies revealed that the N-H functions of **12** interact with Cl^-, Br^-, I^- and HSO_4^- *via* the formation of hydrogen bonds whereas the stronger basic anions interact *via* a N-H abstraction. $H_2PO_4^-$ is only capable to single deprotonate **12** (2 equiv.), while F^- and OAc^- ions undergo a stepwise process: formation of the single deprotonated complex **12** (after 2 equiv. of each respective anion) with a low anion concentration, followed by the twofold deprotonated complex in the presence of higher anion concentration (F^-: 4 equiv.; OAc^-: 7 equiv.). The reduced basicity of $H_2PO_4^-$ and OAc^- ions is reflected in the stronger concentration dependence of the process, that is abstraction of the second proton after addition of 7 equivalents of acetate and only a single deprotonation step by $H_2PO_4^-$ ions.

Table 4.: Equiv. of anions needed to deprotonate **12** one- or twofold and associations constants (K_a) of **13**···X interaction calculated *via* emission titration.

	12			**13**			
	F^-	**OAc^-**	**$H_2PO_4^-$**	**Cl^-**	**Br^-**	**I^-**	**HSO_4^-**
Depro-tonation (equiv.)	2	2	2	-	-	-	-
	4	7	-	-	-	-	-
$K_a(M^{-1})$	n.d.*	n.d.*	n.d.*	33195 ±1232	1572 ±283	n.d.	17804 ±328

*not determined

The remarkable change of the luminescence properties of **12** upon interaction with the anions was shown to be a potential indicator for anion detection through hydrogen bonds. Emission spectroscopic titrations of **12** with chloride, bromide, iodide and hydrogen sulfate hence showed enhancement of the overall emission intensity with a concomitant slight hypsochromic shift of the emission maxima, which confirmes a hydrogen bonding event between the complex and the respective ion. In accordance with the NMR measurements the strongest enhancement of 67% was observed for chloride, followed by bromide (51%), hydrogen sulfate (24%), and iodide (19%) (see Figure 18).

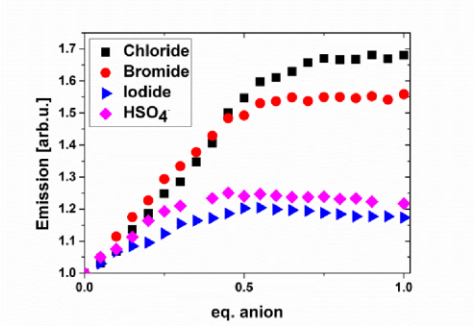

Figure 18: Normalized emission spectral responses of **12** (5 x 10^{-6} M in chloroform, 298 K, λ_{ex} = 378 nm) upon addition of Cl^-, Br^-, I^- and HSO_4^- anions. Reproduced from reference [56] with permission of the publisher John Wiley and Sons.

Job's plot analysis revealed that a stable 2:1 (complex : anion) binding mode is present within NMR and emission titration measurements. Herein an important difference with respect to the

ruthenium(II) complexes (*vide supra*) is displayed which may refer to the reduced charge of the iridium(III) complexes.

Further, ^{1}H-NMR titrations with the weakly basic anions approved a hydrogen bonding event between the latter and **12**. Thereby, the characteristic N-H signal in deuterated chloroform was shown to be low field shifted stepwisely upon addition of up to one equivalent of the aforementioned anions. Thus, the strongest shift(s) of the signal was caused in the order $s(Cl^-) > s(Br^-) > s(I^-) > s(HSO_4^-)$.

In agreement with the above model which takes electrostatic and hydrophilic/hydrophobic interactions with the solvent into consideration, high association constants and a virtually stoichiometric reaction to the respective ion pairs were observed. The high association constants exceed all values obtained for analogous biimidazole ruthenium(II) complexes known thus far.

Since the emission response for the anion-complex interaction provides promising features, but the respective luminescent enhancement was rather small and unselective, further optimization of **12** as optical sensor was carried out (see **13**). Similar to Nocera[55] and Wenger et al.[40], 3,5-dinitrobenzoate was used to quench the excited state of **12** efficiently, that is by about 50% in a 1:1 mixture in chloroform and further addition of up to 8 equivalents lead to a residual luminescence of about 8% with respect to the pristine PF_6 complex. As the hydrogen bonded ion pair between **12···DNBA** (active sensor **13**) shows weak luminescence due to hydrogen bond mediated quenching by the anion, the system was able to be used as a supramolecular luminescence "off-switch" for the improvement of the iridium(III) based sensor **12**.

As it was shown that **12** strongly interacts with weakly basic anions, competitive binding could displace the quencher and restore the luminescence of the ion pair or in other words switch it back on. The weakly basic anions Cl^-, Br^-, I^- and HSO_4^-, were able to establish competing H-bonds with the complex, thus leading to a displacement of DNBA out of the hydrogen bonded ion pair complex. The formation of the competing H-bonds could be followed by emission spectroscopy. Thereby, addition of up to 120 equivalents of F^-, Cl^-, Br^-, I^- and HSO_4^- ions showed a sensitive gradual increase of the emission of **13** of up to 750% for fluoride, 450% for chloride, 405% for hydrogen sulfate, 220% for bromide, and only about 118% for iodide. This regained luminescence can be followed easily by the naked eye (see Figure 19). The outstanding increase by treatment with F^- ions was shown to correspond to a N-H abstraction of the iridium(III) complex (*vice supra*). Additionally, due to the negative charge of the twofold deprotonated **12**, electrostatic repulsion inhibits collision induced quenching by the DNBA anion in solution, therefore leading to strong luminescence.

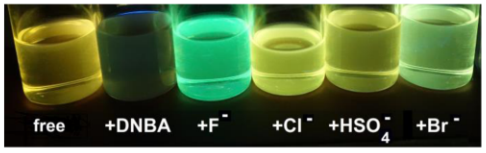

Figure 19: Picture of the different solutions of **12** in chloroform and excess anions. Reproduced from reference [72]. Reproduced by permission of The Royal Society of Chemistry.

The discrimination between chloride and bromide in this system is remarkable, and the general trend in the strengths of luminescence increase due to competing H-bonds with the respective anions, corresponds well to the basicity of the investigated ions. Anion binding constants *via* emission titration experiments of **13** with the respective anions were calculated and found to be 33195 for Cl^-, 17804 for HSO_4^- and only 1572 for I^- (see Table 4).

Competitive molecular recognition of fluoride, chloride, bromide, iodide and hydrogen sulfate *versus* the hydrogen bonded **12···DNBA** (**13**) system therefore displays a powerful tool to increase the ion sensing quality of **12** in terms of luminescence sensitivity.

2.3 Osmium(II) based complexes for anion recognition

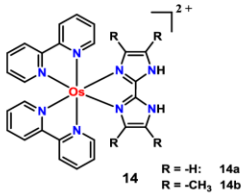

Figure 20.: Osmium(II) coordinated 2,2'-biimidazole complexes with anion recognition features reported by Lahiri et al..[54]

The anion sensing features of the osmium(II) biimidazole complexes **14a** and **14b** have been evaluated by Lahiri and co-workers.[54] The complex-anion interaction was investigated *via* a series of experimental methods, i.e. colorimetry, absorption and ^{1}H NMR spectroscopy, x-ray crystallography, and theoretical (DFT) investigations. In detail, acetonitrile and aqueous medium were used to test the anion sensing features of **14a** and **14b** with tetrabutyl ammonium salts of F^-, CN^-, Cl^-, Br^-, I^-, OAc^- ,SCN^-, NO_3^-, $H_2PO_4^-$ and HSO_4^-. As observed with similar ruthenium(II) and iridium(III)complexes, the strong basic anions like F^-, OAC^-, CN^- and $H_2PO_4^-$ interact with the complexes via N-H abstraction in acetonitrile. This could be followed colorimetrically *via* a colour change from a yellowish to a reddish solution. In contrast, in aqueous medium only CN^- selectively changes the colour of the complexes *via* deprotonation. Colorimetric experiments therefore reveal sensible variations in both **14a** and **14b** based on the solvent medium. The same trend was observed within absorption titrations in acetonitrile, where both complexes are being deprotonated concentration dependently by F^-, CN^-, OAc^-, and $H_2PO_4^-$ (see). Binding constants in acetonitrile on the basis of the absorbance titrations were calculated for the distinct ions and found to be in the range of log(K) = 5.56 up to log(K) = 6.65 (see). However, in aqueous medium only CN^- ions are sensitive to both complexes **14a** and **14b**, visible by a bathochromic shift of the MLCT bands in the absorbance spectrum. Lahiri et al. attributed the exclusive selectivity of **14a** and **14b** for the cyanide ion in aqueous medium to the less negative hydration energy (ΔH_{hyd} = -67 kJ mol^{-1}) as compared to that of the F^- ion (ΔH_{hyd} = -505 kJ mol^{-1}). Further, Lahiri et al. claim that **14a** and **14b** can also function as excellent electrochemical sensors for the selective anions, as they vary the oxidation potential to a conspicuous extend on addition of F^-, CN^-, OAc^- and $H_2PO_4^-$.

Table 5.: Deprotonation processes of complexes **14a** and **14b** and the binding constants between distinct anions determined via absorbance titration.

complex	Action/ Ion	F^-	OH^-	CN^-	OAc^-	$H_2PO_4^-$	Cl^-	Br^-	I^-	HSO_4^-
14a	**Deprot.**	1 4	1 2	1 4	1 -	1 -	- -	- -	- -	- -
14b	**Deprot.**	1 6	1 2	1 6	1 -	- -	- -	- -	- -	- -
14a	**Log(K)[a]**	6.44	n.d.	6.32	6.65	5.67	n.d.	n.d.	n.d.	n.d.
14b	**Log(K)[a]**	5.56	n.d.	5.48	5.77	-	n.d.	n.d.	n.d.	n.d.

[a] Calculated to a 1:1 model; absorption titration; n.d. = not determined

The same trend was endorsed by ^{1}H NMR titration experiments, through vanishing of the NH signal in the lowfield and by a shift of the CH signals affected through the increase of electron density upon deprotonation by the strong basic anions of F^-, CN^- and OAc^-. The hydrogen bond mediated deprotonation process between the receptors and the anions was further proven on the basis of DFT calculations.

The detailed studies reveal that the different strength of hydrogen bonding interactions with the anions, i.e. F^-, CN^-, OAc^-, $H_2PO_4^-$, make **14a** and **14b** effective anion receptors in non-aqueous medium, while the same receptors are perfectly selective towards the CN^- anion in water without any interference from the other investigated anions. However, the sensors exhibit limited application potential as **14a** and **14b** are not luminescent.

2.4 Cobalt imidazole-type complexes for anion recognition

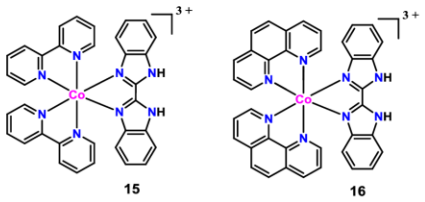

Figure 21.: Cobalt(III) bibenzimidazole metalloreceptors **15** and **16** reported by Nair et al..[73]

Nair et al. focused on two different cobalt(III) bibenzimidazole complexes (**15**) and (**16**) with different ancillary oligopyridyl ligands.[73] Anion sensor studies of the latter were performed with different biologically important anions like F^-, Br^-, I^-, ClO_4^-, OH^- and OAc^-. In contrast to complexes **1**-**14**, which bring about chromogenic recognition of the anions like fluoride or acetate, none of the latter do bring about any vivid colour change in the case of **15** and **16**. However, both complexes were described as suitable candidates for chromogenic recognition of iodide ions, as they selectively would change the colour from colourless to a deep yellow by addition of I^- anions. TBA salts of F^-, OH^- and OAc^- anions were proved to induce slight changes in the ligand centered transitions of the cobalt complexes **15** and **16**, which were assigned to an interaction of the respective anions with the complexes due to their strong basicity. However, **15** and **16** were insensitive to all other anions tested, except iodide, which causes a vivid spectral change in the ligand centered transitions and the hyperchromism was found to be 160% in the case of complex **15**. Ye, Rau and Lahiri et al. have shown, that the ruthenium(II), iridium(III) and osmium(II) complexes containing the bibenzimidazole ligand exhibit no significant changes on the addition of iodide ion, which conclusively indicates that the iodide ion interacts with cobalt complexes with alternate mechanism. Nair et al. claim, that since iodide has a poor tendency to form hydrogen bonds with imidazole ligands, the sensing of iodide by the cobalt(III) complexes should be through the charge transfer complex formation. Accordingly, this should be due to the highly electrophilic cobalt(III) complex interacting with the nucleophilic iodide anion. Further Nair and co-workers demonstrated that **15** exhibits fluorescence quenching upon the addition of I^- and the strong basic anions F^-, OH^- and OAc^-. In case of the latter, the quenching should be a result of the high basicity and the hydrogen bonding ability of the anions. In case of iodide the authors assign the quenching to the heavy atom effect *via* formation of a charge transfer complex. Therefore, they claim that metalloreceptor **15** can also be used as a fluorometric chemosensor for

iodide anions. While the analogous bibenzimidazole complexes **4** and **8** of Ru(II) sense fluoride and acetate *via* a deprotonation process, the analogue cobalt(III) complex **15** has instead been found to be a very good sensor for iodide. Thus, the authors claim that the interaction of anion with second sphere receptor is determined not only by the basicity of the anion or the strength of the hydrogen bond but also depends on the nature of the metal ion used.[73]

2.5. Advancement: unsymmetrically constructed imidazoles as ligands for luminescent anion sensors

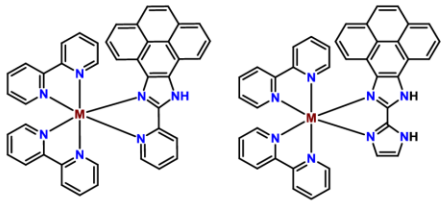

Figure 22: Complexes with unsymmetric imidazole-like ligands with anion recognition features reported by Baitalik et al..

Another advancement was presented by Baitalik and co-workers, which introduced an unsymmetrically constructed imidazole-like ligand as anionic recognition site, incorporating a pyrene functionality with a pyridyl (**17 a,b**) or imidazolyl entity (**18 a,b**).[1,11] The pyrene-4,5-dione core is an interesting ligand because of its rigid, conjugated and planar geometry and its rich photophysical properties. Accordingly, the introduction of the pyrene moiety into the bis-imidazole unit is expected to impart outstanding photophysical properties for efficient optical sensing.[11] The osmium(II) complexes (**17b**, **18b**) in this work are of particular interest because of their absorption spectrum which covers almost the complete visible region and stretches up to the near infrared (NIR, 700-1000 nm) region.[11] Further, the Os(II) complexes are moderately strong emitter with an emission window between 750 and 875 nm, which is of importance for its potential biological applications in imaging and phototherapy.[80–83] Using this new family of complexes, in this approach the emission wavelengths of the receptors are extended to the NIR region, and hence afford a more bio-compatible condition.

The anion recognition features of **17** and **18** were investigated with tetrabutylammonium salts of Cl^-, Br^-, I^-, NO_3^-, ClO_4^-, HSO_4^- and the stronger basic F^-, AcO^-, CN^-, OH^- and $H_2PO_4^-$. The studies of **17** through different spectroscopic techniques revealed that both, the Ru(II) and Os(II) complex, act as "turn-on" luminescence sensors for $H_2PO_4^-$ and serve as "turn-off" sensors toward F^- and AcO^- in acetonitrile, whereas the remaining anions induce only minor changes. The apparent difference between the different anions is, that with the excessive addition of the more basic anions F^- and AcO^- the imidazole N-H proton of the receptor entities are deprotonated, while $H_2PO_4^-$ only interacts through hydrogen-bonding processes. The deprotonation process was confirmed by OH^- ions which induced similar changes in the absorption and emission spectral behaviors. Further, **17a** was stated to act as a suitable lifetime-based sensor for F^- and $H_2PO_4^-$ ions. Baitalik and co-workers also investigated the binding affinities of the complexes **17a**/**17b** toward calf-thymus DNA (CT-DNA) *via* different methods, such as absorption, emission, excited-state lifetime, circular dichroism, and

thermal denaturation of DNA. The intercalative nature of both **17a** and **17b** was proven as well as their characteristic light-switch behaviour.

The anion sensing properties of **18a/b** in acetonitrile were intensively examined through absorption (in acetonitrile and aqueous media), steady-state and time-resolved emission spectroscopy methods. Further, electrochemical investigations, such as cyclic and square wave voltammetric measurements were applied to prove the anion recognition features of the complexes. Similar to **17a/b**, both metalloreceptors can sense F^-, AcO^-, $H_2PO_4^-$ and additionally CN^- ions in acetonitrile without exhibiting selectivity to differentiate the ions. This is in contrast to aqueous media, where both receptors exhibit strong responses only towards CN^- ions. The present metalloreceptors **18a/b** can therefor act as efficient multi-channel sensors for F^-, AcO^-, $H_2PO_4^-$and CN^- in acetonitrile. Further, both complexes exhibit a remarkably selectivity towards cyanide anions in aqueous media even in an excess of other anions as well as in the solide state. An "on-off" effect through CN^- ions is obtained, whereas the other ions almost induce no remarkably colorimetric change. It is of interest to note that unlike in acetonitrile, F^-, AcO^- and $H_2PO_4^-$ do not interfere in aqueous media. The authors quote the greater free energy of hydration for F^-, AcO^- and $H_2PO_4^-$ as a probable reason for the selectivity only towards CN^-. Moreover, the Ru(II) and Os(II) complexes display a visual detection of cyanide ions with a low detection limit of the order of 10^{-8} mol/L.[11]

Additionally, Baitalik and co-workers attempted ^{1}H-NMR spectroscopy to shed light on the mode of interaction between the imidazole NH protons of the metalloreceptors and the selected anions. To this end, they titrated a DMSO-d^6 solution of **18a** with an incremental addition of cyanide ions. During this addition process, a down-field shifting and broadening of the NH signals of **18a** were assigned to initial hydrogen bonding followed by the disappearance of the signal due to complete proton transfer with an excess of the cyanide anion.

2.6 Cation recognition features of a ruthenium(II) bibenzimidazole complex

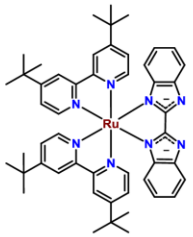

19

Figure 23: Ruthenium(II) bibenzimidazole complex acting as a cation-driven molecular switch presented by Walther et al..

An additional field of application for the bibenzimidazole receptors was investigated by Walther et al. who used the fully deprotonated neutral **19** as a cation recognition sensor.[51] As has been discussed already (*vide supra*), the MLCT absorption band of these type of complex is broadly shifted across the visible light regime with a maximum at approx. $\lambda = 550$ nm compared to the fully protonated analogue. The peripheral formal amide nitrogen atoms of **19** are negatively charged strong Lewis bases and hence ready to bind Lewis acids such as metal cations. The binding withdraws electron

density from the BBI which would in turn reduce its σ–donor strength and increase its π–acceptor strength towards the ruthenium(II) center. Receptor **19** was reacted with the Lewis acids cobalt(II), copper(II), magnesium(II), nickel(II) and zinc(II).

Accordingly, in all cases, binding of the respective metal center was achieved and indeed recognized by a colorimetric response, i.e. a shift of the absorption maximum towards between 510-530 nm. Concomitantly, the emission of the non-luminescent **19** is switched on exclusively by the presence of zinc(II), copper(II) and magnesium(II) metal cations. It is also shown that both the emission intensity and the emission wavelength are dependent on the concentration and the nature of the metal cation. At low $ZnCl_2$:**19** ratios a trinuclar complex is formed, that is bathochromic shifted compared to the dinuclear complex of **19** and zinc(II), which is formed at a 10^4 -fold excess of $ZnCl_2$.

The results clearly show the potential of complex bound imidazole-like ligands to act as sensors for cations. However already published by Walther et al. in 2000 to the best of our knowledge no similar topic was addressed so far.

Conclusion and outlook

We have shown a selection of luminescent biimidazole-like complexes that offer a range of desirable features which make them viable alternatives to organic molecules as luminescent chemosensors. Their photophysical properties are highly sensitive to changes in their supramolecular environment, such as upon coordination or reaction of analytes with the polarized NH recognition motif *via* deprotonation or hydrogen bonding events. The simplicity of the modular synthesis allows facile synthesis of a range of analogues with different functional groups for fine-tuning of their chemical or photophysical properties.[13] In general, all complexes disscussed in this review operate *via* an interaction of the NH function with the different anions by means of deprotonation or a hydrogen bonding mechanism, however to different characteristics. The anion-complex interaction could be verified by ^{1}H NMR specroscopy, UV/Vis and emission titrations and electrochemical measurements such as cyclovoltammetry.

We highlighted the anion recognition features of ruthenium(II) complexes bearing a symmetrically bisimidazole struture motif. One avenue for the improvement of the phosphorescent chemosensors is to introduce selectivity by means of a pocket-like functionality. Through extension of the bisimidazole structure, smaller anions lead to a recognition process whereas large anions could be excluded. Further, iridium(III) based phosphorescent chemosensors for selected anions were presented. Their proven manageability under air atmosphere enhances their application range and is a big asset compared to prior investigations with ruthenium(II) complex fragments. Additionally, the recognition features of related osmium and cobalt complexes were presented. The osmium(II) complexes were proved to be highly selective towards the CN^- anion in water without any interference from the other investigated anions. The cobalt(III) analogue instead has been found to be a very good selective colorimetric sensor for iodide ions. Subsequently, we displayed osmium(II) and ruthenium(II) complexes bearing unsymmetrically constructed imidazole-like ligands that exhibit strong responses only towards CN^- ions in aqueous media. Further they can act as efficient multi-channel sensors for F^-, AcO^- and CN^- in acetonitrile.

In the last part a simple ruthenium(II) bibenzimidazole complex that can act as a cation driven light switch was presented. The feature to detect cations over a significant hypsochromic shift in the absorption spectra or by switching on of the emission enables an efficient way to recognize cations in solution.

One possibility to refine such bisimidazole type complexes in terms of selectivity could be the introduction of a macrocycle entity to receive a defined constrained realm for the detection of ions. In a first procedure this was already performed with ruthenium(II) bibenzimidazole complexes by Rau et al..[84] They could already show that cation complexation by means of copper with the macrocycle is possible. It is obvious that this strategy could be efficient for all other transition metal based imidazole-like sensor systems.

References:

1 S. Mardanya, S. Karmakar, D. Maity and S. Baitalik, *Inorg. Chem.*, 2015, **54**, 513–526.

2 V. W. Manner and J. M. Mayer, *J. Am. Chem. Soc.*, 2009, **131**, 9874–9875.

3 J. H. Alstrum-Acevedo, M. K. Brennaman and T. J. Meyer, *Inorg. Chem.*, 2005, **44**, 6802–6827.

4 E. A. Medlycott and G. S. Hanan, *Chem. Soc. Rev.*, 2005, **34**, 133.

5 W. R. Browne, N. M. O'Boyle, J. J. McGarvey and J. G. Vos, *Chem. Soc. Rev.*, 2005, **34**, 641.

6 V. Balzani, A. Juris, M. Venturi, S. Campagna and S. Serroni, *Chem. Rev.*, 1996, **96**, 759–834.

7 K. E. Erkkila, D. T. Odom and J. K. Barton, *Chem. Rev.*, 1999, **99**, 2777–2796.

8 A. E. Friedman, J. C. Chambron, J. P. Sauvage, N. J. Turro and J. K. Barton, *J. Am. Chem. Soc.*, 1990, **112**, 4960–4962.

9 S. Baitalik, X. Wang and R. H. Schmehl, *J. Am. Chem. Soc.*, 2004, **126**, 16304–16305.

10 P. A. Gale, N. Busschaert, C. J. E. Haynes, L. E. Karagiannidis and I. L. Kirby, *Chem. Soc. Rev.*, 2014, **43**, 205–241.

11 S. Mardanya, S. Karmakar, M. Bar and S. Baitalik, *Dalton Trans.*, 2015, **44**, 21053–21072.

12 R. Martínez-Máñez and F. Sancenón, *Chem. Rev.*, 2003, **103**, 4419–4476.

13 D.-L. Ma, V. P.-Y. Ma, D. S.-H. Chan, K.-H. Leung, H.-Z. He and C.-H. Leung, *Coord. Chem. Rev.*, 2012, **256**, 3087–3113.

14 P. D. Beer, *Acc. Chem. Res.*, 1998, **31**, 71–80.

15 P. D. Beer and J. Cadman, *Coord. Chem. Rev.*, 2000, **205**, 131–155.

16 P. D. Beer and P. A. Gale, *Angew. Chemie Int. Ed.*, 2001, **40**, 486–516.

17 A. P. De Silva, H. Q. N. Gunaratne, T. Gunnlaugsson, A. J. M. Huxley, C. P. McCoy, J. T. Rademacher and T. E. Rice, *Chem. Rev.*, 1997, **97**, 1515–1566.

18 H.-J. Mo, Y. Shen and B.-H. Ye, *Inorg. Chem.*, 2012, **51**, 7174–7184.

19 S.-S. Sun and A. J. Lees, *Chem. Commun.*, 2000, 1687–1688.

20 S. Saha, A. Ghosh, P. Mahato, S. Mishra, S. K. Mishra, E. Suresh, S. Das and A. Das, *Org. Lett.*, 2010, **12**, 3406–3409.

21 N. Kumari, S. Jha and S. Bhattacharya, *J. Org. Chem.*, 2011, **76**, 8215–8222.

22 K.-S. Lee, H.-J. Kim, G.-H. Kim, I. Shin and J.-I. Hong, *Org. Lett.*, 2008, **10**, 49–51.

23 N. Gimeno, X. Li, J. R. Durrant and R. Vilar, *Chem. - A Eur. J.*, 2008, **14**, 3006–3012.

24 S.-S. Sun, A. J. Lees and P. Y. Zavalij, *Inorg. Chem.*, 2003, **42**, 3445–3453.

25 A. Satheshkumar, R. Manivannan and K. P. Elango, *J. Organomet. Chem.*, 2014, **750**, 98–106.

26 A. K. Mahapatra, S. K. Manna, B. Pramanik, K. Maiti, S. Mondal, S. S. Ali and D. Mandal, *RSC Adv.*, 2015, **5**, 10716–10722.

27 P. Molina, A. Tárraga and F. Otón, *Org. Biomol. Chem.*, 2012, **10**, 1711.

28 P. D. Beer, *Coord. Chem. Rev.*, 2003, **240**, 167–189.

29 C. N. Carroll, J. J. Naleway, M. M. Haley and D. W. Johnson, *Chem. Soc. Rev.*, 2010, **39**, 3875.

30 K.-C. Chang, S.-S. Sun, M. O. Odago and A. J. Lees, *Coord. Chem. Rev.*, 2015, **284**, 111–123.

31 F. Wang, L. Wang, X. Chen and J. Yoon, *Chem. Soc. Rev.*, 2014, **43**, 4312.

32 I. Bertini, A. Sigel and H. Sigel, *Handbook on Metalloproteins*, Marcel and Dekker, New York, 2001.

33 S. Rau, L. Böttcher, S. Schebesta, M. Stollenz, H. Görls and D. Walther, *Eur. J. Inorg. Chem.*, 2002, 2800–2809.

34 D. Sorsche and S. Rau, *Eur. J. Inorg. Chem.*, 2014, **2014**, 4244–4249.

35 S. Rau, M. Ruben, T. Büttner, C. Temme, S. Dautz, H. Görls, M. Rudolph, D. Walther, A. Brodkorb, M. Duati, C. O'Connor and J. G.

Vos, *J. Chem. Soc., Dalton Trans.*, 2000, 3649–3657.

36 A. Grüßing, S. Rau, S. Schebesta, A. Scholz, H. Görls and D. Walther, *Z. Anorg. Allg. Chem.*, 2007, 961–970.

37 S. A. Rommel, D. Sorsche, N. Rockstroh, F. W. Heinemann, J. Kübel, M. Wächtler, B. Dietzek and S. Rau, *Eur. J. Inorg. Chem.*, 2015, 3730–3739.

38 M.-A. Haga, *Inorganica Chim. Acta*, 1983, **75**, 29–35.

39 Y. Cui, H.-J. Mo, J.-C. Chen, Y.-L. Niu, Y.-R. Zhong, K.-C. Zheng and B.-H. Ye, *Inorg. Chem.*, 2007, **46**, 6427–6436.

40 Y. Cui, Y.-L. Niu, M.-L. Cao, K. Wang, H.-J. Mo, Y.-R. Zhong and B.-H. Ye, *Inorg. Chem.*, 2008, **47**, 5616–5624.

41 K. Heussner, K. Peuntinger, N. Rockstroh, S. Rau and C. Streb, *Dalton Trans.*, 2015, **44**, 330–337.

42 P. A. Gale, *Coord. Chem. Rev.*, 2001, **213**, 79–128.

43 J. W. Steed, *Chem. Soc. Rev.*, 2009, **38**, 506–519.

44 Z. Xu, S. K. Kim and J. Yoon, *Chem. Soc. Rev.*, 2010, **39**, 1457.

45 H.-J. Mo, J.-J. Wu, Z.-P. Qiao and B.-H. Ye, *Dalton Trans.*, 2012, **41**, 7026–7036.

46 H.-J. Mo, Y.-L. Niu, M. Zhang, Z.-P. Qiao and B.-H. Ye, *Dalton Trans.*, 2011, **40**, 8218.

47 H.-J. Mo, H.-Y. Chao and B.-H. Ye, *Inorg. Chem. Commun.*, 2013, **35**, 100–103.

48 S. A. Rommel, D. Sorsche and S. Rau, *Dalton Trans.*, 2016, **45**, 74–77.

49 D. Sorsche, S. A. Rommel and S. Rau, *Eur. J. Inorg. Chem.*, 2016, **2016**, 1503–1513.

50 M. Haga, T. Ano, T. Ishizaki, K. Kano, K. Nozaki and T. Ohno, *J. Chem. Soc. Dalt. Trans.*, 1994, 263.

51 S. Rau, T. Büttner, C. Temme, M. Ruben, H. Görls, D. Walther, M. Duati, S. Fanni and J. G. Vos, *Inorg. Chem.*, 2000, **39**, 1621–1624.

52 A. M. Bond and M. Haga, *Inorg. Chem.*, 1986, **25**, 4507–4514.

53 M. Haga, *Inorg. Chim. Acta*, 1980, **45**, L183–L184.

54 A. Das, S. M. Mobin and G. K. Lahiri, *Dalton Trans.*, 2015, **44**, 13204–13219.

55 J. C. Freys, G. Bernardinelli and O. S. Wenger, *Chem. Commun.*, 2008, 4267–4269.

56 S. A. Rommel, D. Sorsche, A. Dixit and S. Rau, *Eur. J. Inorg. Chem.*, 2016, **2016**, 40–48.

57 L. Ion, D. Morales, J. Pérez, L. Riera, V. Riera, R. a Kowenicki and M. McPartlin, *Chem. Commun.*, 2006, 91–93.

58 T. Kundu, S. M. Mobin and G. K. Lahiri, *Dalton Trans.*, 2010, **39**, 4232.

59 Z.-Z. Li, Y.-L. Niu, H.-Y. Zhou, H.-Y. Chao and B.-H. Ye, *Inorg. Chem.*, 2013, **52**, 10087–10095.

60 J. A. Dean, Ed., *Lange's Handbook of Chemistry*, Science Press and McGraw-Hill Education, Beijing, 15th edn., 1999.

61 Y. Cui, Y.-L. Niu, M.-L. Cao, K. Wang, H.-J. Mo, Y.-R. Zhong and B.-H. Ye, *Inorg. Chem.*, 2008, **47**, 5616–5624.

62 M. Haga, *Inorg. Chim. Acta*, 1983, **75**, 29–35.

63 C. Pérez-Casas and A. K. Yatsimirsky, *J. Org. Chem.*, 2008, **73**, 2275–2284.

64 N. Rockstroh, K. Peuntinger, H. Görls, D. M. Guldi, F. W. Heinemann, B. Schäfer and S. Rau, *Z. Naturforsch*, 2010, **65b**, 281–290.

65 Y. Yasui, D. K. Frantz and J. S. Siegel, *Org. Lett.*, 2006, **8**, 4989–4992.

66 D. K. Frantz, A. A. Sullivan, Y. Yasui, A. Linden, K. K. Baldridge and J. S. Siegel, *Org. Biol. Chem.*, 2009, **7**, 2347–2352.

67 T. Kundu, A. D. Chowdhury, D. De, S. M. Mobin, V. G. Puranik, A. Datta and G. K. Lahiri, *Dalton Trans.*, 2012, **41**, 4484.

68 K. Monczak, K. Peuntinger, D. Sorsche, F. W. Heinemann, D. M. Guldi and S. Rau, *Chem. Eur. J.*, 2014, **20**, 15426–15433.

69 O. S. Wenger, *Acc. Chem. Res.*, 2013, **46**, 1517–1526.

70 J. C. Freys, G. Bernardinelli and O. S. Wenger, *Chem. Commun.*, 2008, 4267–4269.

71 J. P. Kirby, J. A. Roberts and D. G. Nocera, *J. Am. Chem. Soc.*, 1997, **119**, 9230–9236.

72 S. A. Rommel, D. Sorsche and S. Rau, *Dalton Trans.*, 2016, **45**, 74–77.

73 R. Indumathy, P. S. Parameswaran, C. V. Aiswarya and B. Unni Nair, *Polyhedron*, 2014, **75**, 22–29.

74 R. B. P. Elmes, K. N. Orange, S. M. Cloonan, D. C. Williams and T. Gunnlaugsson, *J. Am. Chem. Soc.*, 2011, **133**, 15862–15865.

75 L. Yang, X. Li, J. Yang, Y. Qu and J. Hua, *ACS Appl. Mater. Interfaces*, 2013, **5**, 1317–1326.

76 Q. Zhao, C. Huang and F. Li, *Chem. Soc. Rev.*, 2011, **40**, 2508–2524.

77 X. Chen, S.-W. Nam, G.-H. Kim, N. Song, Y. Jeong, I. Shin, S. K. Kim, J. Kim, S. Park and J. Yoon, *Chem. Commun.*, 2010, **46**, 8953–8955.

2 Structure of the thesis

The research reported in this thesis includes three main topics concerned with the design of new second-sphere receptor chromophores on the basis of iridium(III) and ruthenium(II) metal centers. Based on previous studies by the groups of Siegel[74,75], Rau[11,76], Ye[7–9,77], and Wenger[78,79], new potential receptors are developed featuring the principal 2,2'-bibenzimidazole receptor ligand.

The particular aspects to be investigated are as follows.

- ❖ Synthesis and profound characterization of the iridium(III) complex of 5,5',6,6'-tetramethyl-2,2'-bibenzimidazole $[(ppy)_2Ir(tmBBI\text{-}H_2)][PF_6]$ (**Ir-K0**) and its homodinuclear analogon **(Ir-K0)$_2$**.
  - Investigation of the basic properties of the iridium(III) chromophores **Ir-K0** and **(Ir-K0)$_2$** and comparison with the well-known ruthenium analogues.
  - Enlightening of the acid-base chemistry of **Ir-K0** *via* ^{1}H-NMR, absorption and fluorescence spectroscopy.
  - The expected significant differences of **Ir-K0** compared to their ruthenium(II) analogue, especially in relation to the emission properties, are suggested to be beneficial regarding photocatalytic purposes.

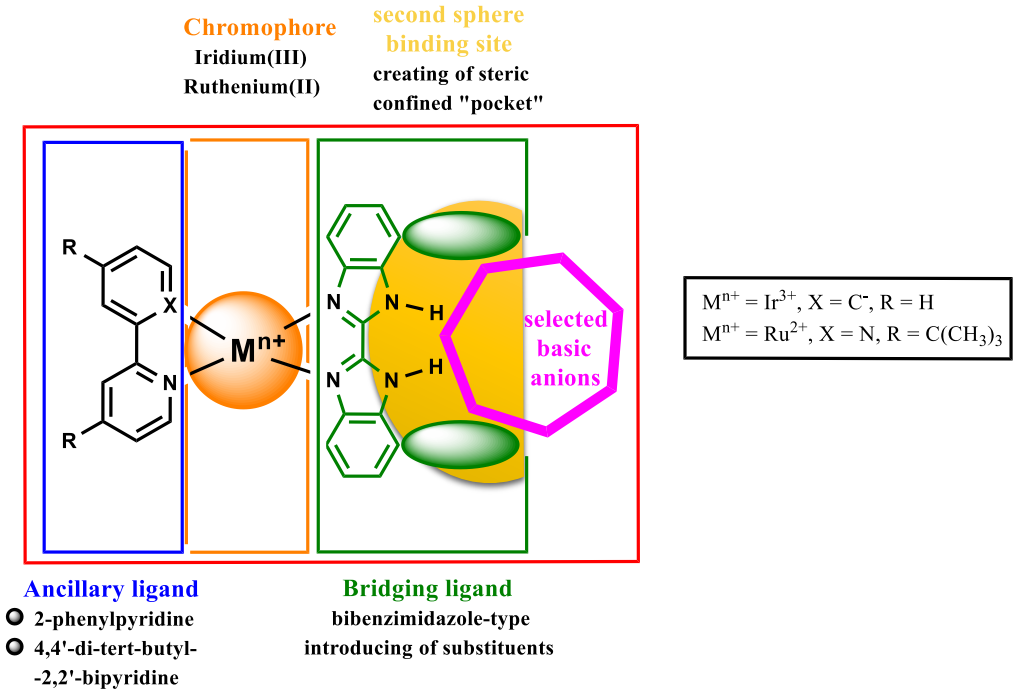

Figure 4: Schematic depiction of the main aspects of the thesis.

- ❖ Investigation of the interaction of the iridium(III)bibenzimidazole model complex **Ir-K0**-H_x (x =0, 1, 2) with selected basic anions.
  - In particular: Investigation of the interaction of **Ir-K0**-H_x (x =0, 1, 2) with halides; further hydrogen sulfate and dihydrogen phosphate *via* ^{1}H-NMR and emission spectroscopic methods.
  - Drawing implications for luminescent sensing.
- ❖ Refinement of the optical sensor system **Ir-K0**-H_x (x =0, 1, 2).

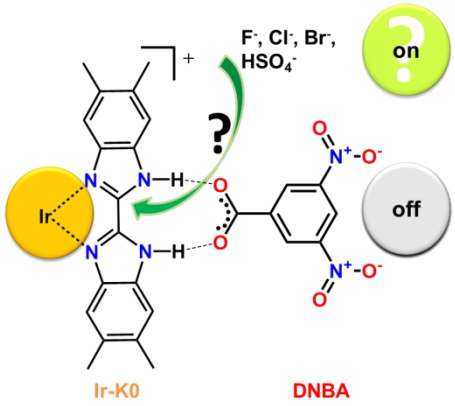

Figure 5: Proposed ON/OFF sensor system resulting of the reaction of the reductive quencher DNBA with **Ir-K0**.

- By using the oxidative quencher 3,5-dinitrobenzoate (DNBA) the resulting hydrogen bonded ion pair between **Ir-K0** and 3,5-dinitrobenzoate (DNBA) should lead to a loss of luminescence - analogous to the reported systems of Nocera[80] and Wenger et al.[81].
- In the presence of weakly basic anions, competitive binding should displace the quencher and restore the luminescence of the ion pair or in other words switch it back on.

- ❖ Synthesis, characterization and investigation of the application potential of bis(2,2'-bipyridine) ruthenium(II) chromophores with 4,4'-disubstituted 2,2'-bibenzmidazole ligands.
  - Analysis of the structure-property relationships by inducing of two rigid substituents.
  - Characterization of the hydrogen bonding interaction between the 2,2'-bibenzimidazole ruthenium(II) chromophores and the halide anions *via* ^{1}H-NMR investigations and fluorescence and absorption spectroscopy.

❖ In a merging project the gained know-how of the two different chromophore should be applied to couple ruthenium(II) and iridium(III) based 2,2'-bibenzimidazole chromophores in one dinuclear complex.

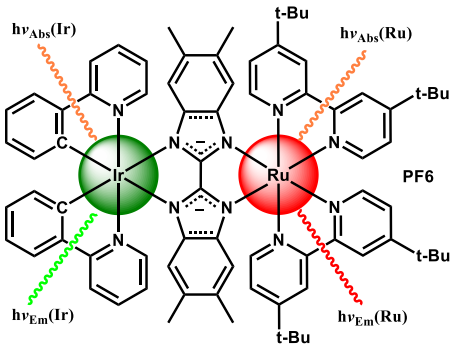

Figure 6: Connecting ruthenium(II) and iridium(III) via 2,2'-bibenzimidazolate as bridging ligand; investigation of combined photophysics.

- Comprehensive characterization of the nature and communication between the different chromophore units *via* the bibenzimidazole bridge.
- Investigation of the application potential as photosensitizer in water reduction experiments.

3 Investigated systems

3.1 Second sphere chemistry of an iridium(III) chromophore

3.1.1 Synthesis, characterization and acid-base chemistry of a luminescent iridium(III) bibenzimidazole system and its homodinuclear analogon

As shown in the introduction, bibenzimidazole complexes of photoactive ruthenium(II), cobalt(III) and osmium(II) have been widely investigated with respect to their hydrogen bonding and anion sensing properties. It was demonstrated that complexes bearing bisimidazole-type ligands are suitable supramolecular sensor systems that can detect anions as well as cations in solution. The absorption features of e.g. photoactive bis(bipyridine)ruthenium(II) complexes in the visible light region are known to change significantly upon deprotonation or hydrogen bonding events.[11,82] Further, in their fully deprotonated state the complexes are featured to act as metalloligands, that is the deprotonated biimidazole sphere can bind a second metal center, e.g. zinc(II), nickel(II), or Cu(I).[11,76,83,84] Binding of these metal centers induces significant changes of the characteristic photophysical properties of the respective complex. This feature is of paramount importance for this and further studies, as it can provide a spectroscopic tool for direct observation of proton release from these molecules.[79]

The versatile applicability of bis(bipyridine)ruthenium(II) complexes however is limited by the fact that only the fully protonated complexes exhibit appreciable luminescence. A significant deactivation pathway is obviously opened through deprotonation, which limits the value of these complexes for photochemical applications.[82] Notably, the triplet-excited state of bis(phenylpyridine)iridium(III) chromophores was shown to generally exhibit a strong mixing of ligand-centered (LC) and metal-centered (MC) states.[85] Together with the long-lived excited states and their high luminescence quantum yields, the greater ligand-field stabilization energy of the third row elements exhibits an important advantage to iridium(III) complexes over ruthenium(II).

In this regard, going from ruthenium(II) to iridium(III) chromophores appeared to be a promising approach in order to connect the switching properties of a bibenzimidazole ligand with the more sophisticated luminescence of a bis(phenylpyridine)iridium(III) complex fragment. Therefore, the aim of this study was the principal translation of the established multifaceted photochemical functionalities of ruthenium(II) bibenzimidazole complexes onto an isostructural iridium(III) chromophore (see Scheme 4).

In the studies we used the 5,5’,6,6’-tetramethyl-2,2’-bibenzimidazole (**L0**) as a (bridging)ligand, which was shown to be a suitable representative of the extended class of bibenzimidazole complexes.[86]

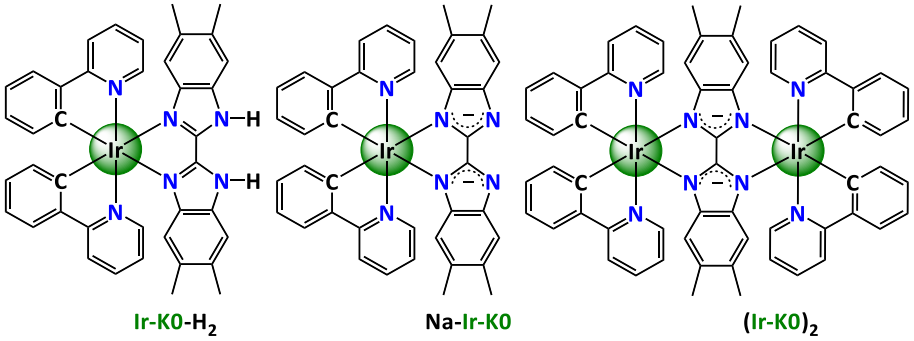

Scheme 4: Schematic representation of the complexes discussed in this paper.

Consequently, the respective iridium chromophore $[(ppy)_2Ir(tmBBI\text{-}H_2)](PF_6)$ (**Ir-K0**) has been synthesized *via* binding of **L0** to the cyclometalated Ir(III) μ-chloro-bridged dimer $[(ppy)_2Ir]_2(\mu\text{-}Cl)_2$. The principal structural characterization of **Ir-K0**-H_x (x = 0, 1, 2) was performed by ESI- mass spectrometry and ^{1}H- and ^{13}C-NMR spectroscopy. The structural expectations, that is the formation of a cis-*bis*-cyclometallated octahedral iridium(III) complex with a peripheral *ortho*-diamine moiety was confirmed. A characteristic signal is given by the two aromatic protons of the ligand **L0** which point towards the ancillary ligands and hence appear upfield shifted to 5.74 ppm due to shielding by the π-electron system of either one phenyl ring. The opposite proton on the outer rim of the complex is characterized by a sharp singlet at 7.5 ppm.

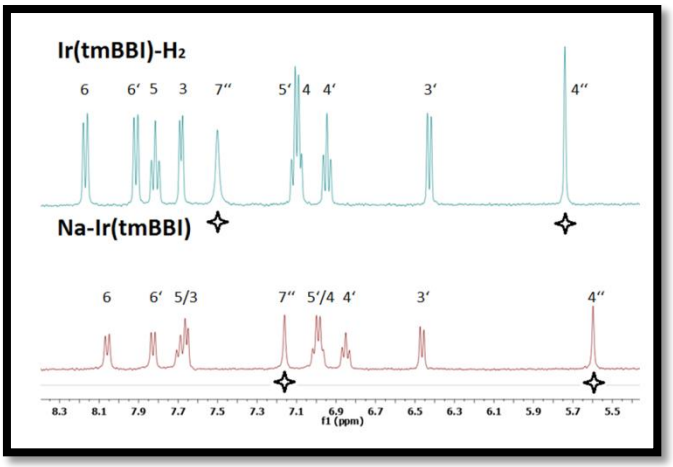

Figure 7: Characteristic ^{1}H-NMR signals of **Ir-K0**-H_2 and Na-**Ir-K0** in DMSO–d_6 in the aromatic region (c = 2.345 mmol/L). The bibenzimidazole related signals are marked with a star.

The ^{1}H-NMR of **Ir-K0**-H_2 provides the expected signal set of two cyclometalated 2-phenylpyridine (**ppy**) units and an iridium(III) together with the peripheral bidentate ligand bibenzimidazole. Similar to analogous ruthenium(II) bibenzimidazole complexes, the aromatic signals 4’’/7’’ on the bibenzimidazole ligand (see Scheme 4) are particularly sensitive to the coordination geometry. As known from the structurally similar ruthenium bipyridyl complex $[(tbbpy)_2Ru(tmBBI\text{-}H_2)][PF_6]_2$ (**R1**), the signal of proton H-4’’ in dimethyl sulfoxide (δ = 5.74 ppm) is highly shielded due to its spatial proximity to one pyridyl

ring of 2-ppy. The opposite proton H-7'' on the outer rim of the complex is downfield shifted by 1.76 ppm to 7.5 ppm with respect to proton H-4''.

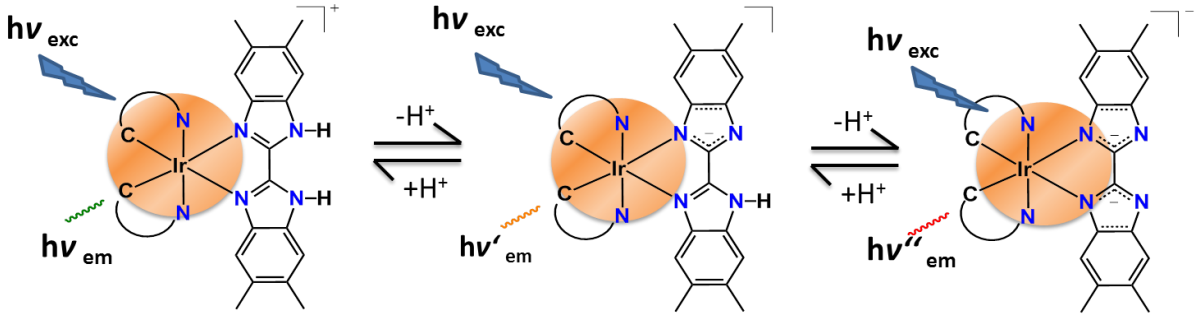

Scheme 5: Acid-base chemistry of **Ir-K0**-H_x (x = 0, 1, 2).

The twofold deprotonated complex Na-**Ir-K0** was synthesized by reaction of **Ir-K0**-H_2 with an excess of sodium hydroxide in methanol. The deprotonation is clearly visible by a significant highfield shift of the proton signals H-4'' and H-7'' in the ^{1}H-NMR spectrum (see Figure 7) in deuterated dimethyl sulfoxide. Additionally, the characteristic NH signal in the lowfield (11.5 ppm), only visible in less polar solvent like chloroform, vanishes upon deprotonation.

The photophysical features of **Ir-K0**-H_x (x = 0, 1, 2) were analyzed and obviously they differ significantly from the isostructural ruthenium(II) complexes. In $Ru(bpy)_3^{2+}$ the MLCT bands are spectrally well separated from intraligand absorptions (IL). However, no clear isolated MLCT bands can be observed in the iridium(III) complexes investigated in this work.[87,88] In line with this, the presented complex shows intense absorption bands in the UV regime which drop significantly at approximately 370 nm.

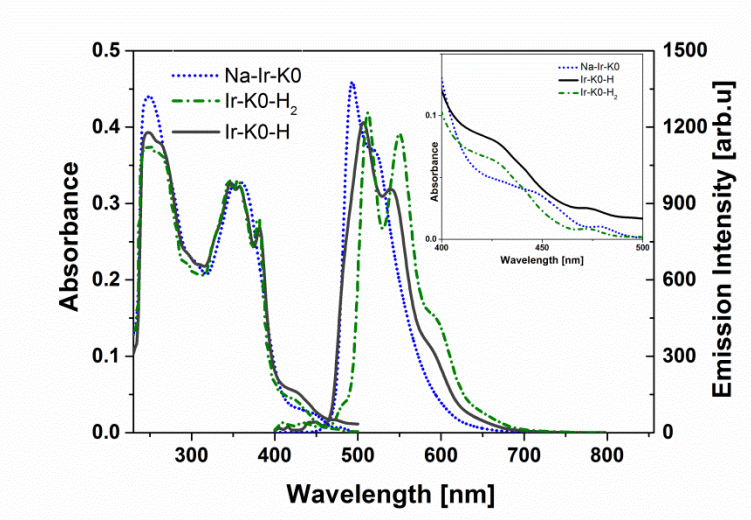

Figure 8: UV/Vis and emission spectra of **Ir-K0**-Hx in chloroform (c = 5 x 10-6 M; excitation at 378 nm); the different protonation states were observed in pure chloroform for Na-**Ir-K0** (blue, dotted), upon the addition of aqueous HCl (for Ir-K0-H, black, solid line), and upon the addition of aqueous HPF_6 (for Ir-K0-H2, green, dash-dot).

Only weak absorption between 400 nm and 500 nm and virtually a negligible absorption at λ = 450 nm is visible with respect to the similar Ru(II) bibenzimidazole complex, which exhibits its characteristic ^{1}MLCT absorption band maxima in this region. The nature of the absorption bands between 300 and 450 nm is suggested to be composed of a mixture of spin-allowed charge-transfer (^{1}CT) transitions that contain contributions from both dπ → π^*_{tmBBI} metal-to-ligand (^{1}MLCT) and π_{ppy} → π^*_{tmBBI} ligand-to-ligand (^{1}LLCT) transitions. The major contribution to the absorption band at around 380 nm was assigned to a mixed dπ → π^*_{ppy} ^{1}MLCT and a ligand centered π → π* (LC) transition on the ppy ligand with respect to the photophysical transitions of $[(ppy)_2Ir(bpy)]^+$.[59]

The acid-base chemistry of **Ir-K0**-H_x (x = 0, 1, 2) has been investigated in chloroform with special care. Therefore the fully deprotonated complex Na-**Ir-K0** was prepared selectively by deprotonation of **Ir-K0**-H_2 with excess sodium hydroxide in methanol. The different protonated complexes **Ir-K0**-H and **Ir-K0**-H_2 have been prepared by adding of either hydrochloric acid or hexafluorophosphoric acid to a solution of the doubly deprotonated complex Na-**Ir-K0**. In contrast to the clear optical response of the analogous ruthenium(II) complexes, only slight and unspecific changes in the UV/vis spectrum can be followed upon deprotonation of **Ir-K0** (see Figure 8)

This is in contrast to the appropriate emission measurements, where a significant change is visible upon deprotonation with all three protonation states being strongly luminescent. The three different protonated complexes exhibit a structured emission band, which was assigned to an emissive excited state that has mixed MLCT and π-π* intraligand (IL) character as frequently observed for cyclometalated Ir complexes.[79,89–92] The doubly protonated complex **Ir-K0**-H_2 shows a structured emission band with two clear maxima at λ = 521 nm and λ = 559 nm together with a sparsely marked shoulder at around λ = 612 nm.

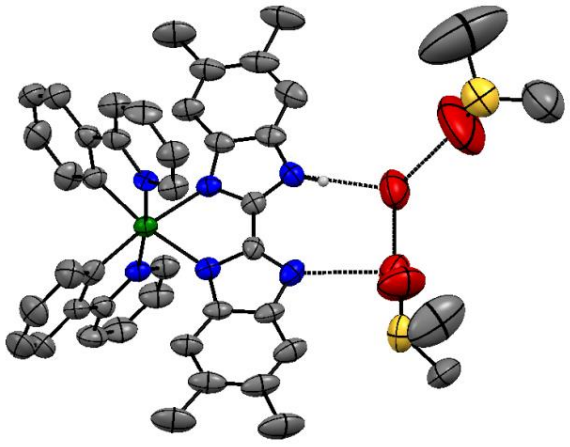

Figure 9:
Solid-state structure of the hydrogen-bond framework of $[(ppy)_2Ir(tmBBI\text{-}H)]\cdot\cdot 2[H_20]\cdot\cdot 2[C_2H_6OS]$ (ellipsoids at 50% probability level; hydrogen atoms that are not involved in the hydrogen-bond framework are omitted for clarity; R1 = 0,0625, wR^2 = 0,1565).

Upon single deprotonation the emission band maximum is blueshifted accompanied by a slight decrease of the luminescence intensity to a maximum at λ = 508 nm with a second one at λ = 548 nm and an

additional shoulder at λ = 589 nm. Finally, the fully deprotonated complex is shifted further into the blue region with only one distinct maximum at λ = 494 nm and a tapered shoulder at λ = 519 nm.

To provide further insight into the hydrogen bond properties of **Ir-K0**-H_x (x = 1, 2) single crystals were grown upon slow diffusion of water into a DMSO solution of the complex. The obtained structure revealed the singly protonated, neutral complex **Ir-K0**-H with a hydrogen bond network that consists of two water molecules and two terminating molecules of dimethyl sulfoxide (see Figure 9).

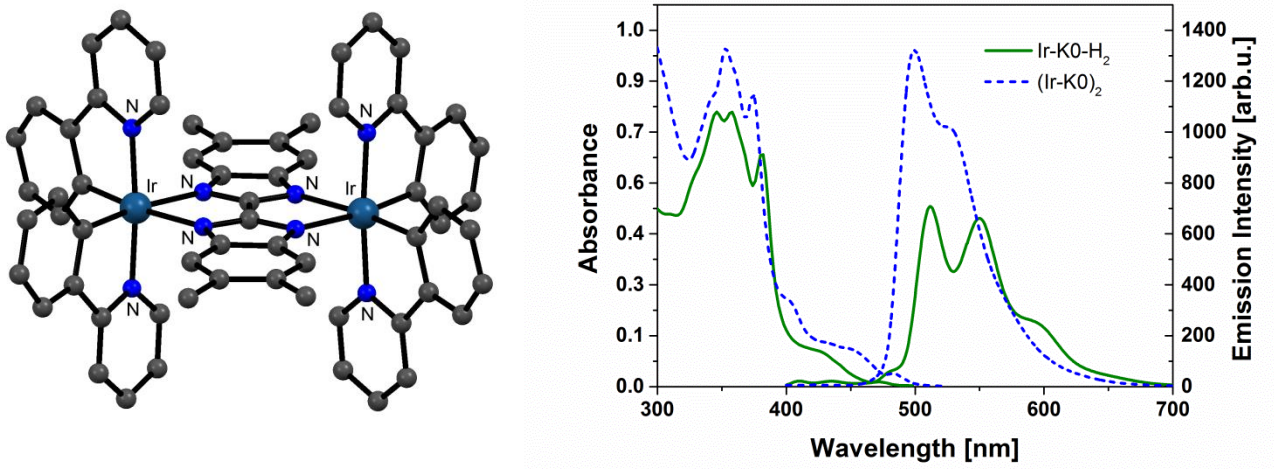

Figure 10: Solid-state structure of **Ir-BBI-Ru** (ellipsoids at 50% probability level; hydrogen atoms that are not involved in the hydrogen-bond framework are omitted for clarity**;** right:photophysical properties of **Ir-K0**-H_2 (green, solid) and **(Ir-K0)$_2$** (mixture of *rac* and *meso*, blue, dashed) in chloroform (c = 5 x 10^{-6} M).

The dinuclear complex **(Ir-K0)$_2$** was synthesised by a microwave assisted reaction of an equimolar amount of the ligand **L0** with the dimer $[(ppy)_2Ir]_2(\mu\text{-}Cl)_2$ in dimethylformamide and triethylamine as a deprotonation agens.[11] Thus, in contrast to systems based on 2,2'-bipyridine or 1,10-phenanthroline, 2,2'-bibenzimidazole represents a suitable bridging ligand as it is able to coordinate a second metal center after deprotonation. The *rac* and *meso* isomers could be separated through fractional crystallization and could selectively be distinguished by ^{1}H NMR spectroscopy. Further, a solid-state structure of the *meso* isomers could be elucidated and was compared to related ruthenium(II) and iridium(III) complexes.

As can be seen in Figure 10 the photophysical properties of **(Ir-K0)$_2$**, especially the emission spectrum, resembles that of the fully deprotonated complex Na-**Ir-K0** with a maximum at λ = 499 nm and a tapped shoulder at λ = 524 nm. Absorption intensity of **(Ir-K0)$_2$** of the MLCT transition and the emission intensity is about twice compared to the mononuclear **Ir-K0**-H_2 and is therefore in accordance with two chromophore units per molecule.

Additionally, time resolved emission studies using a streak camera were performed in order to elucidate more details about the luminescence properties of **Ir-K0**-H_2**,** Na-**Ir-K0** and the dinuclear complex (**Ir-K0)$_2$**. The lifetime of the excited states was ascertained to be approximately 50 ns in oxygen-equilibrated

chloroform solution for all three complexes and is thus comparable to the lifetimes previously observed for other cyclometalated iridium(III) or ruthenium(II) complexes (see Table 1).[68,89,93–98]

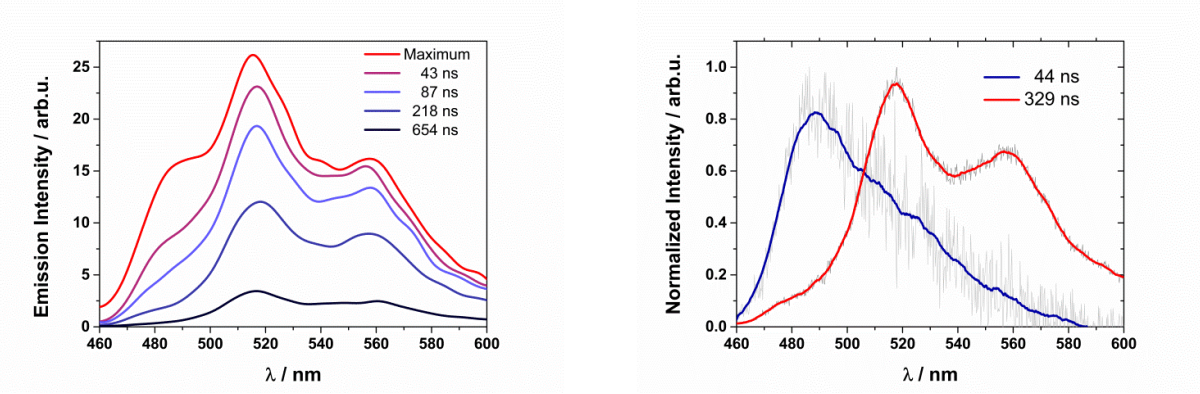

Figure 11: Transient emission features of fully protonated Ir-K0; left: full spectrum at different delay times; right: individual emission spectra corresponding to the indicated life-times.

Ir-K0-H_2 exhibits a special feature, that is the appearance of a second, longer lifetime of 329 ns corresponding to a broad emission spectrum with two maxima at λ = 518 and λ = 558 nm (see Figure 11). This intriguing detail remains subject to further investigations.

Table 1: Photochemical data of the investigated iridium complexes and two related ruthenium compounds. [76]

		λ_{max}/nm		
Complex	solvent [a]	absorption	emission	Lifetime [ns]
Ir-K0-H_2^+	$CHCl_3$	378	521/559	44 (329)
Na-Ir-K0	$CHCl_3$	377	494	57
(Ir-K0)2	$CHCl_3$	375	499	50
[(*bpy)$_2$]$_2$RuBBI	ACN	510/510	700/500	50 /60
(*bpy)$_2$Ru(BBI-H_2)	ACN	473	648	120

[a] air equilibrated

In summary, we could show the coordination of the ancillary ligand 5,5',6,6'-tetramethyl-2,2'-bibenzimidazole (**L0**) to a bis(phenylpyridine)iridium(III) complex fragment to design the octahedral chromophore complex **K0**. Although structurally related to the ruthenium(II) analogon, a diverse and very appealing photophysical behavior is observed. The present result strikingly shows the dependency of the principal photophysics of the iridium(III) bibenzimidazole complexes on the protonation state allowing for protonation state dependent colour tuning from the green to the more blue spectral region. As all three protonation states of the complex are strongly luminescent, the application range is greater compared to conventional ruthenium(II) complexes, which are limited through emission loss upon deprotonation. The complex likewise exhibits a peripheral *cis*-diamine framework that was proved to buildup H-bond supramolecular frameworks and, thus, they could potentially act as anion recognition entities in functional supramolecular photochemistry.

These results are presented comprehensively in the manuscript [SR1][86].

3.1.2 Interaction of an iridium(III)bibenzimidazole complex with different anions: implications for luminescent sensing

In the introduction the recent progress in the field of anion and cation recognition of exclusive transition metal complexes bearing the bisimidazole-type ancillary ligand was summarized. Within the review it was concluded that ruthenium(II) bibenzimidazole complexes are suitable building blocks for the recognition of basic anions and cations. Additionally, in SR1 the supramolecular binding of water with a bibenzimidazole iridium(III) chromophore in the solid-state was presented. Further, the strongly luminescent characteristics of **Ir-K0** in its three protonation states might provide an effective spectroscopic tool for the direct observation of the interactions of the complex with different anions. Therefore it seems promising to further elucidate the potential of these complexes with respect to optical anion sensing with basic anions.

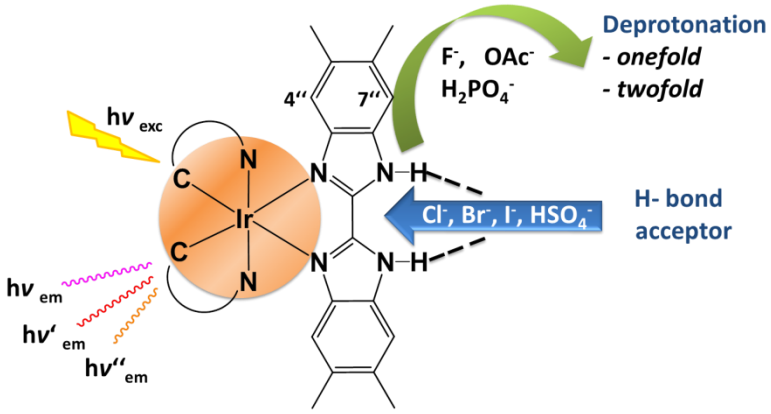

Scheme 6: Schematic representation of the interaction between **Ir-K0**-H_2 and the different investigated anions in this thesis.

In this study the interaction of **Ir-K0**-H_2 with the halides fluoride, chloride, bromide and iodide was targeted. Additionally, hydrogen sulfate, dihydrogen phosphate, and acetate were employed as they are common targets of supramolecular anion sensing through hydrogen bonds (see Scheme 6).

In the following the complex-anion interaction of **Ir-K0**-H_x (x =0,1,2) with the aforementioned anions is investigated by ^{1}H NMR and emission spectroscopic methods. Significant blueshifts of the emission maximum by about 20-25 nm are induced in chloroform when the strong basic anions fluoride, acetate and dihydrogen phosphate are added, indicating a predominant deprotonation of the complex (see Figure 12, right).

Contrary to the behavior described, the weaker basic anions Cl^-, Br^-, I^-, HSO_4^- only induce a moderate shift of the emission spectra in the range of 6–9 nm towards the blue region with a concomitant increase of the emission maximum, which indicates different characteristics of a strong interaction in form of hydrogen bonds, but excludes a deprotonation event of **Ir-K0**-H_2 (see Figure 12, left).

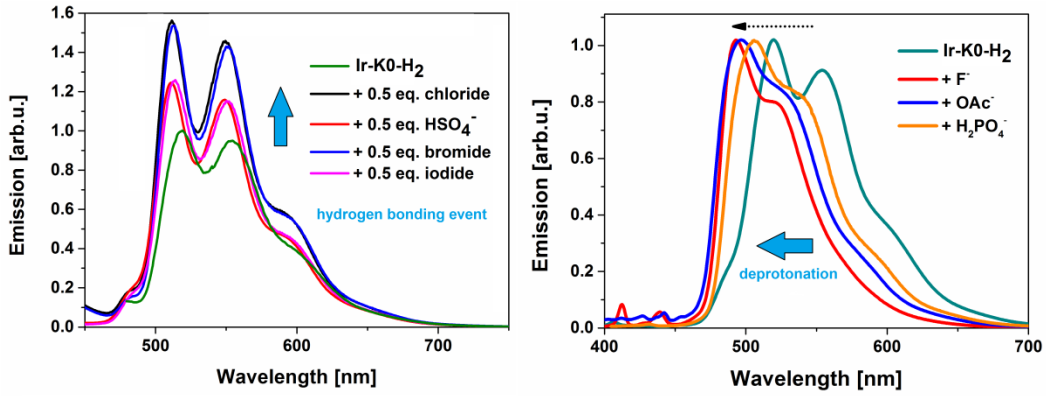

Figure 12: Emission spectra of **Ir-K0**-H_2 in $CDCl_3$- solution (5.0×10^{-6} M); left: normalized emission with respect to the luminescence of pristine **Ir-K0**-H_2 in order to show the relative increase of luminescence; right: all spectra are normalized with respect to the emission maximum; addition of 7 equiv. of various anions.

According to ^{1}H NMR and emission spectroscopy, fluoride anions were shown to cause successive deprotonation of **Ir-K0**-H_2 subsequent to initial hydrogen bonding (see Figure 13 and Figure 15). The first NH abstraction is finalised after addition of two equivalents of fluoride which is in accordance with the formation of hydrogen difluoride (HF_2^-). Despite the comparatively high pk_a value of fluoride the remarkable stability of HF_2^- in solution determines the strength of fluoride as a base. Consequently, the second NH abstraction was observed after addition of another 2 equivalents of the halide. Upon deprotonation, the color of the solution changes from luminous yellow to a bright green, as can be seen with the naked eye (see Figure 14). The characteristic progress of the stepwise deprotonation in the emission spectrum is depicted in Figure 13.

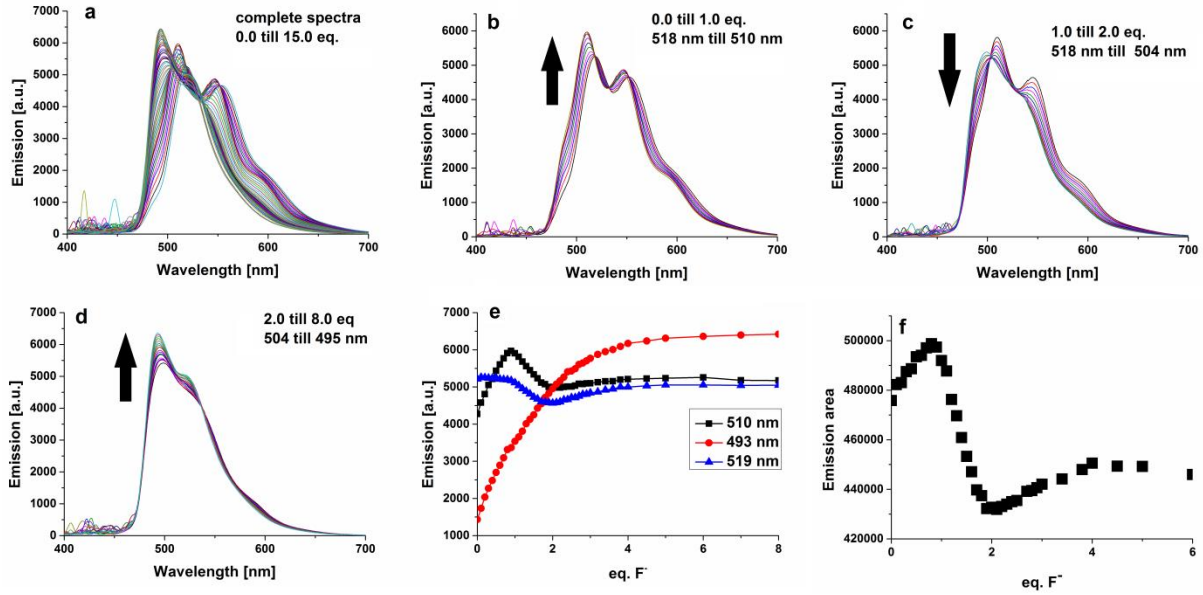

Figure 13: Emission titration of **Ir-K0**-H_2 (5×10^{-6} mol dm^{-3}) in chloroform upon the addition of F^-: (a) 0-15 eq., (b) 0-1 eq., (c) 1-2 eq., (d) 2-8 eq., (e) Emission intensity at 519, 510 and 493 nm vs. eq. of F^-, (f) Emission area vs. eq. of F^-. The arrows depict the shift of the emission spectra upon successive deprotonation.

In the titration experiment the stepwise change of the emission spectra upon NH abstraction indicates that the interaction may involve a four-step process for whom the following equations are suggested.

$[Ir-K0-H_2]^+ + F^- \rightleftarrows [Ir-K0-H_2 \cdots F]$	hydrogen bonding	(1)
$[Ir-K0-H_2 \cdots F] + F^- \rightleftarrows [Ir-K0-H] + [HF_2]^-$	first N-H abstraction	(2)
$[Ir-K0-H] + F^- \rightleftarrows [Ir-K0-H \cdots F]^-$	hydrogen bonding	(3)
$[Ir-K0-H \cdots F]^- + F^- \rightleftarrows [Ir-K0]^+ + [HF_2]^-$	second N-H abstraction	(4)

By titration of increasing equivalents of F^- to a solution of **Ir-K0**-H_2 in [D_6]DMSO the final species that is formed could be verified to be the twofold deprotonated Na-**Ir-K0.** This was assigned by the characteristic highfield shift of H-4'' and H-7'' that also occurs upon deprotonation with basic sodium hydroxide.

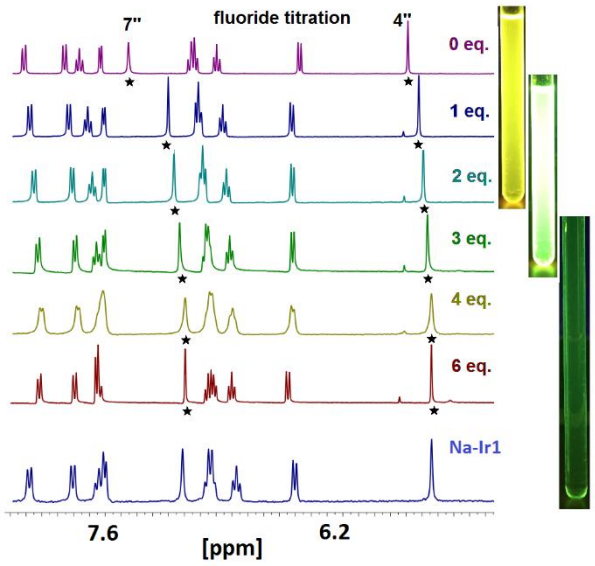

Figure 14: ^{1}H NMR titration of a 2.34 mM solution of **Ir-K0** in [D_6]DMSO with fluoride. Bottom: twofold deprotonated Na-**Ir-K0**.

Likewise for acetate and dihydrogenphosphate the first deprotonation step upon addition of two equivalents of either anion was observed and the appropriate model of dimeric hydrogen dianion (HX_2^-, X = OAc^- or $H_2PO_4^-$) complexes can be applied. For the second NH abstraction, however, more equivalents of acetate (7 eq.) are required and dihydrogenphosphate was shown to only monodeprotonate the complex. This can be suggested as the result of the lesser basicity of these ions and the most likely higher pk_{a_2} value of the second deprotonation step of **Ir-K0**.

Interaction with the weakly basic anions chloride, bromide, iodide and hydrogen sulfate was additionally screened by means of ^{1}NMR and emission spectroscopy. In contrast to [D_6]DMSO the N-H proton of **Ir-K0** can be observed at 12.1 ppm in deuterated chloroform. To examine the nature of interaction between the weaker basic anions and the receptor **Ir-K0**-H_2, a standard ^{1}H NMR titration experiment in chloroform using a start host concentration (2.34 mM) and an increasing amount of the respective TBA salt of the anion (1‑1.5 equiv.) was performed (see Figure 16). The spectral changes obtained, that is a successive shift of the N-H signal into the lowfield, indicates the formation of initial hydrogen bonds between the $BBI_{N\text{-}H}$ groups and the respective anions, however to a different extend.[10,99,100] Upon addition of either one equivalent of the aforementioned anions a characteristic low field shift is obtained, that is a maximum shift for chloride to 14.42 ppm followed by bromide, hydrogen sulfate, and iodide which is shifted to 13.6

ppm (see Figure 15). The most striking shift to δ_{N-H} = 14.42 ppm was observed with chloride. With respect to the almost linear shift of the N-H proton signals until saturation, the binding of the respective anions

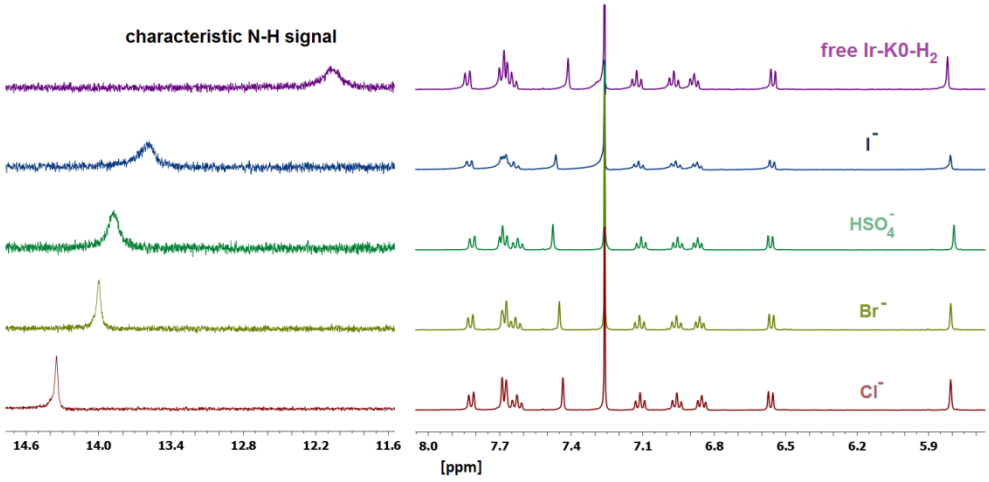

Figure 15: ^{1}H NMR spectra of **Ir-K0**-H_2 in deuterated $CDCl_3$ in the absence and presence of 1 equivalent of anions.

might rather be described as a stoichiometric ion pair formation than a sole hydrogen bonding event (see Figure 16). Nonetheless, the order of binding strength with the investigated ions is suggested to be Cl^- > Br^- > HSO_4^- > I^-. In Figure 16 (left) the typical process of the shift of the N-H signal is depicted for all investigated anions and for chloride in detail in Figure 16 right.

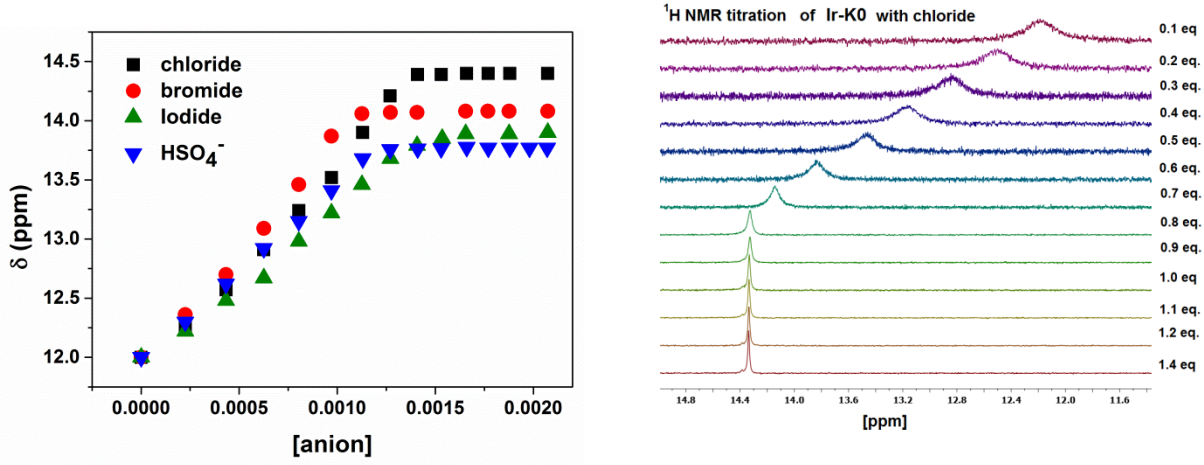

Figure 16: Left: Chemical shift changes of the N-H signal of **Ir-K0**-H_2 in $CDCl_3$ upon addition of different anions; right: Chemical shift changes of the N-H signal of **Ir-K0**-H_2 in $CDCl_3$ upon addition of different anions.

Emission spectroscopic titrations of **Ir-K0**-H_2 with chloride with the aforementioned anions showed enhancement of the overall emission intensity with a concomitant 8 nm hypsochromic shift of the emission maxima (see Figure 17). In accordance with the ^{1}H-NMR measurements the strongest enhancement of 67% was observed for chloride, followed by bromide (51%), hydrogen sulfate (24%), and

iodide (19%). Hence the remarkable luminescence properties of **Ir-K0** were shown to be a potential measure for anion detection through hydrogen bonds. Figure 17 depicts the plot of the emission spectral responses of **Ir-K0**-H_2 (integrated area) upon addition of Cl^-, Br^-, I^- and HSO_4^- anions (left) and exemplarily the progression of the titration with chloride anions (right).

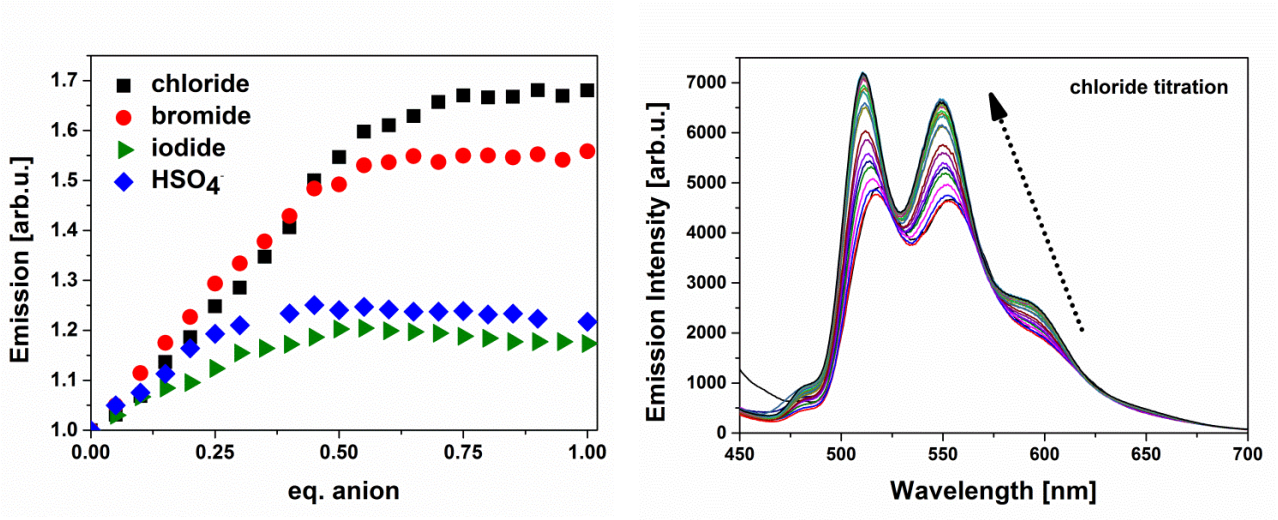

Figure 17: Left: Normalized emission spectral responses (integrated area) of **Ir-K0**-H_2 (5×10^{-6} M in chloroform, 298 K, λ_{ex} = 378 nm) upon addition of Cl^-, Br^-, I^- and HSO_4^- anions; right: emission spectral responses of **Ir-K0**-H_2 (5 x 10^{-6} M in chloroform, 298 K, λ_{ex} = 378 nm) upon addition of Cl^- anions.

The maximum signal shift in Figure 17 occurred up to 0.5 equivalents of the anion with subsequent saturation at 1 equivalent which suggests a stable 2:1 (complex : anion) binding mode. Standard Job's Plot analysis[101] was performed via ^{1}H NMR and emission titration, which confirmed the assumption of a 2:1 binding mode. Herein an important difference with respect to the ruthenium complexes is displayed which exhibit a stable 1:1 (complex : anion) stoichiometry. This deviating behavior may be referred to the reduced charge of the iridium(III) complexes.

To conclude, regarding the assumption of a stable 2:1 binding mode, determination of binding constants was attempted by using the WinEQNMR2[102] software. Thereby, high association constants were observed which to the best of my knowledge exceed all values obtained for analogous biimidazole ruthenium(II) complexes known thus far. However, as described *vice supra* the binding of the respective anions should rather be described as a stoichiometric ion pair formation than a sole hydrogen bonding event.

In conclusion, detailed anion binding studies with **Ir-K0** have shown its potential for the supramolecular recognition of small anions. The strongly basic ions fluoride, acetate, and dihydrogen phosphate cause stepwise deprotonation which can be analyzed through ^{1}H-NMR and emission spectroscopy. The rather weakly basic ions chloride, bromide, iodide and hydrogen sulfate were shown to bind to **Ir-K0** through strong hydrogen bonds with the diamine site. A characteristic proton shift of the respective N-H signal

into the highfield in the ^{1}H-NMR spectrum was visible, coincidentally a deprotonation process could be excluded. Accordingly, the hydrogen bonding event was also visible in the emission titration experiments, where emission of the respective ion pairs was slightly blue shifted and enhanced by up to 67%. Interestingly, the ion binding mechanism involves fast formation of a 2:1 species which distinguishes the iridium sensor from the known ruthenium(II) based systems where a 1:1 stoichiometry dominates. Accordingly, anion binding studies turned out to be a suitable handle for the detailed characterization of the basic H-bond driven supramolecular binding properties of the iridium(III) bibenzimidazole complex.

These results are presented comprehensively in the manuscript [SR2][103].

3.1.3 Supramolecular H-bond driven light switch

In chapter 3.1.2 it was shown that **Ir-K0** provides promising features for being applied as optical sensor for small ions, that is emission enhancement and recognition *via* changes in the ^{1}H-NMR spectrum through hydrogen bonding events. Systematic studies on this system revealed that **Ir-K0** is a convenient hydrogen bond donor for various anions under aerobic conditions like fluoride, chloride, bromide or iodide. Strong bonding interactions between the weakly basic anions and the complex, and a virtually stoichiometric reaction to their respective ion pair was ordinarily observed. However, recognition of the H-bonded ion pair is possible merely through a luminescence increase from an already strongly fluorescent pristine chromophore, that is its PF_6 salt.[103]

Refinement of **Ir-K0** as optical sensor was intended in this study since although the respective emission enhancement provides promising characteristics, however the latter is rather weak and unselective.

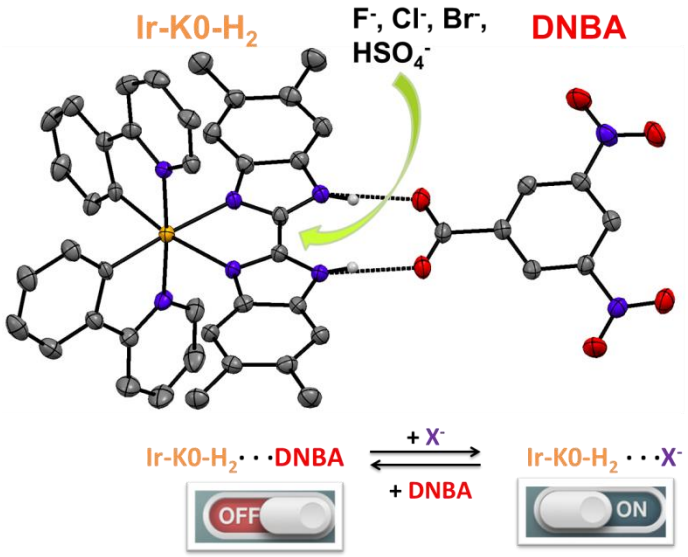

Scheme 7: Scheme of the luminescent On/Off sensor for anions.

Nocera et al. previously reported that the excited state of a phosphorescent ruthenium(II) bipyridine complex, functionalized with an amidinium group, could be efficiently quenched by the electron deficient hydrogen bond acceptor *para*-dinitrobenzoic acid (DNBA).[80] More detailed studies on the quenching of a biimidazole iridium(III) complex with DNBA have been reported by Wenger et al.[81] who claimed that upon excitation of the complex in presence of 3,5-dinitrobenzoate a proton coupled electron transfer is triggered (see Figure 18).

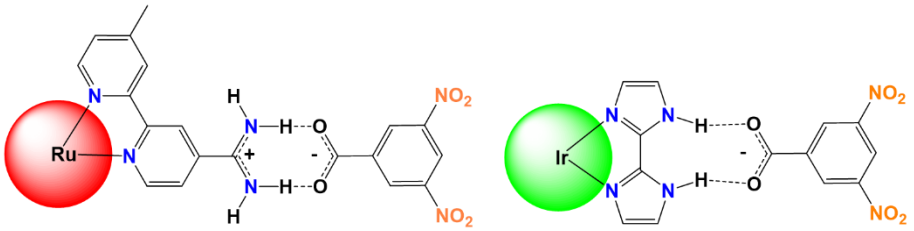

Figure 18: Depiction of literature known reference complexes of Nocera[80] (left) and Wenger et al.[81] (right).

Therefore, the idea was to develop an "off-switch strategy" to enhance the sensitivity of the iridium (III) bibenzimidazole system, employing the proton coupled electron transfer (PCET) quenching mechanism described (*vide supra*). Analogous to the reported systems of Nocera and Wenger et al. a weak luminescence of a hydrogen bonded ion pair between **Ir-K0** and DNBA was expected due to hydrogen bonding mediated quenching by the respective anions. In the presence of weakly basic anions, competitive binding could displace the quencher and restore the luminescence of the ion pair or in other words switch it back on (see Scheme 7).

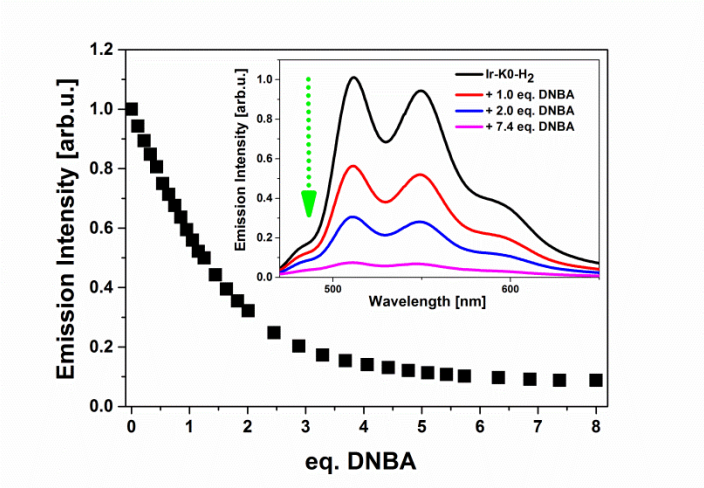

Figure 19: Main: plot of the normalized iridium luminescence intensity as a function of number of equivalents of DNBA added; Inset: luminescence of **Ir-K0**-H_2 as a function of increasing amounts of DNBA

As can be seen in Figure 19, 3,5-dinitrobenzoate quenches the excited state of **Ir-K0** efficiently, that is approximately 50% in a 1:1 mixture in chloroform and after 7 eq. saturation of the quenching kinetics is observed with a residual luminescence of about 8% with respect to the pristine PF_6 complex. This

quenched state of the hydrogen bonded **Ir-K0-H_2**···DNBA (active sensor system, **S**) adduct has been defined within this work as "off" state. Control experiments with the reference complex $[(ppy)_2Ir(bpy)](PF_6)$ **[R2]** were carried out in order to rule out simple outer sphere electron transfer quenching. The hydrogen bond model for **Ir-K0-H_2**···DNBA was approved, as only weak oxidative quenching of **R2** by DNBA down to approximately 53 % upon addition of 7 eq. was observed; the respective kinetics indicating an ordinary bimolecular quenching mechanism due to the lack of H-bonds.
The expected H-bond ion pairing of **Ir-K0**-H_2^+···$DNBA^-$ was further observed in the crystal structure of the donor–acceptor couple where complementary binding of either N-H function towards one oxygen atom of the carboxylic acid group of the DNBA anion exists. Additionally, ^{1}H-NMR titration experiments give further evidence of the complex-DNBA interaction by means of hydrogen bonding events as a shift of the N-H signals directly involved in the salt bridge as well as significant shifts in the aromatic region can be clearly observed in deuterated chloroform.

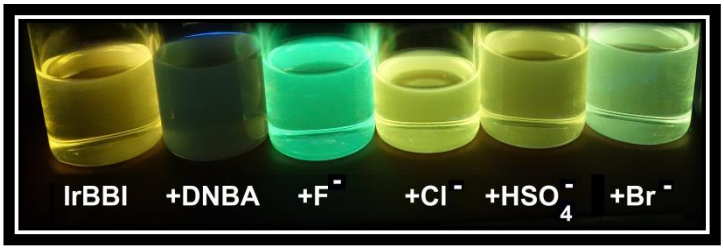

Figure 20: Picture of the different solutions of **Ir-K0** in chloroform and excess anions.

Titration experiments of the **Ir-K0**-H_2^+···$DNBA^-$ (active sensor, **S**) system were carried out with five different anions which were suggested to be able to replace DNBA as H-bond acceptor from the **Ir-K0**-H_2^+···DNBA ion pair and therefore switch the luminescence of the chromophore back "on", that is fluoride, chloride, bromide, iodide and hydrogen sulfate. As presumed, the addition of up to 120 equivalents of the latter anions caused a significant increase in the luminescence intensity of **S**. An increase of up to 750 % for fluoride, 450 % for chloride, 405 % for hydrogen sulfate, 220 % for bromide and the weakest effect of about 118 % for iodide (see Figure 21) was obtained.

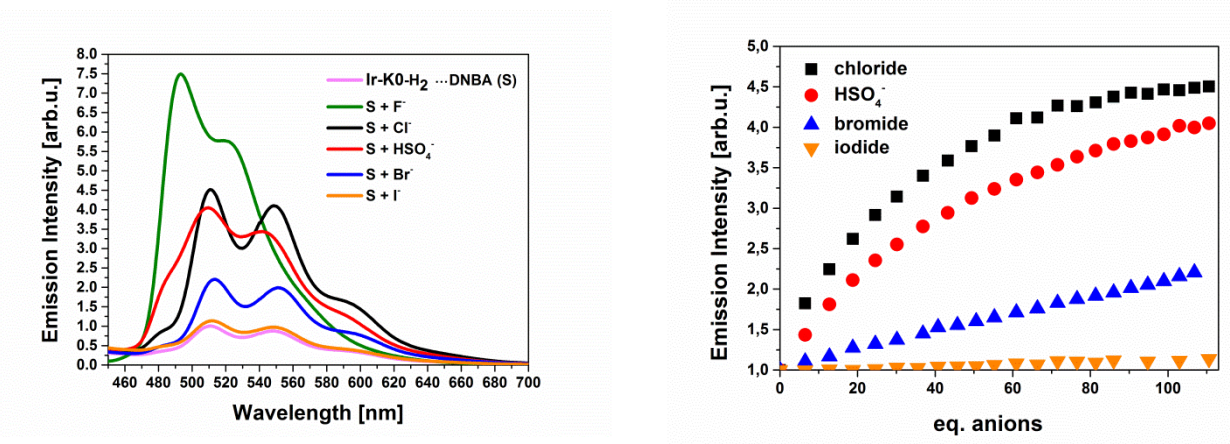

Figure 21: Left: plot of the normalized luminescence intensity of **Ir-K0**-H_2···DNBA (**S**) as a function of the number of equivalents anions added; right: luminescence intensity of **Ir-K0**-H_2···DNBA with 110 eq. of each anion.

The outstanding increase of the emission intensity by treatment with fluoride, including a hypsochromic shift accompanied by a change of the vibronic structure, was shown to correspond to a deprotonation process of the iridium(III) complex with respect to previous reports (Figure 22).[86,103]

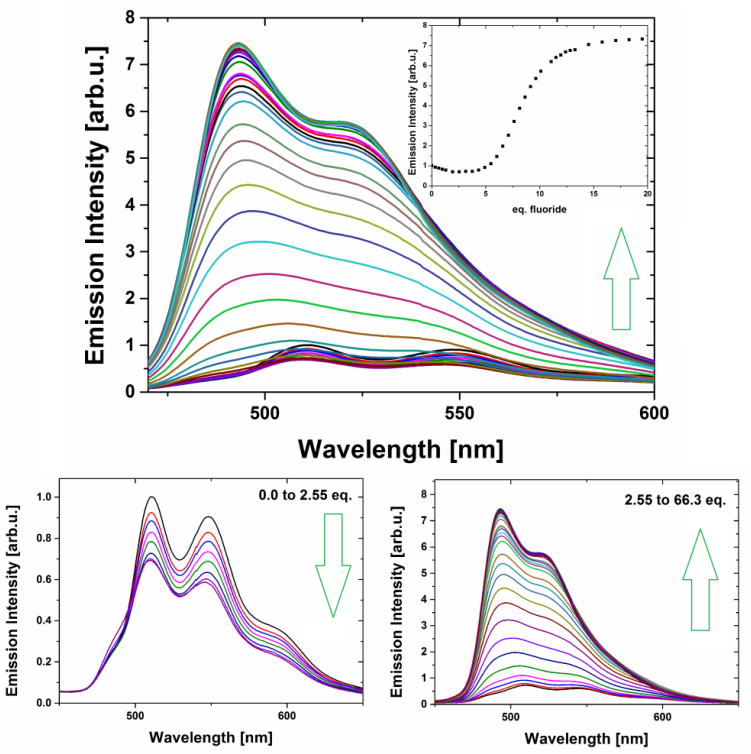

Figure 22: Luminescence of **Ir-K0**-H_2···DNBA (S) as a function of increasing amounts of fluoride (depicted is only one of at least two distinct measurements); inset: plot of the normalized **Ir-K0**-H_2···DNBA luminescence intensity as a function of the number of equivalents of anions added.

Three major effects have to be taken into account for the interaction with fluoride, that is (a) the displacement of the quencher due to deprotonation of the acidic secondary amine functions of the cationic

iridium complex and subsequent breakup of the hydrogen bond framework, (b) the stronger emission of **Ir-K0** in its fully deprotonated state in contrast to the pristine PF_6 complex, and (c) electrostatic repulsion between the negatively charged double deprotonated iridium complex and the anionic quencher 3,5-dinitrobenzoate inhibits collision induced quenching .

Anion	Fluoride	Chloride	Hydrogen sulfate	Bromide
K_a (M^{-1})	n. d.*	33195 (1232)	17804 (283)	1572 (328)

*n.d. = not determined

Table 2: Associations constants (K_a) of **Ir-K0**-H_2···X interaction.

The weakly basic anions instead were shown to cause displacement of DNBA while concomitant establishing competing H-bonds which results in an "on-switching" of the emission of **Ir-K0**. Exemplarily, the general course of the displacement process with chloride ions is depicted in Figure 23 (left). Based on this type of titration, association constants (K_a) between **Ir-K0**-H_2^+···$DNBA^-$ and the investigated anions were determined for a 1 : 1 complex model (see Table 2) using Fit Function **FF1**.

$$\Delta F = \frac{\Delta\varepsilon([H]+[G]+K^{-1}) \pm \sqrt{\Delta\varepsilon^2([H]+[G]+K^{-1})^2 - 4\Delta\varepsilon^2[H][G]}}{2}$$

Fit function FF1[104]

As can be seen in Figure 21 (right part), a remarkable discrimination between chloride and bromide is possible and the general capability to replace DNBA nicely corresponds with the basicity of the anions in a group of the PSE. For the HSO_4^- ion, additional stabilization by the formation of a Y-shaped H-bond framework as reported recently were taken into account.[8–10,77]

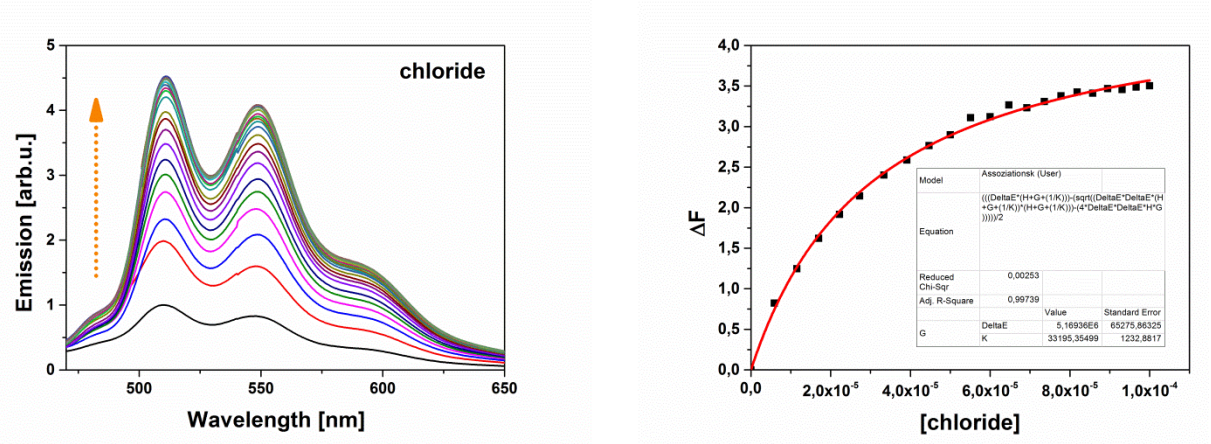

Figure 23: Left: Luminescence of **Ir-K0**-H_2···DNBA as a function of increasing amounts of chloride (depicted is only one of at least two distinct measurements); right: plot of the normalized luminescence intensity of **Ir-K0**-H_2···DNBA as a function of increasing amounts of chloride (depicted is the average of two distinct measurements) and fit according to fit function FF1.

To check for selectivity between the different anions, a titration experiment with a mixture of different anions (Cl^-, Br^-, I^-, HSO_4^-; reading an identical ionic strength as for the individual anions) was carried out. To rule out deprotonation events fluoride anions were excluded. The anion mixture also causes a significant change in the luminescence intensity of the quenched **Ir-K0**-$H_2^+\cdots DNBA^-$ system with saturation behavior at about 214 % of the initial luminescence intensity. Selectivity, however, was not observed as the diverse binding behavior is predominately dependent on the different basicity of the investigated anions.

In conclusion, it was shown that competitive molecular recognition of fluoride, chloride, bromide, iodide and hydrogen sulfate *versus* the electron-accepting 3,5-dinitrobenzoate ion displays a powerful tool to increase the ion sensing quality of **Ir-K0** in terms of luminescence sensitivity. Due to oxidative quenching, the DNBA anion acts as an "off-switch" of the otherwise strongly luminescent iridium complex, providing a significant sensitivity enhancement of **Ir-K0** towards selected anions.

Consequently, the presented supramolecular sensor system exceeds to the best of my knowledge all ruthenium(II) biimidazole-type sensors known in literature so far, regarding a significant increase in luminescence intensity of e.g. 450 % for chloride and as the change in luminescence intensity is pursuable with the naked eye.

These results are presented comprehensively in the manuscript [SR3][105].

3.2 Improvement of an anion sensing strategy for ruthenium(II) complexes through sterically confined 2,2'-bibenzimidazole-type ligands

In the introduction it was revealed that bibenzimidazole ligands provide an elegant direct connection between a *cis*-diimine function for coordination to ruthenium(II), iridium(III) or osmium(II) with an acidic *cis*-diamine function. The latter can act as twofold H-bond donor that is generally suitable to bind one- and two-dentate acceptors.[7,106–108] Additionally, several synthetic modifications have been presented in literature, where the electronic and steric properties of this type of ligand were manipulated.[8,74,84,109,110] Access to -Br, -I, $-NO_2$, $-NH_2$, and imine derivatives of the latter have been reported by Walther *et al.*.[9,109] Additionally, Ye *et al.* presented the nitro derivative as well as the methyl-disubstituted analogue for usage as colorimetric halide sensors.[9] In order to gain selectivity, spatial confinement of the H-bond framework through introduction of substituents in the 4,4'-positions was aspired and the effect of steric confinement was subject of further investigations. [111]

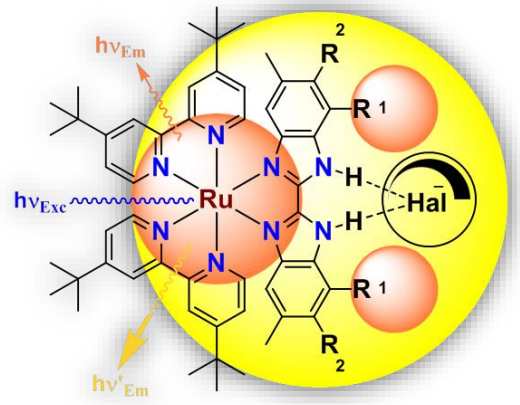

Scheme 8: Schematic depiction of the general concept of functionally dimmed pincer-shaped ruthenium(II) chromophors presented in this work. Upon exchange of the substituents R^1 and R^2 luminescence *hν* of the complexes is dimmed. H-bond binding of halides leads to a significant increase and slightly bathochromic shift of luminescence *hν'*.[111]

Recently, we reported the synthesis of **K1** (see Scheme 9) along with an intensively photophysical and structural characterization of new pincer-shaped ruthenium(II) dyes with versatile supramolecular functions.[84] Thereby the procedure presented by Siegel *et al.* for the synthesis of a wide variety of 4,4'-disubstituted 2,2'-bibenzimidazoles *via* a Negishi coupling route was used.[74,110] In this chapter a direct spatial influence on the H-bond pocket was envisaged through the ability to introduce aromatic substitutents. According to this, another structurally confined complex **K2** was added to the library of 4,4'-disubstituted bibenzimidazol complexes along with the literature known unsubstituted **K0** as a reference (see Scheme 9).

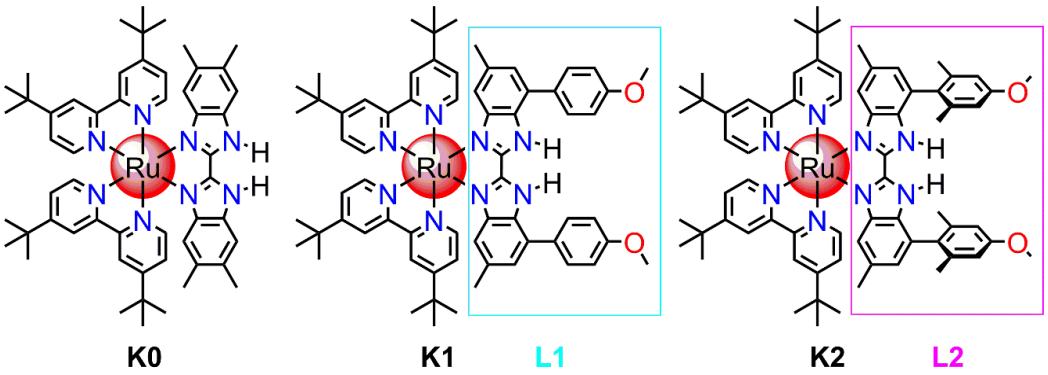

Scheme 9: Ruthenium(II) bibenzimidazole complexes presented in this work; complexes **K1** and **K2** are sterically confined due to anisyl substituents in the 4,4'-positions.

Reference **K0** and **K1** were synthesised according to literature.[84,109] **K2** was synthesized analogue to the synthesis route of previously published **K1** upon acid catalyzed reaction between the boc-protected ligand **L2** and the standard metal precursor $(tbbpy)_2Ru(Cl)_2$.[84,111] As depicted in Scheme 9, the ligands **L1** and **L2** have the same principle structure of the 4,4-di-*para*-anisyl-2,2'-bibenzimidazole, however ligand **L2** is equipped with two additional methyl substituents in ortho position at each anisyl-ring.

The anisyl substituents in **K1** and **K2** provide a constricted pincer-like geometry, whereas in **K0** the hydrogen bond area is virtually open to solvent molecules. ^{1}H-NMR spectroscopic investigations revealed that in **K1** the anisyl substitutents are free to rotate around the $C_{(benzimidazol)}$-$C_{(anisyl)}$ axis at room temperature, whereas for **K2** the characteristic signals give evidence of a rigid C_2 symmetry, where rotation of the dimethylanisyl moiety is sterically hindered. This assignment was made to the differences primarily in the aromatic region of the spectrum, that is two singlets for the eight anisyl protons and a broad singlet of the methoxy group for **K1**. On the other hand for **K2** a sharp peak occurs for the methoxy

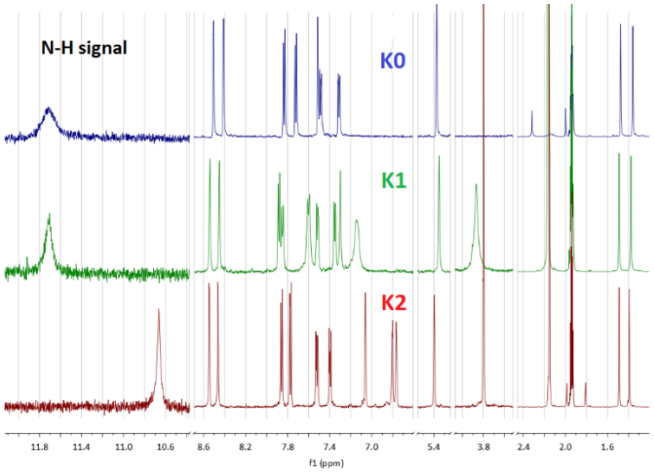

Figure 24: ^{1}H-NMR spectra of **K0** (blue), **K1** (green), and **K2** (red) (10^{-3} M, MeCN-d_3); the three areas (12.5-10 ppm, 8.75-3.5 ppm, 2.5-0.0 ppm) are zoomed differently with respect to the intensity of relevant (non-solvent) signals.[111]

function as well as two aliphatic singlets for the symmetrically inequivalent methyl groups along with two singlets in the aromatic region of the spectrum corresponding to the four remaining anisyl protons.

Further, the characteristic N-H proton signal observed in the lowfield of the recorded ^{1}H-NMR spectrum is significantly upfield shifted compared to **K0** which indicates a slight effect of the π-system of the anisyl substituents at the 4,4-position of the bibenzimidazole.

These results and the thereof deduced structure property correlation lead to the assumption that **K2** should provide a more defined pincer geometry than **K1** (and a fortiori to **K0**), which is more flexible to adapt to small hydrogen bond acceptors.

To get further insight into the supramolecular hydrogen bond network and the structural features of **K1** and **K2**, single crystal X-ray diffraction analysis was performed with four different single crystals grown under varied conditions (exemplarily two of the structures are depicted in Figure 25). The sole appearance of single acceptor binding with the secondary sphere donor entity in all four structures confirmed a distinct confining effect induced by the 4,4'-diaryl substitution pattern. Additionally, the free rotatability of the anisyl rings in **K1** and the lack of rotational freedom of the latter in **K2** have been endorsed. The sole observation of a supramolecular hydrogen bond network with monodentate H-bond acceptors is peculiar, as previously reported structures of ruthenium(II) bibenzimidazole complexes mostly exhibit expanded H-bond frameworks with bidentate or multiple acceptors.[7,76,109,111,112]

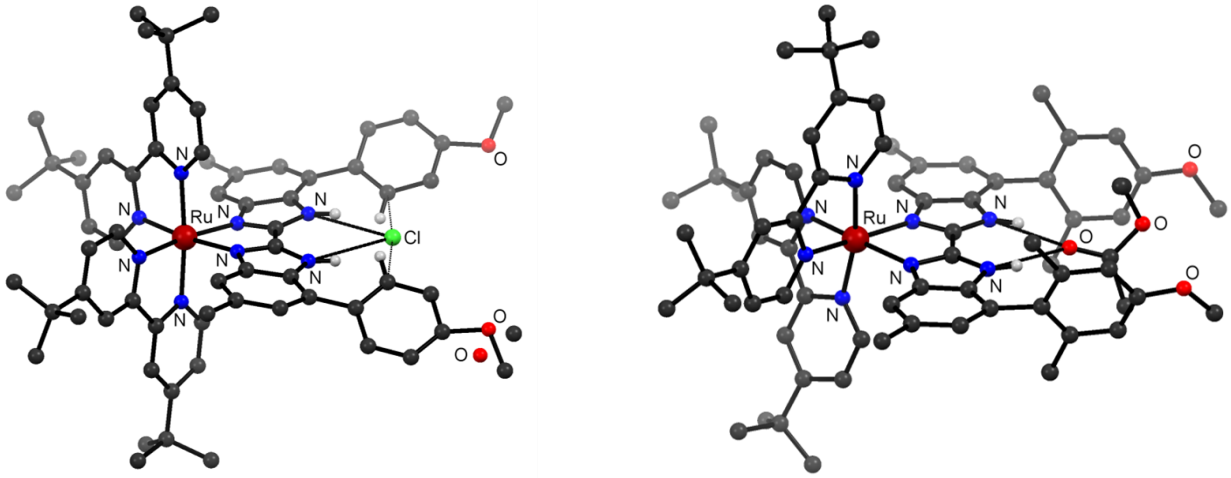

Figure 25: Left: solid-state structure of **K1-Cl**; right: solid-state structure of **K2-EtOAc** (ball-and-stick depiction, hydrogen atoms, counter ions and solvent molecules omitted for clarity, except for the H-bond frameworks).[111]

Photophysical characterization of **K0**, **K1** and **K2** was performed in de-gassed acetonitrile (MeCN) and is depicted in Figure 26. The UV/Vis absorption spectra show in principle the same general features, however, a ligand-centered absorption band at around 350 nm shows two distinct maxima for **K0** and **K2**, whereas the peak in **K1** is only recognized as a shoulder. Along with the observations of the ^{1}H-NMR investigations this was referred to the free rotation of the anisyl substituents in acetonitrile solution at room temperature. Regarding emission spectra it was shown that the emission intensities of **K1** and **K2** are significantly lower as compared to **K0.** The order I(**K0**) > I(**K2**) > **I**(**K1**) was suggested to correspond to the introduction of the substituents and, subsequently the ability to interact with the bibenzimidazol in

terms of π-overlap.[111] Interestingly, the emission maximum of **K2** is slightly shifted bathochromically, while the emission energy of **K0** and **K1** is virtually identical.

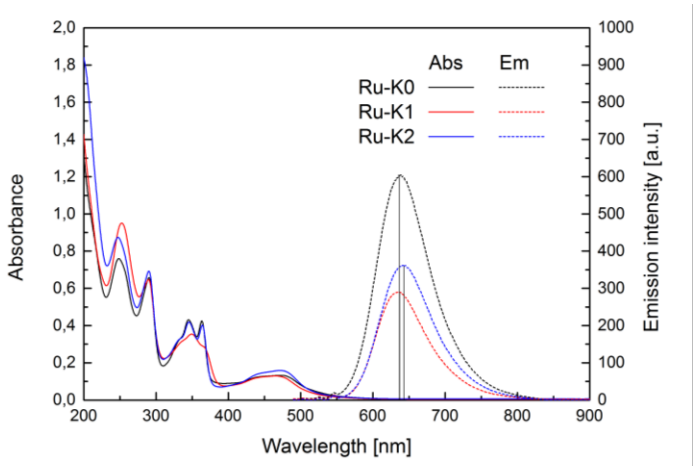

Figure 26: UV/Vis and emission spectra of **K0**, **K1**, and **K2** (10^{-5} M, MeCN).[111]

The supramolecular complex-anion interactions of **K0**, **K1**, and **K2** were investigated intensively *via* different analysis methods, that is ^{1}H-NMR-**,** absorption- and emission titration. In a typical standard titration experiment up to 4 equivalents of fluoride, chloride, bromide, and iodide were added by means of a Hamilton syringe to a 10^{-5} M solution of the complexes in dry acetonitrile with exclusion of oxygen atmosphere. Fluoride and the reference salt TBAOH were shown to immediately deprotonate all three complexes, a process which is even visible by the naked eye, i.e. a transition from bright red to brown to deep violet. Upon recording UV/Vis and emission spectra the deprotonation process was further proved by

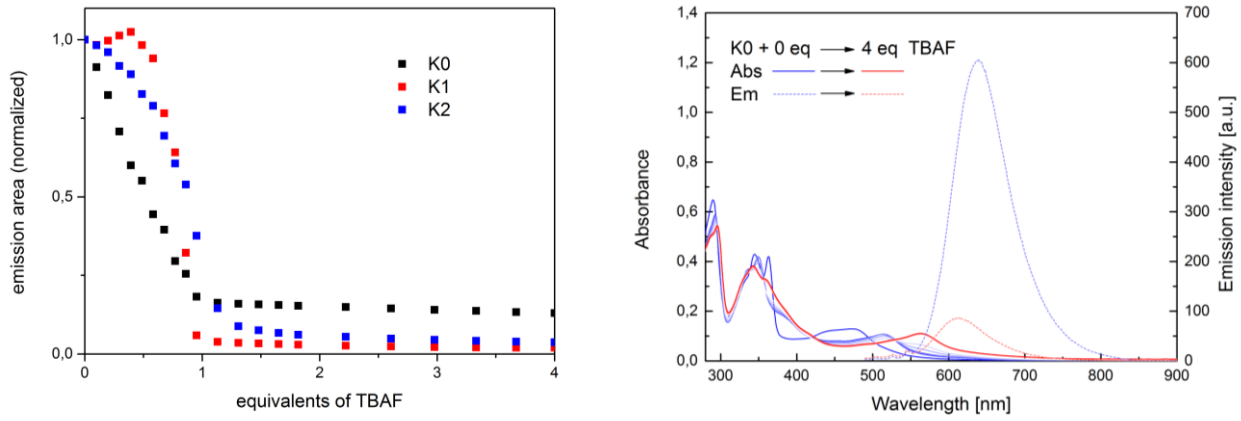

Figure 27: Left: emission quenching of **K0**, **K1**, and **K2** (10^{-5} M, MeCN) upon addition of TBAF, emission area normalized to the respective initial values; right: exemplary UV/Vis (solid line) and emission spectra (dashed line) of **K0** upon addition of TBAF.[111]

the appropriate bathochromic absorption shift accompanied by a quenching of the emission (see Figure 27, right). A slight difference can be seen in the emission spectra, where after the first deprotonation step the emission of **K0** and **K2** is shifted hypsochromically, whereas **K1** exhibits a red shifted emission as

reported previously.[84] Interestingly, the emission behavior suggests a slightly different mechanism for the deprotonation for the different complexes. Thereby, only for **K1** a slight increase within the first 0.5 equivalents of fluoride was observed, indicating strong hydrogen bonding events. Further, after addition of 4 equivalents of fluoride the emission nearly vanishes for **K1** and **K2**, whereas a residual luminescence of about 20 % for **K0** with respect to the pristine luminescence of its PF_6 salt is present.

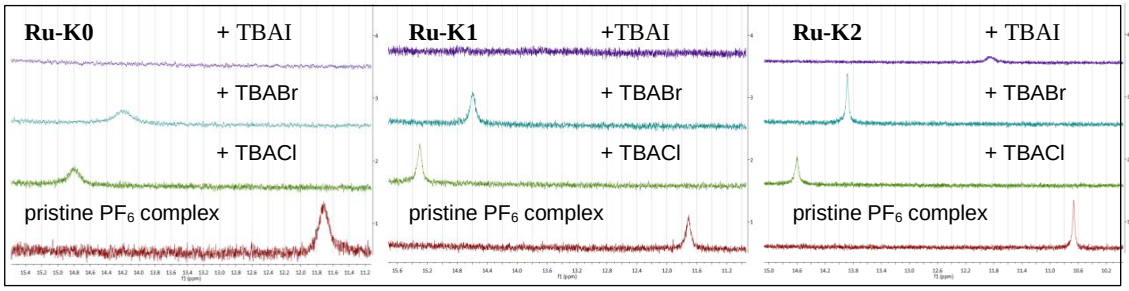

Figure 28: N-H proton signals in the ^{1}H-NMR spectra of **Ru-K0**, **Ru-K1**, and **Ru-K2** upon addition of either one equivalent of tetrabutylammonium chloride, bromide, or iodide in acetonitrile-d_3 solution.

In a second step the anion recognition features of the respective complex have been investigated towards the weaker basic halides chloride, bromide and iodide *via* ^{1}H-NMR measurements. Similar to the investigated iridium(III) complex in chapter 3.1.2, a significant shift of the characteristic N-H signal into the lowfield is obtained upon addition of the respective anion, the characteristic of the shift being in the order of increasing basicity of the ion. For iodide a weak signal only with **K2** was obtained, whereas no signal occurs in the respective spectra of **K0** and **K1**. This may be due to additional stabilization effects through the anisyl-substitution in **K2**.

Table 3: Chemical shift values for **Ru-K0**, **Ru-K1**, and **Ru-K0**.

NMR shifts [ppm] 10^{-3} M MeCN-d_3	pristine PF_6 salt	+ 1 eq TBACl (signal shift Δδ)	+ 1 eq TBABr (signal shift Δδ)	+ 1 eq TBAI (signal shift Δδ)
Ru-K0	11.72	14.79 (3.07)	14.18 (2,46)	---
Ru-K1	11.71	15.30 (3.59)	14.60 (2.89)	---
Ru-K2	10.66	14.60 (3.94)	13.89 (3.23)	11.87 (1.21)

Only a weak response by **K1** and **K2** towards chloride and bromide was obtained by UV-Vis absorption spectroscopy, expressed by a virtually negligible broadening and a slight decrease of the MLCT absorption band around 350 nm. For **K0** no anion response was detectable in the spectra, just as no interaction at all was observed for the respective complex with iodide. This came not as a surprise, as Ye et al. obtained similar results with a ruthenium(II) bibenzimidazole complex.[7]

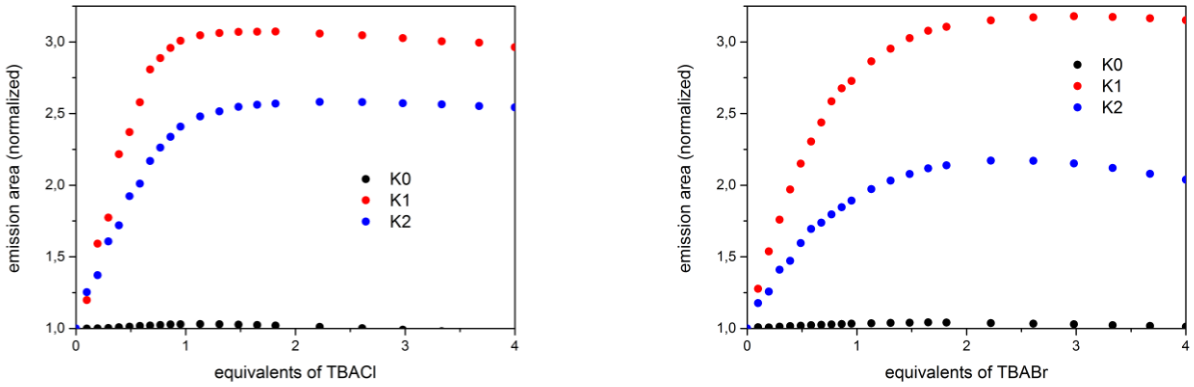

Figure 29: Plot of the emission intensity increase of **K0**, **K1**, and **K2** upon addition of TBACl (left) and TBABr (right), normalized with respect to the initial emission of the pristine PF_6 complexes.[111]

Regarding emission spectroscopic investigations with the complexes, **K0** didn't prove to be a suitable sensor molecule for the detection of chloride, bromide or iodide, as only weak responses were obtained. A much stronger effect was observed when the 4,4-disubstituted complexes **K1** and **K2** were treated with the latter salts, that is a significant increase in luminescence intensity accompanied by a slight bathochromic shift (see Figure 29). Thereby a more than three-fold increase is obtained, for example, by the interaction of chloride and bromide ions with **K1**. As described above, the emission of the pristine PF_6 salts of the complexes **K1** and **K2** is substantially dimmed as compared to **K0** (Figure 26), therefore a more sensitive response in the recognition of anions is possible.

In conclusion, the three different ruthenium(II) bibenzimidazole complexes **K0**, **K1** and **K2** were characterized through various analysis methods, such as ^{1}H-NMR, absorption and emission spectroscopy. Accompanied by single crystal x-ray analysis the anisyl rings in **K1** were characterized as freely rotatable, whereas the latter should be rigid in the scaffold of **K2**.
It was shown, that substitution at the 4,4-position of bibenzimidazole is a powerful tool to increase the sensitivity of colorimetric sensor systems. Due to the functional dimming that has been introduced through expanding the bibenzimidazole scaffold through the attachment of the anisyl substituents, a significant enhancement in luminescence sensitivity has been gained. The latter exceeds to the best of my knowledge all ruthenium(II) bibenzimidazole sensors known in literature so far.

These results are presented comprehensively in the manuscript [SR4].[111]

3.3 Photochemical application of a heterodinuclear bibenzimidazole bridged iridium(III)/ruthenium(II) complex

In the preceding chapters various structures of iridium(III) and ruthenium(II) imidazole-like complexes have been discussed. Accordingly, the mononuclear complexes of Ir(III) and Ru(II) bearing bibenzimidazole as ancillary ligand and their respective homodinuclear compounds are fundamentally characterized and their general photophysical characteristics enlightened.[11,76,86,103,105,107,111,113–116] Although structurally similar, the respective photophysical processes in these complexes are quite different. Therefore, the combination of the unique features of ruthenium complexes, that is a broad visible light absorption with its MLCT absorption maximum beyond 500 nm with the highly emissive triplet states of the iridium chromophore hence appeared promising. In this regard, to the best of my knowledge there is only one photocatalytically active system for hydrogen generation using an iridum(III) bibenzimidazole as photosensitizer known, whereas so far, ruthenium(II) bibenzimidazole complexes have remained unexplored in this regard.[117] The aim was hence to combine the advanced visible-light absorption features of ruthenium(II) complexes with the advantageous luminescent properties of the iridium(III) congener by connecting them within a dinuclear photosensitizer bearing bibenzimidazole as a bridging ligand.

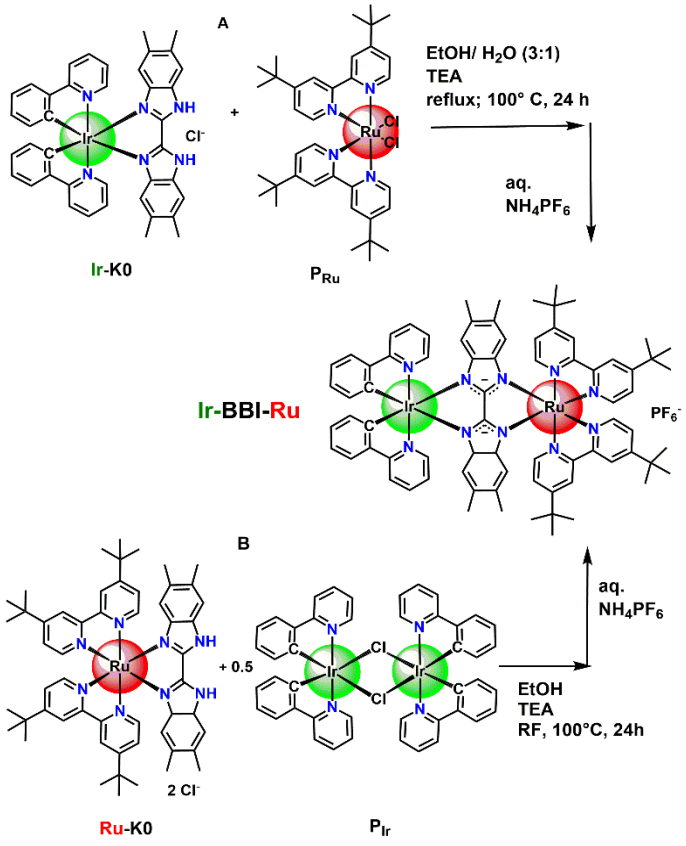

Scheme 10: Depiction of the two different routes A and B to synthesize the heterodinuclear compound **Ir-BBI-Ru.**

The heterodinuclear compound **Ir-BBI-Ru** was synthesised *via* two different routes, starting either with the aforementioned Ir(III) mononuclear compound **Ir-K0** or the Ru(II) analogon **Ru-K0**. Under basic conditions the mononuclear compounds were reacted with the respective precursor $[(tbbpy)_2RuCl_2]$ or $[(ppy)_2Ir(\mu\text{-}Cl)_2]$ to obtain **Ir-BBI-Ru** in good yield. The general structural characterization of the complex was achieved by ^{1}H-NMR spectroscopy and mass spectrometry. The ^{1}H NMR spectrum of **Ir-BBI-Ru** reveals a complex signal set characteristic for a mixture of the racemic isomers ΔΔ and ΛΛ and the *meso* isomers $\Delta_{Ru}\Lambda_{Ir}$ and $\Delta_{Ir}\Lambda_{Ru}$, of the heterodinuclear complex. Interestingly,

four different C-H_{BBI} signals of the bridging ligand are visible in the ^{1}H NMR spectrum and seemingly form two doublets, which is different in **IrBBI-H_2** and **RuBBI-H_2**, where the corresponding signals appear as two singulets (see Figure 30; the protons corresponding to the signals are marked violet). This splitting of the signals was referenced to the different coordination geometries of the C-H_{BBI} signals in the stereoisomers, that is ΛΔ,ΔΛ and ΔΔ,ΛΛ. A *rac:meso* ratio of 60:40 could be calculated by integration of the corresponding signals.

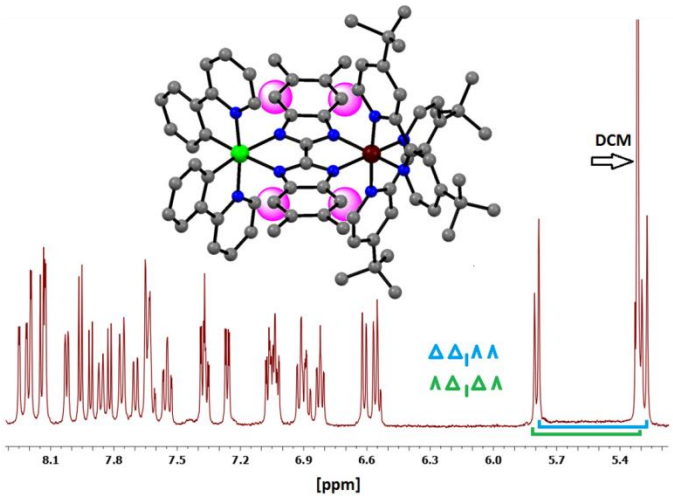

Figure 30: ^{1}H NMR spectrum of **Ir-BBI-Ru** in deuterated dichloromethane; solid-state structure of **Ir-BBI-Ru** (ellipsoids at 50 % probability level; the hydrogen atoms are omitted for clarity.

Further, single crystals were grown to get additional insight into the bonding angles and lengths of the complex (Figure 30). Strikingly, Δ and Λ isomers of the iridium moiety occupy the same position in the crystal lattice and a *rac/meso* ratio of 3:1 ratio was detected. The structure revealed an almost linear arrangement, with a slight preference for binding to the ruthenium complex, characterized by a bending angle of the bibenzimidazole of 183.89° with respect to the iridium center and 176.11° to the ruthenium center. This arrangement is similar to the homodinuclear complexes presented recently.[76,109,115,116]

Intensive photophysical characterization were performed, showing the desired combination of the different properties of the respective homodinuclear complexes in the mixed-metal **Ir-BBI-Ru** complex.[86,111,113,115,118] The UV/Vis spectrum hence exhibits most notably two intense absorption maxima at λ = 358 nm and a maximum at λ = 535 nm. The main part of the intense absorption in the UV regime was assigned to an iridium(III) based transition, whereas the maximum in the red part of the spectrum is mostly characteristic for the ^{1}MLCT transition of the ruthenium(II) entity. Upon excitation of **Ir-BBI-Ru** at λ_{exc} = 350 nm a dual emission occurs, comprising of two distinct emission features, that is one at $\lambda_{max,1}$(em) = 503 nm, and another at $\lambda_{max,2}$(em) = 700 nm (Figure 31). Position and structure of the emission band around 503 nm closely resembles that of the twofold deprotonated **Ir-K0**, whereas the

emission at around 700 nm was assigned to a ruthenium related emission with respect to literature.[10,11,84,86,109,113]

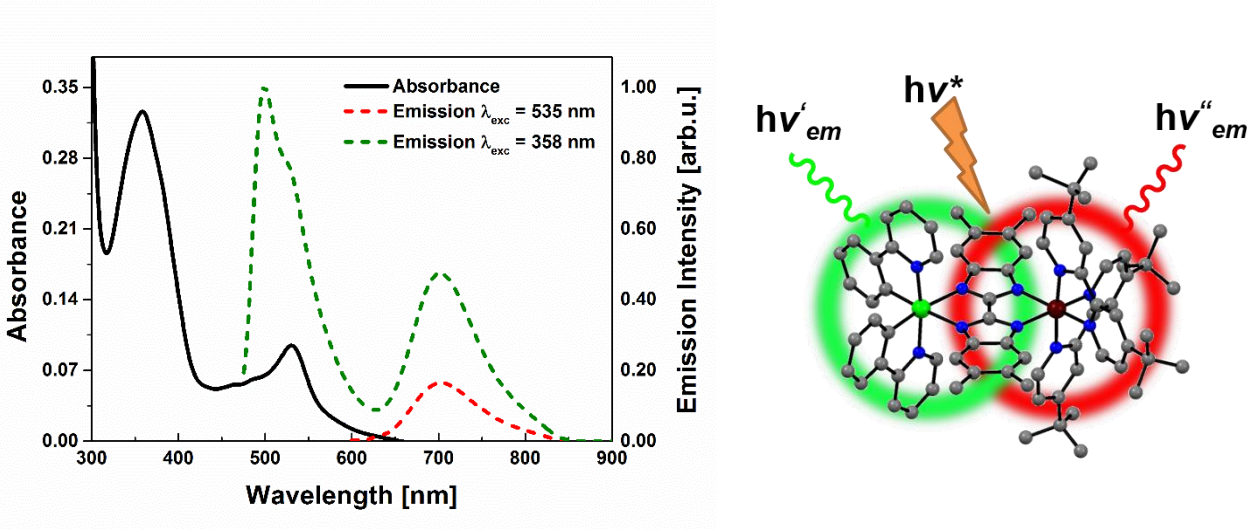

Figure 31: left: UV/Vis (black, solid) and normalized emission spectra (green and red, dashed) of **Ir-BBI-Ru** in dichloromethane ($c = 5 \times 10^{-6}$ M; red: excitation at $\lambda = 535$ nm; green: excitation at $\lambda = 358$ nm).right: Single x-ray crystal structure of **Ir-BBI-Ru** and illustration of the dual luminescene.

Strikingly, upon excitation of the exclusive ^{1}MLCT of ruthenium at $\lambda_{exc} = 535$ nm, only the lowest-lying, distinct weaker Ru-based emission is observed. This observation is special, as most of the mixed-metal bridged Ir(III)/Ru(II) complexes reported in literature exhibit an efficient energy transfer from the iridium(III) to the ruthenium(II) center, resulting in sole emission from the latter.[119–124] Based on the observation that the intensity of the iridium specific emission in the heterodinuclear complex is only about 3% as compared to the mononuclear complex **Ir-K0**, the appearance of the dual luminescence was hence suggested as an efficient but incomplete energy transfer to the weakly emissive ruthenium(II) moiety.

Table 4: General absorption and emission features characterized by the respective spectral band maxima and emission lifetimes.

Complex	λ_{max} [nm]			
	solvent	absorption	emission	lifetime [ns]
Ir-BBI-Ru	CHCl3	358, 530	503, 695	49[b],112[c]
	ACN	353, 517	500, 710	29[b], 36[c]
Ir(tmBBIH$_2$)	CHCl3	378	521/559	44 (329)
Na-Ir(tmBBI)	CHCl3	377	494	57
Ir(tmBBI)Ir	CHCl3	375	499	50
[(tbbpy)$_2$Ru]$_2$(tmBBI)	ACN	510/510	700/700	50/60
(tbbpy)$_2$Ru(tmBBIH$_2$)	ACN	473	648	120

[a] air equilibrated; [b] determined in the spectral interval 510-580 nm, [c] determined in the spectral interval 590-660 nm, respectively

Time resolved emission studies using a streak camera were performed which provided excited state lifetimes of approximately 49 ns in oxygen-equilibrated chloroform solution for the **Ir-BBI-Ru** system. A value, that is very similar to the lifetimes previously observed for the related mononuclear complexes and their dinuclear analogons (see Table 4).[68,92,97,98] Considerable sensitivity towards the solvent polarity was noticed, as the excited state lifetimes are significantly shorter in acetonitrile as compared to those determined in chloroform. Notably, the excited state lifetimes for both emissions are significantly shorter in acetonitrile as compared to those determined in chloroform for **Ir-BBI-Ru**, which indicates considerable sensitivity towards the solvent polarity (see Table 4).

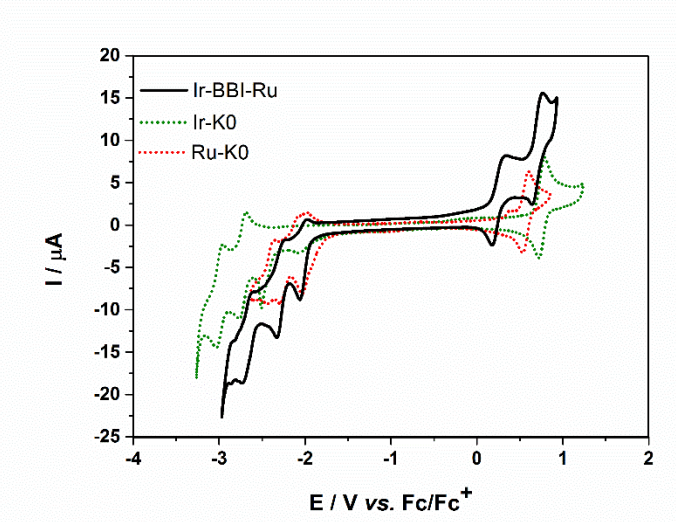

Figure 32: Cyclic voltammogram of **Ir-BBI-Ru** and the mononuclear reference compounds **Ir-K0** and **Ru-K0** in dry acetonitrile using 0.1 M ($^{n}Bu_4N)PF_6$ as supporting electrolyte at a scan rate of 100 mV/s; concentration of the complexes was 1 mM.

Electrochemical analysis of **Ir-BBI-Ru** and of its mononuclear counterparts **Ir-K0** and **Ru-K0** for reference was performed using cyclic voltammetry (ferrocene/ ferrocenium as reference).

According to literature, one reversible oxidation process is observed each for **Ir-K0** and **Ru-K0** related to Ir(III)/Ir(IV) or Ru(II)/Ru(III) oxidation, respectively.[115,116] For **Ir-BBI-Ru** two separated reversible

Table 5: Electrochemical data for oxidation and reduction processes of **Ir-K0**, **Ru-K0** and **Ir-BBI-Ru** in MeCN at a glassy-carbon electrode at 20 °C.

	$E_{1/2}$ / V *vs.* Fc/Fc$^+$					
Compound	Oxidations		Reductions			
Ir-K0	+0.757		-2.075[a]	-2.512[a]	-2.728	2.997
Ru-K0	+0.571	+0.398[a]	-2.002	-2.183	-2.396	
Ir-BBI-Ru	+0.707	+0.261	-2.015	-2.277	-2.676	

[a] irreversible process

oxidation processes were obtained, that is one centered at +0.26 V and the second at +0.71 V. The processes were assigned to the metal oxidations of $Ru^{II/III}$ and $Ir^{III/IV}$, respectively. Interestingly, the first oxidation potential of the binuclear complex is 0.3 V lower than those of the mononuclear complexes, which may be due to the known effect of negatively charged bibenzimidazole bridging ligands on metal based redox potentials (see Table 5). [76,114,117]

The appealing photophysical properties together with the stable metal based redox processes, showed up the potential of **Ir-BBI-Ru** as photosensitizer for visible light driven hydrogen generation from an aqueous solution. To verify the thesis, the known procedure of Cai et al. for structurally related complexes was adapted by using a three-component catalytic system consisting of the photosensitizer **PS**, the water reduction catalyst (WRC) $[Co(bpy)_3]Cl_2$ and triethanolamine (TEOA) as a sacrificial electron donor in a aqueous solution.[117]

The catalytic performance for the three complexes **Ir-BBI-Ru**, **Ir-K0** and **Ru-K0** were measured within an irradiation time of 140 hours after which saturation behaviour was observed. Both iridium(III) containing compounds produced hydrogen with remarkable turnover numbers (TONs) under the selected conditions. However, no hydrogen production could be detected by using **Ru-K0** as a photosensitizer. Since deprotonation of the mononuclear complexes due to the electron donor TEAO is inevitable under the given catalytic conditions, both mononuclear complexes are deprotonated in the catalysis solution. This ineptness to act as photosensitizer was hence assigned to a low energy absorbance of the respective ruthenium complex after deprotonation accompanied by complete quenching of its emission.[82,125]

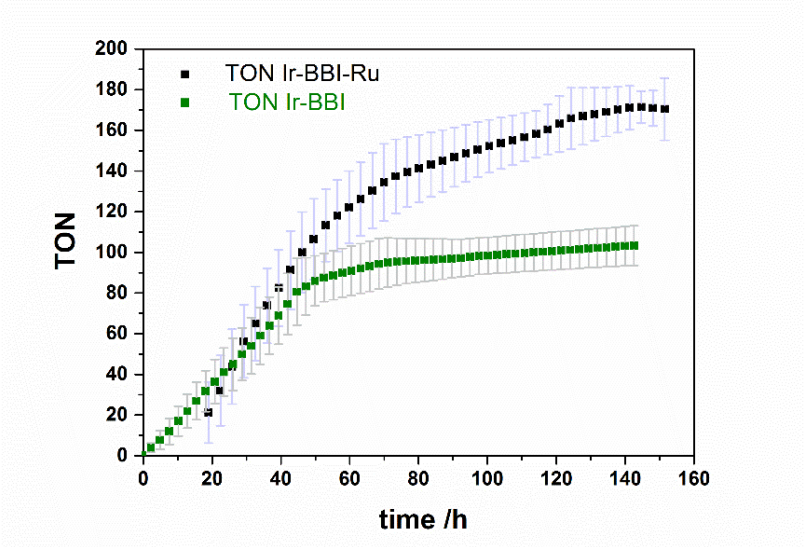

Figure 33: Turnover numbers of the light-driven hydrogen production catalyzed by the covalent system **Ir-BBI-Ru** (black rectangles) and **Ir-K0** (green rectangles); the grey dashes represent the calculated standard deviation of each curve.

In contrast, the analogous iridium complex **Ir-K0** induces inital hydrogen production with an attainable turnover number of about 100 after an irradiation time of 100 h. Further, the heterodinuclear **Ir-BBI-Ru** system displayed significant improvement as compared to the mononuclear complex as a distinct higher TON of about 170 after 140 h irradiation time was reached. Notably, the obtained turnover numbers are in

the range of the results recently published by Cai et. al for a related iridium(III) system, however slightly higher.[117] It has to be mentioned that another irradiation source was used, namely the LED setup established in our group (LED-sticks, wavelength of λ = 470 nm), hence a direct comparison should be avoided. Notably, an induction phase was clearly observed, that is, within the first 20 hours virtually no hydrogen production was detectable when using **Ir-BBI-Ru** as photosensitizer. Conversely, hydrogen production was immediately detectable with the mononuclear **Ir-K0**. The nature of this kind of induction phase remains subject to further investigation.

In summary, the succesful synthesis of the bibenzimidazole bridged iridium(III)/ruthenium(II) chromophore **Ir-BBI-Ru** was presented *via* two different routes. Its photophysical and electrochemical properties have been investigated and it could be shown that the dinuclear chromophore exhibits a superimposition of the properties of its subunits, that is a broad visible light absorption with its MLCT absorption maximum beyond 500 nm with the highly emissive triplet states of the iridium complex. Regarding emission features, a dual emission by an incomplete energy transfer through the bridge was suggested.

Further, the potential of **Ir-BBI-Ru** to be applied as photosensitizer in photochemical processes was strinkingly proven. The obtained kinetic and photophysical data under catalytic conditions suggest an elaborate mechanism for the heterodinuclear photosensitizer and exhibit improved catalytic performance as compared to the sub-component **Ir-K0**. The results spark strong interest to further investigate dinuclear systems in the future to optimize their catalytic effectiveness.

These results are presented comprehensively in the manuscript [SR5].

4 Summary and outlook

Within this work, different novel systems containing photoactive iridium(III) or ruthenium(II) chromophores bearing an imine framework were investigated regarding their application potential as supramolecular sensors and as photocatalysts in the light-driven water reduction.

The functional imine ligand entity is known to interact with anions in its protonated state or cations by means of a covalent binding if deprotonated. The metal ion recognition process is detectable by changes in the light absorbance or the emission properties of the respective pristine complex. Furthermore, a binding of the ions can be followed by ^{1}H-NMR titration measurements.

The iridium(III) bibenzimidazole model complex **Ir-K0** was comprehensively characterized and the universal suitability for application as sensor for small anions was proven. Additionally, a refinement in form of an "off-switch" strategy was presented – the latter leading to a higher selectivity of the supramolecular sensor system.

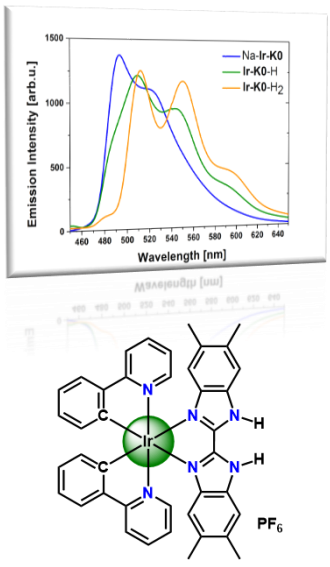

- Strongly luminescent system in all protonation states
- Displays advantageous features regarding photophysical applications

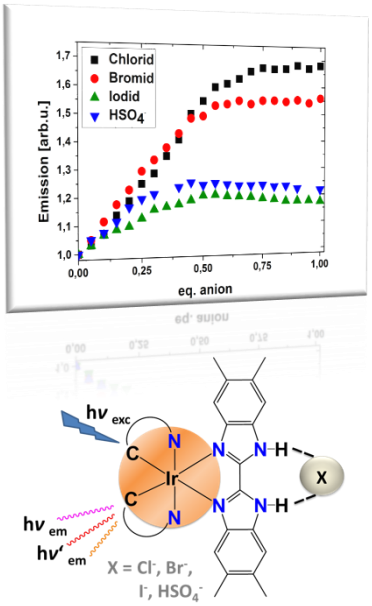

- Potential suitable sensor chromophore for the detection of small, basic molecules *via* ^{1}H-NMR and emission spectroscopic methodes

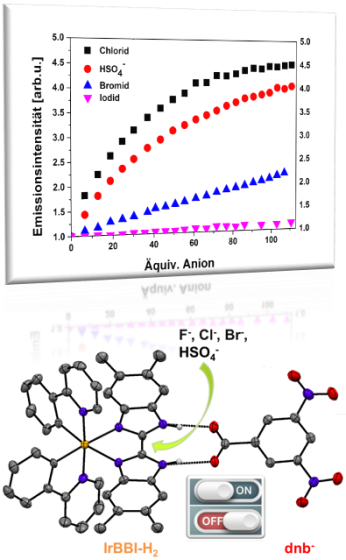

- Optimized sensor system by introducing an „ON-OFF" switch
- Use of oxidative quencher 3,5-dinitrobenzoate
- Increased selectivity of the system

The second part of the thesis dealt with a library of three different ruthenium(II) bibenzimidazole complexes (**K0**, **K1** and **K2**). By introduction of the sterically confining substituents **L1** and **L2**, a selectivity of the binding mode of these chromophores was generated. A significant enhancement in

luminescence sensitivity has hence been achieved due to the functional dimming that was introduced by expanding the bibenzimidazole scaffold *via* the attachment of the anisyl substituents.

In a conclusive project, the heterodinuclear bibenzimidazole bridged iridium(III)/ ruthenium(II) complex **Ir-BBI-Ru** was synthesized in order to investigate the synergy effects of the previously investigated sole chromophore units. Accompanied by a comprehensive investigation of the basic properties of the complex, its applicability as photosensitizer in the light-driven hydrogen production was tested.

In particular, following results were obtained:

- ❖ The iridium(III) bibenzimidazole model complex **Ir-K0** was synthesized and characterized comprehensively. The studies comprised the analogies and differences with respect to the well-established related ruthenium(II) chromophores.

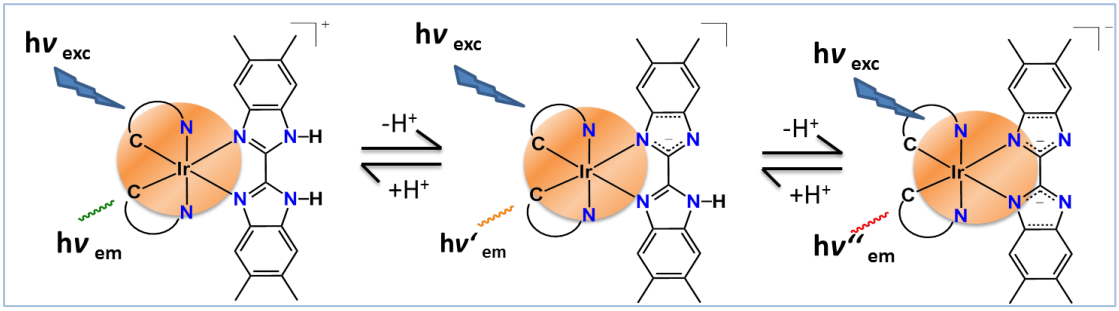

- In this regard the basic photophysical properties of **Ir-K0** were investigated. Although structurally similar to the Ru(II) analogues, the features of **Ir-K0** were shown to be fundamentally different since absorption events mainly occur in the UV regime, comprising of a maximum lower than 360 nm with a weak absorption tailing off up to $\lambda = 450$ nm.
- The dependency of the principal photophysics of **Ir-K0** on the protonation state was investigated. It could be shown, that the mononuclear complex **Ir-K0-H$_x$** (x = 0, 1, 2) is strongly luminescent in all three protonation states, and the emission spectrum is very sensitive to solvents due to the mostly unstable protonation state.
- The model complex **Ir-K0** was compared to related ruthenium(II) bibenzimidazole complexes, where deprotonation leads to a complete quenching of the emission. This observation renders the complex to be advantageous in regard to the usage in photoluminescent applications.
- To the best of our knowledge the first crystallographic investigation of an iridium bibenzimidazole complex with respect to supramolecular aspects was performed, revealing first insights into the hydrogen bond formation ability.

- The homodinuclear complex **(Ir-K0)$_2$** was comprehensively characterized *via* ^{1}H-NMR and photophysical investigations. By using two dimensional NMR it was also possible to prove that two diasteromeric forms of the homodinuclear complexes exist (*meso* and *rac*) and can be separated.
- A crystal structure of the dinuclear **(Ir-K0)$_2$** (*meso* form) was presented and compared with the mononuclear **Ir-K0**-H and three reference compounds.

❖ In an additional study, the aforementioned dependence of the luminescence characteristics of **Ir-K0** on the coordination environment was employed for anion sensing with small anions for the first time. Thereby, different analysis methods, such as ^{1}H-NMR and emission spectroscopy, were applied.

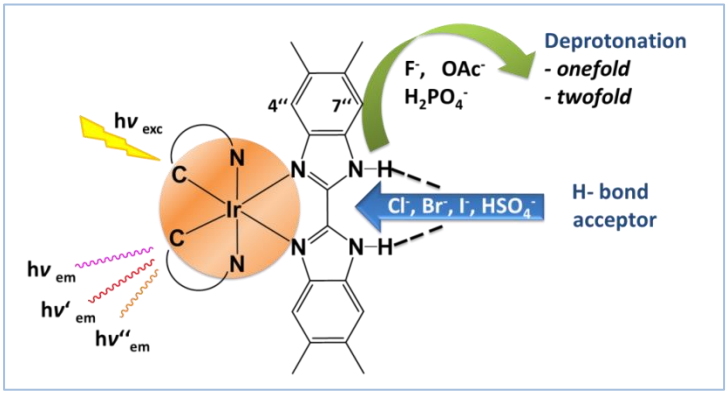

- The detailed anion binding studies with **Ir-K0** have shown its potential for the supramolecular recognition of selected anions. With basic anions such as fluoride, acetate and dihydrogen phosphate in chloroform a deprotonation event was noticeable which could be confirmed by comparison with the selectively synthesized respective protonation states of **Ir-K0**. The mild basic anions such as chloride, bromide, and hydrogen sulfate were found to increase the emission intensity weakly, accompanied by a small hypsochromic shift of the emission. Accordingly, a complete N-H abstraction could be excluded, however weak, but noticeable interactions by means of hydrogen bonding events with the respective anions were proven.
- Interestingly, the ion binding mechanism was shown to involve fast formation of a 2:1 (complex : anion) species which distinguishes the iridium(III) sensor from the known ruthenium(II) based systems where a 1:1 stoichiometry dominates.

❖ In order to refine the sensor sensitivity of the **Ir-K0** system, a supramolecular luminescence "off"-switch strategy was presented.

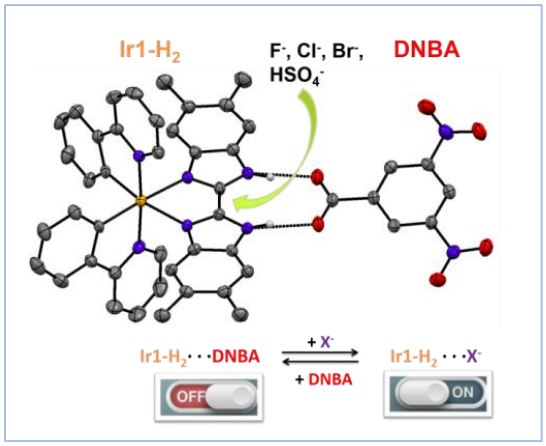

- 3,5-dinitrobenzoate was introduced, as the latter is known to effectively quench the luminescence of N-H acidic chromophores. In the present system the luminescence intensity was quenched to 7 % with regard to the pristine luminescence of the PF_6 salt.
- Competitive hydrogen bonding by the weakly basic anions or competitive deprotonation by the basic anion fluoride lead to a significant luminescence increase of up to 750 %. The "off-switch" strategy was hence shown to display a powerful tool to increase the ion sensing quality of **Ir-K0** in terms of luminescence sensitivity and exceeds all ruthenium(II) biimidazole-type sensors known in literature so far.
- The quenched **Ir-K0**$^{+}$···DNBA^{-} system hence sets benchmark values for anion recognition with phosphorescent bibenzimidazole-type complexes.

❖ In collaboration with Dieter Sorsche an improved anion sensing strategy for ruthenium(II) bibenzimidazole complexes was developed.

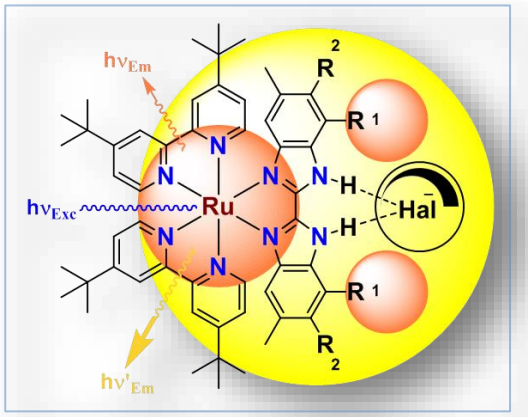

- Following the general synthesis procedures reported by Siegel et al. two new ruthenium(II)bibenzimidazole complexes with sterically demanding substituents adjacent to the α-diamine sphere have been synthesized in this thesis (in collaboration with Dieter Sorsche).
- Accompanied by single crystal x-ray analysis, the anisyl rings in **K1** were characterized as freely rotatable, whereas the latter were supposed to be rigid in the scaffold of **K2**.
- The anion recognition features of the three different ruthenium(II) bibenzimidazole complexes **K0**, **K1** and **K2** were characterized by various analysis methods, such as ^{1}H-NMR, absorption and emission spectroscopy.
- For the weakly basic anions chloride and bromide strong hydrogen binding with **K1** and **K2** was observed with an up to 3-fold increase of emission. In contrast, comparative measurements with the unsubstituted bibenzimidazole complex **K0** showed almost negligible optical response.
- Accordingly, due to the functional dimming that has been introduced by expanding the bibenzimidazole scaffold through the attachment of the anisyl substituents, a significant enhancement in luminescence sensitivity has been gained.

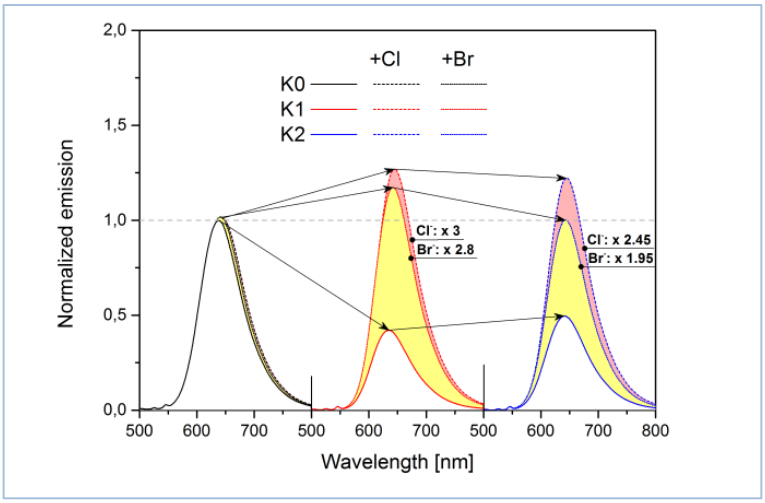

❖ In a conclusive project, the heterodinuclear bibenzimidazole bridged iridium(III)/ ruthenium(II) complex **Ir-BBI-Ru** was synthesized in order to investigate the synergy effect of the prior investigated sole chromophore units. Accompanied by a comprehensive investigation of the basic properties of the complex its applicability as photosensitizer in the light-induced hydrogen production was tested (in collaboration with Dieter Sorsche).

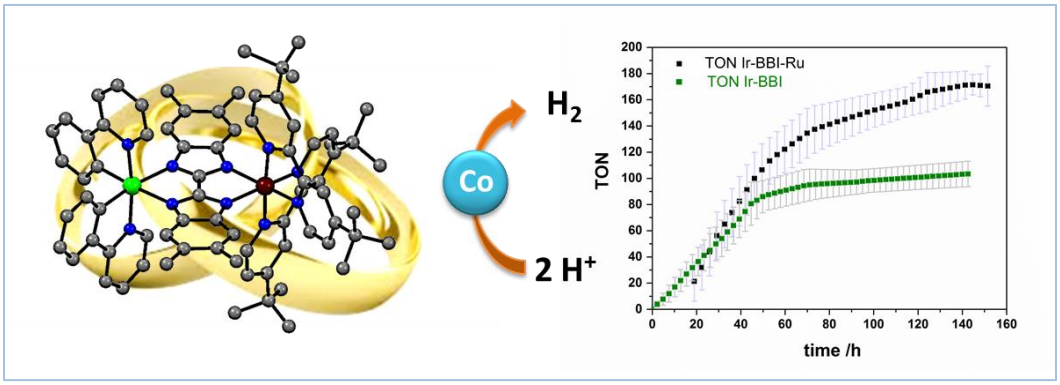

- The successful synthesis of **Ir-BBI-Ru** was presented *via* two different routes.
- Its photophysical and electrochemical properties have been investigated and it could be shown that the dinuclear chromophore exhibits a superimposition of the properties of its subunits, that is a broad visible light absorption with its MLCT absorption maximum beyond 500 nm with the highly emissive triplet states of the iridium(III) entity.
- Regarding emission features, a dual emission by an incomplete energy transfer through the bridge was suggested.
- The potential of **Ir-BBI-Ru** to be applied as photosensitizer in the photocatalytic hydrogen production was proven strikingly. For **Ir-BBI-Ru** an overall turnover number of 170 after 140 h was measured, whereas for **Ir-K0** a slightly reduced TON of 100 was obtained. The obtained kinetic and photophysical data under catalytic conditions suggest an elaborate mechanism for the heterodinuclear photosensitizer and exhibit improved catalytic performance compared to the sub-component **Ir-K0**.

Based on the previous studies it will be promising to coordinate the expanded ligand scaffold of **L1** and **L2** to iridium(III) chromophores. Thereby the strategy of the steric confinement of ruthenium complexes

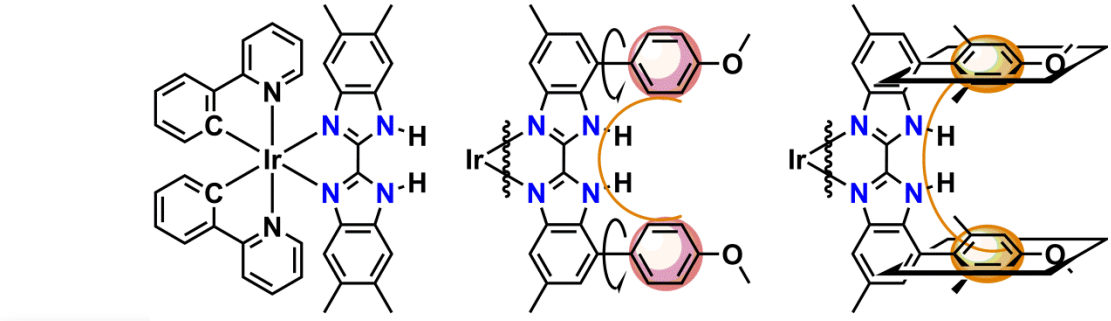

could be combined with the superior luminescence properties of the related iridium(III) complexes, leading conceivably to tailored highly sensitive anion sensors. First attempts have already been realized as it was possible to synthesize the analogue iridium(III) complexes **Ir-K1** and **Ir-K2**. With a library of three novel strongly luminescent Ir(III) complexes a range of application possibilities will be accessible, for example the usage as suitable anion sensors or even as cation sensors, respectively.

Further, the catalytic activity of the heterodinuclear **Ir-BBI-Ru** system sparks strong interest to investigate subsequent dinuclear systems comprising of two different chromophore units to refine their catalytic effectiveness due to synergy effects. Thereby, the focus should especially be on the search for bridging ligands that enable electronic communication between the different chromophore units.

5 References

[1] A. Grüßing, Makrocyclische Funktionseinheiten Mit Exo- Und Endotopen N-Donorsätzen, Friedrich-Schiller-Universität Jena, **2004**.

[2] F. Vögtle, *Supramolekulare Chemie*, Teubner, B. G., Stuttgart, **1992**.

[3] J. W. Steed, J. L. Atwood, *Supramolecular Chemistry*, John Wiley & Sons, Ltd, Chichester, **2000**.

[4] C. J. Pedsersen, *Aldrichimica Acta* **1971**, *4*.

[5] C. D. Gutsche, *Calixarenes, Monographs in Supramolecular Chemistry*, Royal Society Of Chemistry, Cambridge, **1989**.

[6] Y. Cui, H.-J. Mo, J.-C. Chen, Y.-L. Niu, Y.-R. Zhong, K.-C. Zheng, B.-H. Ye, *Inorg. Chem.* **2007**, *46*, 6427–6436.

[7] Y. Cui, Y.-L. Niu, M.-L. Cao, K. Wang, H.-J. Mo, Y.-R. Zhong, B.-H. Ye, *Inorg. Chem.* **2008**, *47*, 5616–5624.

[8] H.-J. Mo, Y.-L. Niu, M. Zhang, Z.-P. Qiao, B.-H. Ye, *Dalton Trans.* **2011**, *40*, 8218.

[9] H.-J. Mo, H.-Y. Chao, B.-H. Ye, *Inorg. Chem. Commun.* **2013**, *35*, 100–103.

[10] Y. Cui, Y. Niu, M. Cao, K. Wang, H. Mo, Y. Zhong, B. Ye, *Inorg. Chem.* **2008**, *47*, 5616–5624.

[11] S. Rau, T. Büttner, C. Temme, M. Ruben, H. Görls, D. Walther, M. Duati, S. Fanni, J. G. Vos, *Inorg. Chem.* **2000**, *39*, 1621–1624.

[12] S. Shinkai, T. Ogawa, Y. Kusano, *Chem. Lett.* **1980**, 283.

[13] M. Shiga, M. Takagi, K. Ueno, *Chem. Lett.* **1980**, 1021.

[14] P. A. Gale, N. Busschaert, C. J. E. Haynes, L. E. Karagiannidis, I. L. Kirby, *Chem. Soc. Rev.* **2014**, *43*, 205–241.

[15] P. A. Gale, *Chem. Commun.* **2011**, *47*, 82–86.

[16] P. D. Beer, P. A. Gale, *Angew. Chemie Int. Ed.* **2001**, *40*, 486–516.

[17] P. D. Beer, *Acc. Chem. Res.* **1998**, *31*, 71–80.

[18] P. D. Beer, J. Cadman, *Coord. Chem. Rev.* **2000**, *205*, 131–155.

[19] S. Mardanya, S. Karmakar, D. Maity, S. Baitalik, *Inorg. Chem.* **2015**, *54*, 513–526.

[20] V. W. Manner, J. M. Mayer, *J. Am. Chem. Soc.* **2009**, *131*, 9874–9875.

[21] J. H. Alstrum-Acevedo, M. K. Brennaman, T. J. Meyer, *Inorg. Chem.* **2005**, *44*, 6802–6827.

[22] E. A. Medlycott, G. S. Hanan, *Chem. Soc. Rev.* **2005**, *34*, 133.

[23] W. R. Browne, N. M. O'Boyle, J. J. McGarvey, J. G. Vos, *Chem. Soc. Rev.* **2005**, *34*, 641.

[24] V. Balzani, A. Juris, M. Venturi, S. Campagna, S. Serroni, *Chem. Rev.* **1996**, *96*, 759–834.

[25] K. E. Erkkila, D. T. Odom, J. K. Barton, *Chem. Rev.* **1999**, *99*, 2777–2796.

[26] A. E. Friedman, J. C. Chambron, J. P. Sauvage, N. J. Turro, J. K. Barton, *J. Am. Chem. Soc.* **1990**,

112, 4960–4962.

[27] S. Baitalik, X. Wang, R. H. Schmehl, *J. Am. Chem. Soc.* **2004**, *126*, 16304–16305.

[28] M. S. Lowry, S. Bernhard, *Chem. Eur. J.* **2006**, *12*, 7970–7977.

[29] M. J. Cook, A. P. Lewis, G. S. G. Mcauliffe, V. Skarda, A. J. Thompson, J. L. Glasper, D. J. Robbins, *J. Chem. Soc. Perkin. Trans. II* **1984**, 1293–1301.

[30] M. Kirch, J. Lehn, J. Sauvage, *Helv. Chim. Acta* **1979**, *62*, 1345–1384.

[31] B. Higgins, B. A. DeGraff, J. N. Demas, *Inorg. Chem.* **2005**, *44*, 6662–6669.

[32] K. K.-W. Lo, W.-K. Hui, C.-K. Chung, K. H.-K. Tsang, D. C.-M. Ng, N. Zhu, K.-K. Cheung, *Coord. Chem. Rev.* **2005**, *249*, 1434–1450.

[33] K. Kalyanasundaram, *Photochemistry of Polypyridine and Porphyrin Complexes*, Academic Press, New York, NY, **1992**.

[34] J. I. Goldsmith, W. R. Hudson, M. S. Lowry, T. H. Anderson, S. Bernhard, *J. Am. Chem. Soc.* **2005**, *127*, 7502–7510.

[35] P. D. Beer, *Coord. Chem. Rev.* **2003**, *240*, 167–189.

[36] M. G. Colombo, A. Hauser, H. U. Guedel, *Inorg. Chem.* **1993**, *32*, 3088–3092.

[37] A. King, R. J. Watts, *J. Phys. Chem.* **1987**, *91*, 1047–1054.

[38] D. M. Roundhill, *Photochemistry and Photophysics of Metal Complexes*, Plenum Press, New York, NY, **1994**.

[39] Y. You, S. Y. Park, *Dalton Trans.* **2009**, *9226*, 1267–1282.

[40] W. J. Finkenzeller, H. Yersin, *Chem. Phys. Lett.* **2003**, *377*, 299–305.

[41] M. K. Nazeeruddin, R. T. Wegh, Z. Zhou, C. Klein, Q. Wang, F. De Angelis, S. Fantacci, M. Grätzel, *Inorg. Chem.* **2006**, *45*, 9245–9250.

[42] H. J. Bolink, L. Cappelli, E. Coronado, A. Parham, P. Stössel, *Chem. Mater.* **2006**, *18*, 2778–2780.

[43] S. T. Parker, J. D. Slinker, M. S. Lowry, M. P. Cox, S. Bernhard, G. G. Malliaras, *Chem. Mater.* **2005**, *17*, 3187–3190.

[44] M. A. Baldo, D. O'Brien, Y. Y, A. Shoustikov, S. Sibley, M. E. Thompson, S. R. Forrest, *Nature* **1998**, *395*, 151–154.

[45] M. A. Baldo, C. Adachi, S. R. Forrest, *Phys. Rev. B* **2000**, *62*, 10967–10977.

[46] E. J. Merino, A. K. Boal, J. K. Barton, *Curr. Opin. Chem. Biol.* **2008**, *12*, 229–237.

[47] F. Shao, B. Elias, W. Lu, J. K. Barton, *Inorg. Chem.* **2007**, *46*, 10187–10199.

[48] F. Shao, J. K. Barton, *J. Am. Chem. Soc.* **2007**, *129*, 14733–14738.

[49] N. D. Silavwe, A. S. Goldman, R. Ritter, D. R. Tyler, *Inorg. Chem.* **1989**, *28*, 1231–1236.

[50] K. A. Belmore, R. A. Vanderpool, J. C. Tsai, M. A. Khan, K. M. Nicholas, *J. Am. Chem. Soc.* **1988**, *110*, 2004–2005.

[51] J. W. Steed, *Chem. Soc. Rev.* **2009**, *38*, 506–519.

[52] P. Anzenbacher, D. S. Tyson, K. Jursíková, F. N. Castellano, *J. Am. Chem. Soc.* **2002**, *124*, 6232–6233.

[53] S. Pang, Y. Zheng, Z. Zhou, C. Tan, Q. Wang, X. Li, *Opt. Mater. (Amst).* **2013**, *35*, 1157–1161.

[54] S. Mardanya, S. Karmakar, M. Bar, S. Baitalik, *Dalton Trans.* **2015**, *44*, 21053–21072.

[55] R. Martínez-Máñez, F. Sancenón, *Chem. Rev.* **2003**, *103*, 4419–4476.

[56] Thomson, "Web of science databases," can be found under https://apps.webofknowledge.com/UA_GeneralSearch_input.do?product=UA&search_mode=GeneralSearch&SID=T1fxZL9orTop2Ra2x2E&preferencesSaved=, **2016**.

[57] D.-L. Ma, V. P.-Y. Ma, D. S.-H. Chan, K.-H. Leung, H.-Z. He, C.-H. Leung, *Coord. Chem. Rev.* **2012**, *256*, 3087–3113.

[58] A. P. De Silva, H. Q. N. Gunaratne, T. Gunnlaugsson, A. J. M. Huxley, C. P. McCoy, J. T. Rademacher, T. E. Rice, *Chem. Rev.* **1997**, *97*, 1515–1566.

[59] S. Ladouceur, E. Zysman-colman, *Eur. J. Inorg. Chem.* **2013**, 2985–3007.

[60] J. N. Demas, E. W. Harris, C. M. Flynn, D. Diemente, *J. Am. Chem. Soc.* **1975**, *97*, 3838–3839.

[61] C. M. Flynn, J. N. Demas, *J. Am. Chem. Soc.* **1973**, *279*, 1973–1974.

[62] J. N. Demas, E. W. Harris, R. P. McBride, *J. Am. Chem. Soc.* **1977**, *99*, 3547–3551.

[63] R. J. Watts, J. S. Harrington, J. Van Houten, *J. Am. Chem. Soc.* **1977**, *99*, 2179–2187.

[64] K. R. Wunschel, W. E. Ohnesorge, *J. Am. Chem. Soc.* **1967**, *89*, 2777–2778.

[65] R. D. Gillard, R. J. Lancashire, P. A. Williams, *J. Chem. Soc. Dalton Trans.* **1979**, 190–192.

[66] M. Nonoyama, *Bull. Chem. Soc. Jpn.* **1974**, *47(3)*, 767–768.

[67] K. A. King, R. J. Watts, *J. Am. Chem. Soc.* **1987**, *109*, 1589–1590.

[68] L. Flamigni, A. Barbieri, C. Sabatini, B. Ventura, F. Barigelletti, *Top. Curr. Chem.* **2007**, *281*, 143–203.

[69] D. Sorsche, Sterically Well-Defined Second-Sphere Receptor Chromophores for Optical Molecular Recognition and Photocatalysis, Universität Ulm, Ulm, **2016**.

[70] S. Ladouceur, E. Zysman-Colman, *Eur. J. Inorg. Chem.* **2013**, *2013*, 2985–3007.

[71] Y. Ohsawa, S. Sprouse, K. A. King, M. K. DeArmond, K. W. Hanck, R. J. Watts, *J. Phys. Chem.* **1987**, *91*, 1047–1054.

[72] R. D. Costa, E. OrtÃ-, H. J. Bolink, S. Graber, S. Schaffner, M. Neuburger, C. E. Housecroft, E. C. Constable, *Adv. Funct. Mater.* **2009**, *19*, 3456–3463.

[73] M. G. Colombo, A. Hauser, H. U. Gudel, I. Anorganische, P. Chemie, U. Bern, *Inorg.chem.* **1993**, *32*, 3088–3092.

[74] Y. Yasui, D. K. Frantz, J. S. Siegel, *Org. Lett.* **2006**, *8*, 4989–4992.

[75] D. K. Frantz, A. A. Sullivan, Y. Yasui, A. Linden, K. K. Baldridge, J. S. Siegel, *Org. Biol. Chem.* **2009**, *7*, 2347–2352.

[76] S. Rau, M. Ruben, T. Büttner, C. Temme, S. Dautz, H. Görls, M. Rudolph, D. Walther, A. Brodkorb, M. Duati, et al., *J. Chem. Soc., Dalton Trans.* **2000**, 3649–3657.

[77] H.-J. Mo, J.-J. Wu, Z.-P. Qiao, B.-H. Ye, *Dalton Trans.* **2012**, *41*, 7026–7036.

[78] O. S. Wenger, *Chem. Eur. J.* **2011**, *17*, 11692–11702.

[79] J. C. Freys, G. Bernardinelli, O. S. Wenger, *Chem. Commun.* **2008**, 4267–4269.

[80] J. P. Kirby, J. A. Roberts, D. G. Nocera, *J. Am. Chem. Soc.* **1997**, *119*, 9230–9236.

[81] J. C. Freys, G. Bernardinelli, O. S. Wenger, *Chem. Commun.* **2008**, 4267–4269.

[82] M. Haga, *Inorg. Chim. Acta* **1983**, *75*, 29–35.

[83] D. Walther, L. Böttcher, J. Blumhoff, S. Schebesta, H. Görls, K. Schmuck, S. Rau, M. Rudolph, *Eur. J. Inorg. Chem.* **2006**, 2385–2392.

[84] D. Sorsche, S. Rau, *Eur. J. Inorg. Chem.* **2014**, *2014*, 4244–4249.

[85] A. F. Henwood, S. Evariste, A. M. Z. Slawin, E. Zysman-Colman, *Faraday Discuss.* **2014**, *00*, 1–18.

[86] S. A. Rommel, D. Sorsche, N. Rockstroh, F. W. Heinemann, J. Kübel, M. Wächtler, B. Dietzek, S. Rau, *Eur. J. Inorg. Chem.* **2015**, 3730–3739.

[87] D. Hanss, J. C. Freys, G. Bernardinelli, O. S. Wenger, *Eur. J. Inorg. Chem.* **2009**, 4850–4859.

[88] S. Kappaun, C. Slugovc, E. J. List, *Int. J. Mol. Sci.* **2008**, *9*, 1527–1547.

[89] A. Auffrant, A. Barbieri, F. Barigelletti, J.-P. Collin, L. Flamigni, C. Sabatini, J.-P. Sauvage, *Inorg. Chem.* **2006**, *45*, 10990–10997.

[90] M. S. Lowry, S. Bernhard, *Chem. - A Eur. J.* **2006**, *12*, 7970–7977.

[91] A. B. Tamayo, S. Garon, T. Sajoto, P. I. Djurovich, I. M. Tsyba, R. Bau, M. E. Thompson, *Inorg. Chem.* **2005**, *44*, 8723–8732.

[92] E. A. Plummer, J. W. Hofstraat, L. De Cola, *Dalton Trans.* **2003**, 2080.

[93] L. Donato, C. E. McCusker, F. N. Castellano, E. Zysman-Colman, *Inorg. Chem.* **2013**, *52*, 8495–8504.

[94] A. Auffrant, A. Barbieri, F. Barigelletti, J. Lacour, P. Mobian, J.-P. Collin, J.-P. Sauvage, B. Ventura, *Inorg. Chem.* **2007**, *46*, 6911–6919.

[95] S. Welter, F. Lafolet, E. Cecchetto, F. Vergeer, L. De Cola, *ChemPhysChem* **2005**, *6*, 2417–2427.

[96] E. A. Plummer, J. W. Hofstraat, L. De Cola, *Dalton Trans.* **2003**, 2080.

[97] R. D. Costa, G. Fernández, L. Sánchez, N. Martín, E. Ortí, H. J. Bolink, *Chem. Eur. J.* **2010**, *16*, 9855–9863.

[98] A. Tsuboyama, T. Takiguchi, S. Okada, M. Osawa, M. Hoshino, K. Ueno, *Dalton Trans.* **2004**, 1115–1116.

[99] S. Fortin, P.-L. Fabre, M. Dartiguenave, A. L. Beauchamp, *J. Chem. Soc. Dalt. Trans.* **2001**, 3520–3527.

[100] Z.-H. Lin, S.-J. Ou, C.-Y. Duan, B.-G. Zhang, Z.-P. Bai, *Chem. Commun.* **2006**, 624–626.

[101] V. M. S. Gil, N. C. Oliveira, *J. Chem. Educ.* **1990**, *67*, 473–478.

[102] M. J. Hynes, *J. Chem. Soc. Dalton Trans.* **1993**, 311–312.

[103] S. A. Rommel, D. Sorsche, A. Dixit, S. Rau, *Eur. J. Inorg. Chem.* **2016**, *2016*, 40–48.

[104] Y. Liu, B.-H. Han, Y.-T. Chen, *J. Phys. Chem. B* **2002**, *106*, 4678–4687.

[105] S. A. Rommel, D. Sorsche, S. Rau, *Dalton Trans.* **2016**, *45*, 74–77.

[106] S. Rau, L. Böttcher, S. Schebesta, M. Stollenz, H. Görls, D. Walther, *Eur. J. Inorg. Chem.* **2002**, 2800–2809.

[107] M.-A. Haga, *Inorganica Chim. Acta* **1983**, *75*, 29–35.

[108] M. Haga, T. Ano, T. Ishizaki, K. Kano, K. Nozaki, T. Ohno, *J. Chem. Soc. Dalt. Trans.* **1994**, 263.

[109] A. Grüßing, S. Rau, S. Schebesta, A. Scholz, H. Görls, D. Walther, *Z. Anorg. Allg. Chem.* **2007**, 961–970.

[110] D. K. Frantz, A. Sullivan, Y. Yasui, A. Linden, K. K. Baldridge, J. S. Siegel, *Org. Biomol. Chem.* **2009**, *7*, 2347–52.

[111] D. Sorsche, S. A. Rommel, S. Rau, *Eur. J. Inorg. Chem.* **2016**, 1503–1513.

[112] K. Halbauer, A. Göbel, A. Sterzik, H. Görls, S. Rau, W. Imhof, *Eur. J. Inorg. Chem.* **2007**, 1508–1514.

[113] M. Haga, *Inorg. Chim. Acta* **1980**, *45*, L183–L184.

[114] A. M. Bond, M. Haga, *Inorg. Chem.* **1986**, *25*, 4507–4514.

[115] M. Haga, T. Matsumura-Inoue, S. Yamabe, *Inorg. Chem.* **1987**, *26*, 4148–4154.

[116] M. Haga, A. M. Bond, *Inorg. Chem.* **1991**, *30*, 475–480.

[117] J. Cai, Z. Yu, Y. Yuan, F. Li, Z. Zou, *ACS Catal.* **2014**, *4*, 1953–1963.

[118] R. Indumathy, P. S. Parameswaran, C. V. Aiswarya, B. Unni Nair, *Polyhedron* **2014**, *75*, 22–29.

[119] K. J. Arm, J. A. G. Williams, *Dalton Trans.* **2006**, 2172–2174.

[120] C. Sabatini, A. Barbieri, F. Barigelletti, K. J. Arm, J. A. G. Williams, *Photochem. Photobiol. Sci.* **2007**, *6*, 397–405.

[121] J. Osío Barcina, N. Herrero-García, F. Cucinotta, L. De Cola, P. Contreras-Carballada, R. M. Williams, A. Guerrero-Martínez, *Chem. Eur. J.* **2010**, *16*, 6033–6040.

[122] S. Welter, F. Lafolet, E. Cecchetto, F. Vergeer, L. De Cola, *ChemPhysChem* **2005**, *6*, 2417–2427.

[123] V. L. Whittle, J. A. G. Williams, *Dalton Trans.* **2009**, 3929–3940.

[124] M. Cavazzini, P. Pastorelli, S. Quici, F. Loiseau, S. Campagna, *Chem. Commun.* **2005**, 5266–5268.

[125] K. Monczak, K. Peuntinger, D. Sorsche, F. W. Heinemann, D. M. Guldi, S. Rau, *Chem. Eur. J.* **2014**, *20*, 15426–15433.

6 Publications

[SR1]: Protonation-Dependent Luminesence of an Iridium(III) Bibenzimidazole Chromophore

Sebastian A. Rommel, Dieter Sorsche, Nils Rockstroh, Frank W. Heinemann, Joachim Kübel, Maria Wächtler, Benjamin Dietzek and Sven Rau*

* *corresponding author*

Published in: *Eur. J. Inorg. Chem.*, **2015**, 3730 – 3734. (DOI: 10.1002/ejic.201500234).

Copyright Reprinted from "Protonation-Dependent Luminesence of an Iridium(III) Bibenzimidazole Chromophore, Sebastian A. Rommel, Dieter Sorsche, Nils Rockstroh, Frank W. Heinemann, Joachim Kübel, Maria Wächtler, Benjamin Dietzek and Sven Rau, *Eur. J. Inorg. Chem.*, **2015**, 3730 – 3734." with permission of the publisher John Wiley and Sons. (License Number: 3910161485883)

In this work, we present the synthesis and a detailed structural and photophysical investigation of the bis(phenylpyridine)iridium(III) complex of 4,4',5,5'-tetramethyl-2,2'-bibenzimidazole (Ir(tmBBI)-H_2) and its homodinuclear complex (Ir(tmBBI)Ir). Their structures were determined by single crystal X-ray diffraction analysis and NMR spectroscopy and detailed UV/Vis and emission studies were performed. Ir(tmBBI)-H_x (x = 0, 1, 2) shows strong protonation state dependent luminescence and is luminescent in all of its three protonation states allowing for protonation state dependent colour tuning from the green to the more blue spectral region. The two diastereomeric forms meso and rac of the dinuclear Ir(tmBBI)Ir could be separated by fractional crystallisation and both showed strong luminescence. The comparison with structurally related ruthenium complexes show pronounced differences of their respective photophysical properties.

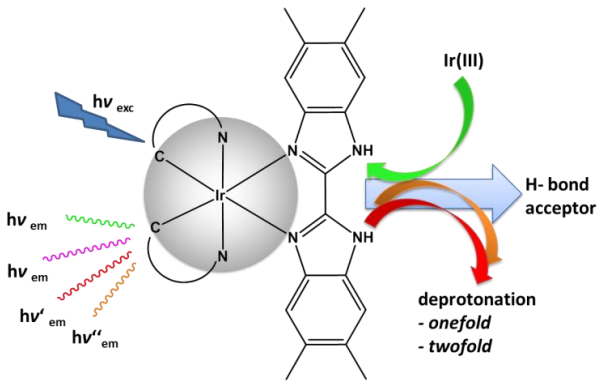

Contribution of the different authors:

Sebastian A. Rommel	Synthesis and complete characteriaztion of the two different complexes. Growing of the crystals suitable for X-ray crystallography of Ir(tmBBI) and Ir(tmBBI)Ir. Writing of the manuscript, concept and results discussion and revision of the manuscript.
Dieter Sorsche	Measurement and refinement of the X-ray structures. Writing, concept and results discussion and revision of the manuscript.
Nils Rockstroh	First synthesis and characterization of Ir(tmBBI) and Ir(tmBBI)Ir. Growing of the crystals of Ir(tmBBI)suitable for X-ray crystallography. Discussion and revision of the manuscript.
Frank W. Heinemann	Measurement and refinement of the X-ray structures, discussion and revision of the manuscript.
Joachim Kübel	Performance of the excited state lifetime measurements.Discussion and revision of the manuscript.
Maria Wächtler	Discussion and revision of the manuscript.
Benjamin Dietzek	Discussion and revision of the manuscript.
Sven Rau	Discussion and revision of the manuscript, concept and results discussion.

EurJIC European Journal of Inorganic Chemistry
ChemPubSoc Europe
FULL PAPER

DOI:10.1002/ejic.201500234

Protonation-Dependent Luminescence of an Iridium(III) Bibenzimidazole Chromophore

Sebastian A. Rommel,[a] Dieter Sorsche,[a] Nils Rockstroh,[b] Frank W. Heinemann,[b] Joachim Kübel,[c] Maria Wächtler,[c] Benjamin Dietzek,[c] and Sven Rau*[a]

Keywords: Iridium / Hydrogen bonds / Photophysics / Luminescence / Chromophores / Color tuning

We present the synthesis and a detailed structural and photophysical investigation of the bis(phenylpyridine)iridium(III) complex of 4,4′,5,5′-tetramethyl-2,2′-bibenzimidazole [Ir(tmBBI)-H_2] and its homodinuclear complex [Ir(tmBBI)Ir]. Their structures were determined by single-crystal X-ray diffraction analysis and NMR spectroscopy, and detailed UV/Vis and emission spectroscopy studies were performed. Ir(tmBBI)-H_x shows strong protonation-state-dependent luminescence and is luminescent in all three of its protonation states, which allows for protonation-state-dependent color tuning from the green to blue spectral region. The diastereomeric *meso* and *rac* forms of the dinuclear Ir(tmBBI)-Ir could be separated by fractional crystallization and both showed strong luminescence. A comparison with structurally related ruthenium complexes showed pronounced differences in their photophysical properties.

Introduction

2,2′-Biimidazoles and 2,2′-bibenzimidazoles are interesting ligands for various kinds of metal centers. The deprotonation of their planar *ortho*-diamine framework causes an increase of σ-donor strength and a decrease of π-acceptor strength.[1–3] Herein, an interesting feature is provided that allows switching of the ligand-field strength and, therefore, the photophysical and electrochemical features of the metal complex with the pH of the matrix.[4] Bibenzimidazole complexes of photoactive bis(bipyridine)ruthenium(II) complexes have been investigated widely with respect to their hydrogen-bonding and anion-sensing properties. Ye and coworkers have confirmed the capability of biimidazole complexes to act as hydrogen-bond donors through NMR and UV/Vis spectroscopy.[5–7] The absorption features in the visible region change significantly upon deprotonation or hydrogen bonding to fluoride or acetate ions. In their fully deprotonated state, these complexes act as metalloligands, that is, the deprotonated biimidazole sphere can bind a second metal center such as zinc(II), nickel(II), or copper(I).[1,2,8,9] The binding of these metal centers results in significant changes to their photophysical properties. This feature, which can be observed for various kinds of bi(benz)imidazole metal complexes, is of paramount importance for this and further studies, as it can provide a spectroscopic tool for the direct observation of proton release from these molecules.[10] The versatile applicability of these complexes is dampened by the fact that only the fully protonated complexes exhibit appreciable luminescence. Deprotonation clearly opens a significant deactivation pathway for these complexes, which limits their value for photochemical applications.

It is important to mention that the ligand-centered metal-to-ligand charge-transfer (^{3}MLCT) excited states of bis(bipyridine)ruthenium(II)bibenzimidazole complexes are located exclusively on the bipyridine ligands.[11] Nonradiative deactivation is possible through variation of the ruthenium-based ground state.[12]

In contrast, the triplet excited states of bis(phenylpyridine)iridium(III) chromophores generally exhibit a strong mix of ligand-centered and metal-centered states. Furthermore, the greater ligand-field stabilization energy of third-row elements imparts an important advantage to Ir^{III} complexes over Ru^{II} complexes. For the second-row elements, the direct population of the triplet metal-centered (^{3}MC) excited state can result in light-induced ligand loss. Consequently, Ir^{III} compounds should in general exhibit greater photostability than their Ru^{II} analogues.[13]

In this regard, a change from ruthenium(II) to iridium(III) chromophores appeared to be a promising approach to connect the switching properties of a bibenzimidazole chromophore with the more sophisticated lumines-

[a] Institute for Inorganic Chemistry I, Ulm University, Albert-Einstein-Allee 11, 89081 Ulm, Germany
E-mail: sven.rau@uni-ulm.de
http://www.uni-ulm.de/nawi/nawi-anorg1
[b] Department Chemie und Pharmazie, Universität Erlangen-Nürnberg, Egerlandstr. 1, 91058 Erlangen, Germany
[c] Leibniz Institute of Photonic Technology (IPHT) Jena e.V., Department Functional Interfaces, Albert-Einstein-Str. 9, 07745 Jena, Germany
Supporting information for this article is available on the WWW under http://dx.doi.org/10.1002/ejic.201500234.

© 2015 Wiley-VCH Verlag GmbH & Co. KGaA, Weinheim

cence of bis(phenylpyridine)iridium(III) complexes. Furthermore, iridium(III) bibenzimidazole complexes are active photosensitizers in water photoreduction.[14–18]

Wenger et al. have presented fundamental work on the photochemistry and photoacidic behavior of a bis(phenylpyridine)iridium(III) biimidazole complexes with a focus on proton-coupled electron-transfer events. The complexes forms hydrogen-bonded 1:1 adducts with benzoate anions and could not be deprotonated when an excess of benzoate anion was added. The photoexcitation of the metal complex in the presence of 3,5-dinitrobenzoate triggers a proton-coupled electron transfer.[10,19]

Here, we present the synthesis and a detailed structural and photophysical investigation of the bis(phenylpyridine)-iridium(III) complex of 4,4′,5,5′-tetramethyl-2,2′-bibenzimidazole [Ir(tmBBI)-H_x] and its homodinuclear complex Ir(tmBBI)Ir (Figure 1). Emission spectroscopy proved to be a powerful method to elucidate the sensitive switch of the electronic structure of Ir(tmBBI-H_x) upon protonation and deprotonation processes. The presented mononuclear complex Ir(tmBBI)-H_x shows promising luminescence properties in all three of its protonation states with protonation-state-dependent shifts for the luminescence wavelength. In contrast to that of its ruthenium(II) analogues, its luminescence is not only retained during successive deprotonation but also increases significantly in intensity after deprotonation. Furthermore, the presented dinuclear complex shows impressive luminescence characteristics in comparison to those of its homodinuclear ruthenium analogue.

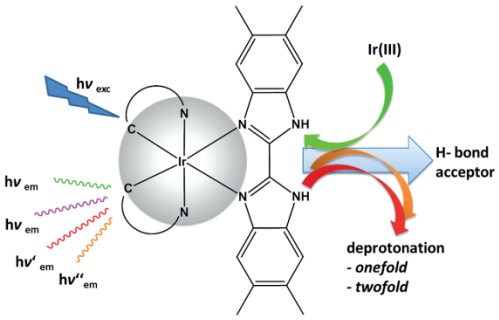

Figure 1. Schematic representation of the building block presented in this work.

Results and Discussion

Synthesis and Characterization of the Complexes

The cyclometalated Ir^{III} μ-chloro-bridged dimer [$(ppy)_2$-$Ir(\mu\text{-}Cl)_2Ir(ppy)_2$] (**1**, ppy = 2-phenylpyridine) was synthesized according to the Nonoyama route by heating $IrCl_3 \cdot 3H_2O$ with 2.5 equiv. of the ligand (2-phenylpyridine) in a mixture of 2-ethoxyethanol and water under reflux.[20] The mononuclear complex $(ppy)_2Ir(tmBBI\text{-}H_2)$ [Ir(tmBBI)-H_2] was obtained by heating the ligand 4,4′,5,5′-tetramethyl-2,2′-bibenzimidazole (tmBBI-H_2, **2**) with the cyclometalated precursor **1** and a catalytic amount of formic acid in a mixture of ethanol/water (5:2) under reflux. After purification through size-exclusion chromatography and recrystallization, Ir(tmBBI)-H_2 was obtained as its hexafluorophosphate salt in a considerable yield (76.6%). The principle structural characterization of the complex was achieved by ^1H and ^{13}C NMR spectroscopy, elemental analysis, and mass spectrometry. The observed ESI-MS signal at m/z = 790 appertains to the monodeprotonated molecular cation Ir(tmBBI)-H. The ^1H NMR spectrum of Ir(tmBBI)-H_2 provides all of the expected signal sets of ppy coordinated to the Ir^{III} center together with a peripheral bidentate ligand. Notably, the aromatic 4′′-/7′′-H signals of the tmBBI-H_2 ligand (**2**) are particularly sensitive to the coordination geometry. Similarly to that of the analogous ruthenium bipyridyl complex [$(tbbpy)_2Ru(tmBBI)\text{-}H_2$]-$[PF_6]_2$ (**R3**, tbbpy = 4,4′-di-*tert*-butyl-2,2′-bipyridine), the 4′′-H signal of **1** in dimethyl sulfoxide (DMSO; δ = 5.74 ppm) is highly shielded owing to its spatial proximity to the pyridyl ring of the phenylpyridine ligand. Therefore, its signal is highfield shifted by 1.76 ppm with respect to that of 7′′-H (δ = 7.50 ppm; see Scheme 1 and Figure 2).

In contrast to 2,2′-bipyridine and 1,10-phenanthroline, 2,2′-bibenzimidazole can act as a bridging ligand to coordinate a second metal center after deprotonation or bind anions through hydrogen bonding in its protonated form.[1] Therefore, the deprotonated complex Na-Ir(tmBBI) was synthesized by stirring the protonated complex Ir(tmBBI)-

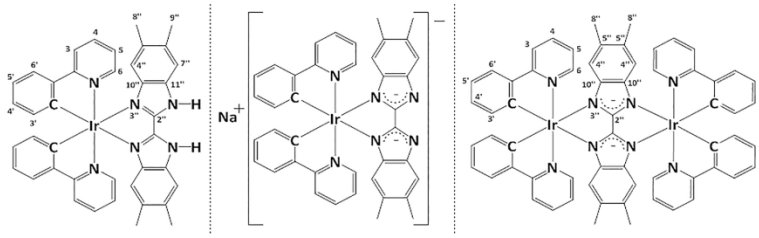

Scheme 1. Schematic representation of the complexes discussed in this paper.

 © 2015 Wiley-VCH Verlag GmbH & Co. KGaA, Weinheim

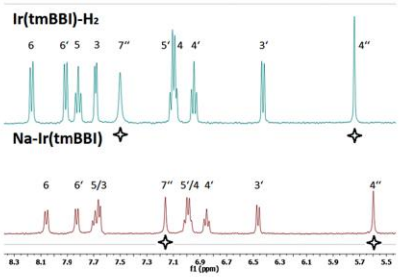

Figure 2. Characteristic ^{1}H NMR signals of Ir(tmBBI)-H_2 and Na-Ir(tmBBI) in [D_6]DMSO in the aromatic region (c = 2.345 mmol/L). The bibenzimidazole-related signals are marked with a star. The complete ^{1}H NMR spectra and the numbering scheme are depicted in the Supporting Information.

H_2 in methanol with excess sodium hydroxide, and the complex was characterized by ^{1}H NMR and optical spectroscopy in dimethyl sulfoxide or chloroform, respectively. In general, the separation of the NMR signals is strongly solvent-dependent.[1] For Ir(tmBBI)-H_2, a signal for the two NH protons is observed at δ = 11.5 ppm in chloroform, whereas no signal can be observed in dimethyl sulfoxide. The clearly visible NH signal of Ir(tmBBI)-H_2 in chloroform disappears upon titration of a solution of the fully protonated complex with tetrabutylammonium hydroxide (TBAOH), and TBA-Ir(tmBBI) did not show any NH signal (see Supporting Information and Figure 1). However, no significant protonation-state-dependent shifts of the ^{1}H NMR signals could be observed in chloroform. In deuterated DMSO, deprotonation leads to significant shifts of the 7′′-/4′′-H and 8′′-/9′′-H signals. In particular, the significant shift of the 7′′-H signal in the ^{1}H NMR spectra by ca. 0.4 ppm is strong evidence for twofold deprotonation. This shift can be ascribed to the higher charge density on the deprotonated bibenzimidazole ligand, which leads to an increased shielding of the hydrogen atoms located on the phenyl ring of the complex.

The dinuclear complex was synthesized by treating an equimolar amount of the ligand tmBBI-H_2 and precursor **1** in dimethylformamide and triethylamine (5:2) in a microwave reaction.[9] Ir(tmBBI)Ir represents a neutral complex.

The combination of two octahedral complex fragments in one molecule leads to three diastereomeric isomers: the *meso* form ΔΛ as well as the ΔΔ and ΛΛ isomers, the racemic mixture of which is referred to as *rac*.[1] The ^{1}H NMR spectra of the mixture (see Figure 3) show a typical signal set for a stereoisomeric pair. The *rac* and *meso* stereoisomers were separated by fractional crystallization, and their characteristic ^{1}H NMR signals are depicted in Figure 3. In contrast to corresponding signals for Ir(tmBBI)-H_2 (Figure 2, top), the signals for 4′′-H and 7′′-H coalesce as doublet, which is shifted by ca. 0.1 ppm upfield with respect to that of 4′′-H in the monomer and indicates a symmetric NMR spectrum. Furthermore, the protons of the CH_3 groups of the BBI ligand give one upfield-shifted signal in the aliphatic region, which confirms the coordination of an identical second iridium moiety. In the respective homodinuclear ruthenium complex [{(tbbpy)$_2$Ru}$_2$(tmBBI)][PF_6]$_2$ (**R2**) or the strongly related [{(dmbpy)$_2$Ru}$_2$(bpym)]$^{4+}$ (dmbpy = 4,4′-dimethyl-2,2′-bipyridine, bpym = 2,2-bipyrimidine) the signals for one pyridine system remain virtually unchanged in both forms.[1,21] However, the signals of two protons of the other pyridine moiety are shifted considerably upfield in the spectrum of the *rac* fraction compared with that of the *meso* form.[1] In our system, the signals of the benzene moiety remain virtually unchanged, whereas the signals for H-3 and H-4 of the pyridine ring are shifted significantly upfield. These results can be explained in terms of a greater anisotropic effect from the ring current of the adjacent phenylpyridine system experienced by 3-H and 4-H, which are directly above the bridging ligand and, therefore, significantly shifted upfield. Furthermore, we were able to calculate a ratio for the *meso* and the *rac* form to be approximately 1:1 for the mixture of both complexes by integration of the signals in the aromatic region of the ^{1}H NMR spectrum.

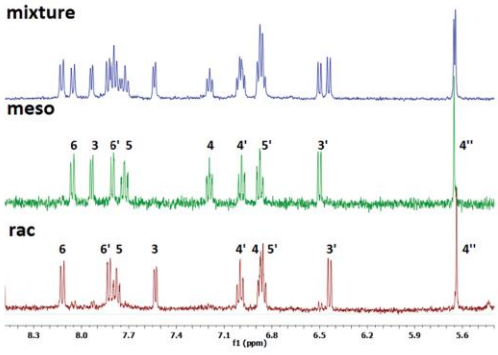

Figure 3. Characteristic signals in the ^{1}H NMR spectra of Ir(tmBBI)Ir in [D_6]DMSO.

The ^{1}H NMR spectrum of the first separated fraction was assigned to the *meso* form as crystals suitable for X-ray diffraction could be obtained from the purified fraction by slow evaporation of a solution of the complex in dimethyl sulfoxide/dichloromethane/ethyl acetate. The ^{1}H NMR data are summarized in Table 1.

Several examples of bibenzimidazole complexes of ruthenium and their structural characterization have been described. By exploiting the hydrogen-bond donor activity of bibenzimidazole toward water, it was shown that these complexes are part of an assembly of highly spatially ordered arrays of mononuclear ruthenium bibenzimidazole complexes. Furthermore, the nature of the hydrogen-bonding activity of these complexes can be reversed from donor to acceptor by deprotonation of the secondary amine group, and in principle there are strong interactions with anions such as fluoride and acetate or weaker interactions with other halides.[1,2,5–8,22,23] Therefore, we attempted to grow

 © 2015 Wiley-VCH Verlag GmbH & Co. KGaA, Weinheim

Table 1. ^{1}H NMR spectroscopic data [ppm] of Ir(tmBBI)-H_2, Na-Ir(tmBBI), Ir(tmBBI)Ir *meso*, and Ir(tmBBI)Ir *rac* in [D_6]DMSO.

Proton:	6	6′	3	5	7′′	5′	4	4′	3′	4′′	9′′	8′′
Ir(tmBBI)-H_2	8.17	7.91	7.82	7.68	7.55	7.12	7.09	6.94	6.41	5.75	2.25	1.94
Na-Ir(tmBBI)	8.06	7.83	7.65	7.69	7.16	7.00	6.98	6.86	6.46	5.60	2.15	1.86
Ir(tmBBI)Ir *meso*	8.06	7.81	7.94	7.72	5.66[a]	6.89	7.20	7.00	6.51	5.66[a]	1.83[a]	1.83[a]
Ir(tmBBI)Ir *rac*	8.12	7.83	7.53	7.77	5.64[a]	6.85	6.88	7.00	6.44	5.64[a]	1.82[a]	1.82[a]

[a] Owing to multiple peak overlap no assignment is possible.

single crystals from an aqueous system (DMSO/water) to provide a closer view of the hydrogen-bond properties of Ir(tmBBI)-H_x (x = 1, 2). The obtained structure revealed the singly protonated, neutral complex Ir(tmBBI)-H with a hydrogen-bond network that consists of two water molecules and two terminating molecules of DMSO (see Figure 4).

In Table 2, the bond lengths and angles of Ir(tmBBI)-H, Ir(tmBBI)Ir, $[(Me\text{-}ppy)_2Ir(biimH_2)]^+$ (**R1**), $[\{(tbbpy)_2Ru\}_2(\mu\text{-}tmBBI)][PF_6]_2$ (**R2**), and $[(tbbpy)_2Ru(tmBBI\text{-}H_2)][PF_6]_2$ (**R3**) are shown. The numbering schemes for Ir(tmBBI)-H and Ir(tmBBI)Ir are depicted in Figures 4 and 5, respectively; all others can be found in the Supporting Information.

The phenylpyridine ligands are oriented with the cyclometalated phenyl ring in the *trans* position with respect to the bibenzimidazole ligand. This observation is in agreement with other known bis-heteroleptic bis(phenylpyridine)-iridium(III) complexes.[24]

In the solid-state structure of Ir(tmBBI)-H two water molecules are hydrogen bonded to the secondary amine functions of the bibenzimidazole core in a conventional manner.[1,5,22,25–28] Owing to the good quality of the data obtained, we were able to locate the protons accurately in the hydrogen-bond framework. The position of the amine proton was assigned with respect to a well-defined Q-peak in an early stage of the refinement. Owing to the uncertainty for the positional parameters of hydrogen atoms, however, it was added to the structure by using the appropriate HFIX command.

Bibenzimidazole ruthenium complexes form hydrogen bonds with bidentate H-bond acceptors, for example, in the presence of water and PF_6 ions, carboxylic acids, or CF_3SO_3 anions.[5,28,29] Here, the peripheral nitrogen atoms form twofold, complementary hydrogen bonds with two water molecules. The H-bond framework is capped by two molecules of dimethyl sulfoxide. The protonated and deprotonated amine functions of the complex fulfil a hydrogen donor and acceptor function simultaneously. In addition, the distances between the N and O atoms [$d_{N\cdots O}$ = 2.80(1) or 2.77(1) Å] evidence that the hydrogen bridges are well-defined.

Many bibenzimidazole complexes, including the reference complexes **R1**, **R2**, and **R3**, show a distorted octahedral coordination geometry. The same geometry could also be stated for the mononuclear iridium(III) complex presented in this work by comparison of the different bond lengths to the various ligands and the deviation of the angles from 180° [<(N5–Ir1–N4) 174.37(11)°, <(C38–Ir1–N3) 170.73(11)°, and <(C27–Ir1–N1) 170.64(11)° for Ir(tmBBI)Ir]. In addition, the angles <(N3–Ir1–N1) 79.49(9)°, <(C27–Ir1–N4) 80.63(12)°, and <(C38–Ir1–N5) 80.62(12)° are smaller than 90° and, therefore, demonstrate a distorted octahedral geometry. In the dinuclear complex Ir(tmBBI)Ir (Figure 5), the bridging ligand binds both

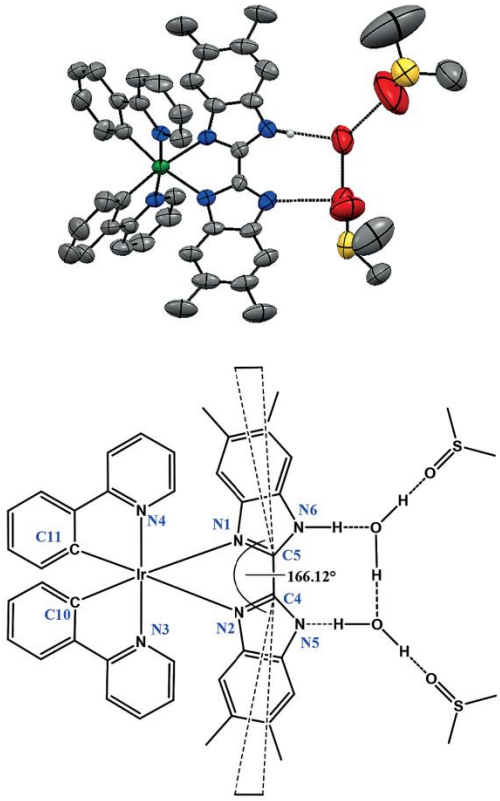

Figure 4. Top: schematic depiction of the solid-state structure of $[(ppy)_2Ir(tmBBI\text{-}H)]\cdot 2[H_2O]\cdot 2[C_2H_6OS]$ with the characteristic bending angle of the bibenzimidazole ligand inscribed. Bottom: solid-state structure of the hydrogen-bond framework of $[(ppy)_2Ir(tmBBI\text{-}H)]\cdot 2[H_2O]\cdot 2[C_2H_6OS]$ (ellipsoids at 50% probability level; the hydrogen atoms that are not involved in the hydrogen-bond framework are omitted for clarity; $R1$ = 0.0625, wR_2 = 0,1565).

 © 2015 Wiley-VCH Verlag GmbH & Co. KGaA, Weinheim

Table 2. Selected bond lengths [Å] and angles [°] of Ir(tmBBI)-H, Ir(tmBBI)Ir, **R1**, **R2**, and **R3**. The numbering scheme is according to that depicted in Figure 2.[1,10]

Ir(tmBBI)Ir		[(Me-ppy)$_2$Ir(biimH$_2$)]$^+$ (**R1**)		Ir(tmBBI)-H		[{(tbbpy)$_2$Ru}$_2$(μ-tmBBI)][PF$_6$]$_2$ (**R2**)		[(tbbpy)$_2$Ru(tmBBI-H$_2$)][PF$_6$]$_2$ (**R3**)	
Ir1–N1	2.201(3)	Ir-N1c	2.169(3)	Ir–N1	2.138(8)	Ru1–N1	2.124(3)	Ru1–N2	2.102(5)
Ir1–N3	2.177(2)	Ir–N4c	2.161(3)	Ir–N2	2.136(8)	Ru1–N2	2.128(3)	Ru1–N1	2.110(4)
Ir1–N4	2.038(3)	Ir–N1a	2.042(3)	Ir–N4	2.061(8)	Ru1–N5	2.032(3)	Ru1–N6	2.052(5)
Ir1–C27	2.005(3)	Ir–C11a	2.019(3)	Ir–C10	2.015(1)	Ru1–N6	2.043(3)	Ru1–N5	2.042(4)
Ir1–N5	2.037(3)	Ir–N1b	2.052(3)	Ir–N3	2.039(7)	Ru1–N8	2.051(3)	Ru1–N8	2.059(4)
Ir1–C38	2.007(3)	Ir–C11b	2.009(4)	Ir–C11	1.990(1)	Ru1–N7	2.028(3)	Ru1–N7	2.058(4)
N3–Ir1–N4	79.49(9)	N4c–Ir–N1c	75.88(10)	N1–Ir1–N2	76.0(3)	N2–Ru1–N1	81.05(12)	N1–Ru1–N2	77.66(12)
C27–Ir1–N4	80.63(12)	C11a–Ir–N1a	80.92(12)	C10–Ir1–N4	80.6(4)	N6–Ru1–N5	78.54(13)	N6–Ru1–N5	79.01(18)
C38–Ir1–N5	80.62(12)	C11b–Ir–N1b	80.07(13)	C11–Ir1–N3	81.5(4)	N7–Ru1–N8	78.54(13)	N7–Ru1–N8	78.93(17)
N5–Ir1–N4	174.37(11)	N1b–Ir–N1a	174.44(12)	N4–Ir1–N3	174.0(3)	N7–Ru1–N5	176.34(14)	N5–Ru1–N8	95.54(17)
C38–Ir1–N3	170.73(11)	C11a–Ir–N4c	172.04(11)	C11–Ir1–N2	171.2(4)	N6–Ru1–N2	169.58(13)	N7–Ru1–N2	93.19(18)
C27–Ir1–N1	170.64(11)	C11b–Ir–N1c	171.93(11)	C10–Ir1–N1	172.4(4)	N7–Ru1–N1	168.89(13)	N6–Ru1–N6	97.79(18)
				N6–C5–C4	130.3(8)			N3–C7–C8	129.7(5)
				N5–C4–C5	128.7(9)			N4–C8–C7	130.3(5)
				N1–C5–C4	116.0(8)			N1–C7–C8	117.4(5)
				N2–C4–C5	116.2(8)			N2–C8–C7	116.8(5)
				deviation α	166.12			deviation α	167.1

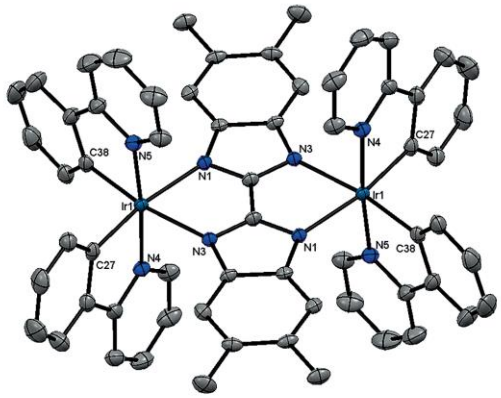

Figure 5. Crystal structure of Ir(tmBBI)Ir; hydrogen atoms and solvent molecules are omitted for clarity.

metal centers equally; therefore, no torsion was determined, which is in agreement with the respective ruthenium(II) dimer [{(tbbpy)$_2$Ru}$_2$(μ-tmBBI)][PF$_6$]$_2$ (**R2**). This linear arrangement is present in homodinuclear complexes, whereas some structures have the bibenzimidazole slightly bent around the metal core. As expected, a similar trend could be observed in the investigated Ir(tmBBI)-H, in which the bibenzimidazole ligand shows a bending angle of 166.12°, which correlates nicely with similar ruthenium or iridium biimidazole complexes, in which the bending angles are (165.9±0.7)°.[2,10,29,30]

The distances between the metal core and the bibenzimidazole ligand X–N$_{BBI}$ (X = Ru^{II} or Ir^{III}) are depicted in Table 2. The bi(benz)imidazole ligand always exhibits longer distances to the metal core than the distances for the comparable ligands phenylpyridine or bipyridine.[1,10] In Ir(tmBBI)-H, the bond lengths $d_{(Ir–NtmBBI)}$ of the iridium core to the nitrogen atoms of the bibenzimidazole ligand are longer [$d_{(Ir–N1)}$ = 2.138(8) Å and $d_{(Ir–N2)}$ = 2.136(8) Å] than the Ir–N Ir–C bond lengths to both phenylpyridine ligands [$d_{(Ir–C11)}$ = 1.990(1) Å, $d_{(Ir–C10)}$ = 2.015(1) Å, $d_{(Ir–N3)}$ = 2.039(7) Å $d_{(Ir–N1)}$ = 2.138(8) Å]. Therefore, on the basis of the data for **R1**, **R2**, and **R3**, it is apparent from the crystal structure that the phenylpyridine ligands bind more strongly to the iridium metal core than the peripheral ligand tmBBI-H.

Furthermore, the structural analysis results imply that the bonding interaction between the metal core and the bridging bibenzimidazole ligand weakens from the mononuclear to the dinuclear complexes for both iridium and ruthenium. If bibenzimidazole is a bridging ligand it has to be doubly deprotonated and becomes a much stronger σ donor.[31,32] The increased σ-donor strength probably causes a decrease of the acceptor abilities. However, as for the previously reported ruthenium complexes, the differences in the ligand properties cannot fully explain the differences in the bond lengths for the mono- and dinuclear complexes.[1]

Photophysical Characterization

The photophysics of ruthenium(II) bibenzimidazole complexes is determined by the protonation state of the bibenzimidazole ligand. Under irradiation, twofold-protonated ruthenium bibenzimidazole complexes (e.g., **R3**) show luminescence, whereas their emission is completely quenched after full deprotonation. This behavior is not found for related iridium-based compounds.

Cai and co-workers investigated a very closely related pair of monodeprotonated mononuclear and dinuclear compounds {[Ir(tfmppy)$_2$]$_2$}$_x$BiBzIm {x = 1, (**R4**), 2 (**R5**); tfmppy = 2-[4-(trifluoromethyl)phenyl]pyridine, BiBzIm = 2,2′-bibenzimidazole}. On the basis of these results, the UV/Vis and emission properties of Ir(tmBBI)-H$_x$ (x = 0, 1, 2) in its different protonation states were investigated (see

 © 2015 Wiley-VCH Verlag GmbH & Co. KGaA, Weinheim

Figure 6). The absorption properties of Ir(tmBBI)-H_x (x = 0, 1, 2) are virtually unchanged irrespective of the protonation steps. An intense band in the UV region was ascribed to spin-allowed $^1\pi$–π^* transitions localized on both coordinated aromatic ligands through reference to the previously well-established photophysical properties of iridium(III) diamine complexes.[15,33–41] The nature of the absorption bands between λ=300 and 450 nm is best described as a mixture of spin-allowed charge-transfer (^{1}CT) transitions that contain contributions from both $d\pi \rightarrow \pi^*_{tmBBI}$ metal-to-ligand charge-transfer (^{1}MLCT) and $\pi_{ppy} \rightarrow \pi^*_{tmBBI}$ ligand-to-ligand charge-transfer (^{1}LLCT) transitions. However, on the basis of investigations on the related complex $[(ppy)_2Ir(bpy)]^+$ (bpy = 2,2′-bipyridine; **R6**), the major contribution to the absorption band at λ = 380 nm should be a mixed $d\pi \rightarrow \pi^*_{ppy}$ ^{1}MLCT and a ligand-centered $\pi \rightarrow \pi^*$ (LC) transition of the ppy ligand.[42] The lower-energy band at λ = 450–550 nm can be associated with direct excitation into the ^{3}MLCT, which is, however, mixed with the $^3\pi$–π^* transition. This assignment is based on the observation of similar absorptions for corresponding iridium complexes.[43] However, unlike $Ru(bpy)_3^{2+}$, for which the MLCT bands are spectrally well separated from intraligand absorptions (IL), no clear isolated MLCT bands can be observed for the iridium(III) complexes investigated in this work.[43,44] This complicates the detection of a trend for the effect of protonation on the MLCT energy through absorption measurements only. In Ir(tmBBI)-H_2 and the related well-established **R6**, ill-defined MLCT transitions are observed as shoulders at λ = 439 [Ir(tmBBI-H_2)] and 477 nm (**R6**) in the absorption spectra.[45] Furthermore, a second mixed IL/MLCT transition is bathochromically shifted (348 nm) compared that of the ruthenium analogue **R6** (337 nm). The reason is the stronger σ-donor character of BBI, which increases the electron density of the iridium core and, therefore, facilitates the transition to a phenylpyridine ligand. In the diprotonated states of the complex, a well-defined shoulder is present at λ = 378 nm; the absence of this shoulder for the completely deprotonated state indicates that protonation has a very small effect on the absorption. On the basis of DFT calculations, Cai and co-workers stated that the electronic distribution between the highest occupied molecular orbital (HOMO) and lowest unoccupied molecular orbital (LUMO) in this type of iridium complexes refers to charge separation. The HOMO accordingly differs depending on the strength of the bonding properties of the ligand backbones. In a dinuclear BBI complex (e.g., **R5**), the HOMO is formed mainly from a combination of Ir 5d orbitals and the entire conjugated system of the BBI bridging ligand, whereas the HOMO for the monodeprotonated mononuclear complex **R4** originates from a combination of Ir 5d orbitals and the deprotonated half of the bibenzimidazole ligand only.[15] Therefore, the protonation state effects the contribution of the bibenzimidazole ligand to the HOMO in this type of complex.

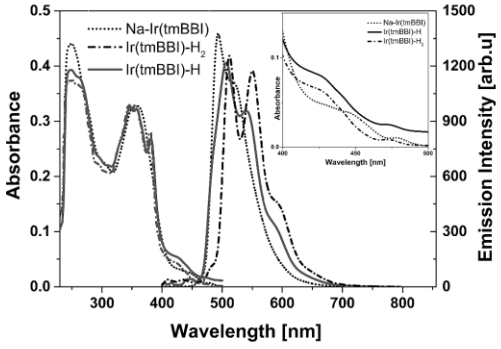

Figure 6. UV/Vis and emission spectra of Ir(tmBBI)-H_x in chloroform (c = 5×10^{-6} M; excitation at 378 nm); the different protonation states were observed in pure chloroform for Na-Ir(tmBBI) (dotted), upon the addition of aqueous HCl [for Ir(tmBBI)-H, solid line] and aqueous HPF_6 [for Ir(tmBBI)-H_2, dash-dot].

As the UV/Vis spectra of the Ir^{III} bibenzimidazole complexes are not affected significantly by the protonation state, we focus on the protonation-state-related changes in the emission spectra. During this investigation, it became apparent that the protonation state of the bibenzimidazole ligand is strongly dependent on the solvent used. In most protic and aprotic solvents (e.g., methanol, acetonitrile, tetrahydrofuran), the partial deprotonation of Ir(tmBBI)-H_2 occurred. The solvent dependency of the photophysical properties of this complex is indicative of emission from MLCT excited states.[45] Finally, the protonation state is unaffected in chloroform; thus, this solvent was applied for the photophysical measurements.

The emission behavior changed significantly upon deprotonation. All three protonation steps show a structured emission band, indicative of an emissive excited state with mixed MLCT and π–π* intraligand (IL) character, as is frequently observed for cyclometalated Ir complexes and recently reported for an iridium biimidazole complex.[10,38,46–48] The doubly protonated complex Ir(tmBBI)-H_2 shows a structured emission band with two clear maxima (λ = 521 and 559 nm) and one shoulder at $\lambda \approx$ 612 nm, which can be completely regenerated from the deprotonated forms Ir(tmBBI)-H_x (x = 0, 1) in solution upon the addition of aqueous HPF_6, a procedure that has been successful with structurally related ruthenium complexes.[8] Upon single deprotonation, the emission is shifted hypsochromically with a slight decrease of the luminescence intensity. Again, the emission consists of two maxima (λ = 508 and 548 nm, the right is one flattened) and one shoulder at λ = 589 nm. Moreover, the emission of the completely deprotonated complex is shifted further into the blue region and only consists of one distinct maximum (λ = 494 nm) and a tapered shoulder (λ = 519 nm).

The most attractive and astonishing feature of this bibenzimidazole complex is that it does not lose its emission during deprotonation. Furthermore, the intensity increases after twofold deprotonation. This is in contrast to the emission of the ruthenium complexes, for which the luminescence decreases during deprotonation and disappears for

 © 2015 Wiley-VCH Verlag GmbH & Co. KGaA, Weinheim

the fully deprotonated form.[1] Deprotonation is a significant deactivation pathway for these complexes and, therefore, limits their value for photochemical applications.

A comparison of Ir(tmBBI)-H_x with the recently presented biimidazole complex $[(Me\text{-}ppy)_2Ir(biimH_2)]^+$ (**R1**) from Wenger and co-workers is interesting.[10] Both systems show similar absorption properties in the wavelength region above 380 nm, and the main contribution originates from a mixed $d\pi \rightarrow \pi^*_{ppy}$ ^{1}MLCT and ligand-centered $\pi \rightarrow \pi^*$ (LC) transition of the ppy ligand. However, a big difference in the range λ = 300–380 nm can be seen. Although the electronic transitions of the bibenzimidazole ligand of Ir(tmBBI)-H_x are clearly visible and lead to an intense absorption band, this contribution is negligible for the biimidazole complex **R1**. A further remarkable difference can be seen in the emission properties of both complexes upon deprotonation, after which inverse behavior is observed. The deprotonation of Ir(tmBBI)-H_x leads to a hypsochromic shift, whereas a shift into the blue is observed for **R1**. In general, the emission range of this type of iridium complexes strongly depends on the type and the functionalization of the ligands used.[49]

A pronounced difference in the photophysical behavior of ruthenium and iridium complexes can be seen in the emission properties of the mononuclear complex and the dinuclear compound Ir(tmBBI)Ir. Both the position and the shape of the emission and absorption spectra of the dinuclear complex exhibit features observed in the twofold-deprotonated Na-Ir(tmBBI) and the partially deprotonated Ir(tmBBI)-H. The absorption spectra of the dinuclear and mononuclear complexes are similar in terms of their shape in the visible region, but the emission of Ir(tmBBI)Ir is twice as intense as that of Ir(tmBBI)-H_2; therefor, the intensity corresponds with the number of independent iridium metal cores (see Figure 7). Similar results were reported by Cai and co-workers.[15]

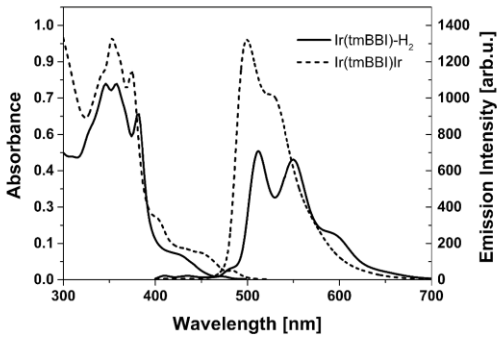

Figure 7. Photophysical properties of Ir(tmBBI)-H_2 (solid) and Ir(tmBBI)Ir (mixture of *rac* and *meso*, dashed) in chloroform ($c = 5 \times 10^{-6}$ M).

In the absorption spectra, a shoulder is observed at $\lambda \approx$ 450 nm, which is bathochromically shifted compared to that of Ir(tmBBI)-H_2 because the two iridium centers withdraw electron density from the BBI ligand and, thus, facilitate a transition into the π^* orbital. Furthermore, a small peak that indicates a protonated state of Ir(tmBBI)-H_x (x = 1, 2) arises at $\lambda \approx$ 374 nm but is slightly shifted hypsochromically (4 nm) owing to the influence of both iridium centers.

Regarding the emission of the complexes in Figure 7, both display vibronically structured emission bands with similar shapes, but the intensity of Ir(tmBBI)Ir is approximately twice that of Ir(tmBBI)-H_2 at identical concentration (Figure 7). This is in good agreement with the expectation for the introduction of a second iridium center. The shape of the emission spectrum resembles that of Na-Ir(tmBBI), but the position of the peak is shifted slightly bathochromically to λ = 499 nm with a tapped shoulder at 524 nm. This change in maximum emission indicates that the formation of the dinuclear complexes exerts an influence on the energy of the emissive states. Compared to the results for the dinuclear ruthenium complexes, for which significant luminescence quenching occurs, the high emission intensity of the iridium(III) dinuclear complex is a significant advantage regarding its range of applications such as its use as a photocenter in photocatalytic reactions.[15]

To elucidate more details about the luminescence properties of the fully protonated complex Ir(tmBBI)-H_2, the fully deprotonated complex Na-Ir(tmBBI), and the dinuclear complex Ir(tmBBI)Ir, time-resolved emission studies with a streak camera were performed. The excited-state lifetimes for all three complexes are ca. 50 ns in oxygen-equilibrated chloroform solutions and, thus, are very similar to the lifetimes previously observed for other cyclometalated iridium complexes.[24,34–36,38,39,50,51] This again contrasts with the behavior observed for the related ruthenium complexes, for which the respective dinuclear species consistently show significantly shorter lifetimes than those of their mononuclear counterparts (see Table 3). For the fully protonated complex Ir(tmBBI)-H_2, a second emission with a lifetime of 329 ns is observed. The time profile of the emission spectra for Ir(tmBBI)-H_2 is very intriguing. In contrast to the spectra of the other two complexes, a pronounced shoulder is visible in the blue part of the spectrum for short decay times with a maximum at $\lambda \approx$ 488 nm. A broad spectrum with two maxima at λ = 518 and 558 nm appears at longer delay times, and the high-energy feature vanishes (Figures 8 and 9). These low-energy features are not observable for the dinuclear complex or the deprotonated complex. Clearly, a far more complicated photochemical behavior is apparent for Ir(tmBBI)-H_2.

Table 3. Photochemical data of the investigated iridium complexes and two related ruthenium compounds.[1]

	Solvent[a]	Absorption λ_{max} [nm]	Emission λ_{max} [nm]	Lifetime [ns]
Ir(tmBBI)-H_2^+	$CHCl_3$	378	521/559	44 (329)
Na-Ir(tmBBI)	$CHCl_3$	377	494	57
Ir(tmBBI)Ir	$CHCl_3$	375	499	50
$[(*bpy)_2]_2$RuBBI	CH_3CN	510/510	700/500	50/60
$(*bpy)_2$Ru(BBI-H_2)	CH_3CN	473	648	120

[a] Air-equilibrated.

 © 2015 Wiley-VCH Verlag GmbH & Co. KGaA, Weinheim

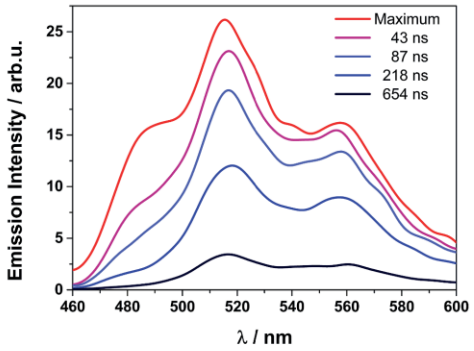

Figure 8. Smoothed time-resolved emission spectra of Ir(tmBBI)-H_2 at different delay times (see Experimental Section and Supporting Information).

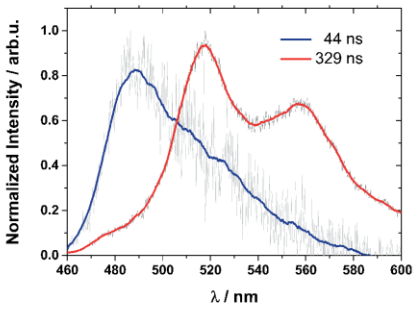

Figure 9. Individual emission spectra of Ir(tmBBI)-H_2 (raw data: grey tones, the colored curves are smoothed; see Experimental Section for details) with respective lifetimes obtained from a global fit of the two-dimensional streak camera dataset.

Conclusions

To the best of our knowledge, this work represents the first crystallographic investigation of the supramolecular aspects of an iridium bibenzimidazole complex. The nature of the hydrogen-bonding activity of iridium bibenzimidazole complexes can be reversed from donor to acceptor by deprotonation of the secondary amine function.

The dependency of the principal photophysics of iridium(III) bibenzimidazole complexes on the protonation state was investigated. The mononuclear complex Ir(tmBBI)-H_x (x = 0, 1, 2) is luminescent in all three of its protonation states, and its emission is very sensitive owing to the mostly unstable protonation state. This is in contrast to ruthenium(II) bibenzimidazole complexes, for which deprotonation leads to the complete quenching of the emission. Furthermore, the emission color can be tuned from yellow to green by successively deprotonating the complex; therefore, a varied emission region between 494 and 700 nm is possible. This luminescent character renders this complex a convenient candidate for applications in photocatalysis, organic light-emitting diode (OLED) technology (e.g., as a chromophore), and even in anion sensing.[5–7,14–16] Preliminary time-resolved emission investigations showed the expected complex behavior for the Ir(tmBBI)-H_2 chromophore. Here, a short-lived high-energy emitting state progresses to a long-lived lower-energy excited state. This behavior has not been observed for the fully deprotonated complex or the dinuclear complex.

The deprotonated complex Na-Ir(tmBBI) represents a very reactive metalloligand, and the introduction of a second metal core is possible. By using two-dimensional NMR spectroscopy, it was also possible to prove that two diastereomeric forms of the homodinuclear complexes exist [Ir(tmBBI)Ir *meso* and Ir(tmBBI)Ir *rac*] and can be separated.

The crystal structure of the dinuclear Ir(tmBBI)Ir (*meso* form) was presented and compared with those of the mononuclear Ir(tmBBI)-H and three reference compounds.

Furthermore, Ir(tmBBI)Ir is highly luminescent, in contrast to its homdinuclear ruthenium analogue, for which luminescence quenching occurs.

Experimental Section

Reactants and Methods: 4,4′,5,5′-Tetramethyl-2,2′-bibenzimidazole (**2**) and tetrakis(2-phenylpyridine-C^2,N)bis(μ-chloro)diiridium(III) (**1**) were synthesized according to published procedures.[52–54]

Technical-grade solvents were purchased from VWR/Prolabo and redistilled under reduced pressure at 40 °C. Spectroscopic-grade methanol, dichloromethane, chloroform, and acetonitrile for spectroscopic measurements were purchased from Roth. All chemicals were purchased from Merck Millipore, Sigma–Aldrich, ABCR, Acros Organics, Alfa Aesar, or VWR/Prolabo and used as purchased (≥95%). Inert reactions were performed under an Argon 4.6 atmosphere by standard Schlenk techniques. Microwave-assisted syntheses were performed with a MLS START 1500 instrument. Size-exclusion chromatography was performed with Sephadex LH-20 (purchased from Pharmacia Fine Chemicals AB, Uppsala, Sweden) as the stationary phase (particle size 25–100 μm). The ^{1}H NMR spectra were recorded at ambient temperature unless otherwise stated with Bruker 400 and 500 MHz spectrometers. All spectra were referenced to the corresponding solvent residual signals (i.e., δ = 1.940 ppm for acetonitrile, 7.260 ppm for chloroform, 5.320 ppm for dichloromethane, and 4.870 ppm for methanol). Mass spectra were recorded with Finnigan MAT SSQ 710 and Thermoquest-Finnigan MAT 95XL instruments. Elemental analysis was performed with an Elementar vario MICRO cube analyzer.

The intensity data for Ir(tmBBI)Ir were collected with a Bruker-Nonius Kappa CCD diffractometer by using graphite-monochromated Mo-K_α radiation (λ = 0.71073 Å). The intensity data for Ir(tmBBI)-H were collected with an Oxford Diffraction Supernova dual source diffractometer with a CCD detector by using Cu-K_α radiation (λ = 1.54178 Å). The data were corrected for Lorentz and polarization effects, and a semi-empirical absorption correction based on multiple scans was applied with SADABS.[56] The struc-

 © 2015 Wiley-VCH Verlag GmbH & Co. KGaA, Weinheim

tures were solved by direct methods (SHELXS2013)[55] and refined by full-matrix least-squares techniques against F_o^2 (SHELXL-2013).[55] All hydrogen atoms were placed in positions of optimized geometry. Mercury 3.3 (Build RC5) was used for structure representations.

The two-dimensional (time and wavelength) emission decay profiles were measured by using a Hamamatsu C4334 streak scope in time-correlated single-photon counting (TCSPC) mode with a time window of 200 ns for the deprotonated (and dinuclear) complex and 1000 ns for the doubly protonated complex. After excitation with the frequency-doubled output of a Ti–sapphire laser (Tsunami, Newport Spectra-Physics GmbH; pulse-to-pulse repetition rate 400 kHz after passing a pulse selector, model 3980, Newport Spectra-Physics GmbH) at λ_{ex} = 405 nm, the luminescence of the sample was collected in a 90°-arrangement, sent through a polarizer set to the magic angle (54.7° relative to the polarization of the excitation pulses), and spectrally dispersed by using a Chromex 250IS imaging spectrograph. The samples were prepared to yield an optical density of 0.1 at the excitation wavelength in a 1 cm quartz cuvette. Global fitting was performed with Scilab.[57] The fits were performed numerically with the convolution included with a Gaussian response function. To properly treat the data recorded for Ir(tmBBI)-H_2, a split ratio was introduced to distribute the initial population of independently decaying species to a parallel kinetic scheme. For better visualization, the transient emission spectra were first averaged over 17 data points (corresponding to ca. 33 ns for the 1000 ns time window and ca. 6.6 ns for the 200 ns time window) and then smoothed by using a 20 point fast Fourier transform (FFT) filter (cutoff frequency ca. 0.11). The individual emission spectra obtained from the global fit were smoothed by calculating the 50 or 20 point rolling average.

[(ppy)$_2$Ir(tmBBI-H$_2$)][PF$_6$] (Ir(tmBBI)-H$_2$): All reactions were performed under inert conditions unless explicitly stated. Formic acid (1 mL) was added to a suspension of **2** (230 mg, 0.21 mmol) and **1** (140 mg, 0.47 mmol) in degassed ethanol and water (5:2), and the mixture was heated to reflux at 115 °C for 24 h. The solution was filtered and concentrated in vacuo, and a solution of NH_4PF_6 (163 mg, 1 mmol) in water (5 mL) was added to precipitate the complex as its hexafluorophosphate salt. The yellowish precipitate was washed with water and ether and purified by size-exclusion chromatography [Sephadex, eluent: chloroform, acetone, methanol (47:30:23)]. The solvent of the product fraction was removed under reduced pressure. The salt was redissolved in ethanol, and a solution of NH_4PF_6 in water was added to precipitate the desired complex; yield 301 mg (76.6%). ^{1}H NMR (DMSO, 400 MHz, 298 K): δ = 8.17 (d, ^3J = 8.1 Hz, 2 H, 6-H), 7.92 (d, ^3J = 7.8 Hz, 2 H, 6′-H), 7.85–7.79 (m, 2 H, 5-H), 7.69 (d, ^3J = 5.7 Hz, 2 H, 3-H), 7.56 (s, 2 H, 7′′-H), 7.15–7.07 (m, 4 H, 4-H, 4′-H), 6.95 (m, 2 H, 5′-H), 6.43 (d, ^3J = 7.5 Hz, 2 H, 3′-H), 5.76 (s, 2 H, 4′′-H), 2.25 (s, 6 H, 9′′-H), 1.94 (s, 6 H, 8′′-H) ppm. ^{13}C{^{1}H} NMR (DMSO, 500 MHz, 298 K): δ = 167.89 (C-2), 149.81 (C-3), 145.72 (C-1′), 139.53 (C-11′′), 138.35 (C-5), 134.73 (C-10′′), 132.62 (C-6′′), 132.95 (C-5′′), 129.45 (C-5′′), 138.35 (C-3′), 132.62 (C-4′), 125.00 (C-6′), 123.98 (C-4), 121.88 (C-5′), 119.74 (C-6), 116.70 (C-7′′), 20.57 (C-8′′, C-9′′) ppm. $C_{40}H_{34}F_6IrN_6P$ (935.93): calcd. C 51.33, H 3.66, N 8.98; found C 50.98, H 4.30, N 8.67. MS (EI): *m/z* = 790 [M – H]$^+$, 501 [(ppy)$_2$Ir]$^+$. Crystals suitable for single-crystal X-ray analysis were obtained by the slow diffusion of water into a dimethyl sulfoxide solution. Crystal Data for [(ppy)$_2$Ir(tmBBI-H)]·2 H_2O·2C_2H_6SO: $C_{44}H_{49}IrN_6O_4S_2$, M_r = 982.21 g mol^{-1}, yellow plate, crystal size 0.1358 × 0.581 × 0.0147 mm, monoclinic, space group $P2_1/n$, a = 11.1899(2) Å, b = 26.1338(4) Å, c = 15.4298(3) Å, β = 107.990(2)°, V = 4291.61(14) Å^3, T = 180(2) K, Z = 4, $\rho_{calcd.}$ = 1.520 Mg/m^3, μ(Cu-K_α) = 7.324 cm^{-1}, F(000) = 1984, 24850 reflections up to h(–13/13), k(–27/32), l(–19/15) measured in the range 7.421 ≤ Θ ≤ 74.493°, completeness Θ_{max} = 99.7%, 8307 independent reflections, R_{int} = 0.0477, 6777 reflections with $F_o > 4\sigma(F_o)$, 538 parameters, 78 restraints, $R1_{obs}$ = 0.0723, wR_{2obs} = 0.1808, R_{1all} = 0.0871, wR_{2all} = 0.1911, GooF = 1.126, largest difference peak and hole: 4.567/–1.600 e/Å^{-3}. Restraints had to be applied to stabilize the geometry and thermal ellipsoids of the DMSO molecules. A well-defined electron-density maximum indicated the position of the amine proton in the hydrogen-bond framework, and the respective proton was added through the appropriate HFIX command in accordance with the neutral charge of the complex and the adjacent hydrogen-bond framework.

[(ppy)$_2$Ir(tmBBI)]Na [Na-Ir(tmBBI)]: A highly concentrated aqueous sodium hydroxide solution (30 mL) was added to a solution of Ir(tmBBI)-H_2 (50 mg, 0.06 mmol) in methanol (30 mL). The desired product complex immediately precipitated as its sodium salt. The mixture was stirred for 24 h, and the resulting precipitate was collected by filtration, washed with water and ether, and dried in vacuo, yield 45 mg (0.055 mmol, 96.4%). ^{1}H NMR (DMSO, 400 MHz, 298 K): δ = 8.06 (d, ^3J = 8.0 Hz, 2 H, 6-H), 7.83 (d, ^3J = 7.7 Hz, 2 H, 6′-H), 7.69–7.65 (m, 4 H, 5-H, 3-H), 7.16 (s, 2 H, 7′′-H), 7.00–6.87 (m, 4 H, 4-H, 4′-H), 6.87–6.85 (m, 2 H, 5′-H), 6.46 (d, ^3J = 7.5 Hz, 2 H, 3′-H), 5.60 (s, 2 H, 4′′-H), 2.15 (s, 6 H, 9′′-H), 1.86 (s, 6 H, 8′′-H) ppm.

[{(ppy)$_2$Ir}$_2$(tmBBI)] [Ir(tmBBI)Ir]: A suspension of **1** (51.2 mg, 47.8 µmol) and **2** (13.0 mg, 44.8 µmol) in dimethylformamide (50 mL) and triethylamine (20 mL) was treated in the microwave for 60 min at 200 W. After the yellow solution cooled to room temp., the addition of water (200 mL) led to the precipitation of the desired product. Subsequently, the product was collected by filtration, washed with water and diethyl ether, and purified by size-exclusion chromatography (Sephadex, eluent: chloroform, acetone, methanol 47:30:23). The two diastereomeric pairs could be separated by fractioned crystallization, yield 24.5 mg (42%). ^{1}H NMR (DMSO, 400 MHz, 298 K, *meso* form): δ = 8.07 (d, ^3J = 8.5 Hz, 4 H, 6-H), 7.94 (d, ^3J = 6.1 Hz, 4 H, 3-H), 7.81 (d, ^3J = 7.8 Hz, 4 H, 6′-H), 7.73–7.71 (m, 4 H, 5-H), 7.21–7.19 (m, 4 H, 4-H), 7.01–6.98 (m, 4 H, 4′-H), 6.90–6.87 (m, 8 H, 5′-H), 6.51 (d, ^3J = 7.7 Hz, 4 H, 3′-H), 5.66 (s, 4 H, 4′′-H), 1.83 (s, 12 H, 8′′-H) ppm. ^{1}H NMR (DMSO, 400 MHz, 298 K, *rac* form): δ = 8.12 (d, ^3J = 8.3 Hz, 4 H, 6-H), 7.83 (d, ^3J = 6.9 Hz, 4 H, 6′-H), 7.80–7.76 (m, 4 H, 5-H), 7.53 (m, ^3J = 5.9 Hz, 4 H, 3-H), 7.02–6.98 (m, 4 H, 4′-H), 6.98–6.84 (m, 8 H, 4-H, 5′-H), 6.440 (d, ^3J = 6.7 Hz, 4 H, 3′-H), 5.64 (s, 4 H, 4′′-H), 1.82 (s, 12 H, 8′′-H) ppm. ^{13}C{^{1}H} NMR (CD_2Cl_2, 100 MHz, 298 K): δ = 168.6 (C-2), 149.7 (C-3), 145.3 (C-1′), 142.5 (C-10′′), 136.1 (C-5), 132.7 (C-4), 128.9 (C-4′ and C-5′′), 123.7 (C-6′), 121.9 (C-3′), 120.8 (C-5′), 118.1 (C-6), 115.4 (C-4′′), 19.8 (C-8′′) ppm. MS (Micro-ESI, chloroform/methanol): *m/z* = 1312 [M + Na – H]$^+$, 1290 [M]$^+$. Crystals suitable for single-crystal X-ray analysis were obtained by the slow evaporation of a solution of the complex in dimethyl sulfoxide/dichloromethane/ethyl acetate. Crystal data for Ir(tmBBI)Ir: $C_{70}H_{72}Ir_2N_8O_4S_4$, M_r = 1602.00 g mol^{-1}, yellow needles, crystal size 0.20 × 0.06 × 0.05 mm, orthorhombic, space group *Pbca*, a = 22.280(5) Å, b = 10.896(2) Å, c = 26.849(5) Å, V = 6518(2) Å^3, T = 150(2) K, Z = 4, $\rho_{calcd.}$ = 1.632 Mg/m^3, μ(Mo-K_α) = 4.263 mm^{-1}, F(000) = 3192, altogether 87357 reflections to h(–28/29), k(–14/14), l(–35/35) measured in the range 3.41 ≤ Θ ≤ 27.88°, completeness Θ_{max} = 99.8%, 7760 independent reflections, R_{int} = 0.0738, 5960 reflections with $F_o > 4\sigma(F_o)$, 403 parameters, 0 restraints, R_{1obs} = 0.0268, wR_{2obs} = 0.0479, R_{1all} = 0.0459, wR_{2all} = 0.0528, GOOF = 1.033, largest difference peak and hole: 0.731/–0.655 e Å^{-3}.

 © 2015 Wiley-VCH Verlag GmbH & Co. KGaA, Weinheim

CCDC-1051673 {for [(ppy)$_2$Ir(tmBBI-H)]·2H$_2$O·2C$_2$H$_6$SO} and -1051663 [for Ir(tmBBI)Ir] contain the supplementary crystallographic data for this paper. These data can be obtained free of charge from The Cambridge Crystallographic Data Centre via www.ccdc.cam.ac.uk/data_request/cif.

Acknowledgments

Financial support by the Carl Zeiss Stiftung (D. S.), the German Federal Environmental Foundation (Deutsche Bundesstiftung Umwelt, DBU) (N. R.), the German Science Foundation (DI 1517/3-1), and the European Cooperation in Science and Technology (COST ACTION CM1202 PERSPECT-H2O) are thankfully acknowledged.

[1] S. Rau, M. Ruben, T. Büttner, C. Temme, S. Dautz, H. Görls, M. Rudolph, D. Walter, A. Brodkorb, M. Duati, C. O'Connor, J. G. Vos, *J. Chem. Soc., Dalton Trans.* **2000**, 3649–3657.
[2] D. Walther, L. Böttcher, J. Blumhoff, S. Schebesta, H. Görls, K. Schmuck, S. Rau, M. Rudolph, *Eur. J. Inorg. Chem.* **2006**, 2385–2392.
[3] D. Boinnard, P. Cassoux, V. Petrouleas, I. J. Savariault, J. Tuchagues, *Inorg. Chem.* **1990**, *29*, 4114–4122.
[4] M.-A. Haga, *Inorg. Chim. Acta* **1980**, *45*, L183–L184.
[5] Y. Cui, Y. Niu, M. Cao, K. Wang, H. Mo, Y. Zhong, B. Ye, *Inorg. Chem.* **2008**, *47*, 5616–5624.
[6] H.-J. Mo, H.-Y. Chao, B.-H. Ye, *Inorg. Chem. Commun.* **2013**, *35*, 100–103.
[7] H.-J. Mo, J.-J. Wu, Z.-P. Qiao, B.-H. Ye, *Dalton Trans.* **2012**, *41*, 7026–7036.
[8] D. Sorsche, S. Rau, *Eur. J. Inorg. Chem.* **2014**, 4244–4249.
[9] S. Rau, T. Büttner, C. Temme, M. Ruben, H. Görls, D. Walther, M. Duati, S. Fanni, J. G. Vos, *Inorg. Chem.* **2000**, *39*, 1621–1624.
[10] J. C. Freys, G. Bernardinelli, O. S. Wenger, *Chem. Commun.* **2008**, 4267–4269.
[11] B. Dietzek, W. Kiefer, J. Blumhoff, L. Böttcher, S. Rau, D. Walther, U. Uhlemann, M. Schmitt, J. Popp, *Chem. Eur. J.* **2006**, *12*, 5105–5115.
[12] C. Kuhnt, M. Karnahl, S. Rau, M. Schmitt, B. Dietzek, J. Popp, *Chem. Phys. Lett.* **2011**, *516*, 45–50.
[13] S. Soman, G. Singh Bindra, A. Paul, R. Groarke, J. C. Manton, F. M. Connaughton, M. Schulz, D. Dini, C. Long, M. T. Pryce, J. G. Vos, *Dalton Trans.* **2012**, 12678–12680 .
[14] Y.-J. Yuan, Z.-T. Yu, J.-G. Cai, C. Zheng, W. Huang, Z.-G. Zou, *ChemSusChem* **2013**, *6*, 1357–1365.
[15] J. Cai, Z. Yu, Y. Yuan, F. Li, Z. Zou, *ACS Catal.* **2014**, *4*, 1953–1963.
[16] Y.-J. Yuan, Z.-T. Yu, H.-L. Gao, Z.-G. Zou, C. Zheng, W. Huang, *Chem. Eur. J.* **2013**, *19*, 6340–6349.
[17] J. I. Goldsmith, W. R. Hudson, M. S. Lowry, T. H. Anderson, S. Bernhard, *J. Am. Chem. Soc.* **2005**, *127*, 7502–7510.
[18] M. B. F. Gärtner, D. Cozzula, S. Losse, A. Boddien, G. Anilkumar, H. Junge, T. Schulz, N. Marquet, A. Spannenberg, S. Gladiali, M. Beller, *Chem. Eur. J.* **2011**, *17*, 6998–7006 .
[19] O. S. Wenger, *Acc. Chem. Res.* **2013**, *46*, 1517–1526.
[20] M. Nonoyama, *Bull. Chem. Soc. Jpn.* **1974**, *47*, 767–768.
[21] H. Masa-aki, A. M. Bond, *Inorg. Chem.* **1991**, *30*, 475–480.
[22] S. Rau, L. Böttcher, S. Schebesta, M. Stollenz, H. Görls, D. Walther, *Eur. J. Org. Chem.* **2002**, 2800–2809.
[23] K. Monczak, K. Peuntinger, D. Sorsche, F. W. Heinemann, D. M. Guldi, S. Rau, *Chem. Eur. J.* **2014**, *20*, 15426–15433.
[24] L. Flamigni, A. Barbieri, C. Sabatini, B. Ventura, F. Barigelletti, *Top. Curr. Chem.* **2007**, *281*, 143–203.
[25] Y. Yasui, D. K. Frantz, J. S. Siegel, *Org. Lett.* **2006**, *8*, 4989–4992.
[26] D. K. Frantz, A. Sullivan, Y. Yasui, A. Linden, K. K. Baldridge, J. S. Siegel, *Org. Biomol. Chem.* **2009**, *7*, 2347–52.
[27] S. Rau, B. Schäfer, A. Grüßing, S. Schebesta, K. Lamm, J. Vieth, H. Görls, D. Walter, M. Rudolph, U. W. Grummt, E. Birkner, *Inorg. Chim. Acta* **2004**, 4496–4503 .
[28] N. Rockstroh, K. Peuntinger, H. Görls, D. M. Guldi, F. W. Heinemann, B. Schäfer, S. Rau, *Z. Naturforsch. B* **2010**, *65*, 281–290.
[29] K. Halbauer, A. Göbel, A. Sterzik, H. Görls, S. Rau, W. Imhof, *Eur. J. Inorg. Chem.* **2007**, 1508–1514.
[30] A. Grüßing, S. Rau, S. Schebesta, A. Scholz, H. Görls, D. Walther, *Z. Anorg. Allg. Chem.* **2007**, 961–970.
[31] M.-A. Haga, *Inorg. Chim. Acta* **1983**, *77*, L39–L41.
[32] M. Haga, T. Matsumura-Inoue, S. Yamabe, *Inorg. Chem.* **1987**, *26*, 4148–4154.
[33] L. Donato, C. E. McCusker, F. N. Castellano, E. Zysman-Colman, *Inorg. Chem.* **2013**, *52*, 8495–8504.
[34] R. D. Costa, G. Fernández, L. Sánchez, N. Martín, E. Ortí, H. J. Bolink, *Chem. Eur. J.* **2010**, *16*, 9855–9863.
[35] E. A. Plummer, J. W. Hofstraat, L. De Cola, *Dalton Trans.* **2003**, 2080–2084.
[36] A. Tsuboyama, T. Takiguchi, S. Okada, M. Osawa, M. Hoshino, K. Ueno, *Dalton Trans.* **2004**, 1115–1116.
[37] S. Welter, F. Lafolet, E. Cecchetto, F. Vergeer, L. De Cola, *ChemPhysChem* **2005**, *6*, 2417–2427.
[38] A. Auffrant, A. Barbieri, F. Barigelletti, J.-P. Collin, L. Flamigni, C. Sabatini, J.-P. Sauvage, *Inorg. Chem.* **2006**, *45*, 10990–10997.
[39] A. Auffrant, A. Barbieri, F. Barigelletti, J. Lacour, P. Mobian, J.-P. Collin, J.-P. Sauvage, B. Ventura, *Inorg. Chem.* **2007**, *46*, 6911–6919.
[40] M. T. Indelli, T. Bura, R. Ziessel, *Inorg. Chem.* **2013**, *52*, 2918–2926.
[41] C. E. McCusker, D. Hablot, R. Ziessel, F. N. Castellano, *Inorg. Chem.* **2012**, *51*, 7957–7959.
[42] S. Ladouceur, E. Zysman-Colman, *Eur. J. Inorg. Chem.* **2013**, 2985–3007.
[43] D. Hanss, J. C. Freys, G. Bernardinelli, O. S. Wenger, *Eur. J. Inorg. Chem.* **2009**, 4850–4859.
[44] S. Kappaun, C. Slugovc, E. J. List, *Int. J. Mol. Sci.* **2008**, *9*, 1527–1547.
[45] K. A. King, R. J. Watts, *J. Am. Chem. Soc.* **1987**, *109*, 1589–1590.
[46] M. S. Lowry, S. Bernhard, *Chem. Eur. J.* **2006**, *12*, 7970–7977.
[47] A. B. Tamayo, S. Garon, T. Sajoto, P. I. Djurovich, I. M. Tsyba, R. Bau, M. E. Thompson, *Inorg. Chem.* **2005**, *44*, 8723–8732.
[48] E. A. Plummer, W. Hofstraat, L. De Cola, *Dalton Trans.* **2003**, 2080–2084.
[49] A. F. Henwood, S. Evariste, A. M. Z. Slawin, E. Zysman-Colman, *J. Chem. Soc. Faraday Trans.* **2014**, 1–18.
[50] L. Donato, C. E. McCusker, F. N. Castellano, E. Zysman-Colman, *Inorg. Chem.* **2013**, *52*, 8495–8504.
[51] S. Welter, F. Lafolet, E. Cecchetto, F. Vergeer, L. De Cola, *ChemPhysChem* **2005**, *6*, 2417–2427.
[52] E. Müller, G. Bernardinelli, J. Reedijk, *Inorg. Chem.* **1995**, *34*, 5979–5988.
[53] B. Schmid, F. O. Garces, R. J. Watts, *Inorg. Chem.* **1994**, *33*, 9–14.
[54] F. O. Garces, K. A. King, R. J. Watts, *Inorg. Chem.* **1988**, *27*, 3464–3471.
[55] G. M. Sheldrick, *Acta Crystallogr., Sect. A* **2008**, *64*, 112–122.
[56] *SADABS*, Bruker AXS Inc., Madison, WI, **2008**.
[57] *Scilab: Free and Open Source Software for Numerical Computation* (OS, version 5.4.1), Scilab Enterprises, Versailles, France, **2012**; available through: http://www.scilab.org.

Received: March 4, 2015
Published Online: July 8, 2015

 © 2015 Wiley-VCH Verlag GmbH & Co. KGaA, Weinheim

Eur. J. Inorg. Chem. **2015** · ISSN 1099–0682

SUPPORTING INFORMATION

DOI: 10.1002/ejic.201500234
Title: Protonation-Dependent Luminescence of an Iridium(III) Bibenzimidazole Chromophore
Author(s): Sebastian A. Rommel, Dieter Sorsche, Nils Rockstroh, Frank W. Heinemann, Joachim Kübel, Maria Wächtler, Benjamin Dietzek, Sven Rau*

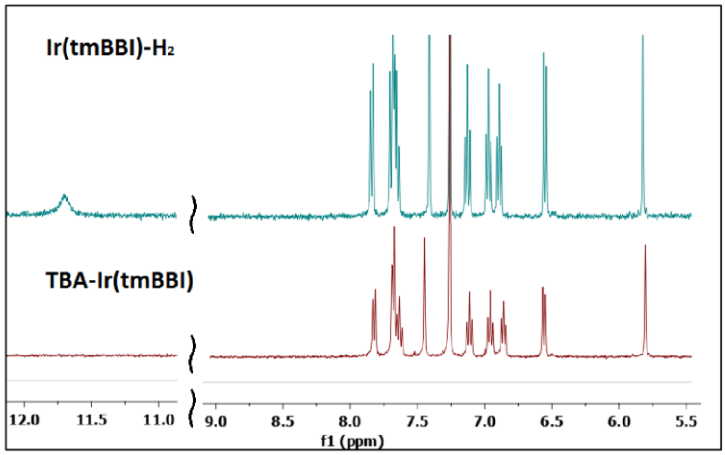

Figure 1. Effect of deprotonation on the characteristic NH signal of **Ir(tmBBI)**-H_x in the ^{1}H NMR spectrum in $CDCl_3$.

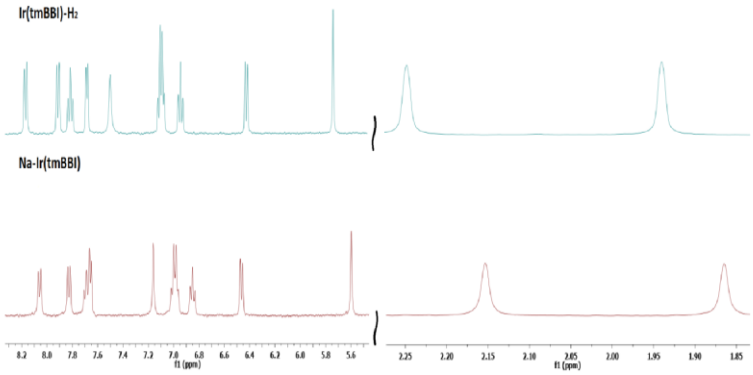

Figure 2. ^{1}H NMR of **Ir(tmBBI)**-H_2 (top) and Na-**Ir(tmBBI)** (bottom) in DMSO-d_6.

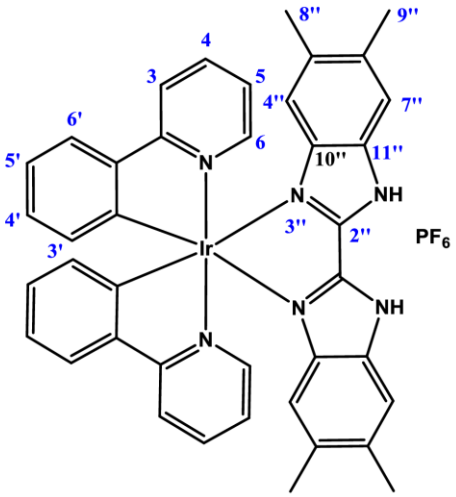

Scheme 1. Numbering scheme for the assignment of the ^{1}H NMR signals of **Ir(tmBBI)**-H_2.

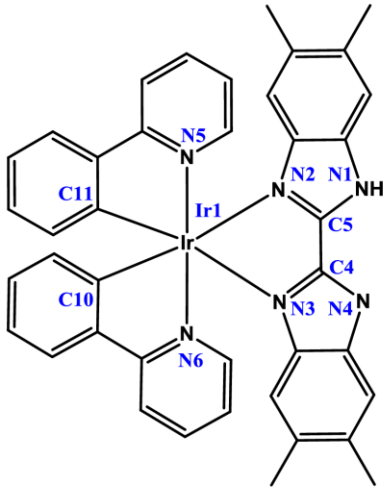

Scheme 2. Numbering scheme of the crystal structure of **Ir(tmBBI)**-H.

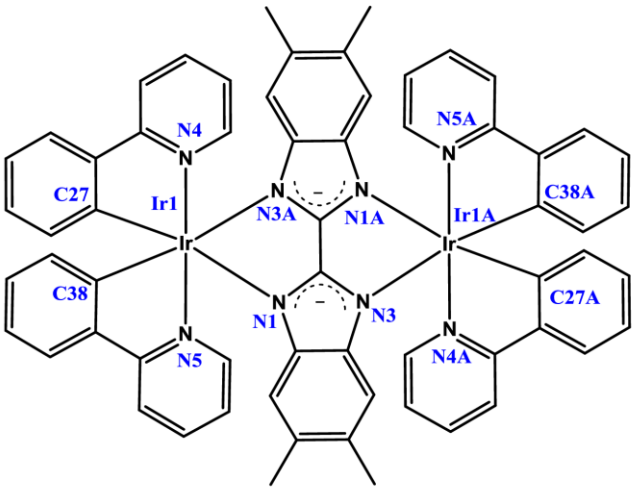

Scheme 3. Numbering scheme of the crystal structure of **Ir(tmBBI)Ir**.

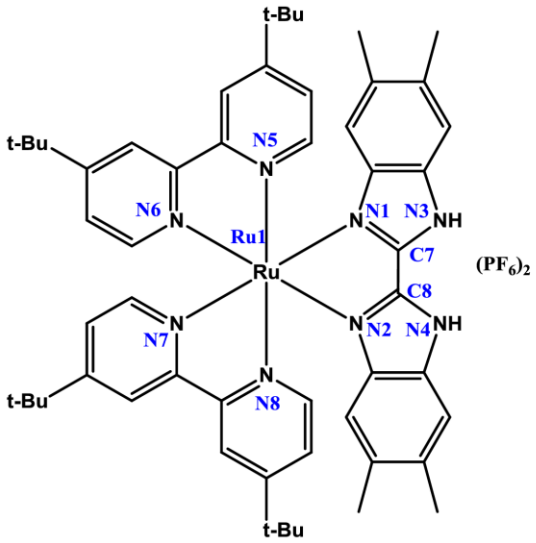

Scheme 4. Numbering scheme of the crystal structure of $[(tbbpy)_2Ru(tmBBI)][PF_6]_2$ (**R3**).

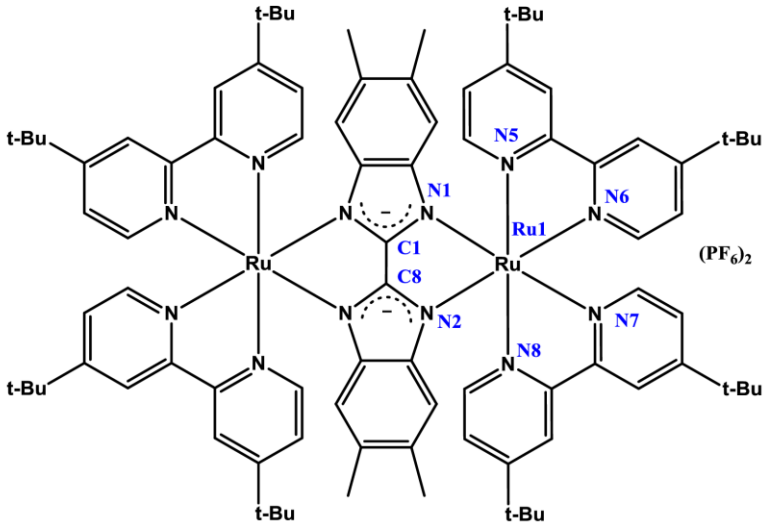

Scheme 5. Numbering scheme of the crystal structure of $[\{(tbbpy)_2Ru\}_2(\mu\text{-}tmBBI)][PF_6]_2$ (**R2**).

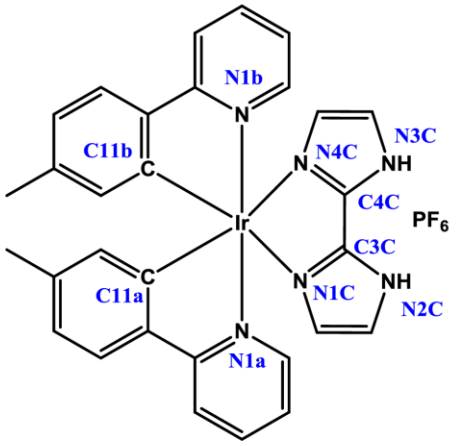

Scheme 6. Numbering scheme of the crystal structure of $[(Me\text{-}ppy)_2Ir(biimH_2)]^+$ (**R1**).

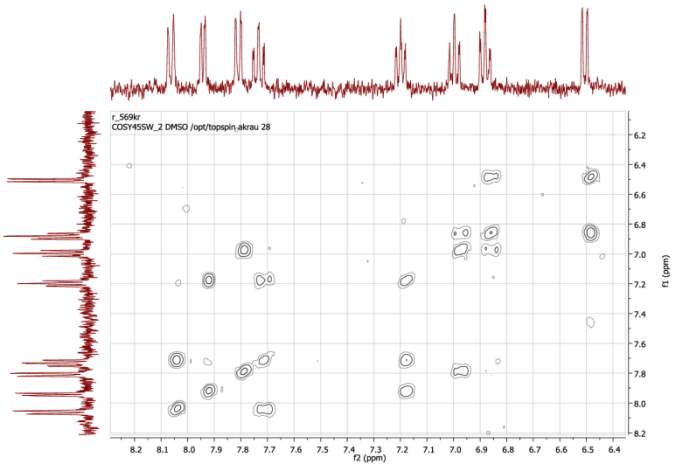

Figure 3. H,H-COSY of **Ir(tmBBI)Ir** *meso* form in DMSO-d_6.

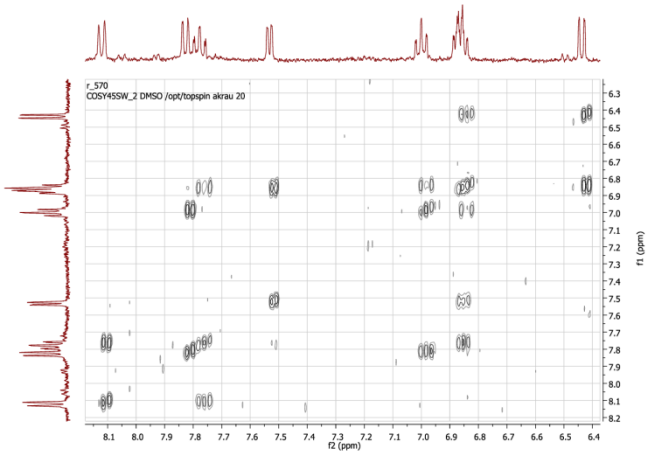

Figure 4: H,H-COSY of **Ir(tmBBI)Ir** *rac* form in DMSO-d_6.

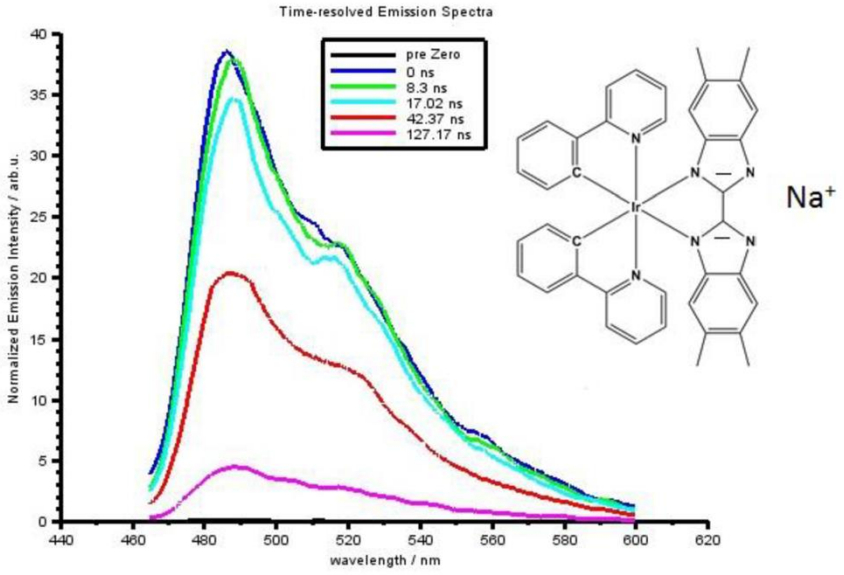

Figure 5. Time resolved emission spectra of Na- **Ir(tmBBI)** at different delay times.

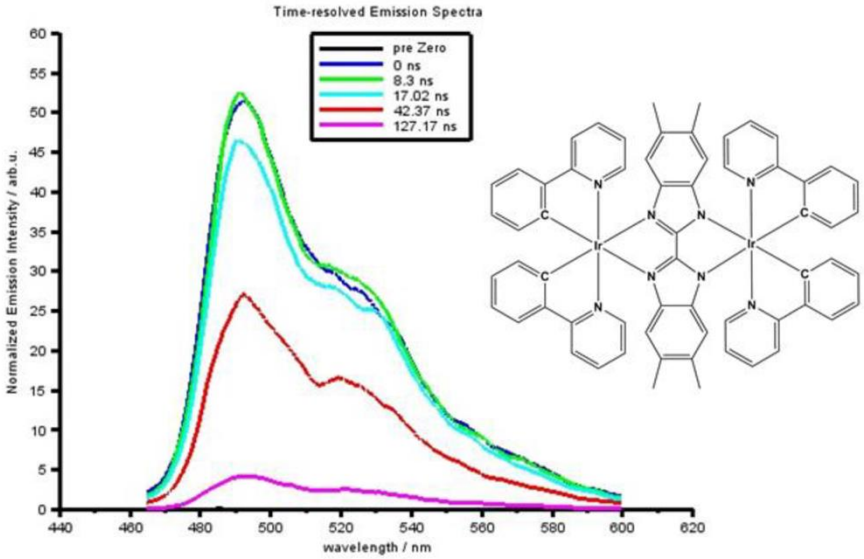

Figure 6. Time resolved emission spectra of **Ir(tmBBI)Ir** at different delay times.

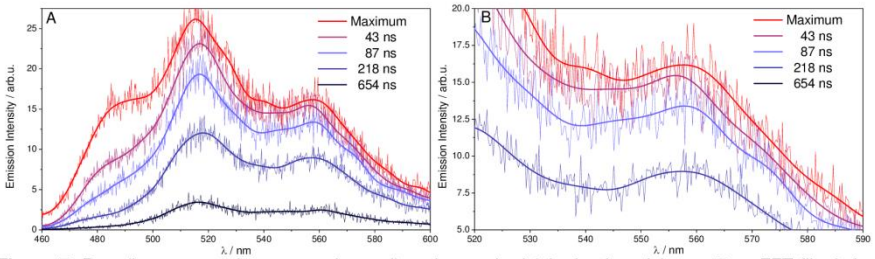

Figure 7. Raw (but averaged, see experimental) and smoothed (obtained applying a 20 pt FFT filter) time resolved emission spectra of **Ir(tmBBI)-H_2** at different delay times. Panel A and B contain the same data, but panel B provides a closer view on the local maximum at ca. 560 nm. It should be noted that the unfavorable signal-to-noise ratio causes slight shifts of the peak, particularly when looking at the 43 ns-curve. The few-nm blue-shift is likely an artifact caused by the smoothing routine.

Table S1. Crystal data and structure refinement for **Ir(tmBBI)Ir**.

Empirical formula	C70 H72 Ir2 N8 O4 S4	
Formula weight	1602.00	
Temperature	150(2) K	
Wavelength	0.71073 Å	
Crystal system	Orthorhombic	
Space group	Pbca	
Unit cell dimensions	a = 22.280(5) Å	□= 90°.
	b = 10.896(2) Å	□= 90°.
	c = 26.849(5) Å	□ = 90°.
Volume	6518(2) $Å^3$	
Z	4	
Density (calculated)	1.632 Mg/m^3	
Absorption coefficient	4.263 mm^{-1}	
F(000)	3192	
Crystal size	0.20 x 0.06 x 0.05 mm^3	
Theta range for data collection	3.41 to 27.88°.	
Index ranges	-28<=h<=29, -14<=k<=14, -35<=l<=35	
Reflections collected	87357	
Independent reflections	7760 [R(int) = 0.0738]	
Completeness to theta = 27.88°	99.8 %	
Absorption correction	Semi-empirical from equivalents	
Max. and min. transmission	0.808 and 0.483	
Refinement method	Full-matrix least-squares on F^2	
Data / restraints / parameters	7760 / 0 / 403	
Goodness-of-fit on F^2	1.033	
Final R indices [I>2sigma(I)]	R1 = 0.0268, wR2 = 0.0479	
R indices (all data)	R1 = 0.0459, wR2 = 0.0528	
Largest diff. peak and hole	0.731 and -0.655 $e·Å^{-3}$	

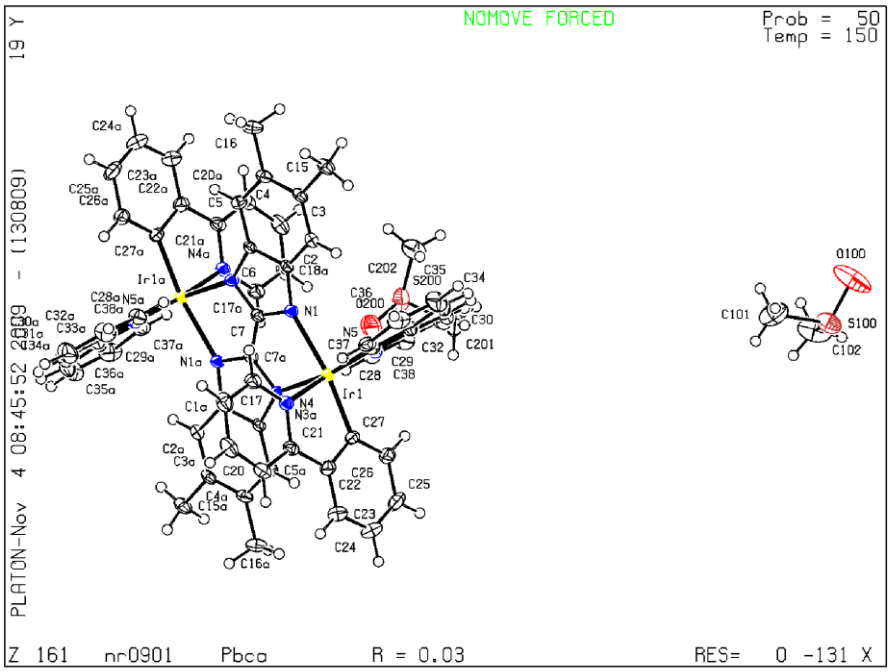

Figure 8. ORTEP depiction of Ir(tmBBI)Ir (ellipsoids at 50% probability).

Table S2. Crystal data and structure refinement for **Ir(tmBBI).**

Empirical formula	C44 H49 Ir N6 O4 S2	
Formula weight	982.21	
Temperature	180(2) K	
Wavelength	1.54178 Å	
Crystal system	Monoclinic	
Space group	P 21/n	
Unit cell dimensions	a = 11.1899(2) Å	□= 90°.
	b = 26.1338(4) Å	□= 107.990(2)°.
	c = 15.4298(3) Å	□ = 90°.
Volume	4291.61(14) $Å^3$	
Z	4	
Density (calculated)	1.520 Mg/m^3	
Absorption coefficient	7.324 mm^{-1}	
F(000)	1984	
Crystal size	0.1358 x 0.581 x 0.0147 mm^3	
Theta range for data collection	7.421 to 72.493°.	
Index ranges	-13<=h<=13, -27<=k<=32, -19<=l<=15	
Reflections collected	24850	
Independent reflections	8307 [R(int) = 0.0477]	
Completeness to theta = 67.679°	99.7 %	
Refinement method	Full-matrix least-squares on F^2	
Data / restraints / parameters	8307 / 78 / 538	
Goodness-of-fit on F^2	1.126	
Final R indices [I>2sigma(I)]	R1 = 0.0723, wR2 = 0.1808	
R indices (all data)	R1 = 0.0871, wR2 = 0.1911	
Largest diff. peak and hole	4.567 and -1.600 $e.Å^{-3}$	

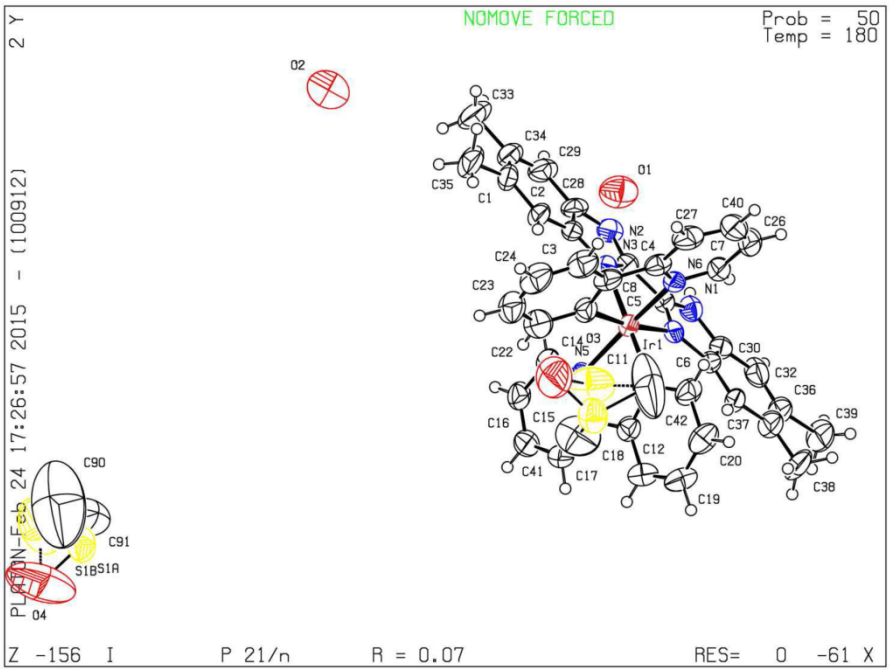

Figure 9. ORTEP depiction of Ir(tmBBI) (ellipsoids at 50% probability).

References

[1] J. C. Freys, G. Bernardinelli, O. S. Wenger, *Chem. Commun.* **2008**, 4267–4269.
[2] S. Rau, M. Ruben, T. Büttner, C. Temme, S. Dautz, H. Görls, M. Rudolph, D. Walther, A. Brodkorb, M. Duati, et al., *J. Chem. Soc. Dalt. Trans.* **2000**, 3649–3657.
[3] S. Rau, T. Büttner, C. Temme, M. Ruben, H. Görls, D. Walther, M. Duati, S. Fanni, J. G. Vos, *Inorg. Chem.* **2000**, *39*, 1621–1624.
[4] SADABS 2008/1, Bruker AXS Inc., **2008**, Madison, WI, U.S.A.
[5] G. M. Sheldrick, *Acta Cryst.* **2008**, *A64*, 112–122.

[SR2]: Interaction of an Iridium(III)- Bibenzimidazole Complex with Anions – Implications for Luminescent Sensing

Sebastian A. Rommel, Dieter Sorsche, Apoorva Dixit and Sven Rau*

* *corresponding author*

Published in: *Eur. J. Inorg. Chem.*, **2016**, 40 – 48. (DOI: 10.1002/ejic.201501108)

Copyright Reprinted from "Interaction of an Iridium(III)- Bibenzimidazole Complex with Anions – Implications for Luminescent Sensing, Sebastian A. Rommel, Dieter Sorsche,Apoorva Dixit and Sven Rau, *Eur. J. Inorg. Chem.*, **2016**, 40 – 48" with permission of the publisher John Wiley and Sons. (License Number: 3910180027115)

The iridium(III) complex $[Ir(ppy)_2(tmBBI\text{-}H_2)](PF_6)$ **(IrBBI-H$_2$) (1)** as an anion receptor has been exploited, where the cis-diamin function of the bibenzimidazole is coupled in such a way to the photophysics of the iridium metal core, that the photophysic is influenced by hydrogen bonds in the ligand periphery. Systematic studies on the system reveal that **IrBBI**-H_2 is a convenient sensor for various anions under aerobic conditions and interacts with Cl^-, Br^-, I^- and HSO_4^- via the formation of hydrogen bonds. Whereas $H_2PO_4^-$ is only capable to mono-deprotonate the **IrBBI**-H_2, it undergoes a stepwise process when F^- and OAc^- are added: formation of the mono-deprotonated complex **IrBBI**-H with a low anion concentration, followed by the double-deprotonated complex **IrBBI**$^-$, in the presence of higher anion concentration. The interaction of various anions with **IrBBI**-H_2 has been investigated *via* emission or NMR titration. According to the conditions chosen, strong binding interactions in form of a 2:1 complex : anion ratio between the less basic anions and the complex, and a virtually stoichiometric reaction to their respective ion pair was observed.

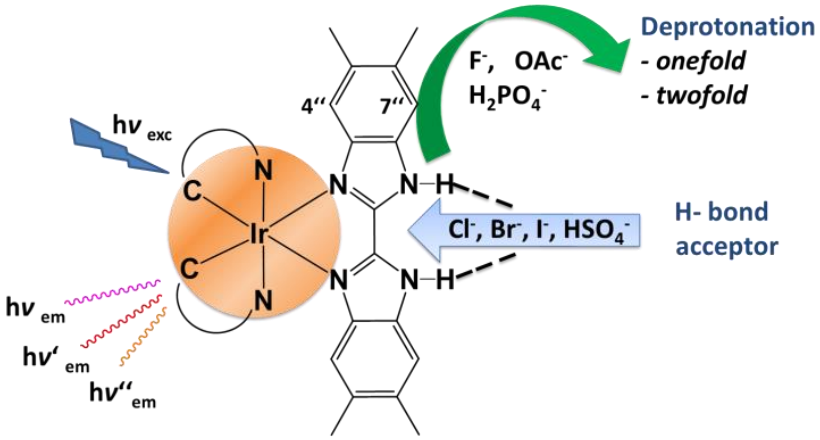

Contribution of the different authors:

Sebastian A. Rommel	Performance of photophysical characterization of the complex, ^{1}H-NMR, emission and UV/Vis titration experiments. Writing of the manuscript.
Dieter Sorsche	Discussion and revision of the manuscript, concept and results discussion.
Apoorva Dixit	Performance of the emission titration measurements, Discussion of the manuscript.
Sven Rau	Discussion and revision of the manuscript, concept and results discussion.

ChemPubSoc Europe
DOI: 10.1002/ejic.201501108
EurJIC European Journal of Inorganic Chemistry
Full Paper

Luminescent Iridium Complexes

Interaction of an Iridium(III)–Bibenzimidazole Complex with Anions – Implications for Luminescent Sensing

Sebastian A. Rommel,[a] Dieter Sorsche,[a] Apoorva Dixit,[a] and Sven Rau*[a]

Abstract: Iridium(III) complex $[Ir(ppy)_2(tmBBI\text{-}H_2)](PF_6)$ (IrBBI-H_2) has been exploited as an anion receptor. In this complex, the *cis*-diamine function of the bibenzimidazole is coupled in such a way to the photophysics of the iridium metal core that the photophysics is influenced by hydrogen bonds in the ligand periphery. Systematic studies on the complex reveal that IrBBI-H_2 is a convenient sensor for various anions under aerobic conditions and interacts with Cl^-, Br^-, I^-, and HSO_4^- by forming hydrogen bonds. Whereas $H_2PO_4^-$ is only capable of mono-deprotonating IrBBI-H_2, a stepwise process is operative when F^- and OAc^- are added: formation of the mono-deprotonated complex IrBBI-H with a low anion concentration, followed by the appearance of double-deprotonated complex $IrBBI^-$ in the presence of higher anion concentration. The interaction of various anions with IrBBI-H_2 has been investigated by emission spectroscopy or NMR titration. According to the conditions chosen, strong binding interactions in the form of a 2:1 complex/anion ratio between the less basic anions and the complex, and a virtually stoichiometric reaction to their respective ion pairs, were observed.

Introduction

There is a surge of interest in the development of specific sensor molecules that are able to act as chromogenic sensors for certain analytes.[1] Selective recognition and sensing of anions is of major interest, because anions are well known to play numerous fundamental roles in a range of chemical, biological, and environmental processes.[2] Sensor molecules should have a receptor entity, specific for a selected analyte, and also a signaling component to translate the analyte-binding-induced changes into a distinct output signal.[1] These changes can be determined by changes in ^1H NMR spectroscopic shifts, redox potentials, and/or by additional spectral investigations (e.g. fluorescence/absorption titrations). Especially analyte–receptor-binding, fluorescence-based sensors have received wider attention, as they are able to achieve high sensitivity and low analyte detection limits.[1]

Among sensor molecules that show changes in spectral properties, which are used for probing, ruthenium–polypyridyl complexes are the most widely investigated systems, because of their chemical stability, excited-state reactivity, luminescence, and redox properties.[3–5] The combination of a $Ru(bpy)_2$ (bpy = 2,2′-bipyridine) moiety and an appropriate ligand, for example, of the imidazole type, was shown to provide a signaling subunit and a binding site for anions through hydrogen bonding at the acidic amine function. When a second sphere coordination interaction takes place on an appropriate ligand, the ruthenium unit gives spectral and electrochemical responses.[1,3,6–18] Regarding these observations, many workgroups have used Ru^{II}–polypyridyl complexes as chromophores, in which functional groups such as amide, pyrrole, pyrimidine, thiourea, urea, and imidazole ligands,[2,19–21] but also other H-bond-donor functionalities, are appended and form hydrogen bonds with anions.[1,5,6,22–28]

Ye,[2,19–21,29] Rau,[30–32] and others,[33–37] for example, have used the Ru^{II}–bpy moiety as a signaling subunit and a 2,2-biimidazole-like ligand ($biimH_2$) as a binding site. The most significant feature of such compositions is that the $biimH_2$ ligand has a classic bifunctionality: the imino moieties can be coordinated to transition metal fragments in a chelating mode, and the amino groups are proved to form twofold hydrogen bonds with various anions, initially as second-sphere coordination. Recent studies on imidazole-type ruthenium–polypyridyl complexes indicate that the optical absorption and emission properties, as well as the redox potential of those complexes, depend directly on the protonation state of the $biimH_2$ ligand.[2,19–21,29–31,38,39] The three different protonation states of these ligands ($biimH_x$, x = 0, 1, 2) are controlled by several factors: (1) the acidity of the metalloreceptor, (2) the basicity of the distinct anions, and (3) the strength and steric demand of the hydrogen bonding, which should be related to the charge and interaction between the hydrogen-bond-donor and -acceptor groups.[2] Ye and coworkers showed that this feature is of pivotal importance and provides an effective spectroscopic and electrochemical handle for the direct observation of the interaction of anionic species.[2,19–21,29] Investigations with various anions and ruthenium–bibenzimidazole-type complexes revealed that the more basic anions fluoride and acetate are able to deprotonate the

[a] *Institute for Inorganic Chemistry I, Ulm University, Albert-Einstein-Allee 11, 89081 Ulm, Germany*
E-mail: sven.rau@uni-ulm.de
http://www.uni-ulm.de/nawi/nawi-anorg1
Supporting information for this article is available on the WWW under http://dx.doi.org/10.1002/ejic.201501108.

© 2016 Wiley-VCH Verlag GmbH & Co. KGaA, Weinheim

ChemPubSoc Europe
EurJIC European Journal of Inorganic Chemistry
Full Paper

BBI ligand, whereas Cl^-, Br^-, I^-, NO_3^-, HSO_4^- and $H_2PO_4^-$ can only build initial hydrogen bonds between the two N–H groups of the BBI-H_2 and themselves (Scheme 1). Therefore, imidazole-type ligands are, in principle, suitable optical sensors for the recognition of various anions.[2,19–21,29] But, to the best of our knowledge, most of the investigated systems need inert conditions, which limits their applicability. Therefore, the necessity to develop systems that can operate under aerobic conditions is obvious. In one of our recent publications, we reported the protonation-state-dependent luminescence of the complex $[Ir(ppy)_2(tmBBI\text{-}H_2)](PF_6)$ (IrBBI-H_2) (ppy = phenylpyridine): The most attractive and astonishing feature of this bibenzimidazole complex is that it does not lose its emission during deprotonation, but the intensity increases after deprotonation.[40] In principle, this feature may provide an effective spectroscopic handle for the direct observation of the interaction of the complex with various anions.

Regarding these preliminary studies, this investigation introduces a reactivity-based, visual, and fluorescence-based anion-sensing strategy with a simple iridium bibenzimidazole complex as fluorophore as a successful application of this approach. As the UV/Vis spectra of the Ir^{III} complexes of bibenzimidazoles are not affected dominantly by the protonation states of the complexes, we focus on the changes in the emission, NMR, and IR absorption spectra, which are caused by the interaction of the complex with various anions. Thereby, iridium(III) complexes of bis(phenylpyridine) have more advantageous photophysics relative to the corresponding complexes with other transition metals.

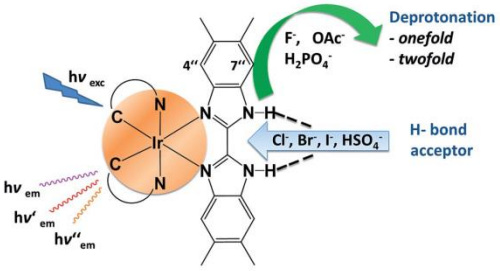

Scheme 1. Schematic representation of the interaction between IrBBI-H_2 and various anions.

Results and Discussion

Studies of Emission Spectra

To develop the design and construction strategy of a second-sphere receptor for anions, the functional complex IrBBI-H_2 was synthesized as published recently and used as a H-bond donor chromophore to investigate its interactions with several anions in solution through spectrophotometric experiments.[40]

Doubly protonated complex IrBBI-H_2 shows a structured emission band with two clear maxima and one slightly developed shoulder (Figure 1).

Upon deprotonation, the emission is not quenched, as is the case with similar ruthenium complexes, but even rises after deprotonation. A stepwise shift towards the blue region of the spectra can be observed upon deprotonation. This was further demonstrated by ^1H NMR spectroscopy, where a significant shift of certain signals could be observed.[40]

When various equivalents of different anions (F^-, OAc^-, $H_2PO_4^-$, Cl^-, Br^-, I^-, HSO_4^-) are added into a 5×10^{-6} M solution of IrBBI-H_2 in chloroform, significant shifts of the emission are induced. Cl^-, Br^-, I^-, and HSO_4^- anions only induce a moderate shift of the emission spectra in the range 6–9 nm towards the blue region and cause an increase in emission, indicating different characteristics of a strong interaction in the form of hydrogen bonds. Contrary to the behavior described upon addition of these four anions, the emission spectra are significantly blue-shifted by about 20–25 nm upon addition of 7 equiv. of F^-, OAc^-, and $H_2PO_4^-$. This phenomenon indicates predominant deprotonation of complex IrBBI-H_x (x = 0, 1, 2) by the three basic anions (Figure 1).

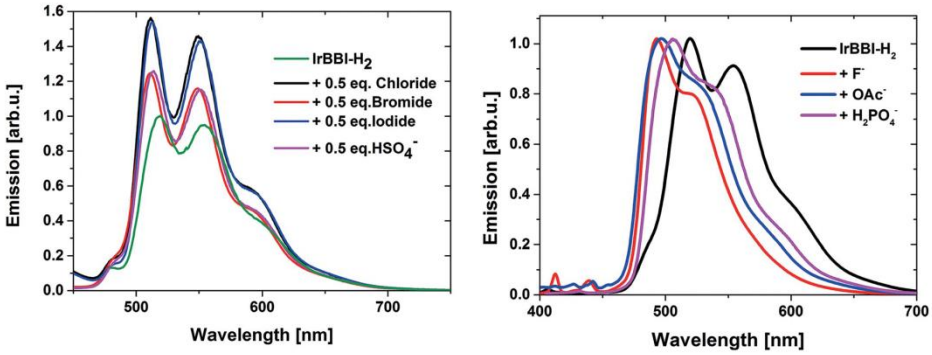

Figure 1. Emission spectra of IrBBI-H_2 in $CDCl_3$ solution (5.0×10^{-6} M); left: normalized emission with respect to the luminescence of pristine IrBBI-H_2 in order to show the relative increase in luminescence; right: all spectra are normalized with respect to the emission maximum; addition of 7 equiv. of various anions.

© 2016 Wiley-VCH Verlag GmbH & Co. KGaA, Weinheim

ChemPubSoc Europe
EurJIC European Journal of Inorganic Chemistry
Full Paper

Interaction with Fluoride

To observe the interesting behavior of IrBBI-H_2 towards fluoride, titration experiments were carried out. Figure 2a–d exhibits the complete profile of spectral displacement, the change in emission intensity of the bands at 519, 510, and 493 nm (Figure 2e) vs. fluoride concentration, and the integrated emission of the spectrum vs. the equivalents of fluoride anions added (Figure 2f). Upon addition of F^- to a solution of IrBBI-H_2, the emission spectrum is gradually blueshifted, and the emission intensity increases. After about 1 equiv. of F^-, the continuous growth reaches a maximum. Subsequently, a constant decrease and additional shift into the blue range occurs up to 2 equiv. of F^-. Thereby, the color of the solution changes from luminous yellow to a bright green, as can be seen with the naked eye (see Figure 3). After two equivalents, the loss in emission intensity is replaced by a more progressive increase, together with a further ongoing blueshift of the emission. After additional 2 equiv., the change in emission spectra stagnates, and the emission remains virtually constant. After a total of 4 equiv. of fluoride, the color of the final solution turns to a bright green. After that, no further change is visible.

The stepwise changes of the emission spectra in the titration experiment indicate that the interaction may involve a four-step process. First, up to 1 equiv. of fluoride addition to the solution of IrBBI-H_2, the stepwise increase of the emission indicates a N–H proton delocalization away from the iridium complex. This may happen in the form of initial hydrogen bonds between the N–H function and the anion and was observed with a similar iridium biimidazole complex by Wenger et al.[37] Generally, the occurrence of two equilibria according to Equations (1) and (2) is assumed.[41]

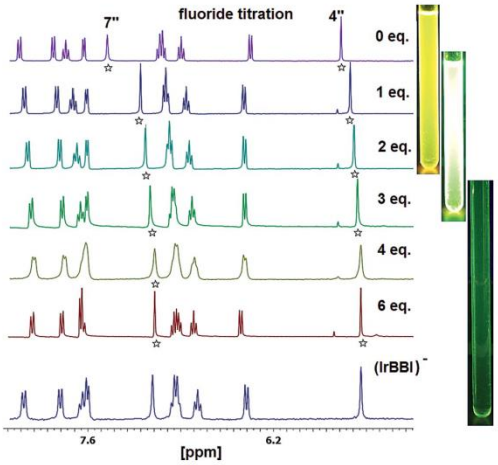

Figure 3. ^1H NMR titration of a 2.34 mM solution of IrBBI-H_2 in [D_6]DMSO with F^-. Bottom: twofold deprotonated $IrBBI^-$.

$$[IrBBI\text{-}H_2]^+ + F^- \rightleftarrows [IrBBI\text{-}H_2\cdots F] \quad (1)$$

$$[IrBBI\text{-}H_2\cdots F] + F^- \rightleftarrows [IrBBI\text{-}H] + [HF_2]^- \quad (2)$$

First, the fluoride anion forms a genuine H-bonded complex. Upon further addition of fluoride, the complex releases an HF molecule, to give the mono-protonated IrBBI-H and the self-complex $[HF_2]^-$.[41] The complete first N–H delocalization is

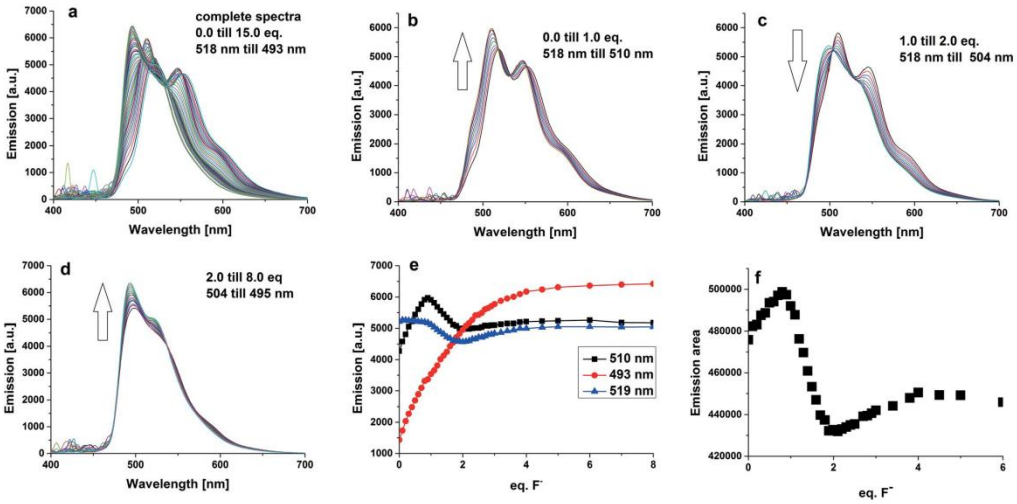

Figure 2. Emission titration of IrBBI-H_2 (5×10^{-6} M) in chloroform upon the addition of: (a) 0–15 equiv., (b) 0–1 equiv., (c) 1–2 equiv., and (d) 2–8 equiv. F^-; (e) emission intensity at 519, 510, and 493 nm vs. number of equivalents of F^-; (f) emission area vs. number of equivalents of F^-. The arrows depict the direction of the shift of the emission spectra upon successive deprotonation.

© 2016 Wiley-VCH Verlag GmbH & Co. KGaA, Weinheim

ChemPubSoc Europe
EurJIC European Journal of Inorganic Chemistry
Full Paper

reached after a total amount of 2 equiv. F^- anions. Further, upon the deprotonation process, the emission shape is significantly altered, as observed by the progressive disappearance of the bathochromic maximum of the curve. The second deprotonation process is completed after another two equivalents of fluoride anions and can be described by Equations (3) and (4), which are equal in trend to the first deprotonation of the complex.

$$[IrBBI\text{-}H] + F^- \rightleftarrows [IrBBI\text{-}H\cdots F]^- \quad (3)$$

$$[IrBBI\text{-}H\cdots F]^- + F^- \rightleftarrows [IrBBI]^+ + [HF_2]^- \quad (4)$$

According to Amendola et al., the peculiar behavior of the fluoride anions can be explained by considering the two overall neutralization equilibria given in Equations (5) and (6).[41]

$$[IrBBI\text{-}H_2]^+ + 2F^- \overset{k_1}{\rightleftarrows} [IrBBI\text{-}H] + [HF_2]^- \quad (5)$$

$$[IrBBI\text{-}H] + 2F^- \overset{k_2}{\rightleftarrows} [IrBBI]^- + [HF_2]^- \quad (6)$$

In order to visualize the deprotonation process, two different types of diagrams were created. In Figure 2e the emission intensity at three different wavelengths vs. the fluoride concentration is depicted, whereas the calculated emission area of each graph vs. $[F^-]$ can be seen in Figure 2f. Both curve shapes clearly indicate a deprotonation step after the addition of 2 and 4 equiv. of fluoride.

To identify the new species that forms upon titration of F^-, various control experiments were performed. By titration of increasing equivalents of F^-, the H signal 7″ and 4″ in the ^1H NMR spectra in $[D_6]$DMSO are progressively shifted to high field (see Figure 3, marked with a star) and remain unchanged upon addition of 4 equiv. of F^- anion. The final displacements for H7″ and H4″ are 0.29 and 0.1 ppm, respectively. The low-field proton signal H7″ is generally more sensitive towards hydrogen bonds at the N–H functions because of their spatial proximity, whereas H4″ mostly responds to the increased electron density on the bibenzimidazole ligand after deprotonation. The observed shifts are typical for a deprotonation process; they were observed for similar ruthenium complexes and recently published for the complex investigated here.[30,37,40,42] The ^1H NMR spectrum after titration of 4 equiv. of fluoride matches well with the spectrum of the twofold deprotonated complex (see Figure 3, bottom). Furthermore, the position of maxima and the shape of the emission spectra after addition of 2 or 4 equiv. fluoride resemble those of the one- and twofold deprotonated IrBBI-H_x (x = 0, 1), respectively, published recently, which demonstrates that a stepwise deprotonation process takes place.[40] Additionally, the fluoride titration was performed in $CDCl_3$, where, in contrast to measurements in $[D_6]$DMSO, the NH signal of the bibenzimidazole is visible (see Figure S4 in the Supporting Information). After titration of 1.5 equiv., the NH_{trnBBI} signal disappears already, which provides evidence for a deprotonation process.

Interaction with the Acetate and Dihydrogen Phosphate Anions

The interaction of IrBBI-H_2 with the acetate (OAc^-) anion was also examined by emission titration experiments. The curve shape obtained upon addition of OAc^- to a solution of IrBBI-H_2 in chloroform is similar to that with F^-, which indicates a stepwise twofold deprotonation. Figure 4 exhibits the complete profile of spectrum displacement (Figure 4a–d), variations in the emission intensity of the bands at 517, 511, and 499 nm (Figure 4e) vs. the number of equivalents of OAc^-, and the calcu-

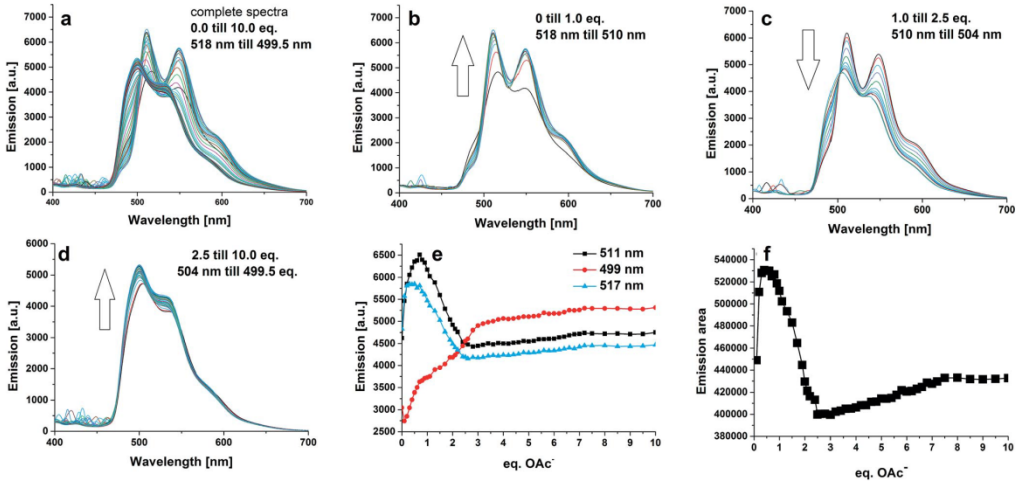

Figure 4. Emission titration of IrBBI-H_2 (5×10^{-6} M) in chloroform upon the addition of OAc^-: (a) 0–10 equiv., (b) 0–1 equiv., (c) 1–2.5 equiv., (d) 2.5–10 equiv., (e) emission intensity at 517, 511, and 499 nm vs. number of equivalents of OAc^-, (f) emission area vs. number of equivalents of OAc^-. The arrows depict the shift of the emission spectra upon successive deprotonation.

© 2016 Wiley-VCH Verlag GmbH & Co. KGaA, Weinheim

ChemPubSoc Europe
EurJIC European Journal of Inorganic Chemistry
Full Paper

lated emission area of the spectrum vs. the number of equivalents of OAc^- (Figure 4f).

When 0–2 equiv. of OAc^- were added into a solution of IrBBI-H_2, the 518 nm band (left of the spectrum) blueshifted to 510 nm, first with an increase, followed by a decrease in emission intensity (see Figure 4a,b). In this step, OAc^- formed complementary hydrogen bonds with the 2 N–H units of IrBBI-H_2, and then one proton was transferred to the OAc^-. The complete first N–H delocalization is reached after a total amount of 2 equiv. OAc^- anions, similar to the results obtained with the F^- titration. This step is defined as:

$$[IrBBI\text{-}H_2]^+ + OAc^- \rightleftarrows [IrBBI\text{-}H\cdots HOAc]^+ \xrightarrow{+\,OAc^-} [IrBBI\text{-}H] + H(OAc)_2^-$$

The continued addition of OAc^- caused a further blueshift of the band shape, which reached its maximum after 7 equiv. No further spectral changes were observed above 7 equiv. of OAc^-. The second step was the removal of the second proton from the BBI ligand. This step can be defined as:

$$[IrBBI\text{-}H] + 2OAc^- \overset{k_2}{\rightleftarrows} [IrBBI]^- + H(OAc)_2^-$$

Accordingly, the interaction of IrBBI-H_2 is primarily related to the basicity of the anion and to the consequent capability of abstracting a hydrogen atom from the H-bond donor. The second deprotonation of fluoride is a special case: Fluoride itself is a less strong base than acetate in chloroform. However, two fluoride ions behave as a strong base and exhibit a large affinity toward H^+ due to the unique stability of the H-bond complex HF_2^-.[41] Since the $H(OAc)_2^-$ dimer is less stable than the HF_2^- analogue, it takes more equivalents of OAc^- to remove the second proton of IrBBI.[2,41,43]

A strong interaction between the metalloreceptor IrBBI-H_2 and OAc^- was confirmed by ^1H NMR titration in [D_6]DMSO solution. A 2.34 mM solution of IrBBI-H_2 in [D_6]DMSO was treated with up to 8 equiv. of OAc^-. Since the N–H signals cannot be observed in [D_6]DMSO, in this case, the chemical shifts of the C–H protons in the H_2BBI ligand (H4″ and H7″) are sufficiently sensitive to the addition of the OAc^- anion, or deprotonation, respectively. The final shifts for H7″ and H4″ after 7 equiv. of acetate resemble the shifts for the fluoride titration experiment after 4 equiv. and reflect a twofold deprotonated $IrBBI^-$ (see Figure 5).

Further investigations were performed with the TBA salt of dihydrogen phosphate. Upon addition of $H_2PO_4^-$ to the solution of IrBBI-H_2, the emission shape undergoes the same transition as that with F^- and $OAc^-$with a shift of the hypsochromic band maximum from 518 to around 504 nm. This shift of 14 nm in the emission band is larger than those observed for Cl^-, Br^-, I^-, or HSO_4^- (vide infra), which indicates that the interaction of receptor IrBBI-H_x (x = 0, 1, 2) with the $H_2PO_4^-$ anion is stronger and refers to the mono-deprotonated species IrBBI-H. The complete profile of the spectral shifts can be found in the Supporting Information (see Figure S1). A strong interaction between the metalloreceptor IrBBI-H_x (x = 0, 1, 2) and the $H_2PO_4^-$ anion was also confirmed by ^1H NMR spectroscopic experiments in $CDCl_3$ solution (see Figure S2). The titration confirmed a mono-

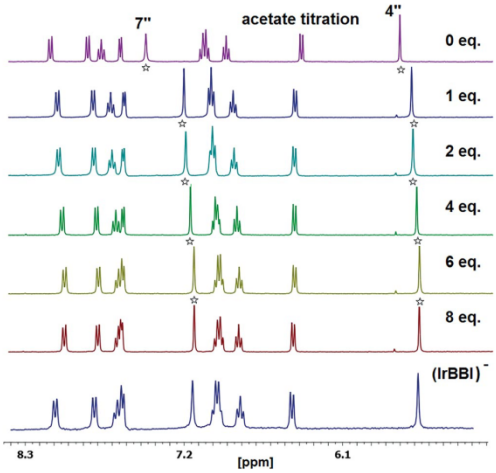

Figure 5. ^1H NMR titration of a 2.34 mM solution of IrBBI-H_2 in [D_6]DMSO with OAc^-.

deprotonation of the complex after 2 equiv. of $H_2PO_4^-$. Figure 6 depicts the ^1H NMR spectrum of the fully protonated IrBBI-H_2 and the deprotonation effect of three different anions, $H_2PO_4^-$ (mono-deprotonation of IrBBI-H_2) and F^-/OAc^- (twofold deprotonation). The main advantage of the iridium system over known sensors, especially ruthenium imidazole type complexes, is the presence of luminescence in all three protonation steps.[40] Whereas the loss of emission of ruthenium bibenzimidazole complexes upon titration with anions can be an effect of deprotonation or an oxidative quenching process, the deprotonation of IrBBI-H_2 with strong basic anions can clearly

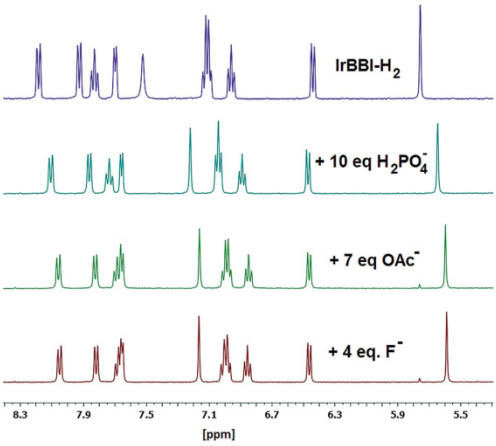

Figure 6. ^1H NMR spectra of IrBBI-H_x (x = 0, 1, 2) (2.34 mM) in [D_6]DMSO with various numbers of equivalents of TBA anion, indicating a onefold deprotonation with $H_2PO_4^-$, and a twofold deprotonation with OAc^- or F^-.

© 2016 Wiley-VCH Verlag GmbH & Co. KGaA, Weinheim

ChemPubSoc Europe
EurJIC European Journal of Inorganic Chemistry
Full Paper

be followed in the emission spectra. A further advantage is the applicability of the system under aerobic conditions, which increases its potential as a sensor system.

Action as Receptor for Cl^-, Br^-, I^-, and HSO_4^-

^{1}H NMR Spectra

During our previous investigations on the IrBBI-H_2 complex, we found that the typical N–H signal of the bibenzimidazole entity is observable in $CDCl_3$, whereas it is missing in [D_6]DMSO. However, the effect of deprotonation can be followed in [D_6]DMSO, whereas in $CDCl_3$ the shift of the ^{1}H NMR signals is much smaller. In order to show the potential of IrBBI-H_2 as an optical sensor for the recognition of various anions, ^{1}H NMR titration experiments were carried out in $CDCl_3$ and [D_6]DMSO solution. When Cl^-, Br^-, I^-, and HSO_4^- were added to a solution of IrBBI-H_2 in [D_6]DMSO, the changes in the spectra were negligible (see Figure S3), unlike the titrations with F^- and OAc^- (Figures 3 and 5), where deprotonation occurred and the titration profile was very different (vide supra). This provides evidence that deprotonation can be excluded for the less basic anions, and hence another type of interaction must take place (e.g. the formation of hydrogen bonds). To examine the nature of interaction between anions and the receptor IrBBI-H_2, we performed a standard ^{1}H NMR titration experiment in $CDCl_3$ using a start host concentration (2.34 mM) and an increasing concentration of various TBA salts (1–2 equiv.). As shown in Figure 7, the fully protonated complex IrBBI-H_2 (purple spectrum) shows a clearly visible ^{1}H NMR BBI_{N-H} signal at δ_{N-H} = 12.01 ppm in chloroform. Upon addition of 1 equiv. of either anion, the appropriate N–H signal exhibits a characteristic shift. These spectral changes indicate the formation of hydrogen bonds between the BBI_{N-H} groups and the anions.[19,34,44,45] The N–H signals exhibit significant downfield shifts as the concentration of anions is increased (see Figures 7 and 8) and reach a maximum shift upon addition of about 0.5–0.6 equiv. of anions. At this molar ratio of 2:1, the N–H proton resonance of IrBBI-H_2 shows no further shift in each titration, indicating that a 2:1 complex/anion ratio has been reached. When adding 1 equiv. TBA iodide to the solution, the smallest shift of the N–H signal up to δ_{N-H} = 13.65 ppm can be observed, which is indicative of the weakest hydrogen bond interaction. The most striking shift was observed with TBA chloride (δ_{N-H} = 14.42 ppm). We therefore assume that the strongest H-bond interaction occurs with the Cl^- anion for this series. Furthermore, a sharpening of the N–H signal can be observed, in the order $Cl^- > Br^- > HSO_4^- > I$ (Figure 7 and Figures S6–S9). In this context, the formation of hydrogen bonds between the observed anions and the BBI ligand of IrBBI-H_2 may lead to a stabilization of the BBI_{N-H} protons.[2]

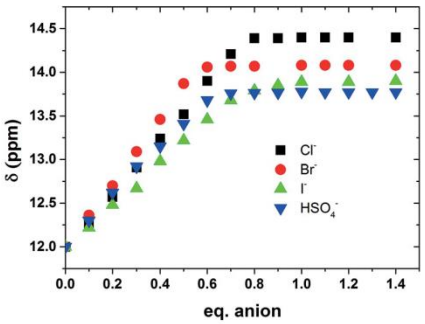

Figure 8. Chemical shift changes of the N–H signal of IrBBI-H_2 in $CDCl_3$ upon addition of various anions.

Determination of binding constants was attempted by using the WinEQNMR2 software.[46] The best fits were obtained by fitting the titration curves and the subsequent calculation to a 2:1/1:1 binding mode. This binding mode was confirmed by a ^{1}H NMR and fluorescence Job plot for all anions (see Figures S5 and S15), and with respect to the literature, it is reasonable to accept this model.[2,19–21,29,35,47] The overall binding constants

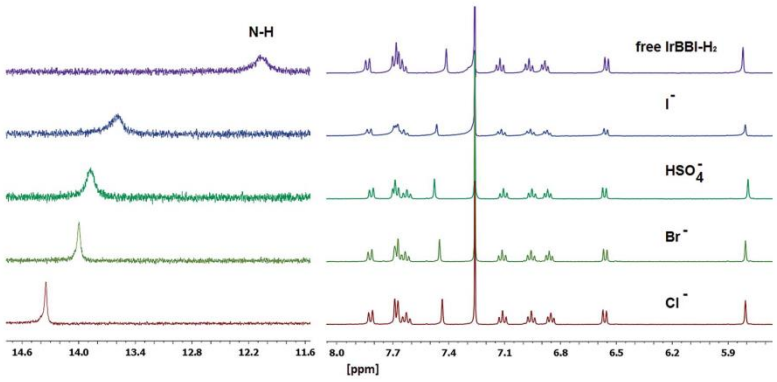

Figure 7. ^{1}H NMR spectra of IrBBI-H_2 in $CDCl_3$ in the absence and presence of 1 equiv. of anions.

© 2016 Wiley-VCH Verlag GmbH & Co. KGaA, Weinheim

ChemPubSoc Europe
EurJIC European Journal of Inorganic Chemistry
Full Paper

of IrBBI-H_2 with these four anions are in the range 10^7–10^8 M^{-1}. It has been reported that, at such strongly binding equilibria, the calculation of binding constants becomes unreliable, and accordingly, our calculations are accompanied by high error values. With respect to the almost linear shift of NMR signals until saturation, the binding of the anions might rather be described as a stoichiometric ion pair formation. Nonetheless, the values obtained from the calculations are sufficient to demonstrate the order of binding strength with the investigated ions: Cl^- > Br^- > HSO_4^- > I^-.

To the best of our knowledge, the obtained association constant values exceed all those reported so far for ruthenium-based sensors, for which a 1:1 stoichiometry is predominant. It has to be mentioned, however, that the corresponding experiments were carried out in acetonitrile, which is a more competitive solvent than chloroform.

Furthermore, the complex–anion interaction can be studied by observing the shift of the hydrogen signals H7′′ and H4′′ in the ^1H NMR spectra (see Figures S10–S14) upon addition of Cl^-, Br^-, I^-, and HSO_4^- anions to a solution of IrBBI-H_2 in $CDCl_3$. Here, H7′′ is gradually shifted downfield with a maximal shift of 0.05 ppm upon addition of up to 2.0 equiv. of HSO_4^- to IrBBI-H_2, which indicates strong interactions between IrBBI-H_2 and the various anions. The magnitude of the displacement follows the order HSO_4^- > I^- > Br^- > Cl^-, which reflects the steric demand of the respective anions and therefore interactions through space. (see the summary in Figure S14). The upfield shift of H4′′ signifies the increase in electron density in IrBBI-H_2 through binding effects. The comparatively large HSO_4^- and I^- ions can certainly interact directly with the H-7′′ as a result of their proximity to the N–H binding site of the amine moiety. This observation reveals that a modification at the 4′′ and 7′′ position of IrBBI-H_2 may influence the selectivity or hydrogen bonding capability towards different anions. This phenomenon was already investigated by Ye and co-workers with similar ruthenium complexes, where the introduction of a methyl or nitro function resulted in a considerable enhancement of the association constants.[2,19–21,29]

Studies of the Emission Spectra in the Presence of Cl^-, Br^-, I^-, and HSO_4^-

The luminescence behavior of IrBBI-H_2 toward Cl^-, Br^-, I^-, and HSO_4^- is quite different from those observed for the F^- and OAc^- anions. As depicted in Figure 9, the emission spectra show an approximate blueshift of 8 nm for all anions tested and an intensity increase of about 67 % (Cl^-), 51 % (Br^-), 24 % (HSO_4^-), and 19 % (I^-) at the maximum upon the addition of various equivalents of these anions (see Figure 10).

This maximum is reached after addition of about 0.5 equiv. of distinct anion to the complex solution. Compared to the more basic anions, for which deprotonation occurs and a further blueshift is observable, the process for the less basic anions stops at the stoichiometric ratio of 2:1 (complex/anion) and saturation behavior is observed. This standard titration is called the "molar ratio method", and together with the Job plot analysis, this is further evidence for a predominantly 2:1 complex/

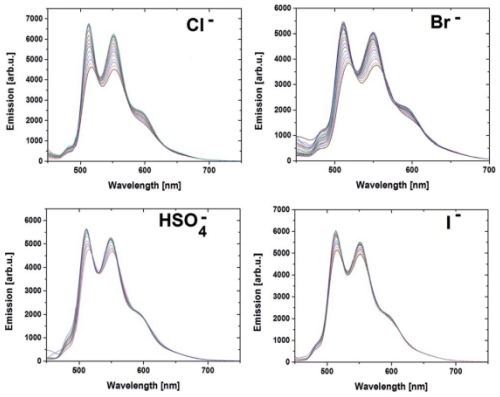

Figure 9. Emission spectral responses of IrBBI-H_2 (5×10^{-6} M in chloroform, 298 K, λ_{ex} = 378 nm) upon addition of Cl^-, Br^-, I^- and HSO_4^- anions.

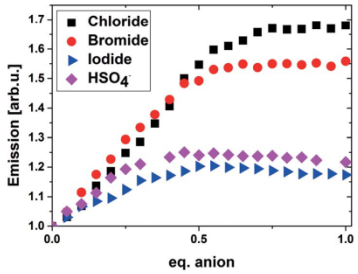

Figure 10. Normalized emission spectral responses (integrated area) of IrBBI-H_2 (5×10^{-6} M in chloroform, 298 K, λ_{ex} = 378 nm) upon addition of Cl, Br^-, I^- and HSO_4^- anions.

anion binding behavior. This enhancement of emission intensity in the order Cl^- > Br^- > HSO_4^- > I^- can be attributed to the formation of hydrogen bonds between IrBBI-H_2 and the anions, which influences the N–H bond and reduces the nonradiative decay of the ^{3}MLCT state through the N–H pathway.

Conclusions

The interaction of the metalloreceptor IrBBI-H_2 with various anions has been investigated. Still, one should keep in mind that the investigated recognition process does not take place within the sophisticated realm of supramolecular chemistry but technically belongs to the nature and congested class of Brønsted acid–base reactions.[41]

It was shown that the photophysics of the complex can be influenced by hydrogen bonds in the periphery of the ligand. Systematic studies on the system reveal that IrBBI-H_2 is a convenient sensor for various anions under aerobic conditions.

© 2016 Wiley-VCH Verlag GmbH & Co. KGaA, Weinheim

ChemPubSoc Europe

EurJIC European Journal of Inorganic Chemistry
Full Paper

The high acidity of the N–H protons in the present complex makes it easy to be deprotonated in the presence of strongly basic anions like F^-, OAc^-, and $H_2PO_4^-$, and they form remarkable hydrogen bonds with weakly basic anions such as Cl^-, Br^-, I^-, and HSO_4^-. The addition of different anions into a solution of this complex gives distinct responses as characterized by emission and NMR spectroscopy. In ^{1}H NMR spectroscopy, it was observed that positions H4″ and H7″ of the bibenzimidazole ligand can also be used as signaling unit, whereas proton H7″ gives additional information about the steric demand of the bound anion. Additional investigation of this pocket effect on anion binding affinity is underway. A fundamental advantage of the iridium-based system is its applicability under aerobic conditions due to its remarkably strong luminescence. We believe that the present work offers new opportunities for future reactivity-based sensing systems.

Experimental Section

Materials and Methods: 4,4′,5,5′-Tetramethyl-2,2′-bibenzimidazole and tetrakis(2-phenylpyridine-C^2,N)bis(μ-chloro)diiridium were synthesized according to published procedures.[48–50] IrBBI-H_2 was synthesized as published recently.[40] Technical grade solvents were purchased from VWR/Prolabo and redistilled under reduced pressure at 40 °C. Methanol, dichloromethane, chloroform, and acetonitrile for spectroscopic measurements were purchased in spectroscopic grade from Roth. Dry solvents were obtained from a MBraun MB SPS-800 system. All chemicals were purchased from Merck Millipore, Sigma Aldrich, ABCR, Acros Organics, Alfa Aesar, or VWR/Prolabo and used as purchased (≥ 95 %). Reactions under inert conditions were performed under an Argon 4.6 atmosphere by means of standard Schlenk techniques. Mass spectra were recorded with a Finnigan MAT SSQ 710 or a Thermoquest-Finnigan MAT 95XL instrument. Elemental analysis was performed with an Elementar Vario MICRO cube instrument.

General Spectroscopic Methods: Chloroform used as solvent for spectral experiments was redistilled under reduced pressure at 40 °C and kept over molecular sieves. Tetrabutylammonium (TBA) salts of F^-, Cl^-, Br^-, I^-, $H_2PO_4^-$, and HSO_4^- were purchased from Alfa Aesar and Merck Chemicals and dissolved in chloroform. Binding constants were performed in duplicate, and the average is reported. All data were processed with the OriginLab software package.

Emission Spectroscopy: Emission spectra were recorded with a JASCO Spectrofluorometer FP-8500 at room temperature. Cuvettes with a 1 cm path length and a 3 mL volume were used for all measurements. For a typical titration experiment, 10 μL aliquots of a TBA salt ($c = 5 \times 10^{-4}$ M) were added stepwise to a 10 mL solution of IrBBI-H_2 ($c = 5 \times 10^{-6}$ M) in chloroform by a syringe. Thereby the TBA salt was dissolved in a solution of IrBBI-H_2 ($c = 5 \times 10^{-6}$ M), so no effect of dilution has to be taken into consideration. The excitation wavelengths were fixed at 378 nm with a slit width of 5 nm and repeated at least twice.

^{1}H NMR Titration: ^{1}H NMR spectra were recorded at ambient temperature, unless otherwise stated, with a Bruker 400 MHz spectrometer with $CDCl_3$ or [D_6]DMSO as a solvent and TMS as an internal standard. For a typical titration experiment, 20 μL aliquots of a (Cl^-, Br^-, I^-, HSO_4^-) TBA salt (5.628 mM in $CDCl_3$) were added to a solution of IrBBI in $CDCl_3$ (2.34 mM). For F^-, OAc^-, and $H_2PO_4^-$, a 2.34 mM solution of IrBBI-H_2 in [D_6]DMSO was titrated with the appropriate amount of anion dissolved in [D_6]DMSO.

Acknowledgments

Financial support by the Carl Zeiss Stiftung by means of a PhD scholarship (to D. S.) is thankfully acknowledged.

Keywords: Iridium · Bibenzimidazole · Anions · NMR titration · Fluorescence

[1] A. Ghosh, B. Ganguly, A. Das, *Inorg. Chem.* **2007**, *46*, 9912–9918.
[2] H.-J. Mo, Y.-L. Niu, M. Zhang, Z.-P. Qiao, B.-H. Ye, *Dalton Trans.* **2011**, *40*, 8218–8225.
[3] A. Juris, V. Balzani, *Coord. Chem. Rev.* **1988**, *84*, 85–277.
[4] P. D. Beer, P. A. Gale, *Angew. Chem. Int. Ed.* **2001**, *40*, 486–516; *Angew. Chem.* **2001**, *113*, 502.
[5] P. D. Beer, *Coord. Chem. Rev.* **2003**, *240*, 167–189.
[6] E. A. Medlycott, G. S. Hanan, *Coord. Chem. Rev.* **2006**, *250*, 1763–1782.
[7] Z. Lin, Y. Zhao, C. Duan, B. Zhang, Z. Bai, *Dalton Trans.* **2006**, 3678–3684.
[8] D. Saha, S. Das, C. Bhaumik, S. Dutta, S. Baitalik, *Inorg. Chem.* **2010**, *49*, 2334–2348.
[9] S. Das, D. Saha, C. Bhaumik, S. Dutta, S. Baitalik, *Dalton Trans.* **2010**, 4162–4169.
[10] C. Bhaumik, S. Das, D. Saha, S. Dutta, S. Baitalik, *Inorg. Chem.* **2010**, *49*, 5049–5062.
[11] P. Anzenbacher, D. S. Tyson, K. Jursíková, F. N. Castellano, *J. Am. Chem. Soc.* **2002**, *124*, 6232–6233.
[12] F. Cheng, N. Tang, J. Chen, F. Wang, L. Chen, *Inorg. Chem. Commun.* **2010**, *13*, 757–761.
[13] A. Ghosh, S. Verma, B. Ganguly, H. N. Ghosh, A. Das, *Eur. J. Inorg. Chem.* **2009**, 2496–2507.
[14] S. Aoki, M. Zulkefeli, M. Shiro, M. Kohsako, K. Takeda, E. Kimura, *J. Am. Chem. Soc.* **2005**, *127*, 9129–9139.
[15] T. Kundu, S. M. Mobin, G. K. Lahiri, *Dalton Trans.* **2010**, *39*, 4232–4242.
[16] X.-F. Shang, J. Li, H. Lin, P. Jiang, Z.-S. Cai, H.-K. Lin, *Dalton Trans.* **2009**, 2096–2102.
[17] V. Balzani, N. Sabbatini, F. Scandola, *Chem. Rev.* **1986**, *86*, 319–337.
[18] T. Lazarides, T. A. Miller, J. C. Jeffery, T. K. Ronson, M. D. Ward, *Dalton Trans.* **2005**, 528–536.
[19] Y. Cui, Y. Niu, M. Cao, K. Wang, H. Mo, Y. Zhong, B. Ye, *Inorg. Chem.* **2008**, *47*, 5616–5624.
[20] H.-J. Mo, H.-Y. Chao, B.-H. Ye, *Inorg. Chem. Commun.* **2013**, *35*, 100–103.
[21] H.-J. Mo, J.-J. Wu, Z.-P. Qiao, B.-H. Ye, *Dalton Trans.* **2012**, *41*, 7026–7036.
[22] C. Padié, K. Zeitler, *New J. Chem.* **2011**, *35*, 994.
[23] P. D. Beer, *Acc. Chem. Res.* **1998**, *31*, 71–80.
[24] P. D. Beer, J. Cadman, *Coord. Chem. Rev.* **2000**, *205*, 131–155.
[25] U. S. Schubert, C. Eschbaumer, *Angew. Chem. Int. Ed.* **2002**, *41*, 2892–2926; *Angew. Chem.* **2002**, *114*, 3016.
[26] A. P. De Silva, H. Q. N. Gunaratne, T. Gunnlaugsson, A. J. M. Huxley, C. P. McCoy, J. T. Rademacher, T. E. Rice, *Chem. Rev.* **1997**, *97*, 1515–1566.
[27] R. Martínez-Máñez, F. Sancenón, *Chem. Rev.* **2003**, *103*, 4419–4476.
[28] W. R. Browne, R. Hage, J. G. Vos, *Coord. Chem. Rev.* **2006**, *250*, 1653–1668.
[29] Y. Cui, H. J. Mo, J. C. Chen, Y. L. Niu, Y. R. Zhong, K. C. Zheng, B. H. Ye, *Inorg. Chem.* **2007**, *46*, 6427–6436.
[30] S. Rau, T. Büttner, C. Temme, M. Ruben, H. Görls, D. Walther, M. Duati, S. Fanni, J. G. Vos, *Inorg. Chem.* **2000**, *39*, 1621–1624.
[31] D. Sorsche, S. Rau, *Eur. J. Inorg. Chem.* **2014**, 4244–4249.
[32] K. Monczak, K. Peuntinger, D. Sorsche, F. W. Heinemann, D. M. Guldi, S. Rau, *Chem. Eur. J.* **2014**, *20*, 15426–15433.
[33] L. A. Beauchamp, S. Fortin, *Inorg. Chem.* **2001**, *40*, 105–112.
[34] S. Fortin, P.-L. Fabre, M. Dartiguenave, A. L. Beauchamp, *J. Chem. Soc., Dalton Trans.* **2001**, 3520–3527.
[35] L. Ion, D. Morales, J. Pérez, L. Riera, V. Riera, R. a. Kowenicki, M. McPartlin, *Chem. Commun.* **2006**, 91–93.
[36] S. Derossi, H. Adams, M. D. Ward, *Dalton Trans.* **2007**, 33–36.
[37] J. C. Freys, G. Bernardinelli, O. S. Wenger, *Chem. Commun.* **2008**, 4267–4269.
[38] S. Rau, M. Ruben, T. Büttner, C. Temme, S. Dautz, H. Görls, M. Rudolph, D. Walther, A. Brodkorb, M. Duati, C. O'Connor, J. G. Vos, *J. Chem. Soc., Dalton Trans.* **2000**, 3649–3657.

© 2016 Wiley-VCH Verlag GmbH & Co. KGaA, Weinheim

ChemPubSoc Europe

EurJIC European Journal of Inorganic Chemistry
Full Paper

[39] A. Grüßing, S. Rau, S. Schebesta, A. Scholz, H. Görls, D. Walther, *Z. Anorg. Allg. Chem.* **2007**, 961–970.
[40] S. A. Rommel, D. Sorsche, N. Rockstroh, F. W. Heinemann, J. Kübel, M. Wächtler, B. Dietzek, S. Rau, *Eur. J. Inorg. Chem.* **2015**, 3730–3739.
[41] V. Amendola, D. Esteban-Gómez, L. Fabbrizzi, M. Licchelli, *Acc. Chem. Res.* **2006**, *39*, 343–353.
[42] M.-A. Haga, *Inorg. Chim. Acta* **1980**, *45*, L183–L184.
[43] C. Pérez-Casas, A. K. Yatsimirsky, *J. Org. Chem.* **2008**, *73*, 2275–2284.
[44] S. Fortin, P.-L. Fabre, M. Dartiguenave, A. L. Beauchamp, *J. Chem. Soc., Dalton Trans.* **2001**, 3520–3527.
[45] Z.-H. Lin, S.-J. Ou, C.-Y. Duan, B.-G. Zhang, Z.-P. Bai, *Chem. Commun.* **2006**, 624–626.
[46] M. J. Hynes, *J. Chem. Soc., Dalton Trans.* **1993**, 311–312.
[47] R. Indumathy, P. S. Parameswaran, C. V. Aiswarya, B. Unni Nair, *Polyhedron* **2014**, *75*, 22–29.
[48] E. Müller, G. Bernardinelli, J. Reedijk, *Inorg. Chem.* **1995**, *34*, 5979–5988.
[49] B. Schmid, F. O. Garces, R. J. Watts, *Inorg. Chem.* **1994**, *33*, 9–14.
[50] F. O. Garces, K. A. King, R. J. Watts, *Inorg. Chem.* **1988**, *27*, 3464–3471.

Received: September 29, 2015
Published Online: November 25, 2015

 © 2016 Wiley-VCH Verlag GmbH & Co. KGaA, Weinheim

Eur. J. Inorg. Chem. **2016** · ISSN 1099–0682

SUPPORTING INFORMATION

DOI: 10.1002/ejic.201501108
Title: Interaction of an Iridium(III)–Bibenzimidazole Complex with Anions – Implications for Luminescent Sensing
Author(s): Sebastian A. Rommel, Dieter Sorsche, Apoorva Dixit, Sven Rau*

^{1}H NMR TITRATIONS Titration Protocol:

^{1}H NMR spectra were recorded on a Bruker 400 MHz spectrometer. Typically, a solution of guest was added to a solution of the host at 293K. The chemical shift of the N-H proton of the host IrBBI-H_2 was monitored for various titration points. The resulting data were analysed using the WinEqNMR2 computer program in experiments where association of guest and host was fast on the NMR timescale.[1] Anion binding titration experiments were carried out using the salt of the non-complexing tetrabutylammonium (TBA) cation as the guest species, titrated into the host species IrBBI-H_2 (in $CDCl_3$). A 5.628 mM solution of anion was added to 0.48 mL of a 2.345 mM solution of IrBBI-H_2. The values of the guest concentration and observed chemical shift were entered into WinEQNMR2 for every titration point, and estimates for the binding constant, limiting chemical shifts and binding stoichiometry were made. The parameters were refined using non-linear least squares analysis to obtain the best fit between observed and calculated chemical shifts; WinEQNMR2 plots the observed shift versus the guest concentration, revealing the accuracy of the experimental data and the suitability of the model used. The input parameters were varied until the best-fit values of the stability constants, together with their errors, converged.[1]

Evaluation of the Complex Stoichiometry.

The stoichiometry of the complexes was determined according to the Job's method of continuous variations. Equimolar amounts of host and guest were dissolved in chloroform. These solutions were distributed among 10 probe samples à 3 mL in such a way that the molar fraction X_H ($X_H = [H]_0/([H]_0 + [G]_0)$) in the resulting solutions decreased from 0.0 to 1.0. The complexation-induced intensity changes were multiplied by X_H and plotted against X_H itself (Job plot).[2]

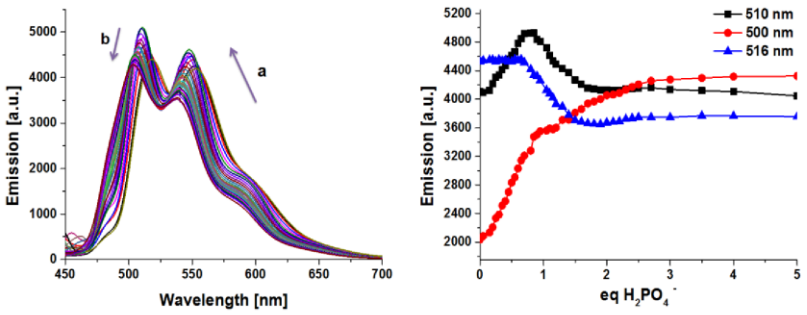

Figure S 1. Left: emission titration of IrBBI (5 x 10^{-6} mol dm^{-3}) in chloroform upon the addition of $H_2PO_4^-$; right: emission intensity at 516, 510 and 500 nm vs. eq. of $H_2PO_4^-$.

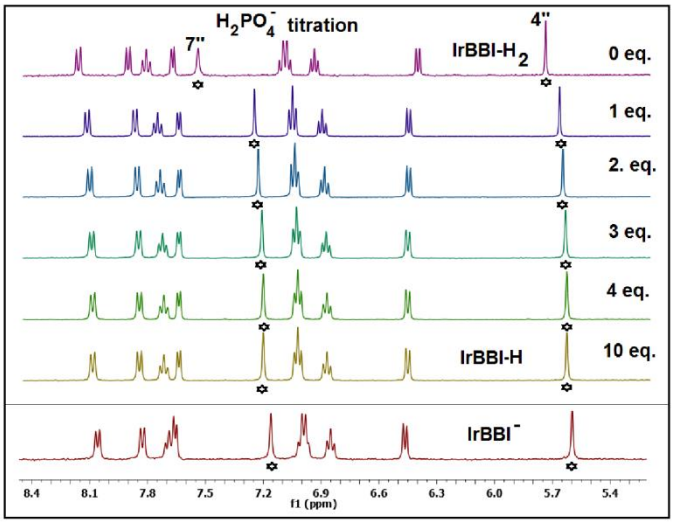

Figure S 2. : ^{1}H NMR spectra of IrBBI-H_x (2.34 mM) in DMSO-d_6 with $H_2PO_4^-$.

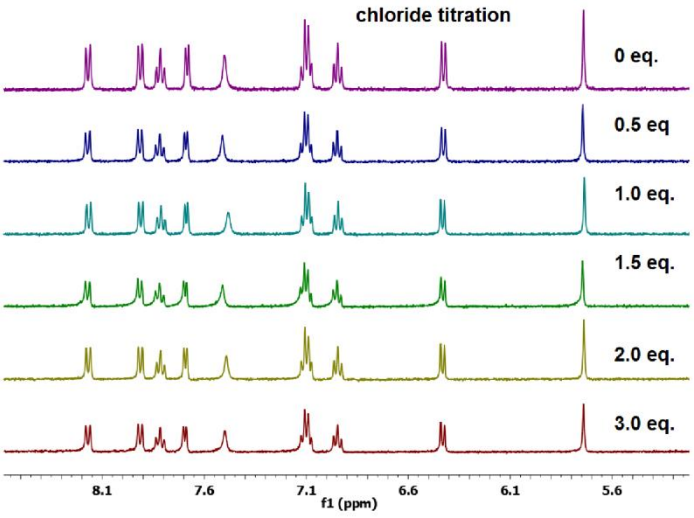

Figure S 3. ^{1}H-NMR spectra of IrBBI-H_2 in DMSO-d6 solution (2.34 mM) and the addition of various equiv. of chloride anions.

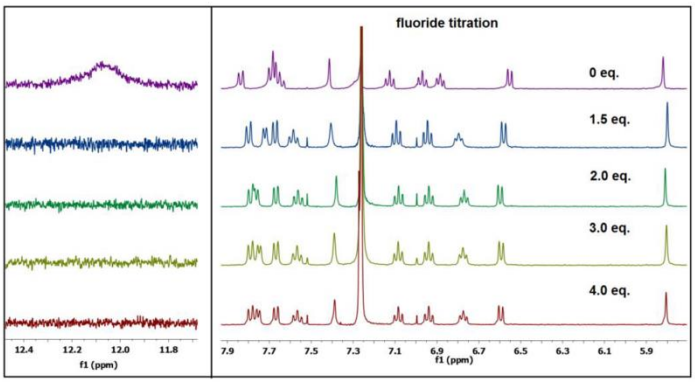

Figure S 4. ^{1}H-NMR spectra of IrBBI-H_x in $CDCl_3$ solution (2.34 mM) and the addition of various equiv. of fluoride anions.

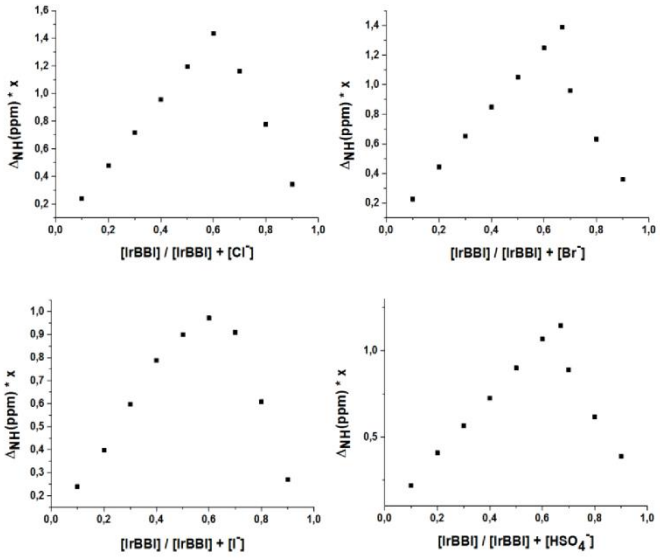

Figure S 5. Job plot analyses for IrBBI-H_2 and Cl^-, Br-, I^-, and HSO_4^- (^{1}H NMR titration, following the NH shift of the complex).[2]

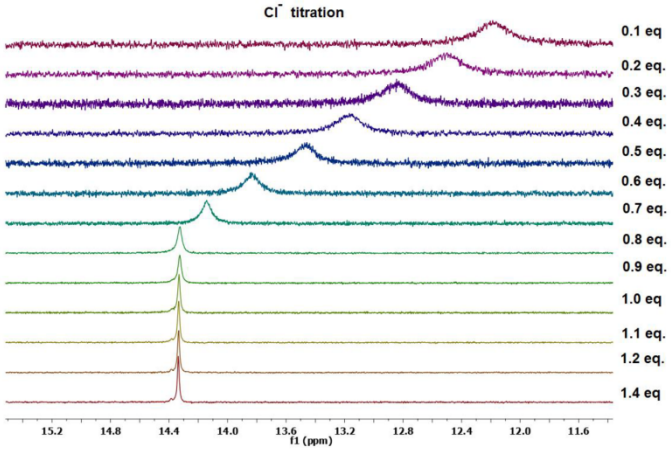

Figure S 6. ^{1}H NMR titration of a 2.345 mM solution of IrBBI-H_2 in $CDCl_3$ with Cl^-. The visible signal can be assigned to the N-H function of the imine moiety of the bibenzimidazole.

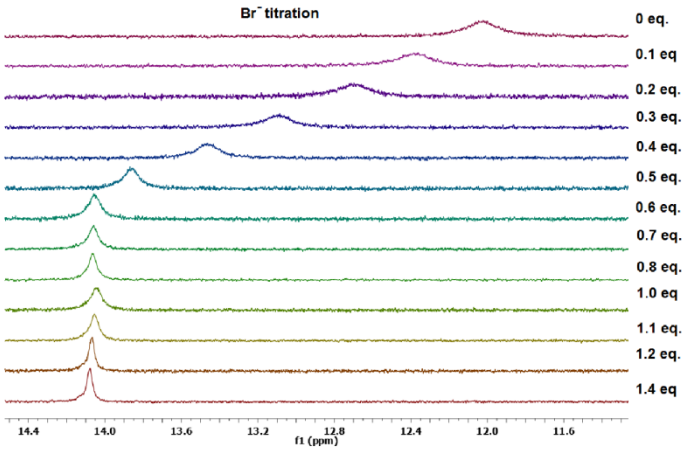

Figure S 7. ^{1}H NMR titration of a 2.345 mM solution of IrBBI-H_2 in $CDCl_3$ with Br^-. The visible signal can be assigned to the N-H function of the imine moiety of the bibenzimidazole.

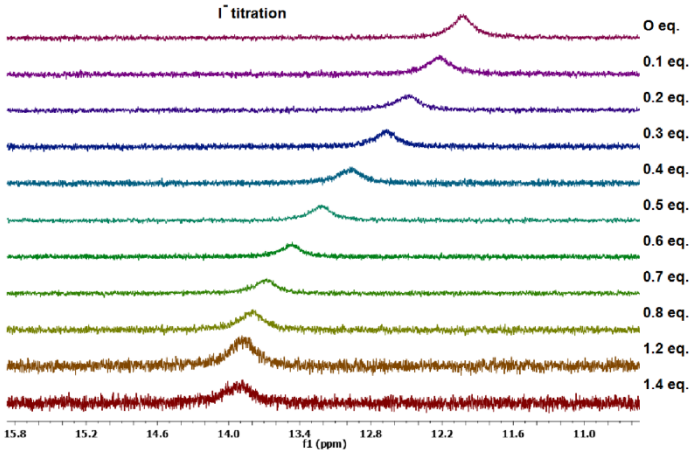

Figure S 8. ^{1}H NMR titration of a 2.345 mM solution of IrBBI-H_2 in $CDCl_3$ with I^-. The visible signal can be assigned to the N-H function of the imine moiety of the bibenzimidazole.

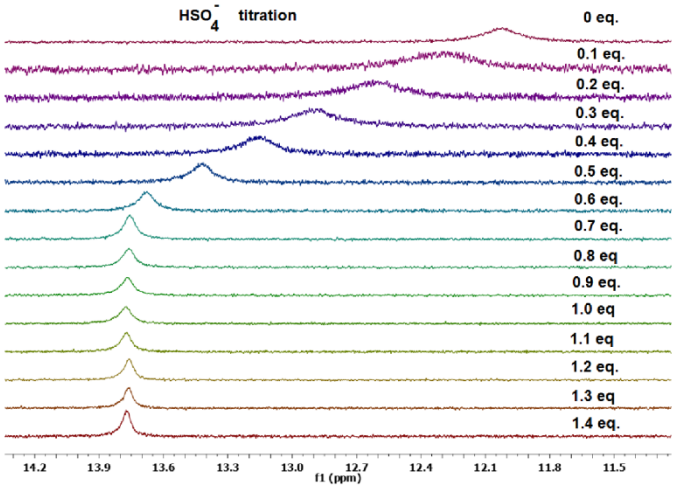

Figure S 9. ^{1}H NMR titration of a 2.345 mM solution of IrBBI-H_2 in $CDCl_3$ with HSO_4^-. The visible signal can be assigned to the N-H function of the imine moiety of the bibenzimidazole.

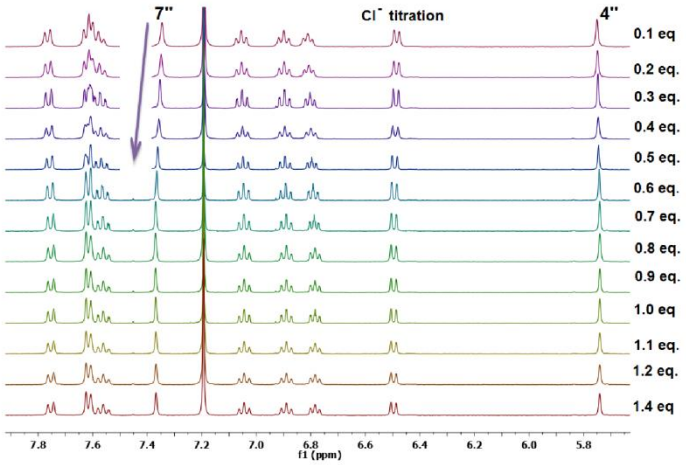

Figure S 10. ^{1}H NMR titration of a 2.345 mM solution of IrBBI-H_2 in $CDCl_3$ with Cl^-.

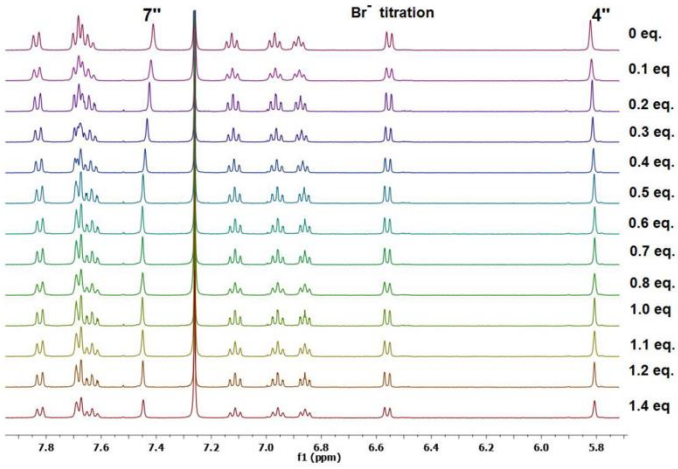

Figure S 11. ^{1}H NMR titration of a 2.345 mM solution of IrBBI-H_2 in $CDCl_3$ with Br^-.

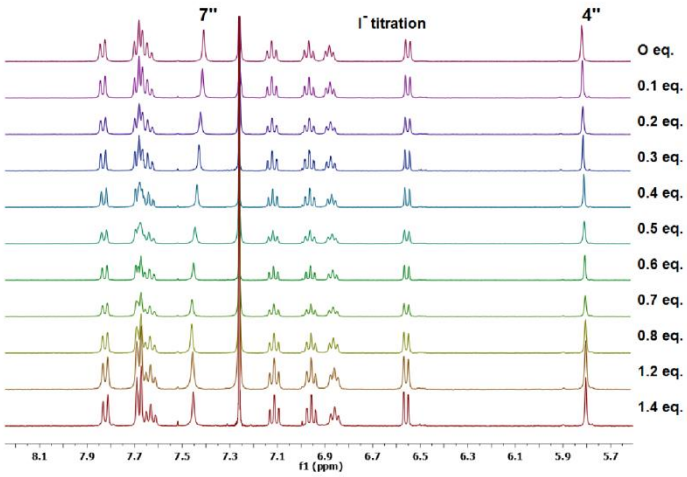

Figure S 12. ^{1}H NMR titration of a 2.345 mM solution of IrBBI-H_2 in $CDCl_3$ with I^-.

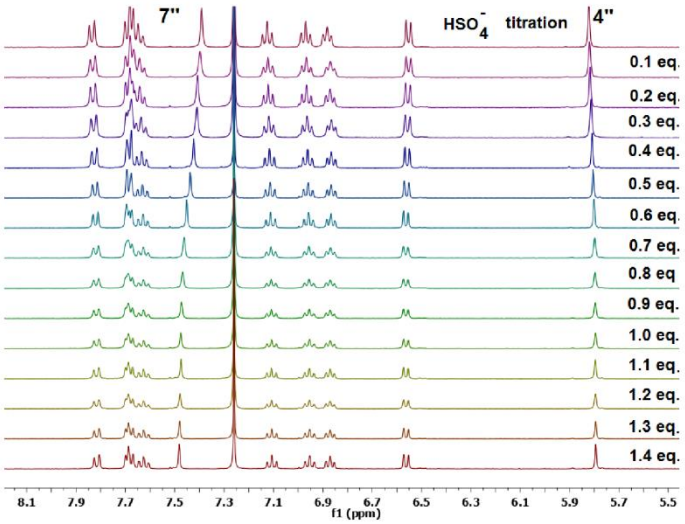

Figure S 13. ^{1}H NMR titration of a 2.345 mM solution of IrBBI-H_2 in $CDCl_3$ withHSO_4^-.

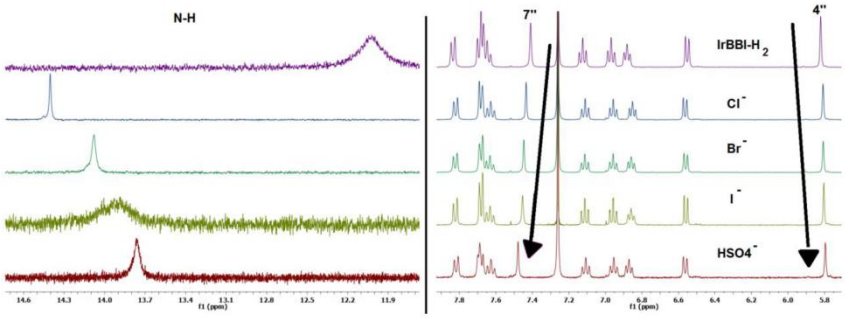

Figure S 14. ^{1}H-NMR spectra of IrBBI-H_2 in $CDCl_3$ solution (2.345 mM) and the addition of 2.0 equiv. of anions.

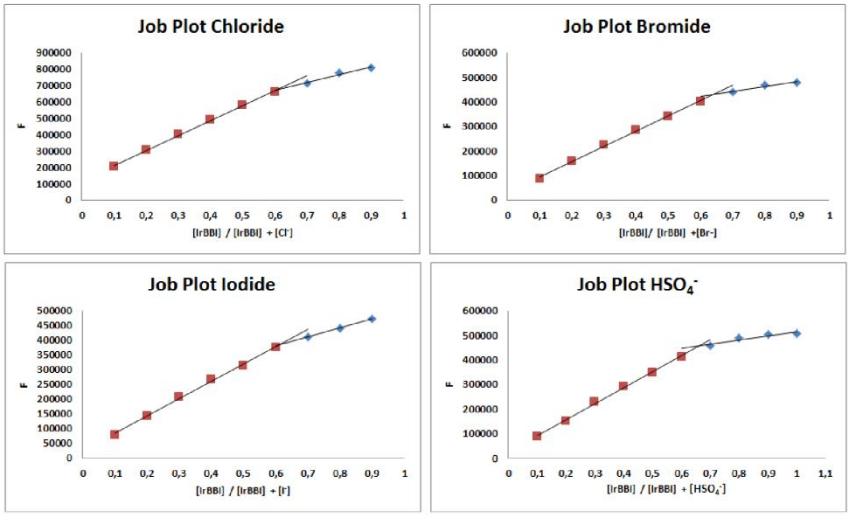

Figure S 15. Job plot analyses for IrBBI-H_2 and Cl^-, Br-, I^-, and HSO_4^- (Emission titration).[2]

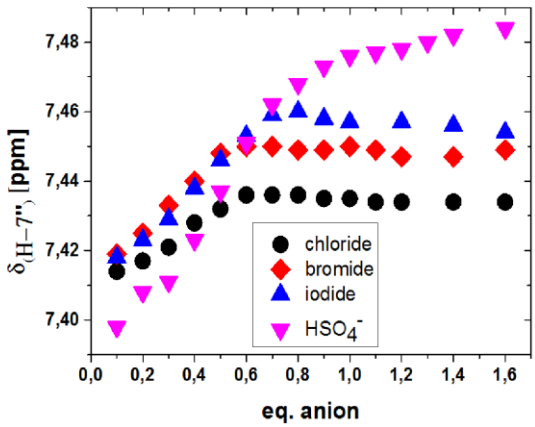

Figure S 16. Chemical shift changes of the H-7'' signal of IrBBI in $CDCl_3$-d_6 upon addition of different anions.

References

1 M. J. Hynes, *J. Chem. Soc. Dalton Trans.*, 1993, 311–312.
2 V. M. S. Gil and N. C. Oliveira, *J. Chem. Educ.*, 1990, **67**, 473–478.

[SR3]: A supramolecular H-bond driven light switch sensor for small anions

Sebastian A. Rommel, Dieter Sorsche and Sven Rau*

* *corresponding author*

Published in: *Dalton Trans*, **2016**, *45*, 74 – 77. (DOI: 10.1039/c5dt04152j)

Copyright Reprinted from "A supramolecular H-bond driven light switch sensor for small anions, Sebastian A. Rommel, Dieter Sorsche and Sven Rau, *Dalton Trans*, **2016**, *45*, 74 – 77". Reproduced by permission of The Royal Society of Chemistry.

A cationic iridium complex with a 2, 2'-bibenzimidazole ligand can act as luminescent sensor for various anions. Strong H-bond supported ion pair bonding with an electron accepting dinitro-benzoate anion switches the luminescence "off". The luminescence of the sensor is switched back "on" when benzoate is replaced by competing H-bonded small anions, therefore leading to enhanced sensitivity of the sensor system.

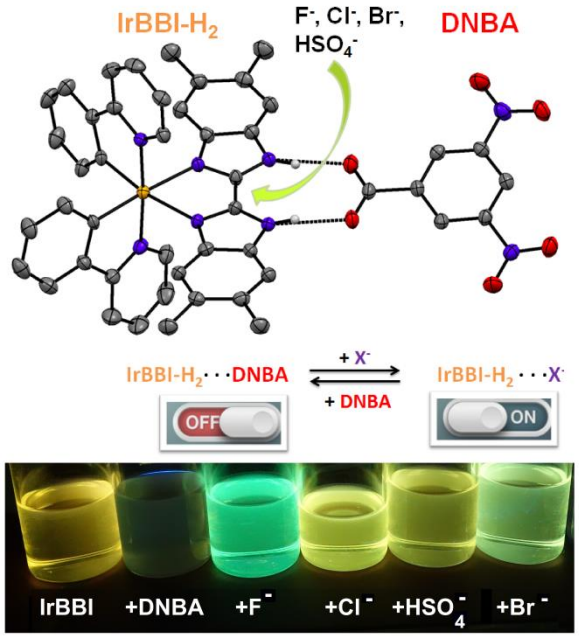

Contribution of the different authors:

Sebastian A. Rommel	Synthesis of the anion sensor. Performance of photophysical characterization of the sensor system, ^{1}H-NMR, emission and UV/Vis titration experiments. Writing of the manuscript.
Dieter Sorsche	Measurement and refinement of the X-ray structures. Writing and revision of the manuscript, concept and results discussion.
Sven Rau	Discussion and revision of the manuscript, concept and results discussion.

Dalton Transactions

COMMUNICATION

View Article Online
View Journal | View Issue

Published on 18 November 2015. Downloaded by Universitat Ulm on 11/01/2016 15:31:23.

Cite this: *Dalton Trans.*, 2016, **45**, 74

Received 22nd October 2015,
Accepted 18th November 2015

DOI: 10.1039/c5dt04152j

www.rsc.org/dalton

A supramolecular H-bond driven light switch sensor for small anions†

S. A. Rommel, D. Sorsche and S. Rau*

A cationic iridium complex with a 2,2′-bibenzimidazole ligand can act as a luminescent sensor for various anions. Strong H-bond supported ion pair bonding with an electron accepting dinitro-benzoate anion switches the luminescence "off". The luminescence of the sensor is switched back "on" when benzoate is replaced by competing H-bonded small anions, therefore leading to an enhanced sensitivity of the sensor system.

Due to their essential roles in biological, environmental and chemical processes, the development of specific phosphorescent sensors for the efficient detection of ions is an important subject in the field of supramolecular chemistry.[1–7] Among the numerous designs of anion receptors, the incorporation of luminescent chromophores into a receptor which are sensitive to interactions between the host and guest molecules has gained increased attention due to their low detection limit and high sensitivity.[8–14] The advantage of luminescence-based sensors is the high sensitivity of luminescence detection compared to other spectroscopic methods.[2] For anion receptors based on hydrogen bonding interactions, various organic compounds with the polarized N–H functional group, such as pyrrole, imidazole, urea, sulfonamide, amide, and thiourea moieties, are capable of providing a hydrogen bonding function to certain anions.[2] For ruthenium complexes various imidazole type sensor systems are known that can be used as anion sensor systems.[1,2,15–24] Further, supramolecular architectures on the bibenzimidazole basis are known.[25] Therefore, we reasoned that d^6 metal complexes of 2,2′-bibenzimidazole (BBI-H_2) would also be particularly interesting candidates. Prior spectroscopic studies on iridium complexes with imidazole type ligands indicated that they provide numerous preferable properties: (a) the MLCT excited states of these molecules are emissive and long-lived (IrBBI-H_2: 44 ns in air equilibrated chloroform; $[Ir(Me\text{-}ppy)_2Biim]^+$ (Biim = biimidazole, ppy = phenylpyridine, **R1**): 1.2 μs in deoxygenated dichloromethane), (b) in the excited state the metal complexes become a potent electron donor, (c) the optical emission spectra of the complexes correspond to the protonation state of the 2,2′-bibenzimidazole ligand and Ir(BBI)-H_X (X = 0, 1, 2) shows strong protonation state dependent luminescence in all three protonation states.[26,27]

We showed elsewhere that the photophysics of the complex **IrBBI-H_2** can be influenced by hydrogen bonds in the ligand periphery. Systematic studies on this system revealed that **IrBBI-H_2** is a convenient hydrogen bond donor for various anions under aerobic conditions like fluoride, bromide or iodide. Strong bonding interactions between the weakly basic anions and the complex, and a virtually stoichiometric reaction to their respective ion pair are generally observed. However, recognition of the H-bonded ion pair is possible merely through a luminescence increase from an already strongly fluorescent pristine chromophore (*i.e.* its PF_6 salt).[28] Therefore, we have developed an off-switch strategy to enhance the sensitivity of the iridium(III) bibenzimidazole system, employing the proton coupled electron transfer (PCET) quenching mechanism described by Nocera *et al.* and Wenger *et al.* The 3,5-dinitro benzoate anion (DNBA) was employed accordingly, in order to efficiently quench the luminescent excited state of **IrBBI-H_2** virtually switching its luminescence "off" in the first place.[26,29,30] The expected H-bond ion pairing of IrBBI-H_2^+···$DNBA^-$ was observed in the crystal structure of the donor–acceptor couple (Fig. 1, top). The N···O distances of 2.690(3) and 2.616(3) Å are comparable to the values reported for **R1** (2.632(4) Å, 2.640(4) Å)[26] and sparsely shorter than those previously observed in the ion pairs of similar complex salts.[31–33]

The formation of hydrogen-bonded IrBBI-H_2^+···$DNBA^-$ pairs in solution can further be observed *via* ^{1}H NMR experiments. A shift of the N–H signals directly involved in the salt bridge as well as the shift of H7″ and H4″ and weaker H3′

Institute for Inorganic Chemistry I, Ulm University, Albert-Einstein-Allee 11, 89081 Ulm, Germany. E-mail: sven.rau@uni-ulm.de; http://www.uni-ulm.de/nawi/nawi-anorg1

†Electronic supplementary information (ESI) available: Experimental procedures, spectral and analytical data, determination of association constants, and crystallographic data for IrBBI-H_2^+–$DNBA^-$. CCDC 1432106. For ESI and crystallographic data in CIF or other electronic format see DOI: 10.1039/c5dt04152j

This journal is © The Royal Society of Chemistry 2016

Published on 18 November 2015. Downloaded by Universitat Ulm on 11/01/2016 15:31:23.

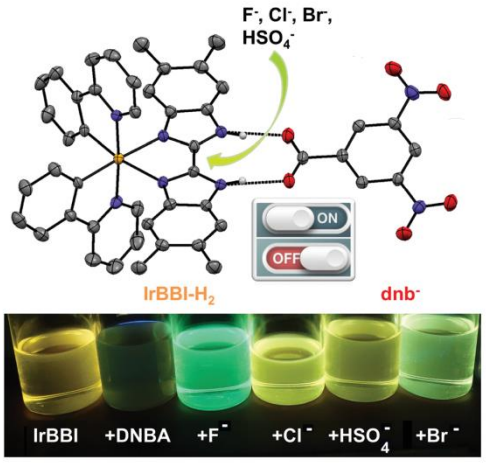

Fig. 1 Top: scheme of the luminescent on/off sensor for anions, bottom: picture of the different solutions of IrBBI in chloroform and excess anions.

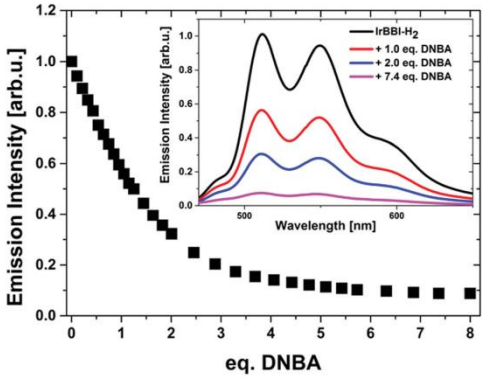

Fig. 2 Main: plot of the normalized iridium luminescence intensity as a function of the number of equivalents of DNBA added; inset: luminescence of IrBBI-H_2 as a function of increasing amounts of DNBA (one measurement of three, average can be found in the ESI†).

(ESI†) can be observed in chloroform, or dichloromethane, when benzoate is added to a solution of the iridium complex (ESI†). Interestingly, the N–H signal in chloroform vanishes completely after addition of one equivalent of benzoate and in DCM it is virtually not visible, therefore no direct calculation of the association constant was possible.

As reported previously, the luminescence spectrum upon photoexcitation of **IrBBI-H_2** at 378 nm in chloroform shows two characteristic band maxima.[28] In the PF_6 salt of **IrBBI-H_2** this emission has a lifetime of 44 ns in air equilibrated chloroform solution,[27] which is indicative of an emissive excited state that has a mixed MLCT and π–π^* intraligand (IL) character as observed for many other cyclometalated Ir complexes.[26,34–40]

As can be seen from Fig. 2, addition of DNBA leads to a dramatic decrease of the iridium luminescence intensity (black squares) due to the oxidative quenching of the MLCT/IL state by the DNBA anion as reported for **R1**.[26] Approximately 50% of the luminescence intensity of the PF_6 salt of **IrBBI-H_2** is quenched upon addition of the first equivalent of DNBA and after 7 eq. saturation of the quenching kinetics is observed at about 8% residual luminescence, which has been defined in this work as the "off" state. In contrast, control experiments with $[Ir(ppy)_2(bipy)]^+$ (bipy = bipyridine; **R2**) show only weak oxidative quenching of **R2** by DNBA down to 53% upon addition of 7 eq., the respective kinetics indicating an ordinary bimolecular quenching mechanism due to the lack of H-bonds (see the ESI†).[26] Accordingly, two effects must be taken into account for this, *i.e.* (i) the formation of tightly bound IrBBI-H_2^+···$DNBA^-$ ion pairs as observed in the solid state, and (ii) efficient electron transfer from the excited iridium complex within the ion pair due to the spatial preorganization.[26]

Titration experiments of the IrBBI-H_2^+···$DNBA^-$ (active sensor, **S**) system were carried out with five different anions which are, in principle, able to replace DNBA as the H-bond acceptor from the IrBBI-H_2–DNBA ion pair and therefore switch the luminescence of the chromophore back "on". (Fig. 3 and 4). As expected, all anions cause a significant change in the luminescence intensity of the IrBBI-H_2^+···$DNBA^-$ system. That is an increase of 750% (fluoride), 450% (chloride), 405% (hydrogen sulfate), 220% (bromide) and the weakest effect of 118% upon titration with iodide (Fig. 3 and 4). Two general mechanisms need to be distinguished here, that is on the one hand (i) deprotonation of the acidic secondary amine functions of the cationic iridium complex by the basic fluoride ions. This is characterized by the hypsochromic shift and change of the vibronic structure of the emission spectrum. This mechanism has the strongest effect, as has been reported elsewhere that the fully deprotonated complex **IrBBI**$^-$ exhibits stronger luminescence compared to the pristine protonated PF_6 salt.[27] Also, due to the negative charge of the latter complex, electrostatic repulsion additionally inhibits collision induced quenching by the DNBA anion in solution. On the other hand (ii) the weakly basic anions Cl^-, HSO_4^-, Br^-, and I^- establish competing H-bonds, whereas the general capability to replace DNBA nicely corresponds to the basicity of the anions. Accordingly, strong effects were observed with Cl^- and HSO_4^-, whereas Br^- and lastly I^- only show a slightly minor effect. Remarkably, the intensity of hydrogen bonded complexes of chloride and hydrogen sulfate is comparable to the value of the **R2**···DNBA interaction, indicating that the residual luminescence quenching corresponds predominantly to the collision induced reaction between an anion stabilized IrBBIH_2^+–X^- ion pair and DNBA.

Generally, the final curve shape after the titration experiment correlated with the fluoride interaction with

Published on 18 November 2015. Downloaded by Universitat Ulm on 11/01/2016 15:31:23.

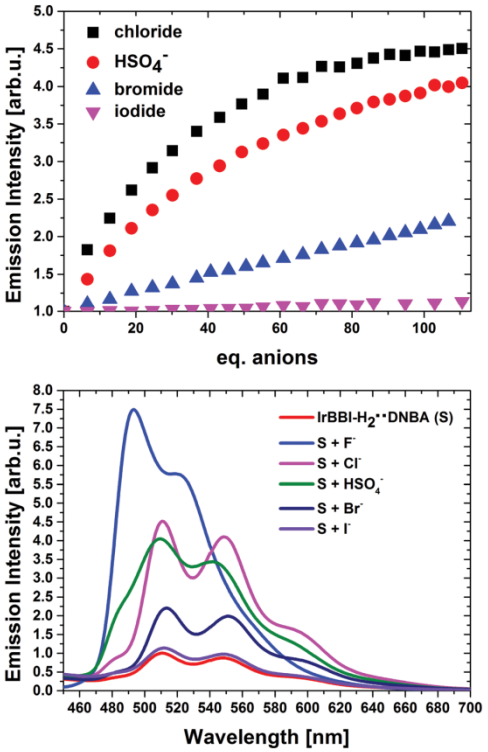

Fig. 3 Top: plot of the normalized luminescence intensity of IrBBI-H_2···DNBA (**S**) as a function of the number of equivalents of anions added; bottom: luminescence intensity of IrBBI-H_2···DNBA with 110 eq. of each anion.

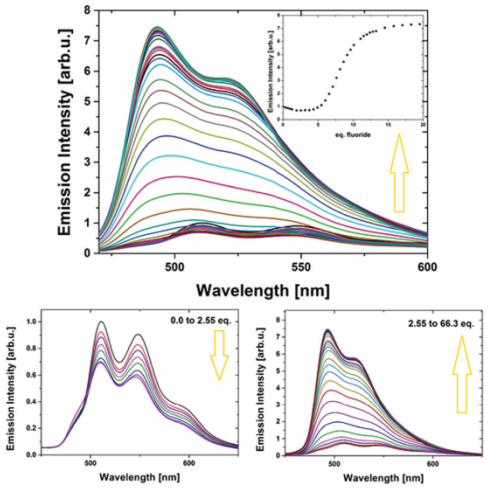

Fig. 4 Luminescence of IrBBI-H_2···DNBA (**S**) as a function of increasing amounts of fluoride (depicted is each only one of at least two distinct measurements); inset: plot of the normalized IrBBI-H_2···DNBA luminescence intensity as a function of the number of equivalents of anions added.

Table 1 Association constants (K_a) of the IrBBI-H_2–X interaction

Anion	Fluoride	Chloride	Hydrogen sulfate	Bromide	Iodide
K_a (M^{-1})	n.d.[a]	33 195 (1232)	17 804 (283)	1572 (328)	n.d.[a]

[a] n.d. = not determined.

IrBBI-H_2^+···$DNBA^-$ resembles the twofold deprotonated species **IrBBI**$^-$, whereas the structured emission of the other ions is characteristic of the fully protonated species of **IrBBI-H_2**. Association constants (K_a) between **IrBBI-H_2** in the presence of 6.86 eq. DNBA and the investigated anions were determined for a 1 : 1 complex model (chloride: K_a (M^{-1}) = 33 195 (1232), hydrogen sulfate: K_a (M^{-1}) = 17 804 (283), bromide: K_a (M^{-1}) = 1572 (328)). This quantitative affinity trend for **IrBBI-H_2** follows that of a simple biimidazole type metal complex and corresponds to the decreasing basicity in a group of the PSE. For the HSO_4^- ion, additional stabilization through the formation of a Y-shaped H-bond framework should be taken into account (Table 1).

In order to check for selectivity between the different anions, a titration experiment with a mixture of different anions (Cl^-, Br^-, I^-, HSO_4^-, having an identical ionic strength as for the individual anions) was carried out. Fluoride anions were excluded, as they deprotonate the sensor system. The anion mixture also causes a significant change in the luminescence intensity of the quenched IrBBI-H_2^+···$DNBA^-$ system and reaches a maximum of 214% of the initial luminescence intensity (ESI†). As the diverse binding behavior is predominately dependent on the different basicity of the investigated anions, selectivity was not observed.

In order to gain selectivity, spatial confinement of the H-bond framework through introduction of substituents in the 7,7′-positions is suggested as the target of ongoing research.[41]

In conclusion, the present results demonstrate that an iridium complex with a 2,2′-bibenzimidazole ligand forms hydrogen-bonded 1 : 1 adducts with 3,5-dinitro-benzoate anions. Due to oxidative quenching, the latter anion acts as an off-switch of the otherwise strongly luminescent iridium complex, providing a significant sensitivity enhancement of **IrBBI-H_2** towards selected anions.

Subsequently, the presented system is superior, to the best of our knowledge, to all ruthenium(II) biimidazole-type sensors known in the literature so far, regarding an increase in the luminescence intensity of *e.g.* 450% for chloride and as the

 This journal is © The Royal Society of Chemistry 2016

Published on 18 November 2015. Downloaded by Universitat Ulm on 11/01/2016 15:31:23.

change in luminescence intensity can easily be followed with the naked eye.

Financial support by the Carl Zeiss Stiftung by means of a PhD scholarship (to D. S.) is thankfully acknowledged.

Notes and references

1 H.-J. Mo, H.-Y. Chao and B.-H. Ye, *Inorg. Chem. Commun.*, 2013, **35**, 100–103.
2 K.-C. Chang, S.-S. Sun, M. O. Odago and A. J. Lees, *Coord. Chem. Rev.*, 2015, **284**, 111–123.
3 P. A. Gale, S. E. García-Garrido and J. Garric, *Chem. Soc. Rev.*, 2008, **37**, 151–190.
4 P. A. Gale and T. Gunnlaugsson, *Chem. Soc. Rev.*, 2010, **39**, 3595.
5 P. A. Gale, N. Busschaert, C. J. E. Haynes, L. E. Karagiannidis and I. L. Kirby, *Chem. Soc. Rev.*, 2014, **43**, 205–241.
6 P. A. Gale, *Chem. Soc. Rev.*, 2010, **39**, 3746–3771.
7 V. Balzani and F. Scandola, *Supramolecular Photochemistry*, Ellis Horwood, New York, 1991.
8 B.-C. Tzeng, Y.-F. Chen, C.-C. Wu, C.-C. Hu, Y.-T. Chang and C.-K. Chen, *New J. Chem.*, 2007, **31**, 202–209.
9 A. Kumar, S.-S. Sun and A. J. Lees, *Coord. Chem. Rev.*, 2008, **252**, 922–939.
10 K.-C. Chang, S.-S. Sun and A. J. Lees, *Inorg. Chim. Acta*, 2012, **389**, 16–28.
11 C.-Y. Hung, A. S. Singh, C.-W. Chen, Y.-S. Wen and S.-S. Sun, *Chem. Commun.*, 2009, 1511.
12 A. S. Singh and S. S. Sun, *J. Org. Chem.*, 2012, **77**, 1880–1890.
13 L. J. Charbonniére, R. Ziessel, M. Montalti, L. Prodi, N. Zaccheroni, C. Boehme and G. Wipff, *J. Am. Chem. Soc.*, 2002, **124**, 7779–7788.
14 S. Sun, J. A. Anspach, A. J. Lees and P. Y. Zavalij, *Organometallics*, 2002, **21**, 685–693.
15 H.-J. Mo, J.-J. Wu, Z.-P. Qiao and B.-H. Ye, *Dalton Trans.*, 2012, **41**, 7026–7036.
16 Y. Cui, Y. Niu, M. Cao, K. Wang, H. Mo, Y. Zhong and B. Ye, *Inorg. Chem.*, 2008, **47**, 5616–5624.
17 Y. Cui, H. J. Mo, J. C. Chen, Y. L. Niu, Y. R. Zhong, K. C. Zheng and B. H. Ye, *Inorg. Chem.*, 2007, **46**, 6427–6436.
18 H.-J. Mo, Y.-L. Niu, M. Zhang, Z.-P. Qiao and B.-H. Ye, *Dalton Trans.*, 2011, **40**, 8218–8225.
19 S. Rau, L. Böttcher, S. Schebesta, M. Stollenz, H. Görls and D. Walther, *Eur. J. Inorg. Chem.*, 2002, 2800–2809.
20 S. Rau, M. Ruben, T. Büttner, C. Temme, S. Dautz, H. Görls, M. Rudolph, D. Walther, A. Brodkorb, M. Duati, C. O'Connor and J. G. Vos, *J. Chem. Soc., Dalton Trans.*, 2000, 3649–3657.
21 D. Sorsche and S. Rau, *Eur. J. Inorg. Chem.*, 2014, 4244–4249.
22 S. Rau, T. Büttner, C. Temme, M. Ruben, H. Görls, D. Walther, M. Duati, S. Fanni and J. G. Vos, *Inorg. Chem.*, 2000, **39**, 1621–1624.
23 N. Rockstroh, K. Peuntinger, H. Görls, D. M. Guldi, F. W. Heinemann, B. Schäfer and S. Rau, *Z. Naturforsch.*, 2010, **65b**, 281–290.
24 A. Grüßing, S. Rau, S. Schebesta, A. Scholz, H. Görls and D. Walther, *Z. Anorg. Allg. Chem.*, 2007, 961–970.
25 F. Sun, Z. Yin, Q.-Q. Wang, D. Sun, M.-H. Zeng and M. Kurmoo, *Angew. Chem., Int. Ed. Engl.*, 2013, **52**, 4538–4543.
26 J. C. Freys, G. Bernardinelli and O. S. Wenger, *Chem. Commun.*, 2008, 4267–4269.
27 S. A. Rommel, D. Sorsche, N. Rockstroh, F. W. Heinemann, J. Kübel, M. Wächtler, B. Dietzek and S. Rau, *Eur. J. Inorg. Chem.*, 2015, 3730–3739.
28 S. A. Rommel, D. Sorsche and S. Rau, *Eur. J. Inorg. Chem.*, 2015, DOI: 10.1002/ejic.201501108.
29 E. R. Young, J. Rosenthal and D. G. Nocera, *Chem. Commun.*, 2008, 2322–2324.
30 J. P. Kirby, J. A. Roberts and D. G. Nocera, *J. Am. Chem. Soc.*, 1997, **119**, 9230–9236.
31 S. Fortin, P.-L. Fabre, M. Dartiguenave and A. L. Beauchamp, *J. Chem. Soc., Dalton. Trans.*, 2001, 3520–3527.
32 S. Derossi, H. Adams and M. D. Ward, *Dalton Trans.*, 2007, 33–36.
33 S. Fortin, P.-L. Fabre, M. Dartiguenave and A. L. Beauchamp, *J. Chem. Soc., Dalton Trans.*, 2001, 3520–3527.
34 M. S. Lowry and S. Bernhard, *Chem. – Eur. J.*, 2006, **12**, 7970–7977.
35 A. B. Tamayo, S. Garon, T. Sajoto, P. I. Djurovich, I. M. Tsyba, R. Bau and M. E. Thompson, *Inorg. Chem.*, 2005, **44**, 8723–8732.
36 T. Sajoto, P. I. Djurovich, A. Tamayo, M. Yousufuddin, R. Bau, M. E. Thompson, R. J. Holmes and S. R. Forrest, *Inorg. Chem.*, 2005, **44**, 7992–8003.
37 E. A. Plummer, J. W. Hofstraat and L. De Cola, *Dalton Trans.*, 2003, 2080–2084.
38 Y. You and W. Nam, *Chem. Soc. Rev.*, 2012, **41**, 7061–7084.
39 P. Coppo, A. Plummer and L. De Cola, *Chem. Commun.*, 2004, 1774–1775.
40 A. Auffrant, A. Barbieri, F. Barigelletti, J.-P. Collin, L. Flamigni, C. Sabatini and J.-P. Sauvage, *Inorg. Chem.*, 2006, **45**, 10990–10997.
41 D. Sorsche, S. A. Rommel and S. Rau, *Eur. J. Inorg. Chem.*, 2015, submitted manuscript.

Electronic Supplementary Material (ESI) for Dalton Transactions.
This journal is © The Royal Society of Chemistry 2015

Supporting Information

A supramolecular H-bond driven light switch sensor for small anions

Sebastian A. Rommel,[a] Dieter Sorsche,[a] and Sven Rau*[a]

[a] Institute for Inorganic Chemistry I, Ulm University, Albert-Einstein-Allee 11, 89081 Ulm, Germany

Table of contents

1. General Information
2. Additional Information

Scheme S1 Numbering scheme for the assignment of the ^{1}H NMR signals of Ir(tmBBI)-H_2.

Fig. S1 ^{1}H NMR titration of IrBBI-H_2 (bottom) in $CDCl_3$ with increasing equivalents of 3,5-dinitro benzoate anion. 4
Fig. S2 Plot of the shift of the NH signal in the ^{1}H NMR titration of IrBBI-H_2 in $CDCl_3$ with increasing equivalents of 3,5-dinitro benzoate anion. 4
Fig. S3 ^{1}H NMR titration of IrBBI-H_2 (bottom) in deuterated DCM with increasing equivalents of 3,5-dinitro benzoate anion..5
Fig. S4 ^{1}H NMR titration of IrBBI-H_2 in deuterated DCM with increasing equivalents of 3,5-dinitro benzoate anion.. 5
Fig. S5 ^{1}H NMR titration of IrBBI-H_2 in deuterated DCM with increasing equivalents of 3,5-dinitro benzoate anion. 6
Fig. S6 ^{1}H NMR titration of IrBBI-H_2 in deuterated DCM with increasing equivalents of 3,5-dinitro benzoate anion. 6
Fig. S7 Main: luminescence of IrBBI-H_2 as a function of increasing amounts of DNBA (depicted is only one measurement of three, average can be found in Fig.S8); inset: plot of the normalized iridium luminescence intensity as a function of number of equivalents of DNBA added. 7
Fig. S8 Plot (polynomial 7th grade) of the average of three measurements of the normalized luminescence intensity of IrBBI-H_2 as a function of number of equivalents of DNBA added. 7
Fig. S9 Main: plot of the normalized luminescence intensity of [Ir(ppy)$_2$(bipy)][PF_6] (R2) as a function of number of equivalents of DNBA added; Inset: scheme of the reagents involved....8
Fig. S10 Luminescence of IrBBI-H_2···DNBA as a function of increasing amounts of chloride (depicted is only one of at least two distinct measurements). 8
Fig. S11 Luminescence of IrBBI-H_2···DNBA as a function of increasing amounts of hydrogen sulfate (depicted is only one of at least two distinct measurements)....9
Fig. S12 Luminescence of IrBBI-H_2···DNBA as a function of increasing amounts of bromide (depicted is only one of at least two distinct measurements). 9
Fig. S13 Plot of the normalized luminescence intensity of IrBBI-H_2···DNBA as a function of increasing amounts of chloride (depicted is the average of two distinct measurements) and fit according to fit function FF1 (vide infra).[5] 10
Fig. S14 Plot of the normalized luminescence intensity of IrBBI-H_2···DNBA as a function of increasing amounts of hydrogen sulfate (depicted is the average of two distinct measurements) and fit according to fit function FF1 (vide infra).[5] 10
Fig. S15 Plot of the normalized luminescence intensity of IrBBI-H_2···DNBA as a function of increasing amounts of bromide (depicted is the average of two distinct measurements) and fit according to fit function FF1 (vide infra).[5] 11
Fig. S 16 Plot of the normalized luminescence intensity of IrBBI-H_2···DNBA (S) as a function of number of equivalents anions added; the "mixture" consists of equal amounts of Cl^-, Br^-, I^-, HSO_4^- anions; the overall ion concentration is 3 x 10^{-4} M. 11
3. Crystallographic data
4. References

1. General Information

Materials and Methods

4,4',5,5'-Tetramethyl-2,2'-bibenzimidazole and Tetrakis(2-phenylpyridine-C^2,N)bis(μ-chloro)diiridium were synthesized according to published procedures.[1–3] IrBBI was synthesized as published recently.[4] Technical grade solvents were purchased from VWR/Prolabo and redistilled under reduced pressure at 40°C. Dry solvents were obtained from a MBraun MB SPS-800 system. All chemicals were purchased from Merck Millipore, Sigma Aldrich, ABCR, Acros Organics, Alfa Aesar or VWR/Prolabo and used as purchased (≥95%). ^{1}H-NMR spectra were recorded at ambient temperature, unless otherwise stated, with a Bruker 400 MHz spectrometer. All spectra were referenced to the corresponding solvent residual signal, i.e. 1.940 ppm for acetonitrile, 7.260 for chloroform, 5.320 for dichloromethane and 4.870 for methanol. Mass spectra were recorded on a Finnigan MAT SSQ 710 or on a Thermoquest-Finnigan MAT 95XL. Elemental analysis was performed on an Elementar vario MICRO cube.

General spectroscopic Methods

Solvent chloroform used for spectral experiments was redistilled under reduced pressure at 40°C and kept over molecular sieves. Tetrabutylammonium (TBA) salts of F^-, Cl^-, Br^-, I^-, and $HSO4^-$ were purchased from Alfa Aesar and Merck Chemicals and dissolved in chloroform. Binding constants were performed in duplicate, and the average is reported. All data were manipulated with the OriginLab software package.

Emission spectroscopy

Emission spectra were performed on a JASCO Spectrofluorometer FP-8500 at room temperature. Cuvettes with a 1 cm path length and a 3mL volume were used for all measurements. For the DNBA quenching experiment aliquots of the TBA-DNBA salt ($c = 2 \times 10^{-5}$ M) were added stepwise to a 2 mL solution of IrBBI-H_2 ($c = 9.04 \times 10^{-7}$ M) in chloroform by a syringe. Thereby the TBA salt was dissolved in a solution of IrBBI-H_2 ($c = 9.04 \times 10^{-7}$ M), so no effect of dilution has to be regarded. For the anion sensor titration we prepared a mixture of IrBBI-H_2 ($c = 9.04 \times 10^{-7}$ M), quenched with 6.86 equivalents of the 3,5-dinitrobenzoate salt. For a typical anion sensor titration experiment 10 μL aliquots of a TBA salt ($c = 3 \times 10^{-4}$ M) were added stepwise to a 2 mL solution of IrBBI-H_2···DNBA ($c = 9.04 \times 10^{-7}$ M) in chloroform by a syringe. Thereby the TBA salt was dissolved in a solution of IrBBI-H_2···DNBA ($c = 9.04 \times 10^{-7}$ M), so no effect of dilution has to be regarded. The excitation wavelengths were fixed at 378 nm with the slit width of 5 nm and repeated at least twice times.

^{1}H NMR Titration

^{1}H NMR spectra were recorded at ambient temperature, unless otherwise stated, with a Bruker 400 MHz spectrometer with $CDCl_3$ as a solvent and TMS as an internal standard. For the titration experiment, aliquots of the TBA salt of 3,5-dinitrobenzoate (0 – 400 μL, 0.0225 M in dichloromethane-d^2) were added to a solution of IrBBI-H_2(200 μL, 4.5 mM in dichloromethane-d^2). The complex concentration was kept constant (1.5 mM).

2. Additional information

Hexafluorophosphate to 3,5-dinitro benzoate anion exchange was effected by adding the respective tetrabutylammonium benzoate salts to a solution of IrBBI-H_2 in dichloromethane. The resulting ion mixture were stirred at room temperature for 5 hours, then evaporated to dryness. The resulting solid was treated with acetonitrile and filtered. Slow addition of diethyl ether to the filtrate induced precipitation of the pure benzoate salts of the iridium complex.

Single crystals of IrBBI-H_2 + (3,5-dinitrobenzoate)- were grown at room temperature by layering diethyl ether above a dichloromethane solution of the iridium complex.

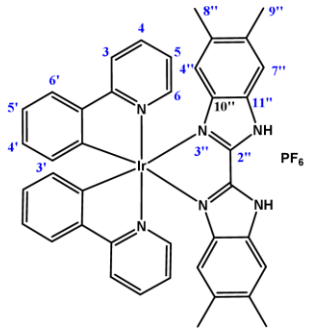

Scheme S2 Numbering scheme for the assignment of the ^{1}H NMR signals of Ir(tmBBI)-H_2.

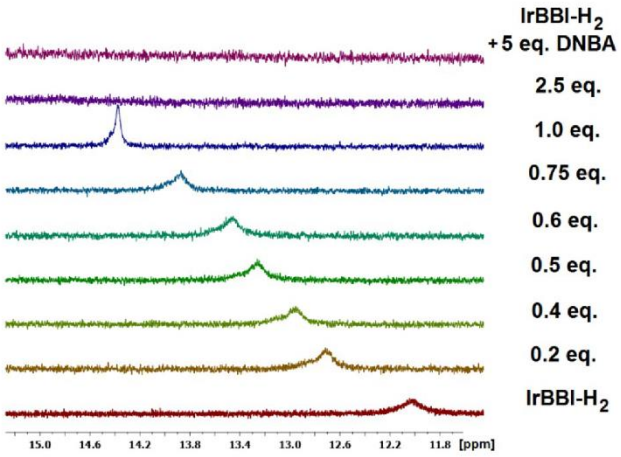

Fig. S1 ^{1}H NMR titration of IrBBI-H_2 (bottom) in $CDCl_3$ with increasing equivalents of 3,5-dinitro benzoate anion. The N-H signal of IrBBI-H_2 is shifting into the lowfield with increasing amount of DNBA. After 1.0 eq. the signal vanishes.

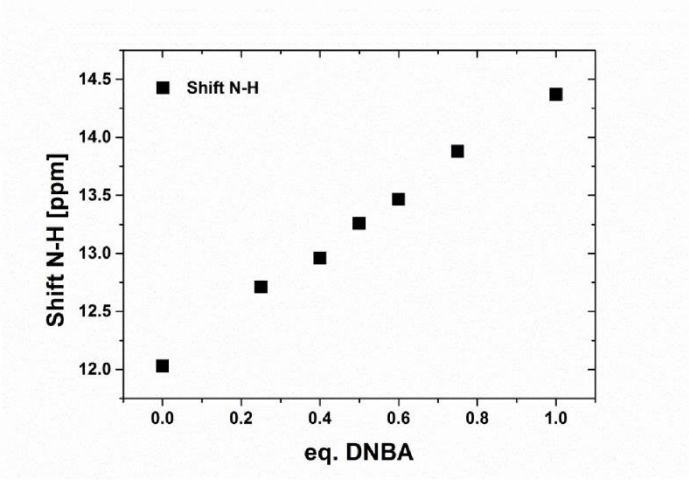

Fig. S2 Plot of the shift of the NH signal in the ^{1}H NMR titration of IrBBI-H_2 in $CDCl_3$ with increasing equivalents of 3,5-dinitro benzoate anion.

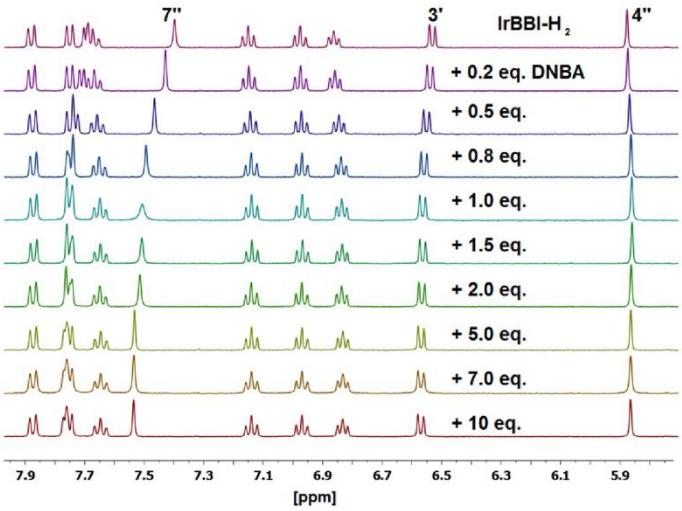

Fig. S3 ^{1}H NMR titration of IrBBI-H_2 (bottom) in deuterated DCM with increasing equivalents of 3,5-dinitro benzoate anion. The proton signals H-7'', H-3' and H-4'' are marked (host concentration = 1.5mM).

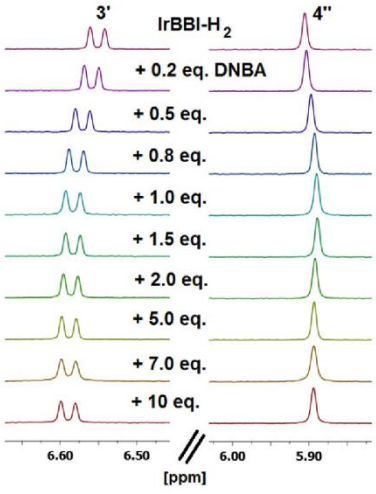

Fig. S4 ^{1}H NMR titration of IrBBI-H_2 in deuterated DCM with increasing equivalents of 3,5-dinitro benzoate anion. Depicted are the proton signals H-3' and H-4'' (host concentration = 1.5mM).

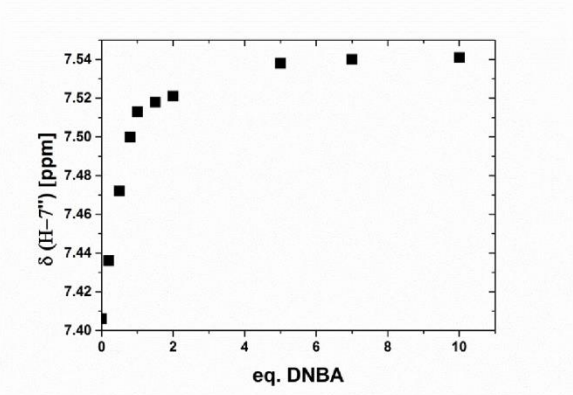

Fig. S5 ^{1}H NMR titration of IrBBI-H_2 in deuterated DCM with increasing equivalents of 3,5-dinitro benzoate anion. Depicted is the shift of the proton signal H-7'' (host concentration = 1.5mM).

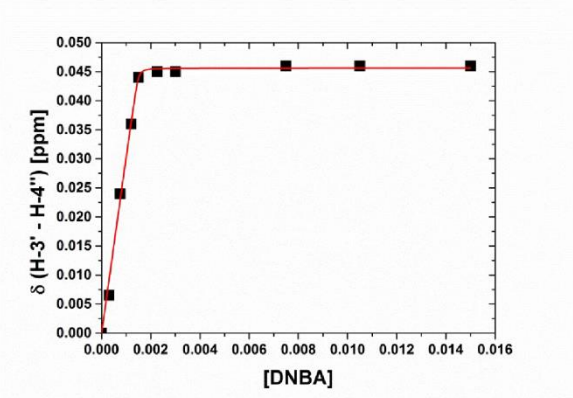

Fig. S6 ^{1}H NMR titration of IrBBI-H_2 in deuterated DCM with increasing equivalents of 3,5-dinitro benzoate anion. Depicted is the difference of the shifts of the proton signals H-3' and H-4''[δ(H-3' – H-4'')]; (host concentration = 1.5mM).

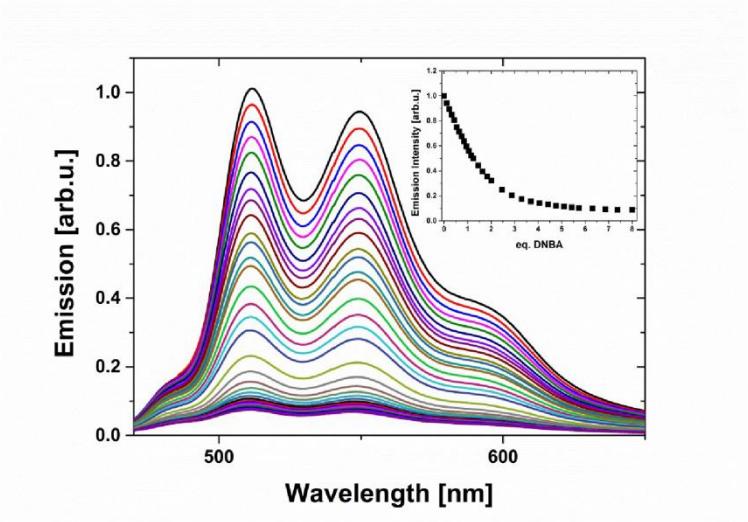

Fig. S7 Main: luminescence of IrBBI-H_2 as a function of increasing amounts of DNBA (depicted is only one measurement of three, average can be found in Fig.S8); inset: plot of the normalized iridium luminescence intensity as a function of number of equivalents of DNBA added.

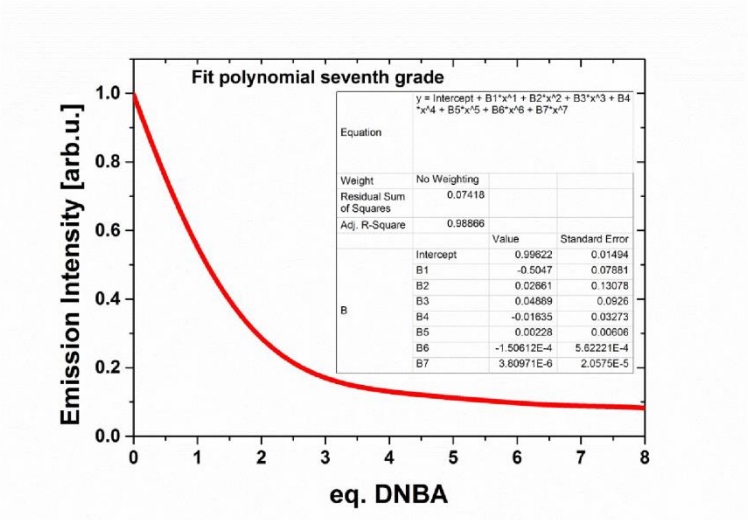

Fig. S8 Plot (polynomial 7th grade) of the average of three measurements of the normalized luminescence intensity of IrBBI-H_2 as a function of number of equivalents of DNBA added.

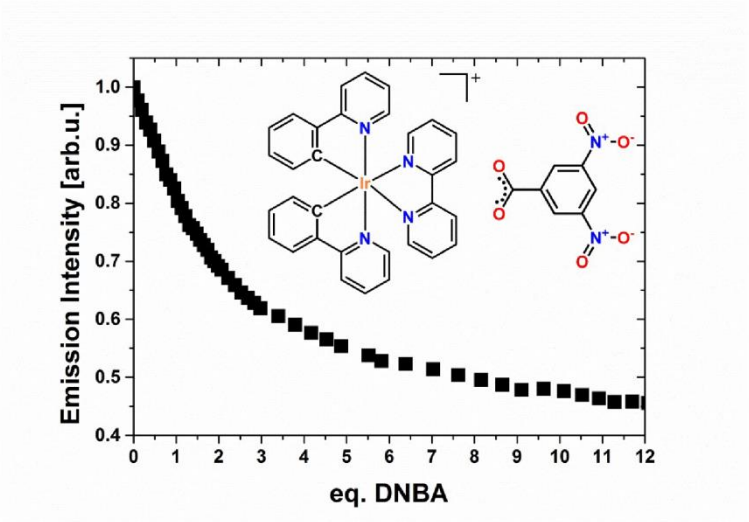

Fig. S9 Main: plot of the normalized luminescence intensity of $[Ir(ppy)_2(bipy)][PF_6]$ (**R2**) as a function of number of equivalents of DNBA added; Inset: scheme of the reagents involved.

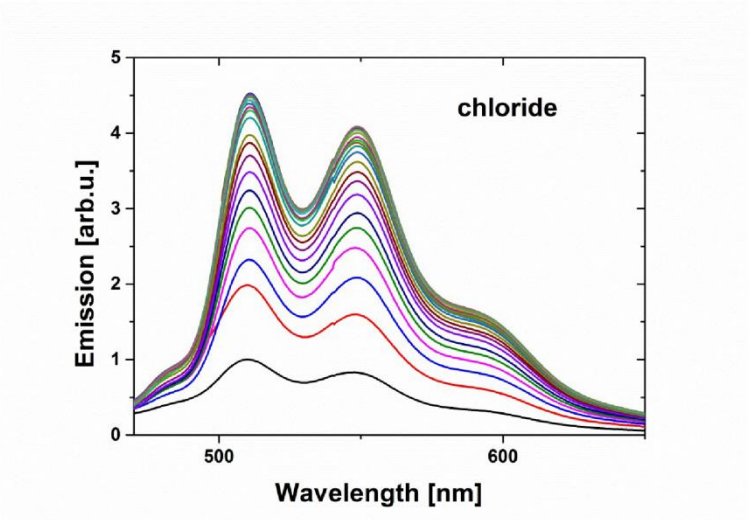

Fig. S10 Luminescence of IrBBI-H_2···DNBA as a function of increasing amounts of chloride (depicted is only one of at least two distinct measurements).

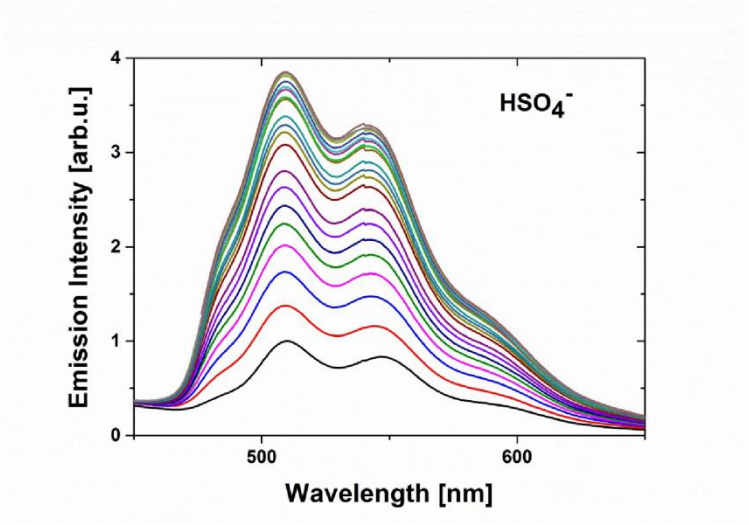

Fig. S11 Luminescence of IrBBI-H_2···DNBA as a function of increasing amounts of hydrogen sulfate (depicted is only one of at least two distinct measurements).

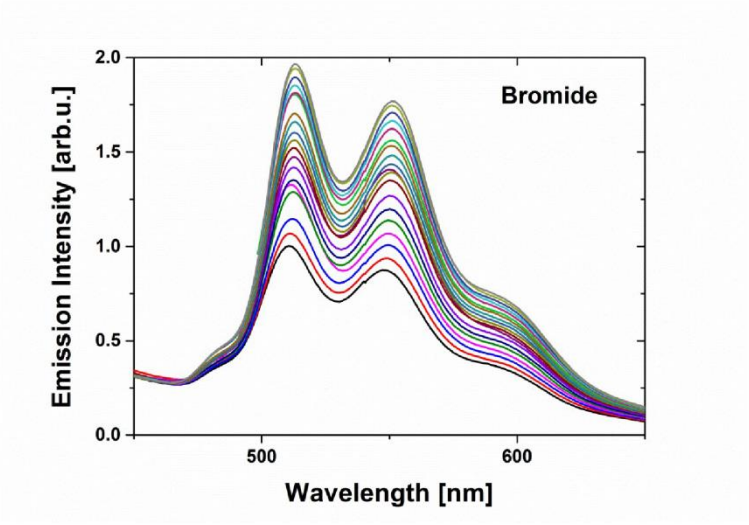

Fig. S12 Luminescence of IrBBI-H_2···DNBA as a function of increasing amounts of bromide (depicted is only one of at least two distinct measurements).

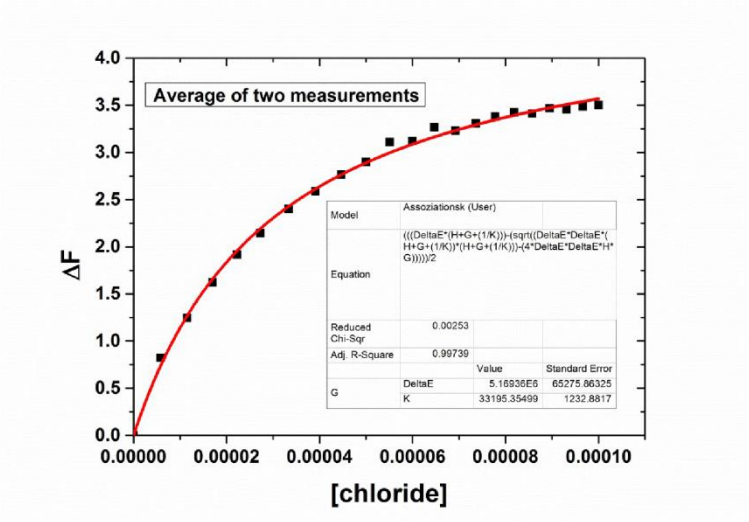

Fig. S13 Plot of the normalized luminescence intensity of IrBBI-H_2···DNBA as a function of increasing amounts of chloride (depicted is the average of two distinct measurements) and fit according to fit function FF1 (*vide infra*).[5]

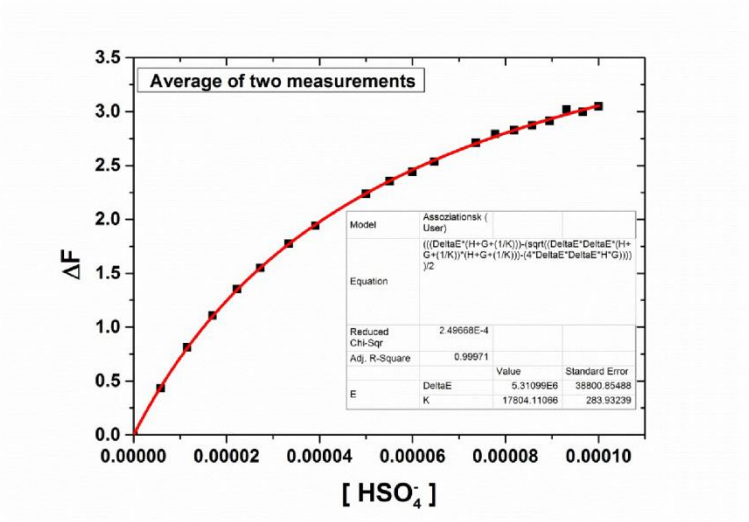

Fig. S14 Plot of the normalized luminescence intensity of IrBBI-H_2···DNBA as a function of increasing amounts of hydrogen sulfate (depicted is the average of two distinct measurements) and fit according to fit function FF1 (*vide infra*).[5]

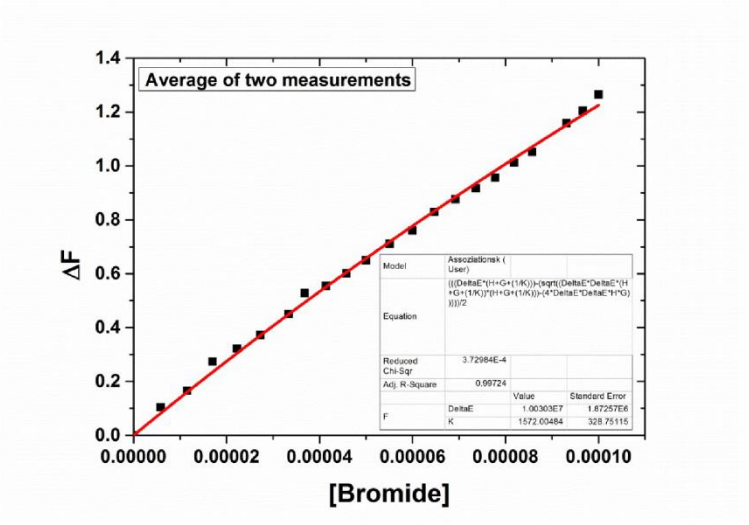

Fig. S15 Plot of the normalized luminescence intensity of IrBBI-H_2···DNBA as a function of increasing amounts of bromide (depicted is the average of two distinct measurements) and fit according to fit function FF1 (*vide infra*).[5]

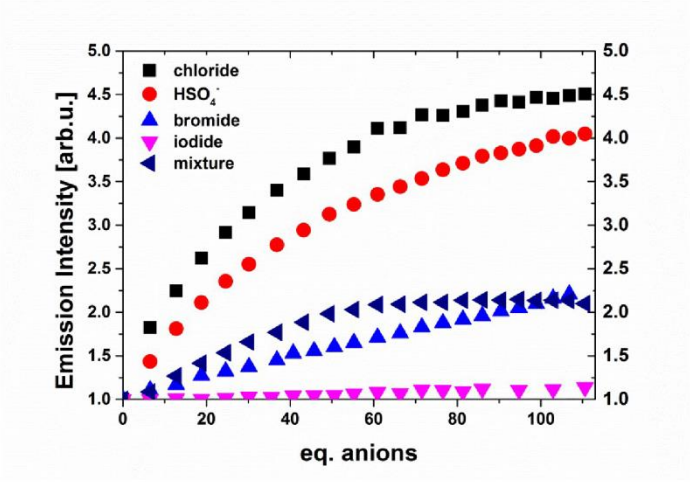

Fig. S 16 Plot of the normalized luminescence intensity of IrBBI-H_2···DNBA (S) as a function of number of equivalents anions added; the "mixture" consists of equal amounts of Cl^-, Br^-, I^-, HSO_4^- anions; the total ion concentration is 3 x 10^{-4} M.

Fit function FF1. Aforementioned binding constants were calculated to the fit function below with respect to literature[5]

$$\Delta F = \frac{\Delta\varepsilon([H] + [G] + K^{-1}) \pm \sqrt{\Delta\varepsilon^2([H] + [G] + K^{-1})^2 - 4\Delta\varepsilon^2[H][G]}}{2}$$

3. Crystallographic data

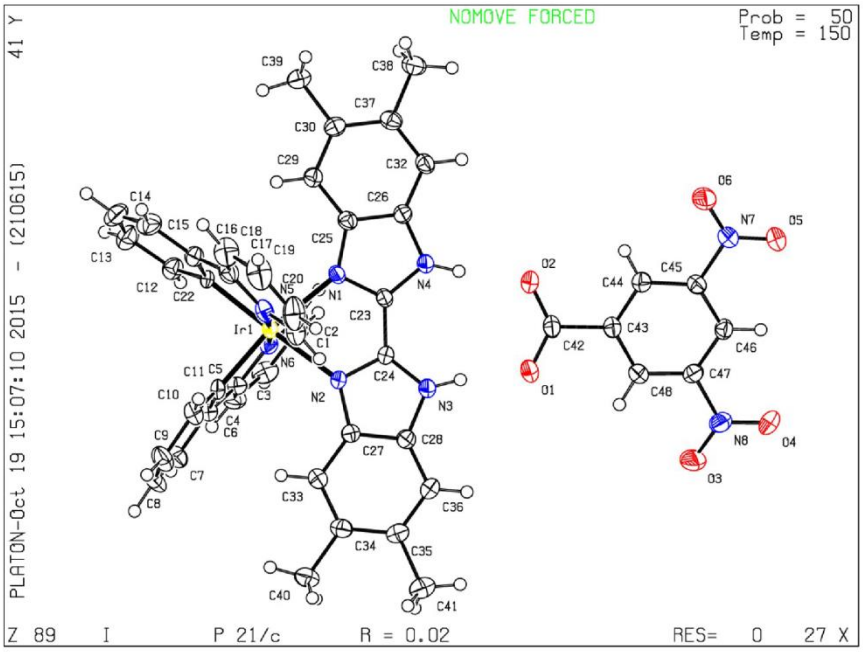

Crystal data for **[(ppy)$_2$Ir(tmBBI)](DNBA)**: C_{47} H_{37} Ir N_8 O_6, M_r = 1002.04 g mol^{-1}, yellow fragment, crystal size 0.1186 x 0.0535 x 0.0246 mm^3, monoclinic, space group P $2_1/c$, a = 12.14320(10) Å, b = 30.0046(4) Å, c = 11.12950(10) Å, β= 92.4390(10)°, V = 4051.38(7) Å^3, T = 150(2) K, Z = 4, $\rho_{calcd.}$ = 1.643 Mg/m^3, μ (Cu-Kα) = 6.897 mm^{-1}, F(000) = 2000, altogether 33117 reflexes up to h(-6/15), k(-35/37), l(-13/13) measured in the range of 7.450° ≤ Θ ≤ 74.469° , completeness Θ_{max} = 99.7 %, 8244 independent reflections, R_{int} = 0.0333, 7209 reflections with $F_0 > 4$ σ(Fo), 563 parameters, 0 restraints, $R1_{obs}$ = 0.0239, $wR2_{obs}$ = 0.0540, $R1_{all}$ = 0.0299, $wR2_{all}$ = 0.0564, GOOF = 1.052, largest difference peak and hole: 0.787/-0.504 e·Å^{-3}. CCDC 1432106 contains the supplementary crystallographic data for this paper. These data can be obtained free of charge from The Cambridge Crystallographic Data Centre via www.ccdc.cam.ac.uk/data_request/cif.

Bond angles

Atom1	Atom2	Atom3	Angle	Atom1	Atom2	Atom3	Angle	Atom1	Atom2	Atom3	Angle
H1	C1	C2	119.0(3)	C12	C22	Ir1	128.0(2)	C35	C41	H41C	109.5(3)
H1	C1	N6	118.8(3)	C16	C22	Ir1	114.6(2)	H41A	C41	H41B	109.5(4)
C2	C1	N6	122.2(3)	C24	C23	N1	117.5(2)	H41A	C41	H41C	109.5(4)
C1	C2	H2	120.5(3)	C24	C23	N4	128.8(3)	H41B	C41	H41C	109.4(4)
C1	C2	C3	118.8(3)	N1	C23	N4	113.6(2)	C23	N1	C25	105.2(2)
H2	C2	C3	120.6(3)	C23	C24	N2	116.1(2)	C23	N1	Ir1	114.6(2)
C2	C3	H3	120.3(3)	C23	C24	N3	130.1(3)	C25	N1	Ir1	140.1(2)
C2	C3	C4	119.4(3)	N2	C24	N3	113.8(2)	C24	N2	C27	104.8(2)
H3	C3	C4	120.3(3)	C26	C25	C29	121.3(2)	C24	N2	Ir1	115.9(2)
C3	C4	H4	120.0(3)	C26	C25	N1	108.1(2)	C27	N2	Ir1	139.2(2)
C3	C4	C5	120.1(3)	C29	C25	N1	130.6(2)	C24	N3	C28	106.3(2)
H4	C4	C5	119.9(3)	C25	C26	C32	120.9(2)	C24	N3	H3A	126.8(3)
C4	C5	C6	126.5(3)	C25	C26	N4	107.2(2)	C28	N3	H3A	126.9(3)
C4	C5	N6	119.6(3)	C32	C26	N4	131.9(2)	C23	N4	C26	105.8(2)
C6	C5	N6	113.9(3)	C28	C27	C33	120.1(3)	C23	N4	H4A	127.1(3)
C5	C6	C7	124.0(3)	C28	C27	N2	108.6(2)	C26	N4	H4A	127.1(3)
C5	C6	C11	115.0(3)	C33	C27	N2	131.3(3)	C17	N5	C21	119.7(3)
C7	C6	C11	120.8(3)	C27	C28	C36	121.6(3)	C17	N5	Ir1	115.3(2)
C6	C7	H7	120.1(3)	C27	C28	N3	106.5(2)	C21	N5	Ir1	124.8(2)
C6	C7	C8	119.6(3)	C36	C28	N3	131.9(3)	C1	N6	C5	119.7(2)
H7	C7	C8	120.3(4)	C25	C29	H29	120.8(3)	C1	N6	Ir1	124.3(2)
C7	C8	H8	119.7(4)	C25	C29	C30	118.4(3)	C5	N6	Ir1	116.0(2)
C7	C8	C9	120.5(3)	H29	C29	C30	120.8(3)	C11	Ir1	C22	87.4(1)
H8	C8	C9	119.8(4)	C29	C30	C37	120.1(3)	C11	Ir1	N1	169.8(1)
C8	C9	H9	119.7(4)	C29	C30	C39	119.8(3)	C11	Ir1	N2	94.6(1)
C8	C9	C10	120.7(3)	C37	C30	C39	120.0(3)	C11	Ir1	N5	97.8(1)
H9	C9	C10	119.6(4)	C26	C32	H32	120.8(3)	C11	Ir1	N6	80.5(1)
C9	C10	H10	119.8(3)	C26	C32	C37	118.4(3)	C22	Ir1	N1	102.3(1)
C9	C10	C11	120.3(3)	H32	C32	C37	120.8(3)	C22	Ir1	N2	176.1(1)
H10	C10	C11	119.8(3)	C27	C33	H33	120.7(3)	C22	Ir1	N5	80.1(1)
C6	C11	C10	118.0(3)	C27	C33	C34	118.5(3)	C22	Ir1	N6	95.2(1)
C6	C11	Ir1	114.5(2)	H33	C33	C34	120.8(3)	N1	Ir1	N2	75.82(9)
C10	C11	Ir1	127.2(2)	C33	C34	C35	120.9(3)	N1	Ir1	N5	86.94(9)
H12	C12	C13	119.4(3)	C33	C34	C40	119.2(3)	N1	Ir1	N6	95.43(9)
H12	C12	C22	119.5(3)	C35	C34	C40	120.0(3)	N2	Ir1	N5	96.31(9)
C13	C12	C22	121.1(3)	C34	C35	C36	120.5(3)	N2	Ir1	N6	88.40(9)
C12	C13	H13	119.7(3)	C34	C35	C41	119.6(3)	N5	Ir1	N6	175.1(1)
C12	C13	C14	120.7(3)	C36	C35	C41	119.8(3)	O4	N8	O3	124.2(3)
H13	C13	C14	119.6(4)	C28	C36	C35	118.4(3)	O4	N8	C47	118.3(3)
C13	C14	H14	120.1(4)	C28	C36	H36	120.8(3)	O3	N8	C47	117.5(3)
C13	C14	C15	119.8(3)	C35	C36	H36	120.8(3)	O5	N7	O6	124.6(3)
H14	C14	C15	120.1(4)	C30	C37	C32	120.8(3)	O5	N7	C45	118.0(2)
C14	C15	H15	120.1(4)	C30	C37	C38	119.4(3)	O6	N7	C45	117.4(2)
C14	C15	C16	119.8(3)	C32	C37	C38	119.8(3)	C44	C43	C48	119.5(3)
H15	C15	C16	120.1(3)	C37	C38	H38A	109.5(3)	C44	C43	C42	120.8(3)
C15	C16	C17	123.4(3)	C37	C38	H38B	109.4(3)	C48	C43	C42	119.6(3)
C15	C16	C22	121.5(3)	C37	C38	H38C	109.5(3)	C43	C44	H44	120.6(3)
C17	C16	C22	114.9(3)	H38A	C38	H38B	109.5(3)	C43	C44	C45	118.9(3)
C16	C17	C18	125.6(3)	H38A	C38	H38C	109.4(3)	H44	C44	C45	120.5(3)
C16	C17	N5	114.4(3)	H38B	C38	H38C	109.5(3)	N8	C47	C48	119.0(3)
C18	C17	N5	120.0(3)	C30	C39	H39A	109.5(3)	N8	C47	C46	118.1(3)
C17	C18	H18	120.2(4)	C30	C39	H39B	109.5(3)	C48	C47	C46	122.9(3)
C17	C18	C19	119.6(3)	C30	C39	H39C	109.4(3)	C43	C48	C47	119.3(3)
H18	C18	C19	120.2(4)	H39A	C39	H39B	109.5(3)	C43	C48	H48	120.3(3)
C18	C19	H19	120.0(4)	H39A	C39	H39C	109.5(3)	C47	C48	H48	120.4(3)
C18	C19	C20	119.9(4)	H39B	C39	H39C	109.5(3)	O1	C42	O2	127.5(3)
H19	C19	C20	120.1(4)	C34	C40	H40A	109.5(3)	O1	C42	C43	115.6(3)
C19	C20	H20	120.7(4)	C34	C40	H40B	109.5(3)	O2	C42	C43	116.9(3)
C19	C20	C21	118.6(4)	C34	C40	H40C	109.5(3)	C47	C46	H46	121.8(3)
H20	C20	C21	120.6(4)	H40A	C40	H40B	109.4(4)	C47	C46	C45	116.4(3)
C20	C21	H21	119.0(4)	H40A	C40	H40C	109.6(4)	H46	C46	C45	121.8(3)
C20	C21	N5	122.1(3)	H40B	C40	H40C	109.4(4)	N7	C45	C44	119.2(3)
H21	C21	N5	119.0(3)	C35	C41	H41A	109.5(3)	N7	C45	C46	117.8(3)
C12	C22	C16	117.1(3)	C35	C41	H41B	109.5(3)	C44	C45	C46	123.0(3)

Bond lengths

Atom 1	Atom 2	Length	Atom 1	Atom 2	Length	Atom 1	Atom 2	Length
C1	H1	0.930(3)	C18	C19	1.376(6)	C37	C38	1.508(5)
C1	C2	1.379(5)	C19	H19	0.929(4)	C38	H38A	0.959(4)
C1	N6	1.349(4)	C19	C20	1.380(6)	C38	H38B	0.960(3)
C2	H2	0.929(4)	C20	H20	0.930(4)	C38	H38C	0.960(4)
C2	C3	1.379(5)	C20	C21	1.378(5)	C39	H39A	0.959(4)
C3	H3	0.930(3)	C21	H21	0.929(4)	C39	H39B	0.959(4)
C3	C4	1.381(5)	C21	N5	1.343(4)	C39	H39C	0.959(3)
C4	H4	0.930(3)	C22	Ir1	2.020(3)	C40	H40A	0.961(4)
C4	C5	1.395(5)	C23	C24	1.454(4)	C40	H40B	0.961(4)
C5	C6	1.459(4)	C23	N1	1.330(4)	C40	H40C	0.960(4)
C5	N6	1.364(4)	C23	N4	1.348(4)	C41	H41A	0.960(4)
C6	C7	1.398(5)	C24	N2	1.337(4)	C41	H41B	0.960(4)
C6	C11	1.416(5)	C24	N3	1.335(4)	C41	H41C	0.960(4)
C7	H7	0.931(3)	C25	C26	1.399(4)	N1	Ir1	2.175(2)
C7	C8	1.377(5)	C25	C29	1.395(4)	N2	Ir1	2.150(2)
C8	H8	0.931(4)	C25	N1	1.393(3)	N3	H3A	0.860(2)
C8	C9	1.377(5)	C26	C32	1.397(4)	N4	H4A	0.861(2)
C9	H9	0.928(4)	C26	N4	1.383(4)	N5	Ir1	2.054(2)
C9	C10	1.396(5)	C27	C28	1.404(4)	N6	Ir1	2.038(2)
C10	H10	0.930(3)	C27	C33	1.404(4)	O1	C42	1.251(4)
C10	C11	1.396(4)	C27	N2	1.386(4)	O2	C42	1.252(4)
C11	Ir1	2.000(3)	C28	C36	1.387(4)	O5	N7	1.218(4)
C12	H12	0.930(3)	C28	N3	1.383(4)	O4	N8	1.225(4)
C12	C13	1.391(5)	C29	H29	0.930(3)	O6	N7	1.220(4)
C12	C22	1.399(4)	C29	C30	1.392(4)	N8	O3	1.227(5)
C13	H13	0.931(3)	C30	C37	1.430(5)	N8	C47	1.465(4)
C13	C14	1.382(5)	C30	C39	1.505(5)	N7	C45	1.475(4)
C14	H14	0.930(4)	C32	H32	0.929(3)	C43	C44	1.393(5)
C14	C15	1.379(5)	C32	C37	1.386(4)	C43	C48	1.389(4)
C15	H15	0.930(3)	C33	H33	0.929(3)	C43	C42	1.522(4)
C15	C16	1.398(5)	C33	C34	1.383(5)	C44	H44	0.929(3)
C16	C17	1.461(5)	C34	C35	1.421(5)	C44	C45	1.387(4)
C16	C22	1.408(4)	C34	C40	1.516(5)	C47	C48	1.380(5)
C17	C18	1.391(5)	C35	C36	1.386(5)	C47	C46	1.383(5)
C17	N5	1.362(4)	C35	C41	1.507(5)	C48	H48	0.930(3)
C18	H18	0.931(4)	C36	H36	0.931(3)	C46	H46	0.931(3)
						C46	C45	1.380(4)

*All bond lengths are given in Å.

Hydrogen bond distances

Atom 1	Atom 2	Length*
N3	O1	2.616(3)
N4	O2	2.690(3)

*All distances are given in Å.

4. References

1 E. Müller, G. Bernardinelli and J. Reedijkt, *Inorg. Chem.*, 1995, **34**, 5979–5988.
2 B. Schmid, F. O. Garces and R. J. Watts, *Inorg. Chem*, 1994, **33**, 9–14.
3 F. O. Garces, K. A. King and R. J. Watts, *Inorg. Chem.*, 1988, **27**, 3464–3471.
4 S. A. Rommel, D. Sorsche, N. Rockstroh, F. W. Heinemann, J. Kübel, M. Wächtler, B. Dietzek and S. Rau, *Eur. J. Inorg. Chem.*, 2015, 3730–3739.
5 Y. Liu, B.-H. Han and Y.-T. Chen, *J. Phys. Chem. B*, 2002, **106**, 4678–4687.

[SR4]: Functional dimming of pincer-shaped bibenzimidazole ruthenium(II) complexes with improved anion sensitive luminescence

Dieter Sorsche, Sebastian A. Rommel and Sven Rau*

* *corresponding author*

Published in: *Eur. J. Inorg. Chem.* **2016**, 1503-1513 (DOI: 10.1002/ejic.201501472)

Copyright Reprinted from "Functional dimming of pincer-shaped bibenzimidazole ruthenium(II) complexes with improved anion sensitive luminescence, Dieter Sorsche, Sebastian A. Rommel and Sven Rau, *Eur. J. Inorg. Chem.* **2016**, 1503-1513" with permission of the publisher John Wiley and Sons (License Number: 3910180469196)

Three bis(4,4'-di-*tert*-butyl-2,2'-bipyridine) ruthenium(II) 2,2'-bibenzimidazole complexes are presented and characterized with respect to their photophysical and structural properties. The 5,5',6,6'-tetramethyl-2,2'-bibenzimidazole (**L0**) and 4,4'-di(*p*-anisyl)-2,2'-bibenzimidazole (**L1**) and the corresponding ruthenium complexes **K0** and **K1** have been reported previously. The new complex **K2** contains the structurally confined ligand 4,4'-di(*o*,*o*'-dimethyl-*p*-anisyl)-2,2'-bibenzimidazole. Due to substitution at the 4,4'-positions, complexes **K1** and **K2** are equipped with a pincer-like geometry as shown by ^{1}H-NMR and XRD studies. The emission intensity of the latter complexes is dimmed as compared to **K0**. However titration experiments with tetrabutylammonium salts of fluoride, chloride, bromide, and iodide exhibit strongly enhanced sensitivity to hydrogen bonding of chloride and bromide, which increases the emission intensity to about 300%, eventually outperforming **K0**. With regard to the luminescence sensitivity, the structurally confined complexes **K1** and **K2** set a new benchmark among ruthenium(II) based colorimetric halide sensors.

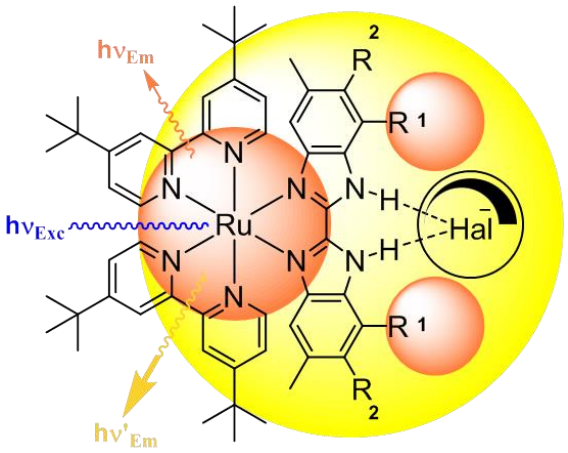

Contribution of the authors

Dieter Sorsche	Synthesis of the complexes. Performance of photophysical characterization of the sensor system, ^{1}H-NMR, emission and UV/Vis titration experiments. Growing of crystals suitable for x-ray analysis. Measurement and refinement of the X-ray structures. Writing of the manuscript.
Sebastian A. Rommel	Co-synthesis of ligands and of the complexes. Preliminary measurements. Discussion and revision of the manuscript.
Sven Rau	Discussion and revision of the manuscript, concept and results discussion.

ChemPubSoc Europe
DOI: 10.1002/ejic.201501472
EurJIC European Journal of Inorganic Chemistry
Full Paper

Luminescent Complexes

Functional Dimming of Pincer-Shaped Bibenzimidazole-Ruthenium(II) Complexes with Improved Anion-Sensitive Luminescence

Dieter Sorsche,[a] Sebastian A. Rommel,[a] and Sven Rau*[a]

Abstract: Three 2,2′-bibenzimidazole-bis(4,4′-di-*tert*-butyl-2,2′-bipyridine)ruthenium(II) complexes are presented and characterized with respect to their photophysical and structural properties. 4,4′,5,5′-Tetramethyl-2,2′-bibenzimidazole (**L0**), 4,4′-di(*p*-anisyl)-2,2′-bibenzimidazole (**L1**), and the ruthenium complexes **K0** and **K1** have been reported previously. The new complex **K2** contains the structurally confined ligand 4,4′-di(*o*,*o*′-dimethyl-*p*-anisyl)-2,2′-bibenzimidazole. Owing to substitution at the 4,4′-positions of the bibenzimidazole ligands, complexes **K1** and **K2** have pincer-like geometries, as shown by ^{1}H NMR spectroscopy and XRD studies. The emission intensities of these complexes are dimmed compared with that of **K0**, whereas titration experiments with tetrabutylammonium (TBA) salts of fluoride, chloride, bromide, and iodide show strongly enhanced sensitivity to hydrogen bonding with chloride and bromide ions, which increases the emission intensity to ca. 300 % of the original value, and they eventually outperform **K0**. With regard to the luminescence sensitivities, **K1** and **K2** set a new benchmark among 2,2′-biimidazole ruthenium(II) colorimetric halide sensors.

Introduction

Small ions, as simple as they are, play numerous fundamental regulatory roles in the environment. Owing to the ubiquitous abundance and versatile functions of small ions, a vast interest has grown in their noninvasive detection through molecular sensors.[1–4] Positively polarized sensor functions such as acidic protic functions can establish strong hydrogen bonds with anions, a feature that has also been employed in recent years for the self-assembly of supramolecular architectures through so-called anion coordination chemistry.[5,6] A potent approach to detect anions through hydrogen bonds is to connect one or more acidic H-donor functions with a luminophore in a way that the absorption and emission properties of the latter are visibly influenced by the appearance and strength of the H-bond interaction.[7,8] On the one hand, polypyridyl-ruthenium(II) complexes are widely applicable molecular tools for the introduction of light in technological and biological applications[9–12] because of their well-known photophysical properties and generally long-lived excited states, in which light energy is absorbed and provided for chemical conversions.[13,14] On the other hand, the vast synthetic variability of the general tris(diimine) framework allows the adjustment of a chromophore for a distinct application.[15–17] For example, 2,2′-bibenzimidazole ligands provide an elegant direct connection between a *cis*-diimine function for coordination to a ruthenium center with an acidic *cis*-diamine function, which acts as a twofold H-bond donor and is generally suitable for the binding of mono- and bidentate acceptors.[18–21] Also, several synthetic modifications have been reported for the manipulation of the electronic and steric properties of these ligands.[22–26] Manipulations of the 4,4′-positions are of particular interest as they define a pincer-like pocket around the hydrogen-bond moiety. Synthetic access to –Br, –I, $–NO_2$, $–NH_2$, and imine derivatives of the latter have been reported by Walther et al., and the nitro derivative as well as a methyl-disubstituted analogue were employed by Ye et al. as colorimetric halide sensors.[22,27] However, the nitro-substituted complex is nonluminescent and, accordingly, sensing through emission has not been reported. Nonetheless, a considerable rise of luminescence intensity has been demonstrated for unsubstituted complexes of 2,2′-bibenzimidazole, and an improvement of this effect could be achieved through the introduction of a small pocket upon the methylation of the 4,4′-positions.[25] By using the procedure presented by Siegel et al. for the synthesis of a wide variety of 4,4′-disubstituted 2,2′-bibenzimidazoles through a Negishi coupling route, we have recently reported the synthesis, photophysical, and structural characterization of new pincer-shaped ruthenium dyes with versatile supramolecular functions.[24]

With the ability to introduce aromatic substituents (Scheme 1, R^1), a direct spatial influence on the H-bond pocket can be envisaged. Therefore, we add another, structurally confined complex to this library of 4,4′-disubstituted bibenzimidazole complexes, for which we can delicately control the geometric orientation of the introduced groups. Our results show that anisyl substitution leads to a significant decrease of the emission intensity of the pristine ruthenium complex as a hexafluorophosphate salt. However, this dimming effect can be re-

[a] *Institute for Inorganic Chemistry I, Ulm University, Albert-Einstein-Allee 11, 89081 Ulm, Germany*
E-mail: sven.rau@uni-ulm.de
https://www.uni-ulm.de/nawi/nawi-anorg1/startseite.html
Supporting information for this article is available on the WWW under http://dx.doi.org/10.1002/ejic.201501472.

© 2016 Wiley-VCH Verlag GmbH & Co. KGaA, Weinheim

ChemPubSoc Europe
EurJIC European Journal of Inorganic Chemistry
Full Paper

versed upon hydrogen bonding between the complexes and weakly basic halides and leads to remarkable anion sensitivity in terms of signal enhancement (see Scheme 1).

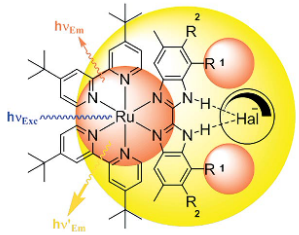

Scheme 1. Schematic depiction of the general concept of functionally dimmed pincer-shaped ruthenium chromophores presented in this work. Upon the exchange of the substituents R^1 and R^2, the luminescence $h\nu$ of the complexes is dimmed, and H-bond binding of halides leads to a significant increase and slight bathochromic shift of luminescence $h\nu'$.

Results and Discussion

Complexes **K0**, **K1**, and **K*** {[(tbbpy)$_3$Ru](PF$_6$)$_2$ for reference spectra; tbbpy = 4,4′-di-*tert*-butyl-2,2′-bipyridine} were synthesized according to literature-known procedures (Scheme 2).[17,23,24] The new complex **K2** was also prepared through a known procedure.[23,24] Although the hydrogen-bond area in **K0** is virtually open to the solvent, the anisyl substituents in **K1** and **K2** provide a pincerlike geometry, and the aryl rings entwine the *cis*-diamine moiety. In **K1**, the anisyl substituents are free to rotate around the C(benzimidazole)–C(anisyl) axis at room temperature, as shown through ^{1}H NMR spectroscopy, in which only two singlets for the eight anisyl protons and a broad singlet of the methoxy group were observed. The ^{1}H NMR spectrum of **K2** generally confirms that the new ligand also binds to ruthenium in a *cis* configuration with respect to its substituents. However, a sharp peak for the methoxy function is found, as well as two aliphatic singlets with equal area for the methyl groups and two singlets in the aromatic region of the spectrum for the four remaining anisyl protons, which is in agreement with a rigid C_2 symmetry in which the rotation of the dimethylanisyl moiety is sterically hindered. It is further noteworthy that the N–H proton signal observed in the low-field end of the recorded spectrum is significantly up-field-shifted; this indicates a slight effect of the π system of the anisyl substituents, which, in an orthogonal orientation with respect to the bibenzimidazole backbone, is oriented towards the *cis*-diamine functionality. In summary, the results strongly suggest that **K2** provides a more defined pincer geometry than **K1**, which is flexible and may generally be able to adapt to a small hydrogen-bond acceptor. A comparison of the ^{1}H NMR spectra of **K0**, **K1**, and **K2** is given in Figure 1. Single crystals of **K2** were grown to verify the aforementioned structural assumptions. Two structures could be characterized in detail: the first one, **K2**-MeOH, shows hydrogen bonding with one molecule of methanol sandwiched between the anisyl substituents, and the second one, **K2**-EtOAc, shows a hydrogen-bond framework with one molecule of ethyl acetate (Figure 2). Notably, in both structures, H bonds are formed between two N–H donor functions and only one O acceptor atom. Similarly, in the structure of **K1** reported recently (**K1**-H$_2$O), one molecule of water was found as a H-bond acceptor.[24] A second structure of **K1**, that is, **K1**-Cl, was obtained within this work and showed one chloride anion bound to the N–H donor functions (Figure 3, left). The general observation of hydrogen bonds with monodentate H-bond acceptors is peculiar, as previously reported structures of bibenzimidazole-ruthenium(II) complexes often show bifurcated H-bond frameworks with bidentate or multiple acceptors.[18,22,28,29]

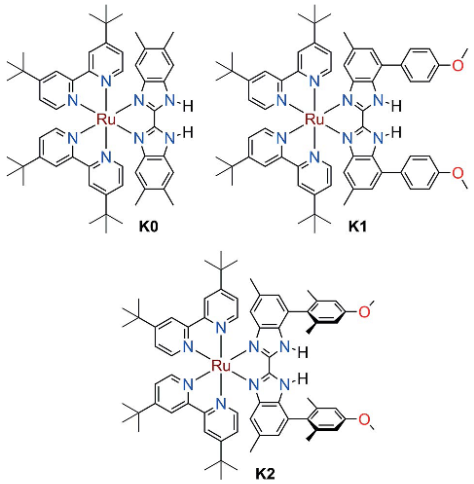

Scheme 2. Bibenzimidazole-ruthenium(II) complexes presented in this work; complexes **K1** and **K2** are pincer-shaped owing to anisyl substituents at the 4,4′-positions, and the latter is sterically confined.

In a recent publication on an iridium(III) complex, we showed that two molecules of water set up an extended H-bond framework with the bibenzimidazole, which is capped by two molecules of dimethyl sulfoxide (DMSO).[30] This aspect has already been discussed in detail for the related ruthenium complexes, and the tendency of bibenzimidazole ligands to bind two H-bond acceptor atoms stems from the rigidity of their framework, in contrast to related diamine/diimine ligands.[19] This is most prominently reflected by the bending of the ligand towards the metal center and subsequent widening of the *cis*-diamine geometry in the respective solid-state structures. The exclusive appearance of single acceptor binding in the four structures discussed in this paper shows that a distinct confining effect of the pincer geometry is introduced by the 4,4′-diaryl substitution pattern. All relevant angles, that is, the bending angles of the bibenzimidazole ligands towards the metal centers, the twist angles of the aryl substituents with the bibenzimidazole, and the opening of the pincer, as characterized by the angle described by the substituents and the distance between the aromatic ring centers (cf. Figure 3, right), as well

© 2016 Wiley-VCH Verlag GmbH & Co. KGaA, Weinheim

ChemPubSoc Europe
EurJIC European Journal of Inorganic Chemistry
Full Paper

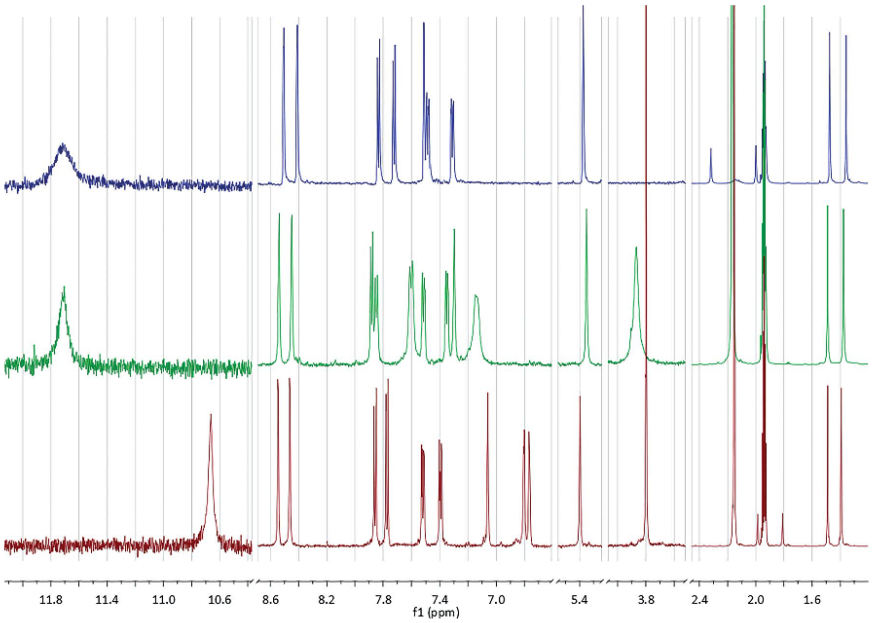

Figure 1. ^{1}H NMR spectra of **K0** (blue), **K1** (green), and **K2** (red; 10^{-3} M, [D_3]MeCN); the three areas (δ = 12.5–10, 8.75–3.5, and 2.5–0.0 ppm) are zoomed differently with respect to the intensity of the relevant (nonsolvent) signals.

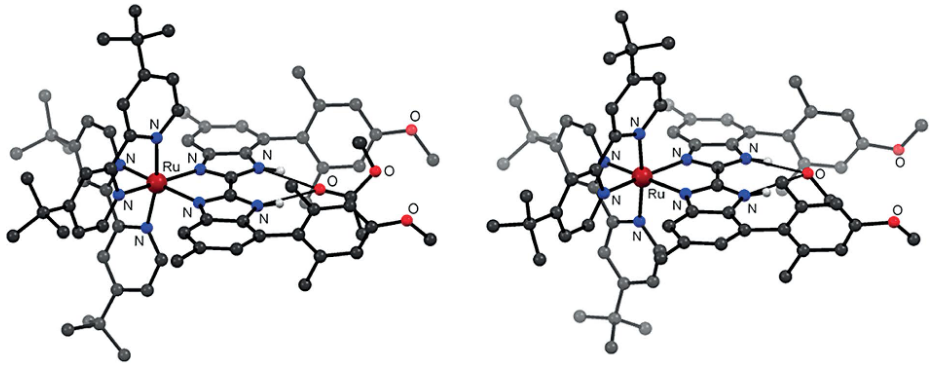

Figure 2. Solid-state structures of **K2**-EtOAc and **K2**-MeOH (ball-and-stick depictions; hydrogen atoms, counterions, and solvent molecules omitted for clarity, except for the H-bond frameworks).

as the H-bond lengths between the respective heteroatoms are listed in Table 1. Strikingly, **K1** and **K2** show very different geometries in the solid-state.

In the structure of **K1**-H_2O, the anisyl substituents tend to rotate in a plane with the bibenzimidazole to adapt an optimum angle to avoid gauche repulsion and maximize overlap with the π systems. Thereby, the pincer geometry is closed to achieve an almost perfectly dense packing with the H-bonded water molecule. In the structure of **K1**-Cl, a similar twist angle of 34.5° is found; however, the pocket size, as characterized by the distance between the anisyl centroids, is considerably larger at 9.376 Å compared with 8.967 Å. This geometry is also reflected in the opening angle of 18.3°, as compared to 14.4°; this angle has virtually no influence on the bibenzimidazole backbone, as characterized by its bending towards the ruthenium center. Strikingly, the twist angles of **K2** in its two solid-state structures are much larger than those of **K1**. As expected from the ^{1}H NMR spectra, the rotation of the anisyl moiety in a

© 2016 Wiley-VCH Verlag GmbH & Co. KGaA, Weinheim

ChemPubSoc Europe
EurJIC European Journal of Inorganic Chemistry
Full Paper

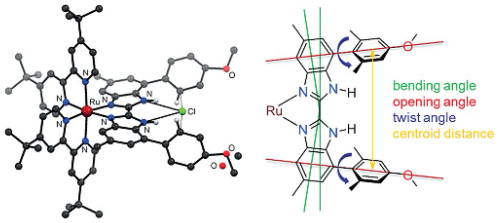

Figure 3. Left: solid-state structure of **K1**-Cl (ball-and-stick depiction; hydrogen atoms, second counterion, and solvent molecules omitted for clarity, except for the H-bond framework); right: color-coded schematic representation of the characteristic values measured in the crystal structures of **K1**-Cl, **K1**-H_2O,[24] **K2**-MeOH, and **K2**-EtOAc, collected in Table 1.

Table 1. Characteristic angles and distances in the solid-state structures of **K1** and **K2**.

	K1-H_2O	**K1**-Cl	**K2**-EtOAc	**K2**-MeOH
Opening angle [°]	14.4(2)	18.3(2)	5.8(2)	4.7(3)
Bending angle [°]	13.3(2)	13.5(2)	12.7(3)	10.0(4)
Torsion angle [°]	32.2(4), 45.4(4)	34.5(6)	76.0(5), 78.1(5)	73.8(7), 74.9(9)
H-bond length [Å]	2.80(2)	3.066	2.820(8)	2.82(7)
Centroid distance [Å]	8.967(5)	9.376(9)	8.360(8)	8.25(1)

plane with the bibenzimidazole is inhibited owing to the steric hindrance imposed by the two methyl groups at the *ortho* positions. Accordingly, to achieve a packing mode as dense as possible, a narrowing of the pincer geometry is observed, as the distances between the anisyl centroids are 8.360 and 8.25 Å, respectively, that is, ca. 0.66 Å less than the distance in **K1**-H_2O, in which only a small oxygen acceptor is also bound in the H-bond framework. This closing of the geometry is further reflected in the almost parallel orientation of the anisyl substituents, characterized by opening angles of 5.8 and 4.7°. A small secondary effect is observed for the bibenzimidazole backbone, which is bent towards the ruthenium center by 12.7° for **K2**-MeOH and only 10.0° for **K2**-EtOAc, compared with an average of 13.4° for the two structures of **K1**. The hydrogen-bond lengths between the *cis*-diamine moieties and oxygen atoms of the H-bond acceptors are virtually equal, whereas, naturally, the hydrogen-bond length is significantly longer for **K1**-Cl, owing to the larger van der Waals radius of the chloride ion. Notably, in the geometry adopted in the chloride complex, the two protons of the anisyl moiety are also oriented towards the anion, in agreement with a positive polarization at the edge of the aromatic system. Such long aryl-H–halide interactions are well-known in supramolecular architectures, in which halide guests are employed as templates for self-assembly.[31,32]

The UV/Vis absorption spectra of **K0**, **K1**, and **K2** show the same general features, but the molar extinction of **K2** in the metal-to-ligand charge-transfer (MLCT) region appears to be slightly higher (Figure 4). Interestingly, a ligand-centered absorption at $\lambda \approx 350$ nm shows two distinct maxima for **K0** and **K2**, whereas the smaller peak is only recognized as a shoulder for **K1**. This may indicate a possible overlap of the anisyl substituents with the π system of the bibenzimidazole, as the ^{1}H NMR spectrum of **K1** indicated that the rotation of the anisyl substituents is unhindered in acetonitrile solution at room temperature. Furthermore, the MLCT absorptions of both **K0** and **K2** are slightly broader at the bathochromic edge, which may infer that the bibenzimidazole π systems are isolated. In **K1**, in contrast, an overlap with the electron-rich anisyl substituents may increase the electron density in the benzimidazole moieties and, therefore, increase the σ-donor strength at the metal center to increase its t_{2g} donor states. The emission spectra show that the emission intensities of **K1** and **K2** are significantly lower than that of **K0** in the order I(**K0**) > I(**K2**) > I(**K1**), which corresponds to the introduction of the substituents and, subsequently, the ability to interact with the bibenzimidazole in terms of π overlap. Although the emission energies of **K0** and **K1** are virtually identical, the emission maximum of **K2** is shifted bathochromically to λ_{max}(Em) = 642 nm.

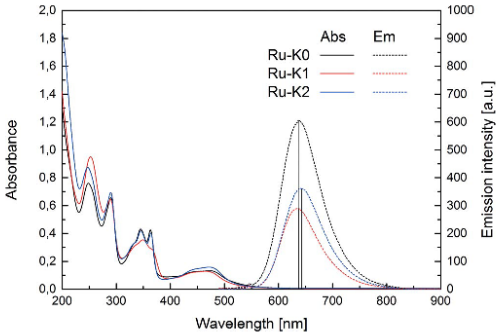

Figure 4. UV/Vis absorption and emission spectra of **K0**, **K1**, and **K2** (10^{-5} M, MeCN).

To investigate the potential of **K0**, **K1**, and **K2** as luminescent anion sensors, standard titration experiments were performed, in which up to 4 equiv. of fluoride, chloride, bromide, and iodide ions were added with a Hamilton syringe to solutions of the complexes in acetonitrile. Emission spectra were recorded at intervals of 10 µL to 100 µL, followed by intervals of 20 µL to 200 µL, and eventually 50 µL steps to 500 µL. For **K1**, a slight increase of emission intensity indicative of a H-bond interaction is observed between 0 and 0.5 equiv. of fluoride ions, followed by a steep quenching trajectory between 0.5 and 1 equiv., and the resulting species remains nonluminescent between 1–4 equiv. Complexes **K2** and **K0** also lose emission quickly between 0 and 1 equiv., although they display a less steep progression, and **K2** reaches its minimum slightly above 1 equiv. (Figure 5, left). Neither **K0** nor **K2** show an initial increase of the emission; however, in contrast to **K1** and **K2**, residual emission above 1 equiv. of fluoride ions is observed for **K0** with ca. 13 % of the initial emission intensity and λ_{max}(Em) = 613 nm. On the basis of previous reports, we concluded that the loss of emission indicates subsequent deprotonation of the amine functions, as deprotonated bibenzimidazole ruthenium complexes are generally nonluminescent.[16,18,20,24,28,33]

As the mono-deprotonated and fully deprotonated bibenzimidazole ruthenium complexes are usually well-distinguishable

© 2016 Wiley-VCH Verlag GmbH & Co. KGaA, Weinheim

ChemPubSoc Europe
EurJIC European Journal of Inorganic Chemistry
Full Paper

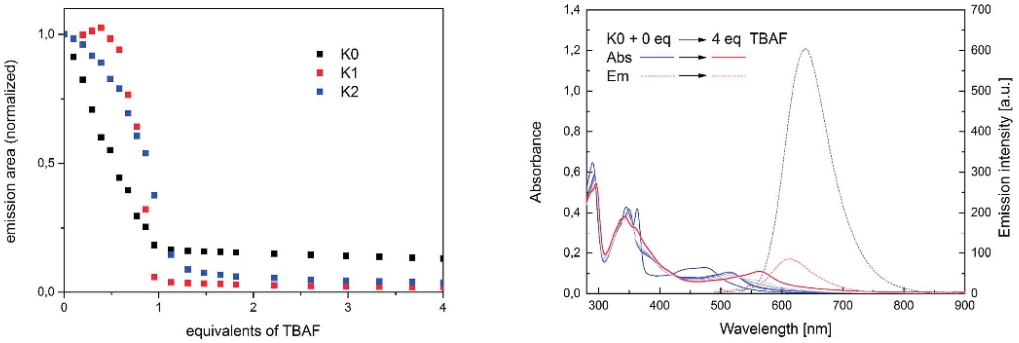

Figure 5. Left: emission quenching of **K0**, **K1**, and **K2** (10^{-5} M, MeCN) upon the addition of TBAF; emission area normalized to the respective initial value. Right: exemplary UV/Vis (solid line) and emission spectra (dashed line) of **K0** upon the addition of TBAF, the spectra of **K1** and **K2** are provided in the Supporting Information.

even with the naked eye through a transition from bright red to brown to deep violet, the UV/Vis spectra of **K0**, **K1**, and **K2** were recorded in acetonitrile upon the addition of either TBAF (for **K0**, cf. Figure 5, right) or TBAOH (for **K0**, Figure 6). The titration experiments with TBAOH show the expected transition for all three complexes, that is, the disappearance of the MLCT absorption band at $\lambda \approx 470$ nm, the intermediate appearance of a bathochromically shifted MLCT absorption with a peak maximum at $\lambda \approx 515$ nm, followed by a transition to the fully deprotonated species with an absorption maximum at $\lambda \approx 555$ nm. In contrast, the emission maxima of **K0** and **K2** shift hypsochromically, and the emission of **K2** eventually vanishes, whereas the emission of **K0** equilibrates at ca. 10 % of the emission of the doubly protonated complex at λ_{max}(Em) = 613 nm. The emission of **K1** shifts slightly bathochromically before it disappears completely, which is in agreement with the mono-deprotonated species that is observed when **K1** is dissolved in methanol.[24]

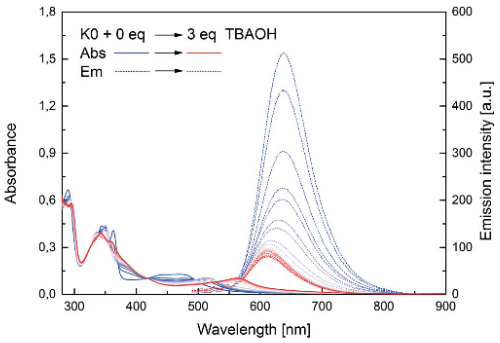

Figure 6. Exemplary absorption and emission spectra of **K0** upon the addition of TBAOH; the spectra of **K1** and **K2** are provided in the Supporting Information.

The respective titration spectra of **K0**, **K1**, and **K2** with fluoride ions match the behavior observed upon deprotonation with TBAOH; therefore, it is reasonable to assume that the interaction between the investigated complexes and TBAF is best described as subsequent deprotonation. Notably, **K0** and **K2** both exhibit hypsochromic emission shifts, whereas that of **K1** is shifted bathochromically. It should further be mentioned that the emission behavior suggests a slightly different mechanism for the deprotonation of **K1**, as the formation of a hydrogen-bond adduct at up to 0.5 equiv. of fluoride ions is indicated. The stoichiometry of fluoride deprotonation with respect to the well-resolved MLCT band shift has been investigated in more detail; a first deprotonation of all complexes at 1 equiv. of fluoride is observed, and the subsequent full deprotonation of **K1** is observed at 4 equiv., whereas it is observed at 6 equiv. for **K0** and **K2**.

To explain the unique behavior of **K1**, one must consider the formation of dimers from the mono-deprotonated complex, as observed in the solid-state structure of **L1**-HCl (Figure 7). For structurally simple biimidazole and bibenzimidazole ruthenium(II) complexes, the dimerization of two mono-deprotonated complexes can occur through shared hydrogen bonds. Ye et al. pointed out that self-association presents a competing process with respect to a potential sensing application and suggested that this process might be inhibited through the introduction of substituents at the 4,4′-positions. However, the obtained structure of **L1**-HCl shows self-association, which is favored by additional intermolecular attraction, that is, a total of four π-stacking interactions between the formally electron-rich anisyl rings and the electron-deficient benzimidazole moieties within the dimer.

This arrangement is possible because of the free rotatability of the substituents in **L1** and **K1**, whereas this effect is most likely hindered in **K2** because of the almost perpendicular arrangement of the benzimidazole and anisyl moieties. In principal, **K0** is capable of forming such dimers; however, they lack the stabilizing π interactions, and a respective effect may not be observed. To verify the ability of **K1** to form dimers, as observed for the ligand, the mono-deprotonated complex was prepared through two approaches: (a) full deprotonation with

© 2016 Wiley-VCH Verlag GmbH & Co. KGaA, Weinheim

ChemPubSoc Europe
EurJIC European Journal of Inorganic Chemistry
Full Paper

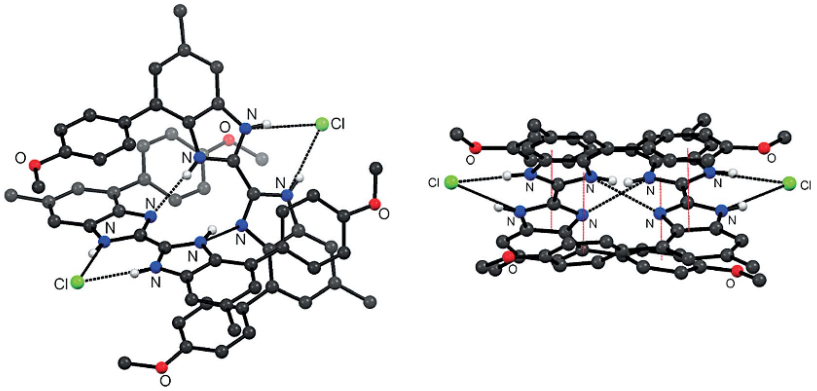

Figure 7. Solid-state structure of the HCl adduct **L1**-HCl (ball-and-stick depiction; hydrogen atoms and solvent molecules omitted for clarity, except for the H-bond framework), which shows dimer formation; the black lines indicate hydrogen bonds, and the red lines indicate π-stacking interactions.

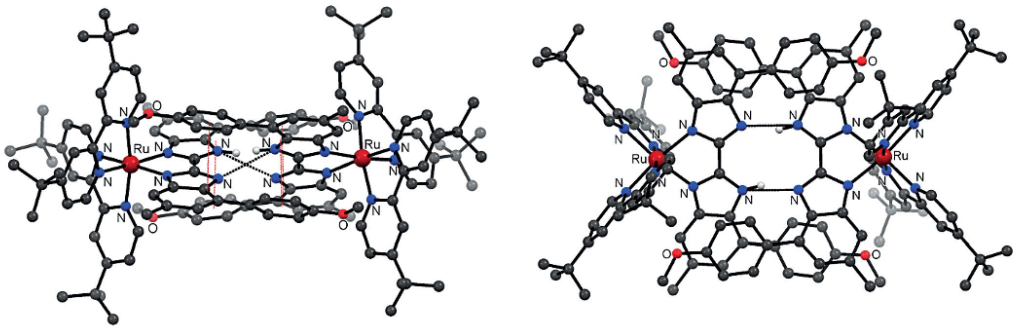

Figure 8. Solid-state structures of the dimer $(\mathbf{K1})_2$ [ball-and-stick depiction, left: structure (a), side-view; right: structure (b), top view; hydrogen atoms and solvent molecules omitted for clarity, except for the H-bond framework]; the black lines indicate hydrogen bonds, and the red lines indicate π-stacking interactions.

aqueous sodium hydroxide and subsequent addition of the mildly acidic, sterically demanding phenylphosphonic acid and (b) full deprotonation with trimethylamine and subsequent treatment with water. The obtained structures of $(\mathbf{K1})_2$ nicely show the same dimer of the intertwined monoprotonated complex, accompanied by either (a) four phenylphosphonate counterions that share a hydrogen-bond network through six protons or (b) two hexafluoridophosphate counterions, as well as solvent molecules for both structures. The observed dimerization behavior is very similar to that of the ligand (Figure 8). The respective values for the π stacking and H-bond lengths as well as the characteristic angles are collected in Table 2.

It has been shown in the literature that hydrogen bonds through the *cis*-diamine functionality of the bibenzimidazole usually affect the electron density around the corresponding protons, the signals of which in some cases can be observed by ^{1}H NMR spectroscopy. Accordingly, spectra (10^{-3} mol L^{-1} in [D_3]acetonitrile) of all complexes upon addition of either 1 equiv. of TBACl, TBABr, and TBAI were recorded (Figure 9).[25]

Table 2. Characteristic angles and distances of the solid-state structures of **L1**-HCl and $(\mathbf{K1})_2$ (a) and (b).

Complex	π stacking anisyl–imidazole [Å]	*d*(N–H···N) [Å]	Twist anisyl–imidazole [°]
L1-HCl	3.331	2.874	43.2
$(\mathbf{K1})_2$ (a)	3.311	2.821	36.8
$(\mathbf{K1})_2$ (b)	3.377	2.877	40.2

The obtained spectra nicely show a deshielding of the acidic protons, indicative for hydrogen bonding with chloride and bromide. With iodide the signal could only be observed for **K2**, whereas it disappeared in the spectra of **K0** and **K1** (cf. Table 3). The signal shifts for **K1** are somewhat larger as compared to those of **K0**, whereas the N-H signals of the pristine PF_6 salts appear at the same position. As mentioned before, the N-H proton signal of **K2** is slightly more shielded as compared to the case of **K0** and **K1**. Accordingly, all signals of the chloride and bromide adducts are shifted upfield as compared to those

© 2016 Wiley-VCH Verlag GmbH & Co. KGaA, Weinheim

ChemPubSoc Europe
EurJIC European Journal of Inorganic Chemistry
Full Paper

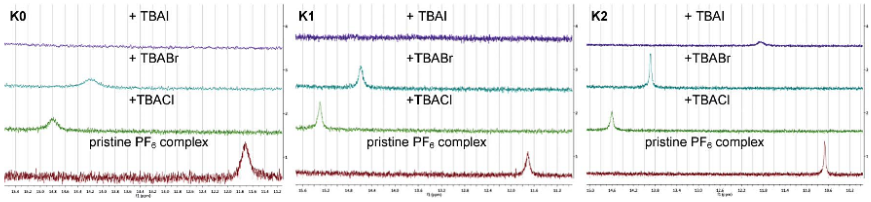

Figure 9. Low-field region (N–H signals) of the ^{1}H NMR spectra of **K0** (left), **K1** (middle), and **K2** (right): pristine PF_6 complexes (bottom/red), upon the addition of 1 equiv. of TBACl (green), TBABr (blue), and TBAI (purple).

Table 3. ^{1}H NMR chemical shifts [ppm] of the N–H protons of **K0**, **K1**, and **K2** upon the addition of 1 equiv. of Cl^-, Br^-, or I^- ions; 10^{-3} M [D_3]MeCN.

Complex	Pristine PF_6 salt	1 equiv. of TBACl (signal shift $\Delta\delta$)	1 equiv. of TBABr (signal shift $\Delta\delta$)	1 equiv. of TBAI (signal shift $\Delta\delta$)
K0	11.72	14.79 (3.07)	14.18 (2.46)	–
K1	11.71	15.30 (3.59)	14.60 (2.89)	–
K2	10.66	14.60 (3.94)	13.89 (3.23)	11.87 (1.21)

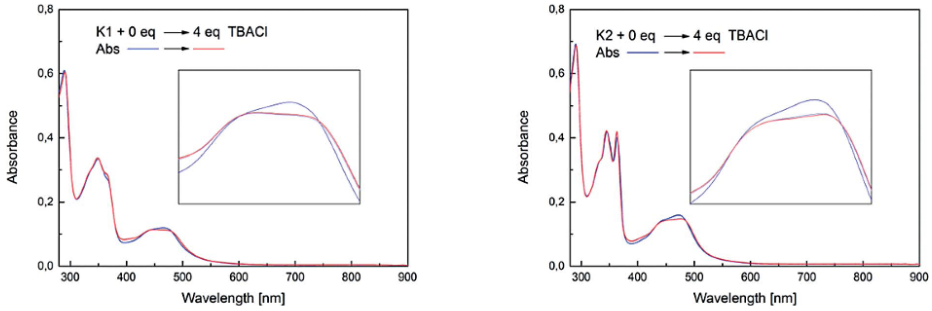

Figure 10. UV/Vis spectra of **K1** (left) and **K2** (right; 10^{-5} M, MeCN) upon the addition of TBACl; inset: zoom of the MLCT absorption band (λ = 410–500 nm).

of the respective adducts of **K0** and **K1**. Nonetheless, the remaining difference is not as predominant as with the PF_6 complexes, and – accordingly – the total signal shift as characterized by the difference between initial positions and positions in the presence of Cl^- and Br^- is the highest for **K2** (cf. Table 3, parentheses).

Titration experiments with chloride, bromide, and iodide ions were performed, as described for the fluoride and hydroxide titrations. The UV/Vis spectra of all complexes show a sensitive response to addition of chloride and bromide ions, that is, a slight broadening and decrease in the absorptivity of the MLCT absorption bands, which is indicative of a strong H-bond interaction between the halide ions and the bibenzimidazole ligands. However, these effects are hard to distinguish by the naked eye and show a rapid saturation that is not useful for the determination of an exact concentration of the analyte (Figure 10).

In the emission spectra, only a slight increase in intensity along with a bathochromic shift of the emission was observed for **K0** upon the addition of chloride and bromide ions to ca. 5 % before it even decreased linearly upon the further addition of the halide solution. This came as a surprise with respect to the behavior of similar complexes that had been reported previously. The main difference in **K0** compared with reported systems is the four methyl substituents; however, the basicity of bibenzimidazole ligands has a crucial effect on their hydrogen-bond properties. For **K0**, the inductive effect of the methyl groups has already been proven to cause unusual reactivity compared with that of unsubstituted analogues.[34,35] To validate our method, we performed titration experiments with the TBA halide salts with **K*** as a reference compound and observed a comparable decrease in emission intensity to that observed for **K0** after the addition of 1 equiv. of salt; it was concluded that, in addition to hydrogen bonding, some minor effects connected with our method caused the eventual linear behavior observed.

Although **K0** is not a suitable sensor molecule for the detection of chloride, bromide, or iodide ions, a much stronger effect was observed when **K1** and **K2** were treated with the latter salts, that is, a significant increase in luminescence intensity was accompanied by a slight bathochromic shift (Figure 11). The luminescence intensity of **K1** increases to 303 % of the initial value upon the addition of 1 equiv. of chloride ions and to ca. 279 % of the initial value in the presence of bromide ions. Likewise, the luminescence intensity of **K2** increases to ca. 244 % of the initial value when treated with chloride ions and to

© 2016 Wiley-VCH Verlag GmbH & Co. KGaA, Weinheim

ChemPubSoc Europe
EurJIC European Journal of Inorganic Chemistry
Full Paper

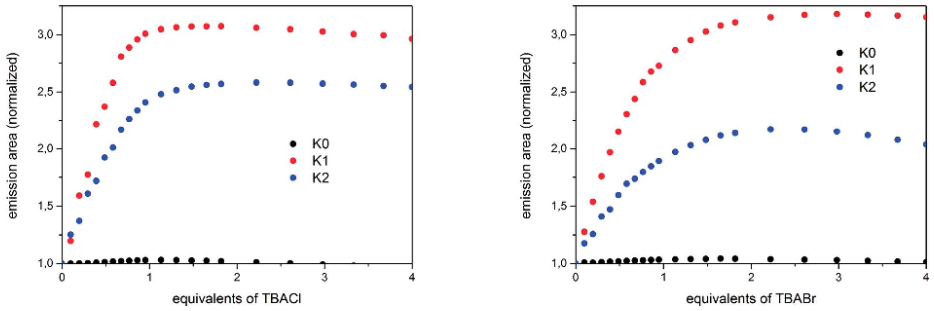

Figure 11. Plot of the emission intensity area increase of **K0**, **K1**, and **K2** upon the addition of TBACl (left) and TBABr (right), normalized with respect to the initial emission of the pristine PF_6 complexes.

193 % of the initial value when treated with bromide ions. Upon the addition of 1 equiv. of bromide ions, the emission intensities for **K0** and **K2** are approximately equal within the experimental error, that is, the H bonding of these halides nicely cancels the initial dimming of luminescence through the introduction of the anisyl substituents (Figure 12). Both **K1** and **K2** eventually outperform **K0** significantly in terms of luminescence intensity upon the addition of 1 equiv. of chloride ions, **K1** also outperforms **K0** in the presence of bromide ions, and their remarkably higher sensitivity compared with that of **K0** is retained.

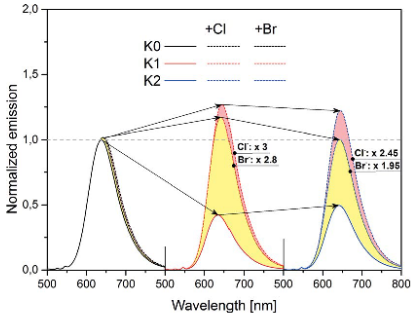

Figure 12. Comparison of the emission spectra of **K0** (left, black lines), **K1** (middle, red lines), and **K2** (right, blue lines); solid lines, white area: pristine PF_6 salts; dotted lines, yellow area: upon the addition of 1 equiv. of TBABr; dashed lines, red area: upon the addition of 1 equiv. of TBACl.

Therefore, through the functional dimming that has been introduced by the attachment of the anisyl substituents, a significant enhancement in luminescence sensitivity has been gained that, to the best of our knowledge, exceeds those of all previously reported ruthenium(II) bibenzimidazole sensors. To quantify the interactions of the investigated complexes with chloride and bromide ions, association constants were calculated from the obtained data.[36] Owing to the eventual decrease in the emission of **K0** after the addition of 1 equiv., no reliable fit could be generated. In contrast, the association between **K1** and chloride ions is too strong, as illustrated by the almost linear progression between 0 and 1 equiv., after which a virtually linear saturation is observed. The obtained value of 1.8×10^6 L mol^{-1} was calculated with a mean error of 25 %, and we strongly suggest that the interaction is described as a stoichiometric ion-pair formation rather than a dynamic equilibrium. Smaller association constants were determined for **K1** with bromide ions and for **K2** with both chloride and bromide ions, as reflected by the respective errors; the values are collected in Table 4. Titrations with iodide ions showed only minor effects on either complex, that is, only a linear decrease in the emission of **K0** and slight increases of the emissions of **K1** and **K2** by ca. 40 and 20 %, respectively. The respective absorption spectra showed virtually no response in the MLCT region. All of the obtained values from the emission spectra that characterize the respective sensor–ion interaction are summarized in Table 4.

Table 4. Luminescence properties of **K0**, **K1**, and **K2** upon the addition of 1 equiv. of Cl^-, Br^-, or I^- ions.

Complex	Ion	Luminescence increase[a] [%]	λ_{max}(Em) [nm]	log K_a[b]
K0	Cl^-	103	645	–
K0	Br^-	103	641	5.13[c] (16 %)
K0	I^-	97	641	–
K1	Cl^-	303	645	6.26 (25 %)
K1	Br^-	279	642	5.63 (7 %)
K1	I^-	111	639	–
K2	Cl^-	244	646	5.82 (14 %)
K2	Br^-	193	646	5.63 (15 %)
K2	I^-	106	643	–

[a] Relative to the initial value of the pristine PF_6 complexes upon the addition of 1 equiv. TBAX. [b] Calculated if possible, fit errors are given in parentheses. [c] Calculated only within 0–1 equiv. owing to the subsequent decrease above 1 equiv.

Conclusions

The three complexes **K0**, **K1**, and **K2** have been synthesized and fully characterized with respect to their geometric features. All of the complexes exhibit a *cis*-diamine functionality, which, in principle, can interact with H-bond acceptors such as small anions. Complexes **K1** and **K2** exhibit additional anisyl functionalities adjacent to the diamine function. In **K1**, this geometry is

© 2016 Wiley-VCH Verlag GmbH & Co. KGaA, Weinheim

ChemPubSoc Europe

EurJIC European Journal of Inorganic Chemistry
Full Paper

flexible, as the anisyl substituent can rotate and, therefore, modify the size of the cavity within the pincerlike geometry. Additional anion–dipole interactions between aryl protons and a chloride guest were observed in the crystal. The solid-state structures represent the H-bonding capabilities of the protonated complexes **K1** and **K2** as well as the nature of the structural restrictions. The structures obtained from the ligand **L1** and deprotonated **K1** emphasize their unique supramolecular interactions owing to the modularity and flexibility of the ligand. The emission spectra show that the introduction of the anisyl substituents is accompanied by a dimming of the luminescence of **K1** and **K2** compared with that of **K0**. The treatment of all of the complexes with fluoride ions leads to deprotonation. The interaction of **K0** with iodide ions is negligible within the experimental error, only a slight response occurs for **K2**, and a more pronounced response occurs for **K1**. However, the UV/Vis spectra suggest predominant interactions with the complex periphery. The addition of chloride or bromide ions eventually cancels and even reverses the luminescence dimming of **K1** and **K2** with an eventual increase to 300 % compared with the luminescence of the pristine material. This enhanced sensitivity and selectivity for chloride and bromide ions among the halide ions is a promising finding for the further development of ruthenium(II) bibenzimidazole based anion sensors.

Experimental Section

General: Technical-grade solvents were purchased from VWR/Prolabo and redistilled under reduced pressure at 40 °C. Dry degassed acetonitrile was purified from the HPLC-grade solvent from VWR/Prolabo with an MBraun SPS 800 solvent purification system. All chemicals were purchased from Sigma–Aldrich, ABCR, Acros Organics, Alfa Aesar, or VWR/Prolabo and used as purchased (≥95 %). Microwave-assisted syntheses were performed with an MLS START 1500 system. The ^{1}H NMR spectra were recorded at ambient temperature, unless otherwise stated, with a Bruker 400 MHz spectrometer. All spectra were referenced to the corresponding residual solvent signals, that is, δ = 1.940 ppm for acetonitrile and δ = 5.320 ppm for dichloromethane. X-ray crystallography was performed with a SuperNova (Dual Source) diffractometer, equipped with an ATLAS detector, from Agilent Technologies. The structures were refined by full-matrix least-squares techniques against F_o^2 (SHELXL 2013).[37] The hydrogen atoms were included at calculated positions with fixed thermal parameters. All non-hydrogen atoms were refined anisotropically. The electronic absorption spectra were recorded with a JASCO V-670 spectrophotometer, and the emission spectra were recorded with a JASCO FP-8500 spectrofluorometer. 10^{-4} M stock solutions of **K***, **K0**, **K1**, and **K2** as well as 2×10^{-3} M stock solutions of the tetrabutylammonium salts of OH^-, F^-, Cl^-, Br^-, and I^- were prepared under a protective argon atmosphere in a UNILAB glovebox from MBraun. Sample solutions (2 mL) were prepared by 1:10 dilution of the complex solutions in gas-tight emission cuvettes, 1 mL TBA halide solutions were prepared by dilution of the investigated complex solution (100 µL) and the TBA halide solution (100 µL). The TBA halide solution (500 µL) was then transferred to a Hamilton® syringe and added to the cuvette through a septum in defined portions without the removal of the syringe between measurements. The solutions were continuously stirred during the measurements and TBA halide addition, and a new septum was used for every run. Data manipulations were performed with the Origin Pro 9.0.0G (32-bit) b45 software from OriginLab Corporation (© 1991–2012).

4,4′,5,5′-Tetramethyl-2,2′-bibenzimidazole (tmBBI, **L0**), 1,1′-bis(*tert*-butoxycarbonyl)-4,4′-bis(4-methoxyphenyl)-6,6′-dimethyl-2,2′-bibenzimidazole (dmBBI^{phOMe}boc$_2$, **L1**), 1,1′-bis(*tert*-butoxycarbonyl)-4,4′-bis(2,6-dimethyl-4-methoxyphenyl)-6,6′-dimethyl-2,2′-bisbenzimidazole (dmBBI^{dmphOMe}boc$_2$, **L2**), bis(4,4′-di-*tert*-butyl-2,2′-bipyridine)(4,4′,5,5′-tetramethyl-2,2′-bibenzimidazole) ruthenium(II) dihexafluoridophosphate (**K1**), and bis(4,4′-di-*tert*-butyl-2,2′-bipyridine)4,4′-bis(2,6-dimethyl-4-methoxyphenyl)-6,6′-dimethyl-2,2′-bibenzimidazole ruthenium(II) dihexafluoridophosphate (**K1**) were synthesized by literature procedures.[17,23,24,38] The ruthenium precursor complex bis(4,4′-di-*tert*-butyl-2,2′-bipyridyl)dichloridoruthenium(II) [(tbbpy)$_2$Ru(Cl)$_2$] was synthesized according to the efficient microwave-assisted method reported previously[17] from ruthenium(III) chloride hydrate (35–40 % ruthenium, purchased from Degussa). Tris(4,4′-di-*tert*-butyl-2,2′-bipyridine)ruthenium(II) hexafluoridophosphate (**K***) was obtained as a side-product from the synthesis. Bis(4,4′-di-*tert*-butyl-2,2′-bipyridyl)dichloridoruthenium(II) was separated by silica column chromatography and recrystallized as the hexafluoridophosphate salt.

Complex K2: To a suspension of **L2** (73.1 mg, 0.1 mmol) in ethanol (30 mL) and water (20 mL), formic acid (1 mL) was added, and the mixture heated to reflux at 115 °C. A solution of bis(4,4′-di-*tert*-butyl-2,2′-bipyridine)dichloridoruthenium(II) (70.8 mg, 0.1 mmol) in ethanol (20 mL) was added dropwise over 1 h, and the solution was stirred and heated for a further 12 h. After cooling, the crude mixture was filtered through Celite® 545. A solution of NH_4PF_6 (81.5 mg, 0.5 mmol) in water (10 mL) was added to precipitate the product complex as a hexafluorophosphate salt. The resulting precipitate was collected by filtration, washed three times each with water and ether, and dried in vacuo, yield 131.3 mg (0.09 mmol, 90 %). ^{1}H NMR (CD_2Cl_2, 298 K, 400 MHz, cf. Scheme S1): δ = 8.32 (d, $^4J_{H,H}$ = 1.5 Hz, 2 H, tbbpy 3-H or 3′-H), 8.26 (d, $^4J_{H,H}$ = 1.5 Hz, 2 H, tbbpy 3-H or 3′-H), 7.85 (d, $^3J_{H,H}$ = 6.0 Hz, 2 H, tbbpy 6-H or 6′-H), 7.73 (d, $^3J_{H,H}$ = 6.0 Hz, 2 H, tbbpy 6-H or 6′-H), 7.55 (dd, $^3J_{H,H}$ = 6.0, $^4J_{H,H}$ = 1.5 Hz, 2 H, tbbpy 5-H or 5′-H), 7.39 (dd, $^3J_{H,H}$ = 6.0 Hz, $^4J_{H,H}$ = 1.5 Hz, 2 H, tbbpy 5-H or 5′-H), 7.01 (s, 2 H, BBI 5-H), 6.72 (s, 2 H, BBI 8-H or 8′-H), 6.68 (s, 2 H, BBI 8-H or 8′-H), 5.40 (s, 2 H, BBI 7-H), 5.32 (solvent residual signal) 3.79 (s, 6 H, BBI OMe), 2.18 (s, 6 H, BBI Me), 1.98 (s, 6 H, BBI OMe or OMe′), 1.79 (s, 6 H, BBI OMe or OMe′), 1.50 (s, 18 H, tbbpy *t*Bu), 1.41 (s, 18 H, tbbpy *t*Bu) ppm. ^{13}C{^{1}H} NMR (CD_2Cl_2, 298 K, 100 MHz): δ = 162.71, 161.94, 159.97, 159.30, 157.37, 152.49, 152.00, 142.38, 138.32, 138.13, 135.84, 129.75, 127.88, 126.79, 125.93, 124.76, 120.70, 120.63, 114.16, 113.69, 113.60, 68.26, 55.53, 35.91, 35.76, 30.63, 30.41, 21.90, 20.66, 20.46 ppm. UV/Vis (10^{-5} M, MeCN): λ_{max} = 472 nm (MLCT). Emission spectroscopy (10^{-5} M, MeCN): λ_{max} = 642 nm.

Crystal Data for K1-Cl: $C_{66}H_{74}Cl_2N_8O_2Ru$, M_r = 1183.30 g mol^{-1}, red hexagonal plate, crystal size 0.1527 × 0.0965 × 0.0135 mm, monoclinic, space group *C*2/*c*, a = 15.3857(5) Å, b = 29.5222(13) Å, c = 13.7004(5) Å, β = 97.165(3)°, V = 6174.4(4) Å^3, T = 150(2) K, Z = 4, $\varrho_{calcd.}$ = 1.273 Mg/m^3, μ(Mo-K_α) = 0.390 mm^{-1}, F(000) = 2480, total 18853 reflections to h(–18/19), k(–36/31), l(–17/16) measured in the range 3.499 ≤ Θ ≤ 26.371°, completeness Θ_{max} = 99.7 %, 6309 independent reflections, R_{int} = 0.0398, 5258 reflections with $F_o > 4\sigma(F_o)$, 377 parameters, 2 restraints, R_{1obs} = 0.0512, wR_{2obs} = 0.1438, R_{1all} = 0.0644, wR_{2all} = 0.1570, GOOF = 0.611, largest difference peak and hole: 1.304/–0.604 e Å^{-3}. Restraints were applied to fix the disordered methoxy groups in a reasonable fashion. In the crystal lattice, it is assumed that the anisyl substituents move between two alter-

© 2016 Wiley-VCH Verlag GmbH & Co. KGaA, Weinheim

ChemPubSoc Europe

EurJIC European Journal of Inorganic Chemistry

Full Paper

native positions, as was reflected by a largely distorted, anisotropically smeared oxygen atom. The best refinement was obtained upon splitting the methoxy group over two alternative positions with site occupancies of 52.1 and 47.9 %. Residual electron density maxima in a disordered arrangement were removed by using the Platon SQUEEZE[39,40] procedure. The corresponding electron count of 46 electrons per void roughly corresponds to one molecule of acetone per void, whereas the respective volume of 194 Å^3 is considerably larger than that expected, which is generally in accordance with the observed disorder.

Crystal Data for K2-MeOH: $C_{73}H_{94}F_{12}N_8O_5P_2Ru$, M_r = 1554.57 g mol^{-1}, red prism, crystal size 0.1443 × 0.1077 × 0.0595 mm, triclinic, space group $P\bar{1}$, a = 14.7205(5) Å, b = 15.9255(4) Å, c = 18.5618(6) Å, α = 76.484(2)°, β = 67.234(3)°, γ = 81.893(2)°, V = 3895.1(2) Å^3, T = 180(2) K, Z = 2, $\varrho_{calcd.}$ = 1.325 Mg/m^3, μ(Cu-K_α) = 2.709 mm^{-1}, F(000) = 1640, total 42562 reflections to h(–17/18), k(–19/19), l(–23/23) measured in the range 7.386 ≤ Θ ≤ 74.496°, completeness Θ_{max} = 99.7 %, 15887 independent reflections, R_{int} = 0.0489, 13257 reflections with F_o > 4σ(F_o), 937 parameters, 17 restraints, R_{1obs} = 0.0738, wR_{2obs} = 0.2099, R_{1all} = 0.0876, wR_{2all} = 0.2202, GOOF = 1.045, largest difference peak and hole: 1.245/–1.027 e Å^{-3}. The FLAT restraint was applied to the anisyl substituents, which otherwise drifted slightly irregularly inwards to the ligand cavity. The C–O bond lengths in two methanol molecules and one P–F bond length in one of the counterions were restrained by using the DFIX command. Residual electron density maxima indicated the appearance of another molecule of methanol in the unit cell, but the respective refinement was unstable. Therefore, the Platon SQUEEZE[39,40] procedure was applied. The calculated electron count of twelve electrons merely indicates the presence of one strongly disordered molecule of water in a void volume of 124 Å^{-3}.

Crystal Data for K2-EtOAc: $C_{78}H_{98}F_{12}N_8O_6P_2Ru$, M_r = 1634.65 g mol^{-1}, red fragment, crystal size 0.1067 × 0.0772 × 0.0629 mm, triclinic, space group $P\bar{1}$, a = 15.6267(5) Å, b = 16.0298(4) Å, c = 17.9392(4) Å, α = 91.364(2)°, β = 103.432(2)°, γ = 111.221(2)°, V = 4045.4(2) Å^3, T = 180(2) K, Z = 2, $\varrho_{calcd.}$ = 1.342 Mg/m^3, μ(Cu-K_α) = 2.646 mm^{-1}, F(000) = 1704, total 44213 reflections to h(–19/18), k(–20/16), l(–18/22) measured in the range 7.384 ≤ Θ ≤ 74.492°, completeness Θ_{max} = 99.7 %, 16477 independent reflections, R_{int} = 0.0332, 14505 reflections with F_o > 4σ(F_o), 964 parameters, 4 restraints, R_{1obs} = 0.0520, wR_{2obs} = 0.1417, R_{1all} = 0.0598, wR_{2all} = 0.1483, GOOF = 1.081, largest difference peak and hole: 1.464/–1.989 e Å^{-3}. The DFIX command was applied to fix the geometry of the unbound ethyl acetate solvent molecule.

Crystal data for L1-HCl: $C_{62}H_{56}Cl_8N_8O_4$, M_r = 1260.74 g mol^{-1}, pale yellow prism, crystal size 0.3215 × 0.1651 × 0.1234 mm, monoclinic, space group $P2_1/c$, a = 23.5769(6) Å, b = 18.4780(5) Å, c = 14.1490(4) Å, β = 97.378(3)°, V = 6113.0(3) Å^3, T = 170(2) K, Z = 4, $\varrho_{calcd.}$ = 1.370 Mg/m^3, μ(Cu-K_α) = 3.804 mm^{-1}, F(000) = 2608, total 25076 reflections to h(–29/17), k(–22/21), l(–17/17) measured in the range 7.435 ≤ Θ ≤ 73.809°, completeness Θ_{max} = 99.7 %, 11964 independent reflections, R_{int} = 0.0244, 10034 reflections with F_o > 4σ(F_o), 800 parameters, 68 restraints, R_{1obs} = 0.0527, wR_{2obs} = 0.1440, R_{1all} = 0.0618, wR_{2all} = 0.1542, GOOF = 1.042, largest difference peak and hole: 1.845/–0.714 e Å^{-3}. Some intramolecular Cl–Cl distances in the distorted solvent molecules were fixed by using the DANG restraint, and the ellipsoids of the respective chlorine atoms were restrained by using the ISOR command.

Crystal data for $(K1)_2$ (a): $C_{146}H_{176}F_{12}N_8O_6P_2Ru_2$, M_r = 2764.11 g mol^{-1}, violet rectangular prism, crystal size 0.3262 × 0.2562 × 0.0598 mm, monoclinic, space group $P2_1/n$, a = 25.8355(4) Å, b = 23.7914(3) Å, c = 26.2326(4) Å, β = 110.056(2)°, V = 15146.4(4) Å^3, T = 150(2) K, Z = 4, $\varrho_{calcd.}$ = 1.212 Mg/m^3, μ(Cu-K_α) = 2.399 mm^{-1}, F(000) = 5794, total 126354 reflections to h(–32/30), k(–24/29), l(–32/32) measured in the range 7.427 ≤ Θ ≤ 74.495°, completeness Θ_{max} = 99.7 %, 30885 independent reflections, R_{int} = 0.0463, 22164 reflections with F_o > 4σ(F_o), 1659 parameters, 27 restraints, R_{1obs} = 0.0738, wR_{2obs} = 0.2099, R_{1all} = 0.0876, wR_{2all} = 0.2202, GOOF = 1.080, largest difference peak and hole: 1.924/–1.264 e Å^{-3}. The DFIX, DANG, and ISOR restraints were applied to some *tert*-butyl groups to achieve a stable refinement. The methyl groups of both acetonitrile molecules were calculated with fixed coordinates for all atoms to avoid shift errors related to the positioning of the hydrogen atoms. Two more molecules of *tert*-butyl methyl ether per formula unit were indicated by the residual electron densities but could not be integrated in a stable model. Therefore, the Platon SQUEEZE[39,40] procedure was applied, and the calculated electron count of 156 electrons in two voids was correlated to two molecules of the nonsolvent.

Crystal data for $(K1)_2$ (b): $C_{166}H_{195}N_{17}N_{17}O_{18}P_4Ru_2$, M_r = 3042.40 g mol^{-1}, violet prism, crystal size 0.3322 × 0.181 × 0.0888 mm, monoclinic, space group $P2_1/n$, a = 29.1278(5) Å, b = 15.1725(4) Å, c = 38.3664(7) Å, β = 90.825(2)°, V = 16953.9(6) Å^3, T = 180(2) K, Z = 4, $\varrho_{calcd.}$ = 1.192 Mg/m^3, μ(Mo-K_α) = 0.280 mm^{-1}, F(000) = 6408, total 113099 reflections to h(–36/35), k(–14/18), l(–46/47) measured in the range 3.408 ≤ Θ ≤ 26.372°, completeness Θ_{max} = 99.7 %, 34581 independent reflections, R_{int} = 0.0624, 18255 reflections with F_o > 4σ(F_o), 1795 parameters, 27 restraints, R_{1obs} = 0.0563, wR_{2obs} = 0.1505, R_{1all} = 0.1062, wR_{2all} = 0.1650, GOOF = 0.737, largest difference peak and hole: 1.358/–0.921 e Å^{-3}. DFIX and DANG restraints were used to stabilize the geometry of distorted solvent molecules, ISOR was used for two methyl substituents of one *tert*-butyl group. The diethyl ether molecules were refined isotropically, and two further molecules of diethyl ether and acetonitrile could not be stably integrated in the refinement. Therefore, the Platon SQUEEZE[39,40] procedure was applied here, and the electron count in the respective voids reflects the assumed presence of acetonitrile (41/42 electrons) and diethyl ether (85 electrons each).

CCDC 1431043 [for $(\mathbf{K1})_2$ (a)], 1431044 [for $(\mathbf{K1})_2$ (b)], 1431045 (for **K1**-Cl), 1431046 (for **K2**-EtOAc), 1431047 (for **K2**-MeOH), and 1431048 (for **L1**-HCl) contain the supplementary crystallographic data for this paper contain the supplementary crystallographic data for this paper. These data can be obtained free of charge from The Cambridge Crystallographic Data Centre.

Acknowledgments

Financial support by the Carl-Zeiss-Stiftung, Germany through a PhD scholarship to D. S. is thankfully acknowledged.

Keywords: Ruthenium · N ligands · Anions · Sensors · Luminescence

[1] P. D. Beer, S. R. Bayly, *Top. Curr. Chem.* **2005**, *255*, 125–162.
[2] P. D. Beer, E. J. Hayes, *Coord. Chem. Rev.* **2003**, *240*, 167–189.
[3] J. F. Callan, A. P. de Silva, D. C. Magri, *Tetrahedron Lett.* **2005**, *61*, 8551–8588.
[4] P. D. Beer, *Acc. Chem. Res.* **1998**, *31*, 71–80.
[5] J. Lehr, T. Lang, O. A. Blackburn, T. A. Barendt, S. Faulkner, J. J. Davis, P. D. Beer, *Chem. Eur. J.* **2013**, *19*, 15898–15906.
[6] K. Ng, A. R. Cowley, P. D. Beer, *Chem. Commun.* **2006**, 3676–3678.

© 2016 Wiley-VCH Verlag GmbH & Co. KGaA, Weinheim

ChemPubSoc Europe

EurJIC European Journal of Inorganic Chemistry
Full Paper

[7] M. C. Llinàs, J. Farran, M. V. Capparelli, G. Anguera, D. Sánchez-García, J. Teixidó, S. Borrós, *Tetrahedron Lett.* **2014**, *55*, 4667–4670.
[8] D. Saha, S. Das, C. Bhaumik, S. Dutta, S. Baitalik, *Inorg. Chem.* **2010**, *49*, 2334–48.
[9] V. Balzani, A. Credi, M. Venturi, *Chem. Soc. Rev.* **2009**, *38*, 1542–50.
[10] S. Saha, J. F. Stoddart, *Chem. Soc. Rev.* **2007**, *36*, 77–92.
[11] W. T. Eckenhoff, R. Eisenberg, *Dalton Trans.* **2012**, *41*, 13004–13021.
[12] C. Mari, G. Gasser, *CHIMIA Int. J. Chem.* **2015**, *69*, 176–181.
[13] M. G. Pfeffer, T. Kowacs, M. Wächtler, J. Guthmuller, B. Dietzek, J. G. Vos, S. Rau, *Angew. Chem. Int. Ed.* **2015**, *54*, 6627–6631; *Angew. Chem.* **2015**, *127*, 6727.
[14] M. G. Pfeffer, B. Schäfer, G. Smolentsev, J. Uhlig, E. Nazarenko, J. Guthmuller, C. Kuhnt, M. Wächtler, B. Dietzek, V. Sundström, S. Rau, *Angew. Chem. Int. Ed.* **2015**, *54*, 5044–5048; *Angew. Chem.* **2015**, *127*, 5132.
[15] A. Kroll, K. Monczak, D. Sorsche, S. Rau, *Eur. J. Inorg. Chem.* **2014**, 3462–3466.
[16] K. Monczak, K. Peuntinger, D. Sorsche, F. W. Heinemann, D. M. Guldi, S. Rau, *Chem. Eur. J.* **2014**, *20*, 15426–15433.
[17] S. Rau, B. Schäfer, A. Grüßing, S. Schebesta, K. Lamm, J. Vieth, H. Görls, D. Walther, M. Rudolph, U. W. Grummt, E. Birkner, *Inorg. Chim. Acta* **2004**, *357*, 4496–4503.
[18] Y. Cui, Y.-L. Niu, M.-L. Cao, K. Wang, H.-J. Mo, Y.-R. Zhong, B.-H. Ye, *Inorg. Chem.* **2008**, *47*, 5616–24.
[19] S. Rau, L. Böttcher, S. Schebesta, M. Stollenz, H. Görls, D. Walther, *Eur. J. Inorg. Chem.* **2002**, 2800–2809.
[20] M.-A. Haga, *Inorg. Chim. Acta* **1983**, *75*, 29–35.
[21] M. Haga, T. Ano, T. Ishizaki, K. Kano, K. Nozaki, T. Ohno, *J. Chem. Soc., Dalton Trans.* **1994**, 263.
[22] A. Grüßing, S. Rau, S. Schebesta, A. Scholz, H. Görls, D. Walther, *Z. Anorg. Allg. Chem.* **2007**, *633*, 961–970.
[23] Y. Yasui, D. K. Frantz, J. S. Siegel, *Org. Lett.* **2006**, *8*, 4989–92.
[24] D. Sorsche, S. Rau, *Eur. J. Inorg. Chem.* **2014**, 4244–4249.
[25] H.-J. Mo, Y.-L. Niu, M. Zhang, Z.-P. Qiao, B.-H. Ye, *Dalton Trans.* **2011**, *40*, 8218–8225.
[26] D. K. Frantz, A. A. Sullivan, Y. Yasui, A. Linden, K. K. Baldridge, J. S. Siegel, *Org. Biomol. Chem.* **2009**, *7*, 2347–52.
[27] H.-J. Mo, H.-Y. Chao, B.-H. Ye, *Inorg. Chem. Commun.* **2013**, *35*, 100–103.
[28] S. Rau, M. Ruben, T. Buttner, C. Temme, S. Dautz, H. Görls, M. Rudolph, D. Walther, A. Brodkorb, M. Duati, C. O'Connor, J. G. Vos, *J. Chem. Soc., Dalton Trans.* **2000**, 3649–3657.
[29] K. Halbauer, A. Göbel, A. Sterzik, H. Görls, S. Rau, W. Imhof, *Eur. J. Inorg. Chem.* **2007**, 1508–1514.
[30] S. A. Rommel, D. Sorsche, N. Rockstroh, F. W. Heinemann, J. Kübel, M. Wächtler, B. Dietzek, S. Rau, *Eur. J. Inorg. Chem.* **2015**, 3730–3739.
[31] J. A. Wisner, P. D. Beer, M. G. B. Drew, M. R. Sambrook, *J. Am. Chem. Soc.* **2002**, *124*, 12469–12476.
[32] F. Szemes, D. Hesek, Z. Chen, S. W. Dent, M. G. B. Drew, A. J. Goulden, A. R. Graydon, A. Grieve, R. J. Mortimer, T. Wear, J. S. Weightman, P. D. Beer, *Inorg. Chem.* **1996**, *35*, 5868–5879.
[33] S. Rau, T. Büttner, C. Temme, M. Ruben, H. Görls, D. Walther, M. Duati, S. Fanni, J. G. Vos, *Inorg. Chem.* **2000**, *39*, 1621–1624.
[34] K. Heussner, K. Peuntinger, N. Rockstroh, S. Rau, C. Streb, *Dalton Trans.* **2015**, *44*, 330–337.
[35] N. Rockstroh, K. Peuntinger, H. Görls, D. M. Guldi, F. W. Heinemann, B. Schäfer, S. Rau, *Z. Naturforsch. B* **2010**, *65*, 281–290.
[36] Y. Liu, B. Han, Y. Chen, *J. Phys. Chem. B* **2002**, *106*, 4678–4687.
[37] G. M. Sheldrick, *Acta Crystallogr., Sect. A* **2008**, *64*, 112–22.
[38] E. Muller, G. Bernardinelli, J. Reedijk, *Inorg. Chem.* **1995**, *34*, 5979–5988.
[39] A. L. Spek, *Acta Crystallogr., Sect. D* **2009**, *65*, 148–155.
[40] A. L. Spek, *J. Appl. Crystallogr.* **2003**, *36*, 7–13.

Received: December 22, 2015
Published Online: September 3, 2016

 © 2016 Wiley-VCH Verlag GmbH & Co. KGaA, Weinheim

Eur. J. Inorg. Chem. **2016** · ISSN 1099–0682

SUPPORTING INFORMATION

DOI: 10.1002/ejic.201501472
Title: Functional Dimming of Pincer-Shaped Bibenzimidazole-Ruthenium(II) Complexes with Improved Anion-Sensitive Luminescence
Author(s): Dieter Sorsche, Sebastian A. Rommel, Sven Rau*

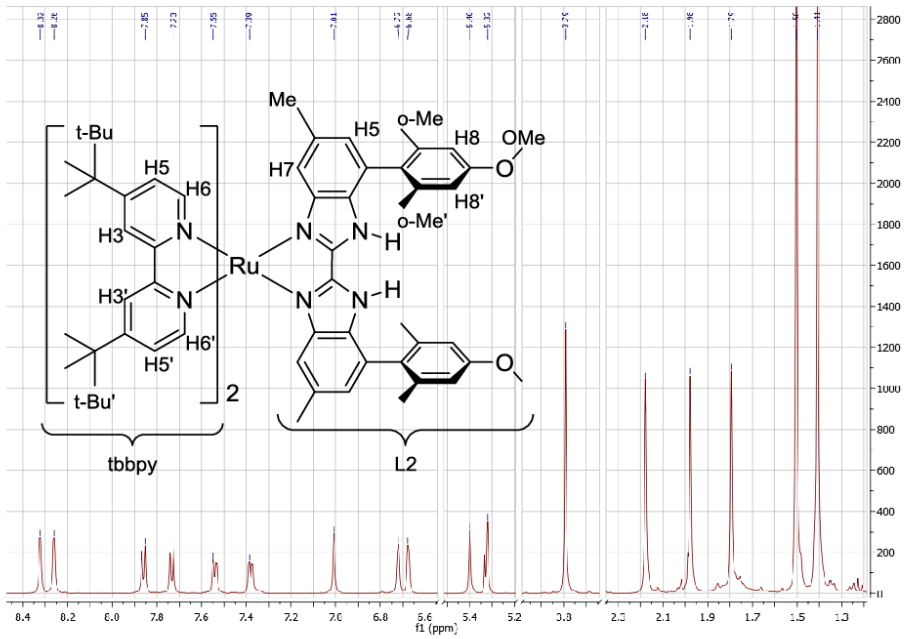

Figure SF1. ^{1}H-NMR spectrum of **K2** in $CDCl_2$ and schematic representation with labels for all protons as used in the experimental section.

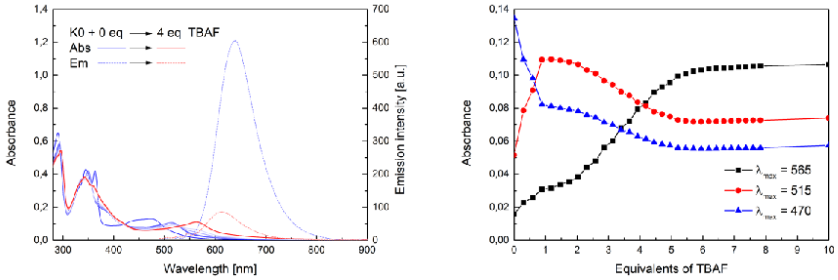

Figure SF2. left: UV/Vis absorption (solid line) and emission (dashed line) spectra of **K0** upon stepwise addition of TBAF to a 10^{-5} M solution in acetonitrile; right: plot of the absorptance at wavelengths characteristic to the MLCT absorption bands of the fully protonated (470 nm), mono protonated (515) and deprotonated (565) complex.

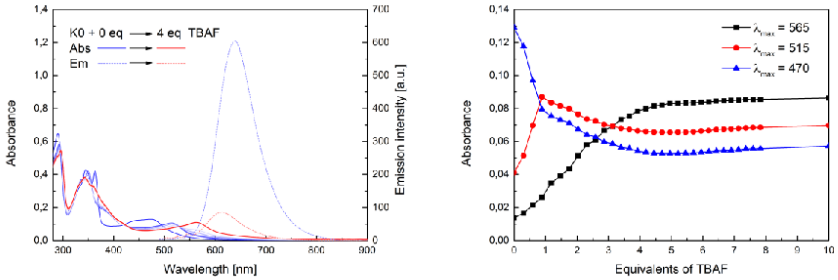

Figure SF3. left: UV/Vis absorption (solid line) and emission (dashed line) spectra of **K1** upon stepwise addition of TBAF to a 10^{-5} M solution in acetonitrile; right: plot of the absorptance at wavelengths characteristic to the MLCT absorption bands of the fully protonated (470 nm), mono protonated (515) and deprotonated (565) complex.

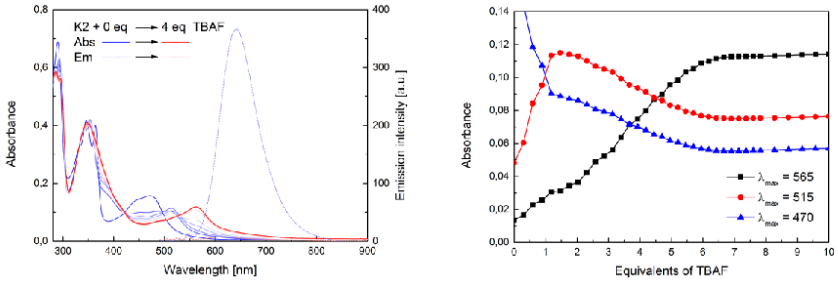

Figure SF4. left: UV/Vis absorption (solid line) and emission (dashed line) spectra of **K2** upon stepwise addition of TBAF to a 10^{-5} M solution in acetonitrile; right: plot of the absorptance at wavelengths characteristic to the MLCT absorption bands of the fully protonated (470 nm), mono protonated (515) and deprotonated (565) complex.

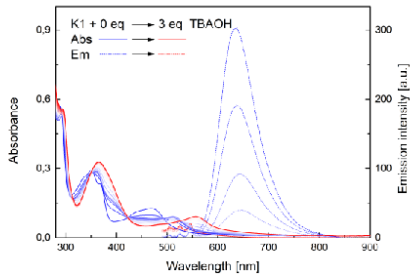

Figure SF5. UV/Vis absorption (solid line) and emission (dashed line) spectra of **K1** (10^{-5} M acetonitrile) upon stepwise addition of TBAOH.

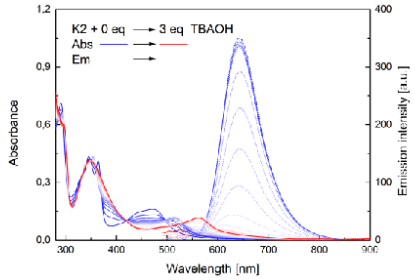

Figure SF6. UV/Vis absorption (solid line) and emission (dashed line) spectra of **K1** (10^{-5} M acetonitrile) upon stepwise addition of TBAOH.

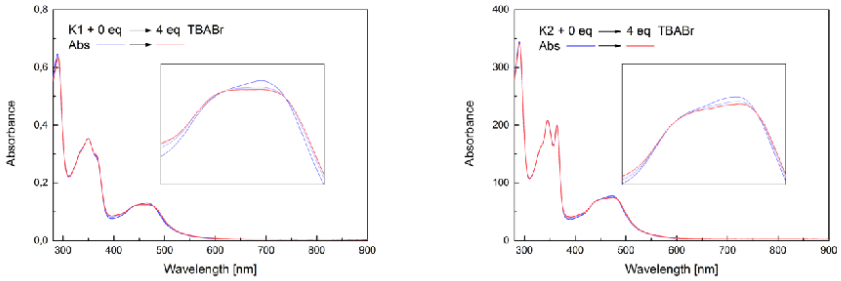

Figure SF7. UV/Vis spectra of **K1** (left) and **K2** (right) (10^{-5} M, MeCN) upon addition of TBACl; inlay: zoom of the MLCT absorption band (410-500 nm).

Figure SF8. Emission spectra of **K0** (10^{-5} M, MeCN) upon stepwise addition of TBACl (left) and TBABr (right); inlay (right) plot of emission area versus concentration of TBA halide, and fit according to fit function **FF1** (*vide infra*).

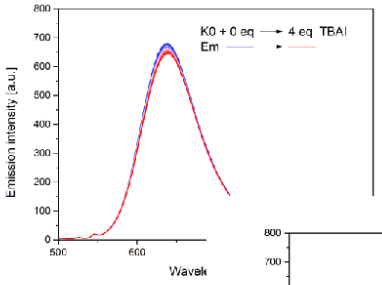

Figure SF9. Emission spectra of **K0** (10^{-5} M, MeCN) upon stepwise addition of TBACl (left) and TBABr (right); inlay plot of emission area versus concentration of TBA halide, and fit according to fit function **FF1** (*vide infra*).

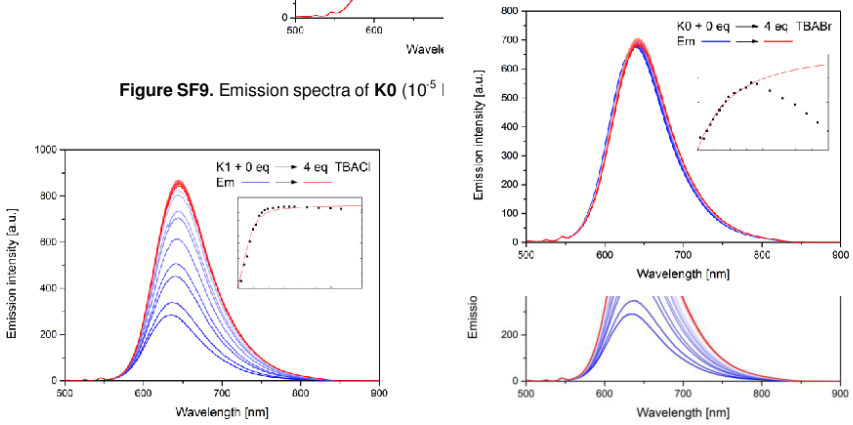

Figure SF10. Emission spectra of **K1** (10^{-5} M, MeCN) upon stepwise addition of TBACl (left) and TBABr (right); inlay plot of emission area versus concentration of TBA halide, and fit according to fit function **FF1** (*vide infra*).

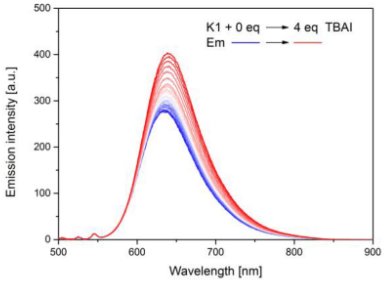

Figure SF11. Emission spectra of **K1** (10^{-5} M, MeCN) upon stepwise addition of TBAI.

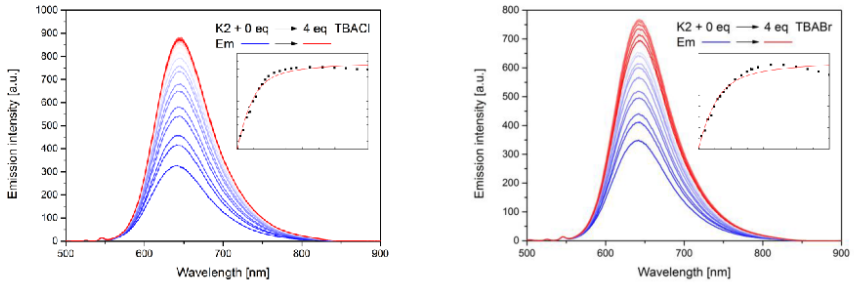

Figure SF12. Emission spectra of **K2** (10^{-5} M, MeCN) upon stepwise addition of TBACl (left) and TBABr (right); inlay: plot of emission area versus concentration of TBA halide, and fit according to fit function **FF1** (*vide infra*).

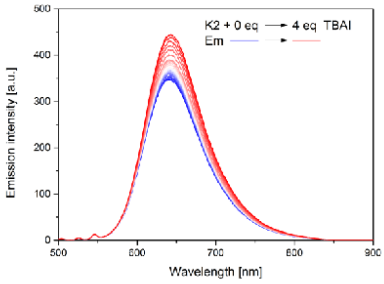

Figure SF13. Emission spectra of **K2** (10^{-5} M, MeCN) upon stepwise addition of TBAI.

Fit function FF1. Aforementioned binding constants were calculated to the fit function below with respect to literature[1]

$$\Delta F = \frac{\Delta\varepsilon([H]+[G]+K^{-1}) \pm \sqrt{\Delta\varepsilon^2([H]+[G]+K^{-1})^2 - 4\Delta\varepsilon^2[H][G]}}{2}$$

Table 1. Crystal data and structure refinement for **K1-Cl**.

Empirical formula	C66 H74 Cl2 N8 O2 Ru	
Formula weight	1183.30	
Temperature	150(2) K	
Wavelength	0.71073 Å	
Crystal system	Monoclinic	
Space group	*C* 2/c	
Unit cell dimensions	a = 15.3857(5) Å	a= 90°.
	b = 29.5222(13) Å	b= 97.165(3)°.
	c = 13.7004(5) Å	g = 90°.
Volume	6174.4(4) $Å^3$	
Z	4	
Density (calculated)	1.273 Mg/m^3	
Absorption coefficient	0.390 mm^{-1}	
F(000)	2480	
Crystal size	0.1527 x 0.0965 x 0.0135 mm^3	
Theta range for data collection	3.499 to 26.371°.	
Index ranges	-18<=h<=19, -36<=k<=31, -17<=l<=16	
Reflections collected	18853	
Independent reflections	6309 [R(int) = 0.0398]	
Completeness to theta = 25.242°	99.7 %	
Refinement method	Full-matrix least-squares on F_0^2	
Data / restraints / parameters	6309 / 2 / 377	
Goodness-of-fit on F_0^2	0.611	
Final R indices [I>2sigma(I)]	R1 = 0.0512, wR2 = 0.1438	
R indices (all data)	R1 = 0.0644, wR2 = 0.1570	
Largest diff. peak and hole	1.304 and -0.604 $e.Å^{-3}$	

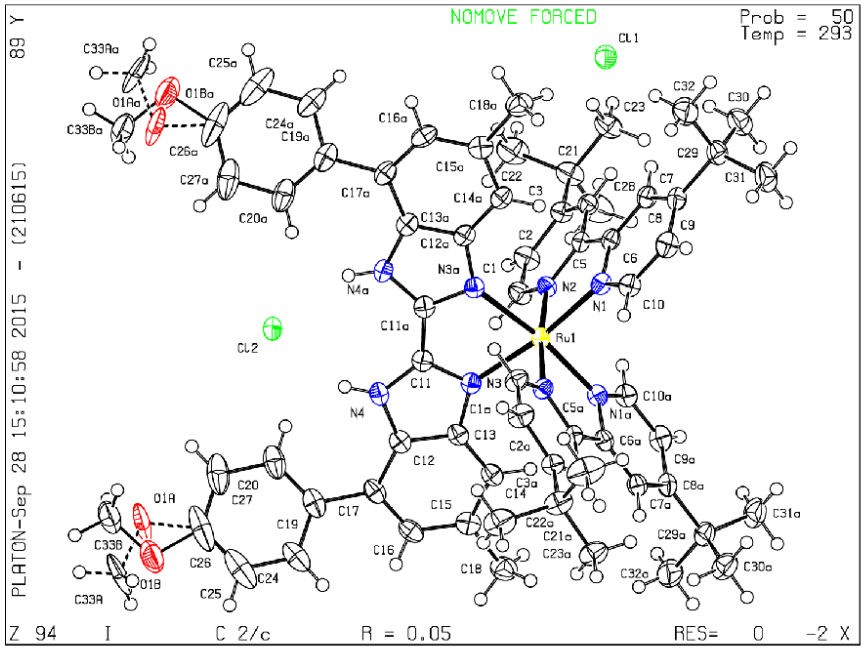

Figure SF14: ORTEP representation of **K1-Cl**, ellipsoids at 50% probability.

Table 2. Crystal data and structure refinement for **K2-MeOH**.

Empirical formula	C73 H94 F12 N8 O5 P2 Ru	
Formula weight	1554.57	
Temperature	180(2) K	
Wavelength	1.54178 Å	
Crystal system	Triclinic	
Space group	*P* -1	
Unit cell dimensions	a = 14.7205(5) Å	a= 76.484(2)°.
	b = 15.9255(4) Å	b= 67.234(3)°.
	c = 18.5618(6) Å	g = 81.893(2)°.
Volume	3895.1(2) $Å^3$	
Z	2	
Density (calculated)	1.325 Mg/m^3	
Absorption coefficient	2.709 mm^{-1}	
F(000)	1640	
Crystal size	0.1443 x 0.1077 x 0.0595 mm^3	
Theta range for data collection	7.386 to 74.496°.	
Index ranges	-17<=h<=18, -19<=k<=19, -23<=l<=23	
Reflections collected	42562	
Independent reflections	15887 [R(int) = 0.0489]	
Completeness to theta = 67.679°	99.7 %	
Refinement method	Full-matrix least-squares on F_0^2	
Data / restraints / parameters	15887 / 16 / 916	
Goodness-of-fit on F_0^2	1.045	
Final R indices [I>2sigma(I)]	R1 = 0.0738, wR2 = 0.2099	
R indices (all data)	R1 = 0.0876, wR2 = 0.2202	
Largest diff. peak and hole	1.245 and -1.027 $e.Å^{-3}$	

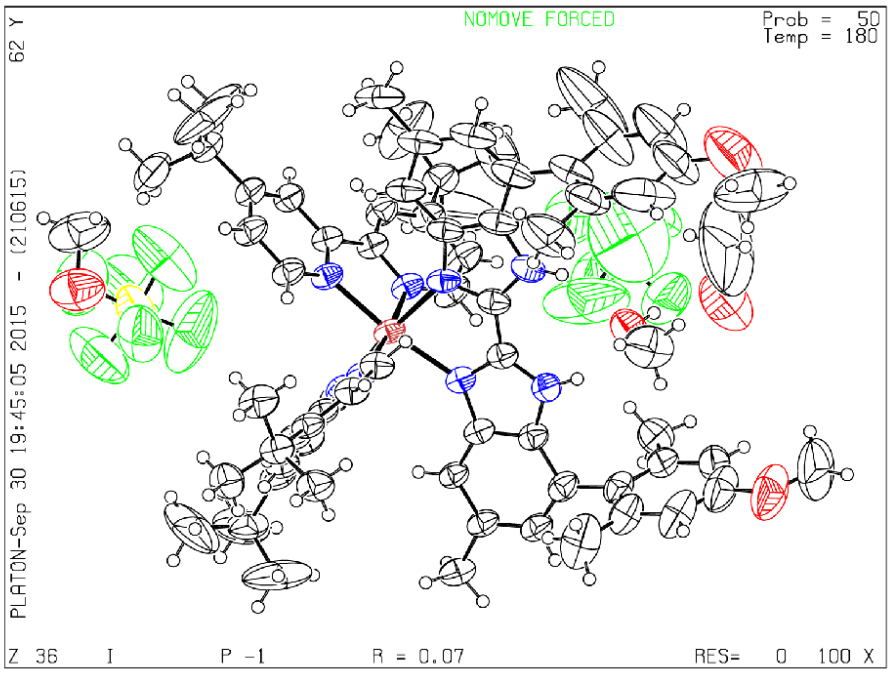

Figure SF15: ORTEP representation of **K2-MeOH**, ellipsoids at 50% probability.

Table 3. Crystal data and structure refinement for **K2-EtOAc**.

Empirical formula	C78 H98 F12 N8 O6 P2 Ru	
Formula weight	1634.65	
Temperature	180(2) K	
Wavelength	1.54178 Å	
Crystal system	Triclinic	
Space group	*P* -1	
Unit cell dimensions	a = 15.6267(5) Å	a= 91.364(2)°.
	b = 16.0298(4) Å	b= 103.432(2)°.
	c = 17.9392(4) Å	g = 111.221(2)°.
Volume	4045.4(2) $Å^3$	
Z	2	
Density (calculated)	1.342 Mg/m^3	
Absorption coefficient	2.646 mm^{-1}	
F(000)	1704	
Crystal size	0.1067 x 0.0772 x 0.0629 mm^3	
Theta range for data collection	7.384 to 74.492°.	
Index ranges	-19<=h<=18, -20<=k<=16, -18<=l<=22	
Reflections collected	44213	
Independent reflections	16477 [R(int) = 0.0332]	
Completeness to theta = 67.679°	99.7 %	
Refinement method	Full-matrix least-squares on F_0^2	
Data / restraints / parameters	16477 / 4 / 964	
Goodness-of-fit on F_0^2	1.081	
Final R indices [I>2sigma(I)]	R1 = 0.0520, wR2 = 0.1417	
R indices (all data)	R1 = 0.0598, wR2 = 0.1483	
Largest diff. peak and hole	1.464 and -0.989 $e·Å^{-3}$	

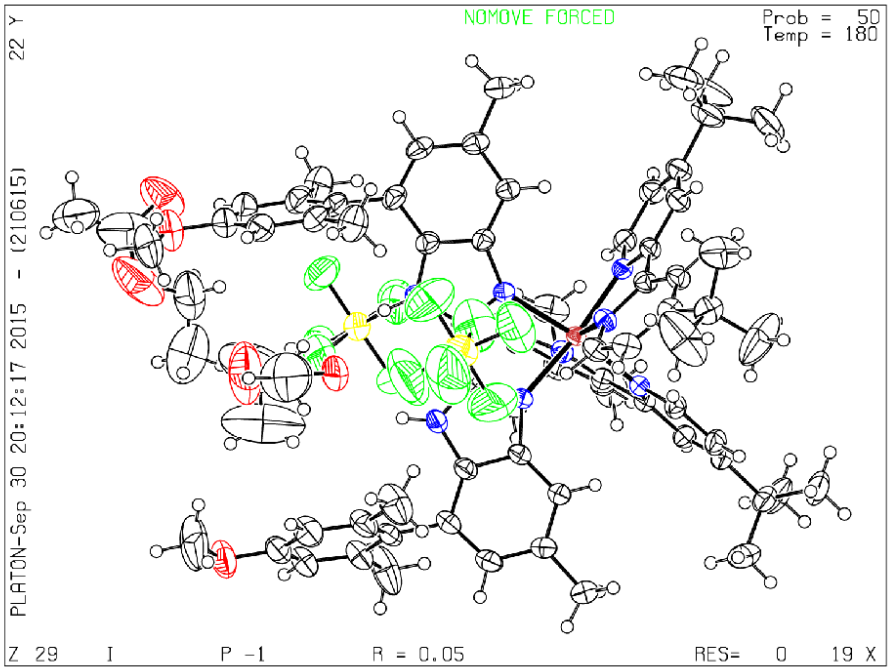

Figure SF16. ORTEP representation of **K2-EtOAc**, ellipsoids at 50% probability.

Table 4. Crystal data and structure refinement for **L1-HCl**.

Empirical formula	C62 H56 Cl8 N8 O4	
Formula weight	1260.74	
Temperature	270(2) K	
Wavelength	1.54184 Å	
Crystal system	Monoclinic	
Space group	*P* 2_1/c	
Unit cell dimensions	a = 23.5769(6) Å	a= 90°.
	b = 18.4780(5) Å	b= 97.378(3)°.
	c = 14.1490(4) Å	g = 90°.
Volume	6113.0(3) $Å^3$	
Z	4	
Density (calculated)	1.370 Mg/m^3	
Absorption coefficient	3.804 mm^{-1}	
F(000)	2608	
Crystal size	0.3215 x 0.1651 x 0.1234 mm^3	
Theta range for data collection	7.435 to 73.809°.	
Index ranges	-29<=h<=17, -22<=k<=21, -17<=l<=17	
Reflections collected	25076	
Independent reflections	11964 [R(int) = 0.0244]	
Completeness to theta = 67.684°	99.7 %	
Refinement method	Full-matrix least-squares on F_0^2	
Data / restraints / parameters	11964 / 68 / 800	
Goodness-of-fit on F_0^2	1.042	
Final R indices [I>2sigma(I)]	R1 = 0.0527, wR2 = 0.1440	
R indices (all data)	R1 = 0.0618, wR2 = 0.1542	
Largest diff. peak and hole	0.845 and -0.714 $e.Å^{-3}$	

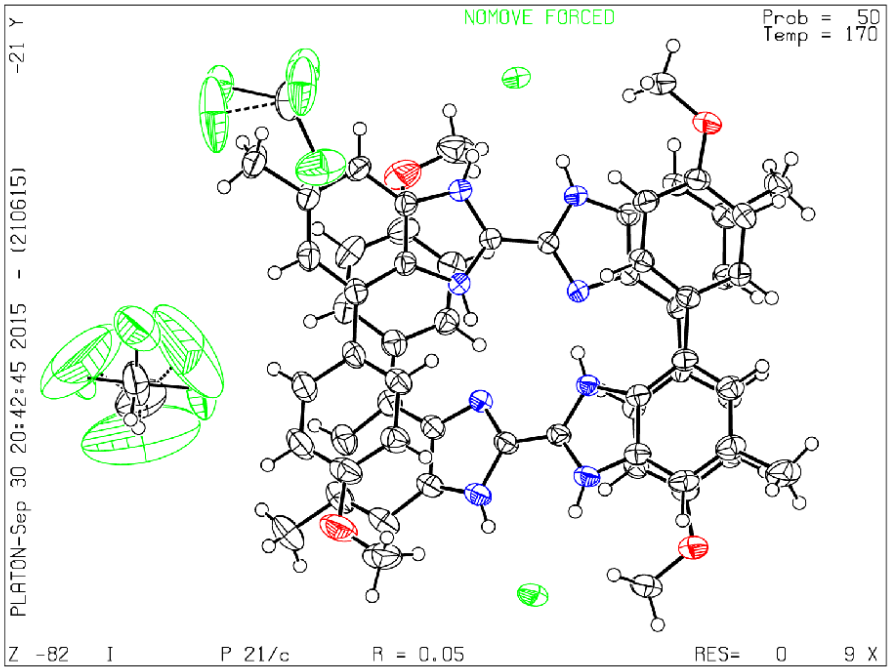

Figure SF16. ORTEP representation of **L1-HCl**, ellipsoids at 50% probability.

Table 5. Crystal data and structure refinement for **$(K1)_2$ (a)**.

Empirical formula	C146 H176 F12 N18 O6 P2 Ru2	
Formula weight	2764.11	
Temperature	150(2) K	
Wavelength	1.54178 Å	
Crystal system	Monoclinic	
Space group	$P\,2_1/n$	
Unit cell dimensions	a = 25.8355(4) Å	a= 90°.
	b = 23.7914(3) Å	b= 110.056(2)°.
	c = 26.2326(4) Å	g = 90°.
Volume	15146.4(4) $Å^3$	
Z	4	
Density (calculated)	1.212 Mg/m^3	
Absorption coefficient	2.399 mm^{-1}	
F(000)	5794	
Crystal size	0.3262 x 0.2562 x 0.0598 mm^3	
Theta range for data collection	7.427 to 74.495°.	
Index ranges	-32<=h<=30, -24<=k<=29, -32<=l<=32	
Reflections collected	126354	
Independent reflections	30885 [R(int) = 0.0463]	
Completeness to theta = 67.679°	99.7 %	
Refinement method	Full-matrix least-squares on F_0^2	
Data / restraints / parameters	30885 / 27 / 1659	
Goodness-of-fit on F_0^2	1.080	
Final R indices [I>2sigma(I)]	R1 = 0.0717, wR2 = 0.1998	
R indices (all data)	R1 = 0.0943, wR2 = 0.2167	
Largest diff. peak and hole	1.924 and -1.264 $e·Å^{-3}$	

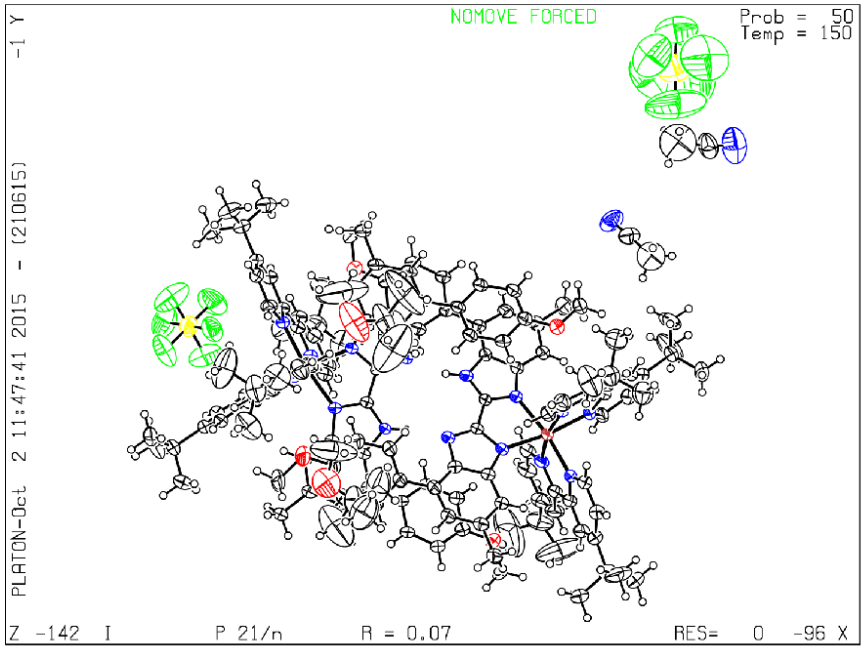

Figure SF17. ORTEP representation of **$(K1)_2$ (a)**, ellipsoids at 50% probability.

Table 6. Crystal data and structure refinement for **(K1)$_2$ (b)**.

Empirical formula	C166 H195 N17 O18 P4 Ru2	
Formula weight	3042.40	
Temperature	180(2) K	
Wavelength	0.71073 Å	
Crystal system	Monoclinic	
Space group	*P* 2_1/n	
Unit cell dimensions	a = 29.1278(5) Å	a= 90°.
	b = 15.1725(4) Å	b= 90.825(2)°.
	c = 38.3664(7) Å	g = 90°.
Volume	16953.9(6) Å^3	
Z	4	
Density (calculated)	1.192 Mg/m^3	
Absorption coefficient	0.280 mm^{-1}	
F(000)	6408	
Crystal size	0.3322 x 0.181 x 0.0888 mm^3	
Theta range for data collection	3.408 to 26.372°.	
Index ranges	-36<=h<=35, -14<=k<=18, -46<=l<=47	
Reflections collected	113099	
Independent reflections	34581 [R(int) = 0.0624]	
Completeness to theta = 25.242°	99.7 %	
Refinement method	Full-matrix least-squares on F_0^2	
Data / restraints / parameters	34581 / 27 / 1795	
Goodness-of-fit on F_0^2	0.737	
Final R indices [I>2sigma(I)]	R1 = 0.0563, wR2 = 0.1505	
R indices (all data)	R1 = 0.1062, wR2 = 0.1650	
Largest diff. peak and hole	1.358 and -0.921 e·Å^{-3}	

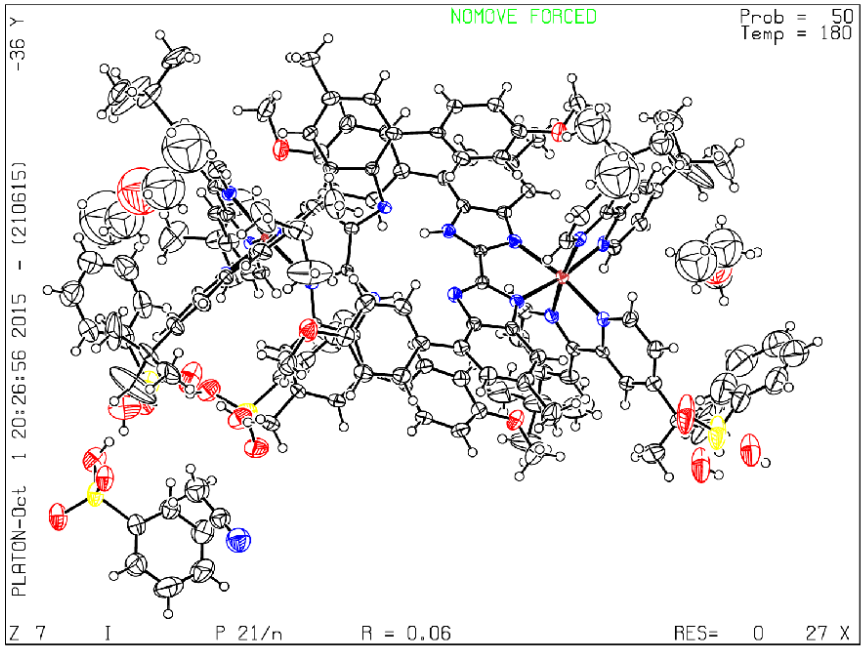

Figure SF18. ORTEP representation of **$(K1)_2$ (b)**, ellipsoids at 50% probability.

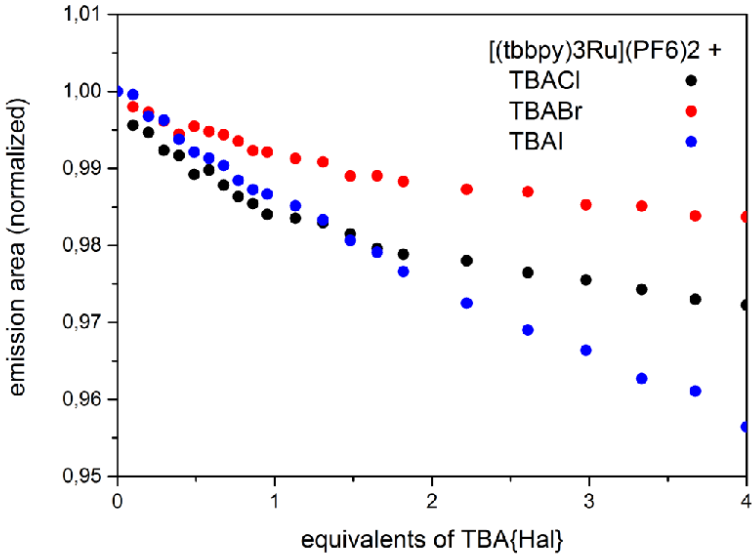

Figure SF19. Quenching of **K*** with TBACl, TBABr, and TBAI characteristic to methodology applied in this paper.

[1] Y. Liu, B. Han, Y. Chen, *J. Phys. Chem. B* **2002**, *106*, 4678–4687.

[SR5]: Visible-light sensitized photocatalytic hydrogen generation using a dual emissive heterodinuclear cyclometalated iridium(III)/ruthenium(II) complex

Sebastian A. Rommel, Dieter Sorsche, Stefanie Schönweiz, Joachim Kübel, Nils Rockstroh, Benjamin Dietzek, Carsten Streb and Sven Rau*

* *corresponding author*

Published in: *Journal of Organomet. Chem.* **2016**, in press.
DOI: 10.1016/j.jorganchem.2016.04.002

Copyright Reprinted from "Visible-light sensitized photocatalytic hydrogen generation using a dual emissive heterodinuclear cyclometalated iridium(III)/ruthenium(II) complex, Sebastian A. Rommel, Dieter Sorsche, Stefanie Schönweiz, Joachim Kübel, Nils Rockstroh, Benjamin Dietzek, Carsten Streb and Sven Rau, *Journal of Organomet. Chem.* **2016**" with permission of the publisher Elsevier Limited The Boulevard, Langford Lane Kidlington, Oxford, OX5 1GB, UK. (License Number: 3912400498568)

The synthesis, spectroscopic and electrochemical properties of the heterodinuclear iridium(III)/ruthenium(II) photosensitizer **Ir-BBI-Ru**, i.e. $[(ppy)_2Ir\text{-}(tmBBI)\text{-}Ru(^tbbpy)_2][PF_6]$ (ppy = 2-phenylpyridine; tmBBI = 5,5',6,6'-tetramethyl-2,2'-bibenzimidazole; ^{t}bbpy = 4,4'-di-*tert*-butyl-2,2'-bipyridine) are presented in this manuscript. The absorbance of the dinuclear complex lies well within the visible light spectrum, showing mainly absorption features typical for dinuclear ruthenium(II) bibenzimidazole complexes. The complex exhibits characteristic emission properties of both individual metal centers, indicative of an incomplete energy transfer. The application of **Ir-BBI-Ru** as visible-light absorbing photosensitizer in the field of photocatalytic water reduction is demonstrated by considerable hydrogen generation with the Co(II) catalyst $[Co(bpy)_3][PF_6]_2$ and triethanolamine as sacrificial donor.

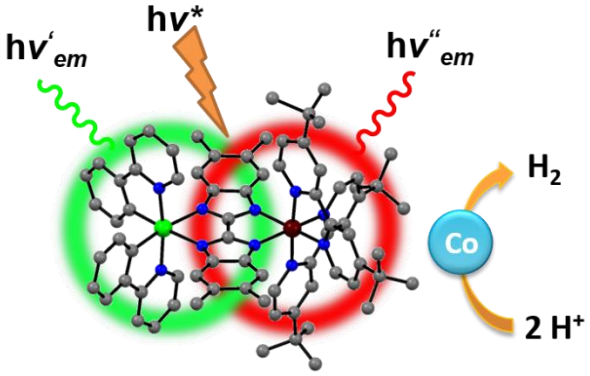

Contribution of the authors

Sebastian A. Rommel	Synthesis of the dinuclear complex Ir-BBI-Ru. Synthesis of the mononuclear complexes Ir-K0 and Ru-K0 as reference. Performance of photophysical and electrochemical characterization of the sensor system. Performance of the catalysis measurements. Writing of the manuscript.
Dieter Sorsche	Measurement and refinement of the X-ray structures. Writing of the manuscript.
Stefanie Schönweiz	Performance of the electrochemical measurements of Ir-BBI-Ru and writing of the corresponding paragraph in the manuscript.
Joachim Kübel	Performance of the excited state lifetime measurements.Discussion and revision of the manuscript.
Nils Rockstroh	First synthesis and characterization of Ir-BBI-Ru. Discussion and revision of the manuscript.
Benjamin Dietzek	Discussion and revision of the manuscript.
Sven Rau	Discussion and revision of the manuscript, concept and results discussion.

ARTICLE IN PRESS

Journal of Organometallic Chemistry xxx (2016) 1–8

Contents lists available at ScienceDirect

Journal of Organometallic Chemistry

journal homepage: www.elsevier.com/locate/jorganchem

Visible-light sensitized photocatalytic hydrogen generation using a dual emissive heterodinuclear cyclometalated iridium(III)/ruthenium(II) complex

Sebastian A. Rommel [a, 1], Dieter Sorsche [a, 1], Stefanie Schönweiz [a], Joachim Kübel [b, c], Nils Rockstroh [a], Benjamin Dietzek [b, c], Carsten Streb [a], Sven Rau [a, *, 2]

[a] Institute for Inorganic Chemistry I, Ulm University, Albert-Einstein-Allee 11, 89081 Ulm, Germany
[b] Leibniz Institute of Photonic Technology (IPHT) Jena e.V., Department Functional Interfaces, Albert-Einstein-Str. 9, 07745 Jena, Germany
[c] Institute of Physical Chemistry and Abbe Center of Photonics, Friedrich Schiller University Jena, Helmholtzweg 4, 07743 Jena, Germany

ARTICLE INFO

Article history:
Received 12 February 2016
Received in revised form
1 April 2016
Accepted 6 April 2016
Available online xxx

Keywords:
Dinuclear complex
Dual luminescence
Water reduction
Iridium(III)
Ruthenium(II)
Bibenzimidazole

ABSTRACT

The synthesis, spectroscopic and electrochemical properties of the heterodinuclear iridium(III)/ruthenium(II) photosensitizer **Ir-BBI-Ru**, i.e. $[(ppy)_2Ir\text{-}(tmBBI)\text{-}Ru(^tbbpy)_2][PF_6]$ (ppy = 2-phenylpyridine; tmBBI = 5,5′,6,6′-tetramethyl-2,2′-bibenzimidazole; ^{t}bbpy = 4,4′-di-*tert*-butyl-2,2′-bipyridine) are presented. Its absorbance lies well within the visible light spectrum, showing absorption features typical for dinuclear ruthenium(II) bibenzimidazole complexes. The complex exhibits characteristic emission properties of both metal centers, indicative of an incomplete energy transfer. The application of **Ir-BBI-Ru** as visible-light absorbing photosensitizer in the field of photocatalytic water reduction is demonstrated by considerable hydrogen generation with a Co(II) catalyst and triethanolamine as sacrificial donor.

© 2016 Published by Elsevier B.V.

1. Introduction

Luminescent transition metal complexes are highly relevant compounds for a manifold of applications such as artificial lighting technologies, bioanalytical sensing, and photocatalysis [1–8]. Research in this area is aiming at optimizing the photophysical properties of such complexes for a certain purpose in terms of visible light absorption, emission properties and lifetimes of the respective electronically excited states. A particular synthetic tool is the use of bridging ligands in order to combine the properties of two distinct chromophore units [9–15]. The nature of the bridging ligand determines the photophysical properties of the metal centers both through the ligand-field and the amount of electronic communication it allows between the bridged metal centers [16]. Two well-established types of luminescent transition metal complexes are tris(bipyridine) ruthenium(II) and cyclometalated tris- or bis((phenyl)pyridine)iridium(III) derivatives [6,17–21]. Although structurally similar, the photophysical processes in these complexes are quite different. The ruthenium complexes of this type usually exhibit broad absorption in the visible regime attributed to a singlet metal-to-ligand charge transfer excitation, formally creating an excited ruthenium(III)/bipyridine(-e$^-$) state, which undergoes rapid intersystem crossing to generate the respective long-lived luminescent triplet state [17]. Iridium(III) chromophores, in contrast absorb mostly in the UV regime with only weak absorption above 400 nm. The absorption features of these complexes are ascribed to mixed ^{3}MLCT/^{3}LC excited states, which can be populated directly due to strong spin-orbit coupling of the 5d metal center [22–27]. We have recently reported several examples of ruthenium(II) and iridium(III) complexes with derivatives of 2,2′-bibenzimidazole as third ligand for supramolecular interactions and chemical sensing [28–30]. Both types of chromophores exhibit strong though fundamentally different photophysical responses to changes of their environment. For example, the ruthenium(II) complexes show significant broadening and a bathochromic shift of the visible-light absorbance accompanied by

* Corresponding author.
E-mail address: sven.rau@uni-ulm.de (S. Rau).
[1] Both authors contributed equally.
[2] http://www.uni-ulm.de/nawi/nawi-anorg1.

http://dx.doi.org/10.1016/j.jorganchem.2016.04.002
0022-328X/© 2016 Published by Elsevier B.V.

Please cite this article in press as: S.A. Rommel, et al., Journal of Organometallic Chemistry (2016), http://dx.doi.org/10.1016/j.jorganchem.2016.04.002

a stepwise quenching of their emission upon deprotonation [30]. The analogous iridium(III) complexes, in contrast, exhibit almost no significant change of the absorption, but remain strongly luminescent at varying wavelengths upon deprotonation [10,28,29].

Previously, Dietzek et al. showed that bibenzimidazoles are suitable candidates to facilitate excited-state excitation migration taking place within a polynuclear complex [31]. Further, to the best of our knowledge only one photocatalytically active system for hydrogen generation from an aqueous solution using an iridium(III) bibenzimidazole as photosensitizer has been reported to date, whereas so far, ruthenium(II) bibenzimidazole complexes remain unexplored in this regard [9]. The aim of this work was hence to combine the advanced visible-light absorption features of ruthenium(II) complexes with the advantageous luminescent properties of the iridium(III) congener by connecting them within a dinuclear bibenzimidazolate bridged photosensitizer.

We present the synthesis, spectroscopic and electrochemical properties of **Ir-BBI-Ru** and will show strong visible-light absorption and dual emission from both chromophore units. Time-resolved photophysical analysis was carried out to grasp the underlying processes, and the new complex is shown to act as an advantageous photosensitizer in light-driven photocatalytic hydrogen generation.

2. Results and discussion

2.1. Synthesis and characterization of the complex

The heterodinuclear complex **Ir-BBI-Ru** was synthesized *via* two different routes, i.e. either binding of the ruthenium complex fragment ($(^{t}bbpy)_2Ru^{2+}$ from its dichlorido precursor ($^{t}bbpy$ = *tert*-butyl-bipyridine, route A) to the metalloligand $[(ppy)_2IrBBI]^-$ (**IrBBI**$^-$, ppy = 2-phenylpyridine, BBI = 5,5′,6,6′-tetramethyl-2,2′-bibenzimidazole), or analogous binding of the iridium complex fragment $(ppy)_2Ir^+$ from the respective bis(μ-chlorido) bridged dimeric precursor to the metalloligand $[(^{t}bbpy)_2RuBBI]$ (**RuBBI**) (route B, see Scheme 1). The respective fragments have been synthesized according to literature procedures [32,33]. The reactions were carried out in protic media (route A: mixture of ethanol/water (3:1); route B: ethanol) under inert conditions and upon addition of triethylamine (TEA) in order to deprotonate the bibenzimidazole complexes and generate the respective metalloligands. Precipitation of the hexafluorophosphate salt and subsequent purification through silica column chromatography (ACN/water 4:1, v/v) and size-exclusion chromatography (sephadex®, methanol) yielded **Ir-BBI-Ru** in moderate yields (76%, route A, or 66%, route B). The principle structural characterization of the complex was achieved by NMR spectroscopy and mass spectrometry. The observed ESI-MS signal at m/z = 1427.524 and 713.762 appertain to the one- or twofold positively charged $(Ir\text{-}BBI\text{-}Ru)^+$ or $(Ir\text{-}BBI\text{-}Ru)^{2+}$, respectively.

The ^{1}H NMR spectrum of **Ir-BBI-Ru** (see Fig. 1) reveals a complex signal set characteristic for a mixture of the *meso* isomers $\Delta_{Ru}\Lambda_{Ir}$ and $\Delta_{Ir}\Lambda_{Ru}$, and the racemic isomers ΔΔ and ΛΛ of the heterodinuclear complex. The signals in the aromatic and aliphatic region agree with the expected number of protons of **Ir-BBI-Ru** and the spectrum provides all of the expected signal sets of 2 different coordinating (**ppy** and **^{t}bbpy**) as well as one peripheral bridging ligand (**BBI**). However, due to the superimposition of a majority of the signals no accurate assignment of the proton signals is possible.

Notably, however, there are the two doublet like signal sets at δ = 5.81/5.79 ppm and δ = 5.30/5.28 ppm, which correspond to the four C–H signals located at the bibenzimidazole (see Fig. 1). The aromatic $C\text{–}H_{BBI}$ signals are particularly sensitive to the coordination geometry as observed at structural similar mononuclear bibenzimidazole complexes [10,30,34–36]. The bis(phenylpyridine)iridium(III) complex of 5,5′,6,6′-tetramethyl-2,2′-bibenzimidazole [**IrBBI-H$_2$**] shows only two different $C\text{–}H_{BBI}$ signals in deuterated dichloromethane, i.e. one at δ = 5.91 (H-7″) and the other at δ = 7.41 (H-4″) (see ESI). The same signal splitting is observed at the structural similar ruthenium complex [**RuBBI-H$_2$**], where the more highfield shifted $C\text{–}H_{BBI}$ signal is strongly shielded owing to its spatial proximity to the pyridyl ring of the **ppy** or **^{t}bbpy** ligand. In contrast to corresponding signals for **IrBBI-H$_2$** or **RuBBI-H$_2$**, in **Ir-BBI-Ru**, however, four different $C\text{–}H_{BBI}$ signals are visible in the ^{1}H NMR spectrum and seemingly form two doublets. This refers to the different coordination geometries of the $C\text{–}H_{BBI}$ signals in the stereoisomers, i.e. ΛΔ,ΔΛ (Fig. 1, black marked) and ΔΔ,ΛΛ (orange marked). By integration of the two signals at δ = 5.81/5.79 a ratio of 60/40 for ΔΔ,ΛΛ/ΛΔ,ΔΛ was calculated. Similarly, in the single crystal a *rac*/*meso* ratio of 3:1 ratio was detected. Strikingly, Δ and Λ isomers of the iridium moiety occupy the same position in the crystal lattice.

In Table 1, the bond lengths and angles of Ir-(tmBBI)-Ir (**R1**) [10], **Ir-BBI-Ru**, $[\{(^{t}bbpy)_2Ru\}_2(\mu\text{-tmBBI})][PF_6]_2$ (**R2**) [34] and $[(^{t}bbpy)_2Ru(tmBBI\text{-}H_2)][PF_6]_2$ (**R3**) [37] are shown. The numbering scheme for **Ir-BBI-Ru** is depicted in Fig. 2, all others can be found in the Supporting Information.

The phenylpyridine ligands in the iridium moiety are oriented with the cyclometalated phenyl ring in the *trans* position with respect to the bibenzimidazole ligand. This observation is in agreement with other known bis-heteroleptic bis(phenylpyridine)-iridium(III) complexes [10,24].

For the homo-dinuclear complexes **Ir-(tmBBI)-Ir** and **Ru-(tmBBI)-Ru** a linear arrangement of the bridging ligand has been reported which reflects symmetric binding to both metal centers [10,34]. In the respective mononuclear structures, in contrast, it is well known that the bibenzimidazole is slightly bent towards the metal center with bending angles around 165.9° (±0.7°) [10,30,34,38–41]. In the presented heterodinuclear complex **Ir-BBI-Ru** a slight distortion of the bridging ligand geometry in contrast to the homodinuclear congeners is observed. That is, the bibenzimidazole ligand exhibits a bending angle of 183.89° with respect to the iridium center and 176.11° to the ruthenium center, which is in agreement with the slightly longer $Ir\text{–}N_{(BBI)}$ distances as compared to the respective $Ru\text{–}N_{(BBI)}$ distances in the mononuclear complexes.

All distances and angles characteristic to the coordination polyhedra of the mononuclear, the homodinuclear, and the presented heterodinuclear complex are presented in Table 1. The bi(benz)imidazole ligand always exhibits longer distances to the metal core than the distances for the comparable ligands phenylpyridine or bipyridine, respectively [10,34,39].

2.2. Photophysical characterization

The absorption spectrum of **Ir-BBI-Ru** (see Fig. 3) exhibits the characteristic features of the respective homodinuclear complexes, i.e. most notably two intense absorption maxima at 358 nm and a maximum at 535 nm [10,30,42–44]. For the reference compound **Ir-BBI-H$_2$** only ill-defined MLCT transitions were observed in the UV/Vis spectrum and unlike $Ru(bpy)_3^{2+}$, for which the MLCT bands are spectrally well separated from intraligand absorptions (IL), no clear isolated MLCT band for the iridium part of **Ir-BBI-Ru** can be observed here [10]. The absorption band in the 400–500 nm region is due to a singlet, spin-allowed MLCT transition centered on the ruthenium moiety, together with a weak contribution of spin-forbidden MLCT transitions (singlet–triplet) from the iridium part at the UV edge [45].

Most of the ligand bridged Ir(III)/Ru(II) dinuclear complexes

Please cite this article in press as: S.A. Rommel, et al., Journal of Organometallic Chemistry (2016), http://dx.doi.org/10.1016/j.jorganchem.2016.04.002

ARTICLE IN PRESS

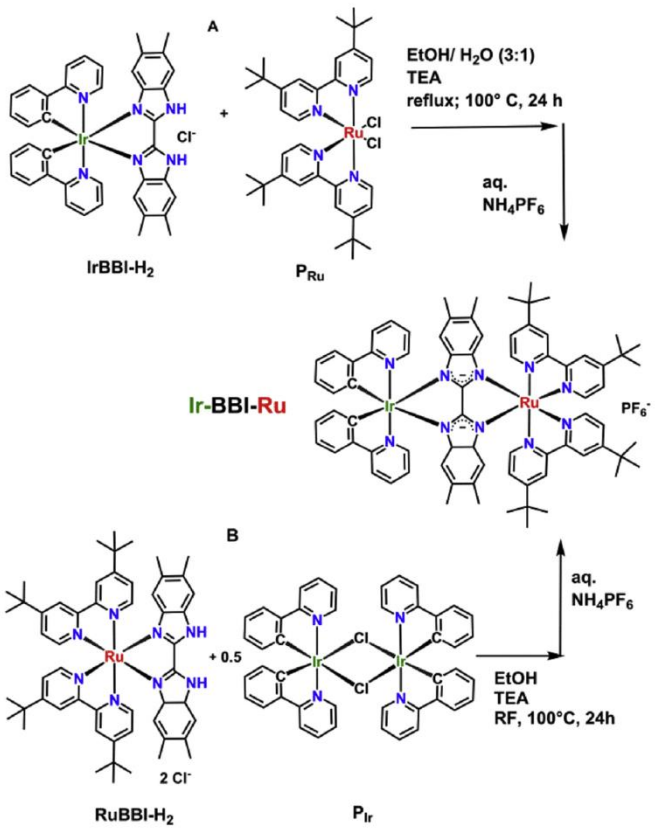

Scheme 1. Depiction of the two different routes A and B to synthesize the heterodinuclear compound **Ir-BBI-Ru**.

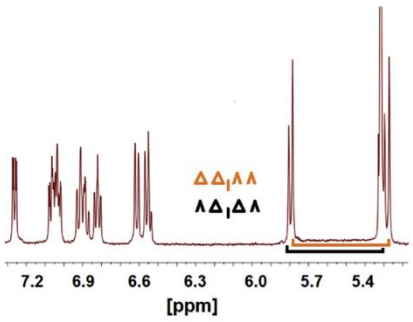

Fig. 1. ^{1}H NMR spectrum of **Ir-BBI-Ru** in deuterated dichloromethane.

reported in literature exhibit an efficient energy transfer from the iridium(III) to the ruthenium(II) center, resulting in sole emission from the latter [45–50]. Upon excitation of **Ir-BBI-Ru** at $\lambda_{exc} = 350$ nm two distinct emission features are observed (Table 2, Fig. 3), i.e. one at $\lambda_{max,1}(em) = 503$ nm, and one at $\lambda_{max,2}(em) = 700$ nm. The position and structure of the emission band around 503 nm closely resembles that of the twofold deprotonated **IrBBI**$^-$ in dichloromethane, whereas the emission at around 700 nm can be assigned to a ruthenium related emission with respect to literature [10,35,36,41,43,51]. Upon excitation of the ruthenium specific absorption at 535 nm, only the lowest-lying, Ru-based emission is observed (Fig. 4). This finding can be rationalized as expected, since the Ir(III) chromophores do not absorb light at wavelengths longer than 400 nm.

Fluorescence excitation spectra recorded at an emission at $\lambda = 503$ nm and at $\lambda = 700$ nm exhibit nearly identical features in the UV regime, i.e. two distinct maxima at 290/281 nm and 358 nm. Upon excitation at 358 nm the emission bands at 520 and at 700 nm can be recorded simultaneously. The appearance of dual emission from **Ir-BBI-Ru** indicates that the bridging bibenzimidazolate ligand prevents coupling of the two chromophores within the complex. Comparative measurements under identical optical density of the luminescence of **IrBBI-H$_2$** have shown that the intensity of the iridium specific emission in the heterodinuclear complex is only about 3% as compared to the mononuclear complex, which in turn is a rather strong indication for an efficient but incomplete energy transfer to the weakly emissive ruthenium(II) moiety (see ESI).

Please cite this article in press as: S.A. Rommel, et al., Journal of Organometallic Chemistry (2016), http://dx.doi.org/10.1016/j.jorganchem.2016.04.002

ARTICLE IN PRESS

Table 1
Selected bond lengths [Å] and angles [°] of Ir-BBI-Ru, R1, R2 and R3. The numbering scheme is according to that depicted in Fig. 2 [10,37].

Ir(-tmBBI)-Ir (**R1**)		**Ir-(tmBBI)-Ru**		**Ir-(tmBBI)-Ru**		$[(ppy)_2Ir(tmBBI\text{-}H_2)][PF_6]$ (**IrBBI, R2**)		$[(^tbbpy)_2Ru(tmBBI\text{-}H_2)][PF_6]_2$ (**RuBBI, R3**)	
Ir1–N1	2.201(3)	Ir1–N1A	2.066(3)	Ru1–N5	2.130(5)	Ir–N1	2.138(8)	Ru1–N2	2.102(5)
Ir1–N3	2.177(2)	Ir1–N2A	2.005(3)	Ru1–N6	2.122(5)	Ir–N2	2.136(8)	Ru1–N1	2.110(4)
Ir1–N4	2.038(3)	Ir1–N3	2.198(6)	Ru1–N7	2.035(5)	Ir–N4	2.061(8)	Ru1–N6	2.052(5)
Ir1–C27	2.005(3)	Ir1–C4	2.194(6)	Ru1–N8	2.047(6)	Ir–C10	2.015(1)	Ru1–N5	2.042(4)
Ir1–N5	2.037(3)	Ir1–C1A	2.037(3)	Ru1–N9	2.025(5)	Ir–N3	2.039(7)	Ru1–N8	2.059(4)
Ir1–C38	2.007(3)	Ir1–C1C	2.073(3)	Ru1–N10	2.048(5)	Ir–C11	1.990(1)	Ru1–N7	2.058(4)
N3–Ir1–N4	79.49(9)	N3–Ir1–N4	79.8(2)	N10–Ru1–N9	79.0(2)	N1–Ir1–N2	76.0(3)	N1–Ru1–N2	77.66(12)
C27–Ir1–N4	80.63(12)	C1A-Ir1-N2A	82.3(1)	N8–Ru1–N7	78.4(2)	C10–Ir1–N4	80.6(4)	N6–Ru1–N5	79.01(18)
C38–Ir1–N5	80.62(12)	C1C–Ir1–N1A	80.6(1)	N5–Ru1–N6	80.6(2)	C11–Ir1–N3	81.5(4)	N7–Ru1–N8	78.93(17)
N5–Ir1–N4	174.37(11)	C1C–Ir1–N3	170.0(2)	N10–Ru1–N7	176.3(2)	N4–Ir1–N3	174.0(3)	N5–Ru1–N8	95.54(17)
C38–Ir1–N3	170.73(11)	C1A-Ir1-N4	174.6(2)	N5–Ru1–N8	170.7(2)	C11–Ir1–N2	171.2(4)	N7–Ru1–N2	93.19(18)
C27–Ir1–N1	170.64(11)	N1A-Ir1-N2A	171.9(1)	N6–Ru1–N9	170.1(1)	C10–Ir1–N1	172.4(4)	N6–Ru1–N6	97.79(18)
						N6–C5–C4	130.3(8)	N3–C7–C8	129.7(5)
		Deviation α_{Ir}	183.89	Deviation α_{Ru}	176.11°	N5–C4–C5	128.7(9)	N4–C8–C7	130.3(5)
						N1–C5–C4	116.0(8)	N1–C7–C8	117.4(5)
						N2–C4–C5	116.2(8)	N2–C8–C7	116.8(5)
						Deviation α	166.12	Deviation α	167.1

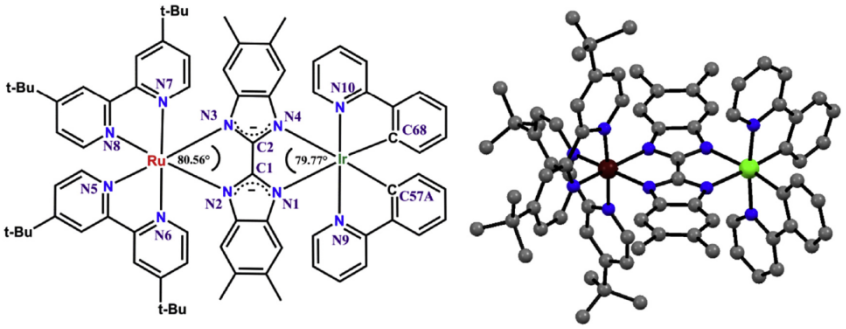

Fig. 2. Left: schematic depiction of the solid-state structure of **Ir-BBI-Ru**.; right: solid-state structure of **Ir-BBI-Ru** (ellipsoids at 50% probability level; the hydrogen atoms are omitted for clarity; R1 = 0.0634, wR2 = 0.1654).

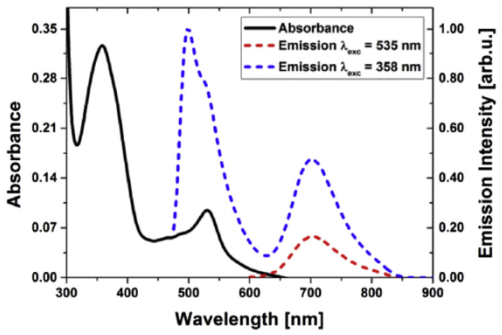

Fig. 3. UV/Vis (black, solid) and normalized emission spectra (blue and red, dotted) of **Ir-BBI-Ru** in dichloromethane ($c = 5 \times 10^{-6}$ M; red: excitation at λ = 535 nm; blue: excitation at λ = 358 nm). (For interpretation of the references to colour in this figure legend, the reader is referred to the web version of this article.)

In order to elucidate the unusual luminescence properties of **Ir-BBI-Ru** in more detail, time resolved emission studies using a streak camera were performed, which allows to record time-resolved emission spectra. This way, for each band in the emission spectrum the decay kinetics can be resolved and the corresponding emission lifetime can be determined: The lifetime of the iridium based (bright, i.e. emitting) excited state in **Ir-BBI-Ru** is approximately 49 ns in oxygen-equilibrated chloroform solution, which is very similar to the lifetimes previously observed for related cyclometalated iridium complexes (see Table 3) [24,52–54].

Table 2
Photophysical data of the investigated complex **Ir-BBI-Ru** and related Ir(III) or Ru(II) compounds [10,34].

Complex	Solvent[a]	λ_{max}/nm		Lifetime [ns]
		Absorption	Emission	
Ir-BBI-Ru	$CHCl_3$	358, 530	503, 695	49[b],112[c]
	ACN	353, 517	500, 710	29[b], 36[c]
Ir(tmBBI)-H_2^+	$CHCl_3$	378	521/559	44 (329)
Na–**Ir(tmBBI)**	$CHCl_3$	377	494	57
Ir(tmBBI)Ir	$CHCl_3$	375	499	50
$[(^tbpy)_2Ru]_2tmBBI$	ACN	510/510	700/700	50/60
$(^tbpy)_2Ru(tmBBI\text{-}H_2)$	ACN	473	648	120

[a] Air equilibrated.
[b] Determined in the spectral interval 510–580 nm.
[c] Determined in the spectral interval 590–660 nm, respectively.

Please cite this article in press as: S.A. Rommel, et al., Journal of Organometallic Chemistry (2016), http://dx.doi.org/10.1016/j.jorganchem.2016.04.002

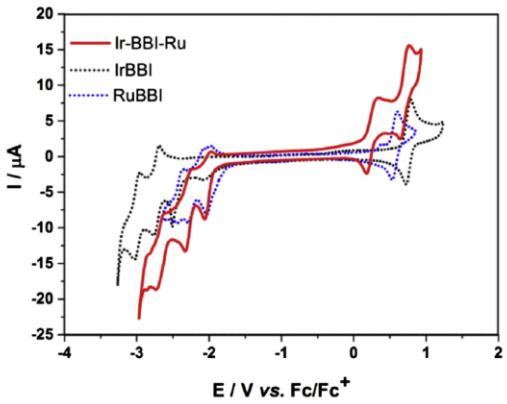

Fig. 4. Cyclic voltammogram of **Ir-BBI-Ru** and the mononuclear reference compounds **IrBBI-H$_2$** and **RuBBI-H$_2$** in dry acetonitrile using 0.1 M (^{n}Bu$_4$N)PF$_6$ as supporting electrolyte at a scan rate of 100 mV/s; concentration of the complexes was 1 mM.

Earlier investigations on the related system **Ir(BBI)-H$_x$** (x = 2, 0) and the homodinuclear **Ir-BBI-Ir** also provide values for the excited state lifetime of approximately 50 ns (see Table 3). On the other hand, the lifetime of the bright ruthenium based excited state is 112 ns under identical experimental conditions. Notably, the excited state lifetimes for both emissions are significantly shorter in acetonitrile (see Table 2) as compared to those determined in chloroform for **Ir-BBI-Ru**, which indicates considerable sensitivity towards the solvent polarity (see ESI). A more detailed photophysical investigation is out of the scope of this contribution.

2.3. Electrochemical properties

Comparative electrochemical analysis of **Ir-BBI-Ru** and its mononuclear reference compounds **IrBBI-H$_2$** and **RuBBI-H$_2$** was performed using cyclic voltammetry (dry, de-gassed ACN, (^{n}Bu$_4$N)PF$_6$ as supporting electrolyte, ferrocene/ferrocenium as reference). Table 3 shows recorded oxidation and reduction potentials of mono- and binuclear bibenzimidazole complexes, respectively. For the mononuclear **IrBBI-H$_2$** and **RuBBI-H$_2$** complexes, one reversible oxidation process is observed related to Ir(III)/Ir(IV) or Ru(II)/Ru(III) oxidation, respectively [44,13]. For the Ru species the reversible redox wave is centered at +0.57 V, whereas the oxidation wave is shifted anodically by 0.19 V for the iridium species, which is in accordance with previously reported homodimetallic Ru(II) and Ir(III) complexes [55]. For **IrBBI-H$_2$** the oxidation could mainly be associated with Ir-centered orbitals and σ band Ir–C orbitals derived from the removal of an electron belonging to the highest occupied molecular orbital (HOMO) of the iridium [9]. The heterodinuclear complex **Ir-BBI-Ru** shows two reversible oxidation processes centered at +0.26 V and +0.71 V related to Ru$^{II/III}$ and Ir$^{III/IV}$, respectively. Notably, the first oxidation potential of the binuclear complex is 0.3 V lower than those of the mononuclear complexes, which may be due to the known effect of negatively charged bibenzimidazole bridging ligands on metal based redox potentials [9,34,56]. Further, this indicates an electron-donor property of the BBI bridging ligand in the dinuclear Ir(III)/Ru(II) system [9,44,57].

Table 3
Electrochemical data for oxidation and reduction processes of **IrBBI-H$_2$**, **RuBBI-H$_2$** and **Ir-BBI-Ru** in MeCN at a glassy-carbon electrode at 20 °C.

Compound	$E_{1/2}$/V *vs.* Fc/Fc$^+$					
	Oxidations		Reductions			
Ir-BBI-H$_2$	+0.757		−2.075[a]	−2.512[a]	−2.728	2.997
Ru-BBI-H$_2$	+0.571	+0.398[a]	−2.002	−2.183	−2.396	
Ir-BBI-Ru	+0.707	+0.261	−2.015	−2.277	−2.676	

[a] Irreversible process.

3. Hydrogen production experiments

Stimulated by the appealing photophysical properties and stable metal based redox processes, we were keen to investigate the potential of **Ir-BBI-Ru** as photosensitizer for visible light driven hydrogen generation from an aqueous solution. Following the procedure reported by Zou et al. for structurally related mono- and heterodinuclear iridium(III) complexes, we used a three-component catalytic system consisting of the photosensitizer **PS**, the water reduction catalyst (WRC) [Co(bpy)$_3$]Cl$_2$ and triethanolamine (TEOA) as a sacrificial electron donor in a mixture of acetone and water (4:1, v/v) under an inert argon atmosphere [9]. Quantitative determination of the generation of hydrogen was conducted by gas chromatography analysis of the gas phase of the reaction system (for details, see ESI). Control experiments have been performed by excluding the photosensitizer from the system. Thereby no significant amounts of hydrogen were detectable.

In a typical photocatalytic experiment, the three-component system was used in a 10 mL solution of acetone/water (4:1, v/v) containing PS (10 μM), [Co(bpy)$_3$]Cl$_2$ (0.33 mM), and TEOA (0.19 M) at a pH value of pH = 8.0, i.e. lower than the pK$_a$ of TEOA. Other than Zou et al., who used a 300 W xenon lamp equipped with a cutoff filter (irradiation wavelength >420 nm), samples in this work were irradiated by 470 nm LEDs [9].

For the three complexes **Ir-BBI-Ru**, **IrBBI-H$_2$** and **RuBBI-H$_2$**, we measured their catalytic performance within an irradiation time of 140 h after which saturation behaviour was observed. Since deprotonation of the mononuclear complexes is inevitable under the selected catalytic conditions due to the electron donor, both mononuclear complexes are deprotonated in the catalysis solution. Whereas both iridium(III) containing compounds were able to produce hydrogen under the said conditions, no hydrogen was detected by using **RuBBI-H$_2$** as a **PS**. As discussed earlier, the respective ruthenium complex exhibits a low energy absorbance accompanied by complete quenching of its emission and is therefore no suitable **PS** [57,58]. The analogous iridium complex, in contrast, induces initial hydrogen production with an attainable TON of about 100 after an irradiation time of 100 h.

With the heterodinuclear **Ir-BBI-Ru** system hydrogen evolution could also be induced with a TON of about 170 after 140 h. The TON values obtained for the mononuclear **IrBBI-H$_2$** and **Ir-BBI-Ru** are in the range of the results produced by Cai et al. for their [[Ir(tfmppy)$_2$]$_X$(BiBzIm)] (X = 1,2) system [tfmppy = 2-(4-(trifluoromethyl) phenyl)-pyridine, BiBzIm = 2,2′-bibenzimidazole) [9]. However, in our case for both **PS**s a longer hydrogen production rate is observed as well as slightly higher overall TONs. It should be noted that in this report a different irradiation source was used, however the influence of the latter on the kinetics and efficiency of the catalysis is unclear.

Interestingly, an induction phase was clearly observed when using **Ir-BBI-Ru** as **PS** in contrast to the mononuclear iridium **PS**. Therefore, UV/Vis and emission measurements under catalysis conditions were performed to investigate the process occurring during the induction phase (see ESI). Upon perpetual irradiation of the catalysis solution a successive degradation process is observable according to the decrease of absorbance intensity. Regarding emission, the freshly degassed catalysis solution exhibits the

Please cite this article in press as: S.A. Rommel, et al., Journal of Organometallic Chemistry (2016), http://dx.doi.org/10.1016/j.jorganchem.2016.04.002

discussed features (*vide supra*), i.e. the iridium(III) based emission band maxima at around 500 nm and the ruthenium(II) based band at 700 nm. Upon irradiation, the iridium(III) specific emission increases immediately by a manifold, whereas the weak ruthenium specific emission band remains unchanged (see ESI). After around 4 h the changes in the UV/Vis and emission spectra are negligible, indicating the formation of a stable system. Thereby, the emission intensity at 502 nm is increased thirtyfold with constant ruthenium specific emission at 700 nm. The mechanistic details remain subject of further investigations. In sum, both the mononuclear iridium complex and the heterodinuclear complex are promising **PSs** for visible light driven hydrogen production (see Fig. 5).

4. Conclusions

The succesful synthesis of a heterodinuclear 4,4′,5,5′-tetramethyl-2,2′-bibenzimidazolate bridged iridium(III)/ruthenium(II) chromophore **Ir-BBI-Ru** was presented. Its photophysical and electrochemical properties have been investigated and compared to related complexes. A crystal structure of **Ir-BBI-Ru** was provided and compared with three structurally similar reference compounds.

By coupling a ruthenium and an iridium moiety to the bridging ligand bibenzimidazole, a dinuclear complex is obtained, which in principle combines the advantageous visible light absorbing properties of its ruthenium moiety with the sophisticated luminescence properties of its iridium-phenylpyridine moiety. In addition, a rare case of dual luminescence from both moieties is observed, whereas the iridium based emission in the covalently bound dyad **Ir-BBI-Ru** is significantly quenched by approximately 97% as compared to the mononuclear complex **IrBBI-H$_2$**.

Emission lifetimes of the iridium(III) specific emission is in the range of other related transition-metal bibenzimidazole complexes. Excited state lifetime measurements revealed a complex behaviour with different structured emission spectra in different solvents. Further studies, including quantum efficiency and transient absorption measurements are under investigation.

As fine tuning of the emission colour and a modification of the photophysical properties of iridium(III) complex fragments can be easily performed by a change in the ligand structure, the use of these materials for electroluminescent devices is conceivable. Further, the presented electrochemical and photophysical results clearly indicate that the complex exhibits the potential to work as a photosensitizer in photochemical processes. The obtained kinetic and photophysical data under catalytic conditions suggest an elaborate mechanism for the heterodinuclear photosensitizer and spark strong interest to further investigate this system in the future.

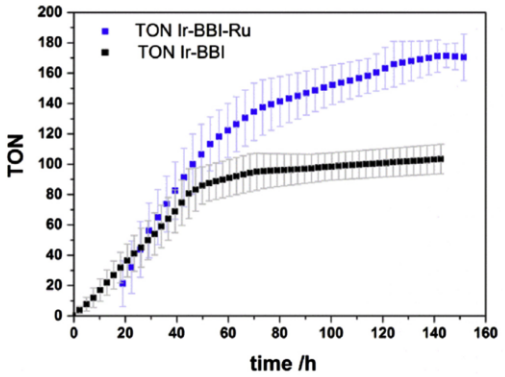

Fig. 5. Turnover numbers of the light-driven hydrogen production catalyzed by the covalent system **Ir-BBI-Ru** (blue rectangles) and **IrBBI-H** (black rectangles); the grey dashes represent the calculated standard deviation of each curve. (For interpretation of the references to colour in this figure legend, the reader is referred to the web version of this article.)

5. Experimental

5.1. Reactants and methods

The ruthenium precursor complex bis(4,4′-di-*tert*-butyl-2,2′-bipyridyl)dichloridoruthenium(II) [(tbbpy)$_2$Ru(Cl)$_2$] was synthesized according to an efficient microwave-assisted method presented in the literature starting from Ruthenium(III) chloride hydrate (35–40% Ruthenium) purchased from Degussa [33]. 4,4′,5,5′-Tetramethyl-2,2′-bibenzimidazole, tetrakis(2-phenylpyridine-C^2,N)bis(μ-chloro)diiridium [32,59,60] and the mononuclear complexes **IrBBI-H$_2$** and **RuBBI-H$_2$** were synthesized according to published procedures [10,36].

Technical grade solvents were purchased from VWR/Prolabo and redistilled under reduced pressure at 40 °C. Dichloromethane, chloroform and acetonitrile for spectroscopic measurements were purchased in spectroscopic grade from Roth. All chemicals were purchased from Merck Millipore, Sigma Aldrich, ABCR, Acros Organics, Alfa Aesar or VWR/Prolabo and used as purchased (≥95%). Inert reactions were performed under an Argon 4.6 atmosphere by means of standard Schlenk techniques. Size exclusion chromatography was carried out with Sephadex LH-20 as stationary phase (particle size 25–100 μm), purchased from Pharmacia Fine Chemicals AB, Uppsala, Sweden. ^{1}H NMR spectra were recorded at ambient temperature, unless otherwise stated, with a Bruker 400 MHz spectrometer and Bruker 500 MHz spectrometer. All spectra were referenced to the corresponding solvent residual signal, i.e. 1.940 ppm for acetonitrile, 7.260 for chloroform, 5.320 for dichloromethane and 4.870 for methanol. Mass spectra were recorded on a Finnigan MAT SSQ 710 or on a Thermoquest-Finnigan MAT 95XL.

X-ray crystallography was performed on a SuperNova (Dual Source) diffractometer, equipped with an ATLAS detector, from Agilent Technologies. The structures were refined by full-matrix least squares techniques against Fo^2 (SHELXL 2013) [61]. The hydrogen atoms were included at calculated positions with fixed thermal parameters. All non-hydrogen atoms were refined anisotropically.

Intensity data for **Ir-BBI-Ru** were collected on an Oxford Diffraction Supernova, dual source with a CCD detector diffractometer using Cu-k$_\alpha$ radiation ($\lambda = 1.54178$ Å). Data were corrected for Lorentz and polarization effects, a semi-empirical absorption correction based on multiple scans using SADABS [62] was applied. Structures were solved by direct methods (SHELXS2013 [61]) and refined by full-matrix least-squares techniques against F$_0^2$(SHELXL-2013 [61]). All hydrogen atoms were placed in positions of optimized geometry. Mercury 3.3 (Build RC5Mercury 3.3 (Build RC5)) was used for structure representations.

5.2. Electrochemistry

DC cyclic voltammetry (CV) experiments were performed using a CH Instruments CHI 620E electrochemical workstation equipped with a standard three-electrode arrangement: working electrode: glassy carbon electrode (d = 1.6 mm), quasi reference electrode: Ag wire (in a glass frit containing electrolyte with the same concentration as the concentration of electrolyte in the analysed solution),

Please cite this article in press as: S.A. Rommel, et al., Journal of Organometallic Chemistry (2016), http://dx.doi.org/10.1016/j.jorganchem.2016.04.002

counter electrode: Pt wire. All potentials are reported relative to the ferrocene/ferrocenium internal standard. CV experiments were performed in dry acetonitrile using (^{n}Bu4)NPF$_6$ as supporting electrolyte. All solutions were purged with argon for at least 3 min to remove O_2 and kept under a slight positive Ar pressure while performing the experiment.

5.3. Excited state lifetime measurements

The two-dimensional (time and wavelength) emission decay profiles were measured using a Hamamatsu streak scope C4334 in photon counting mode using a time-window of 500 ns. After excitation with the frequency-doubled output of a Ti-sapphire laser (Tsunami, Newport Spectra-Physics GmbH; pulse-to-pulse repetition rate 400 kHz after passing a pulse selector, model 3980, Newport Spectra-Physics GmbH) at λ_{exc} = 365 nm the luminescence of the sample was collected in a 90°-arrangement and spectrally dispersed using a Chromex 250IS imaging spectrograph. Selected horizontal (spectral) and vertical (temporal) intervals were integrated using the HPDTA software delivered with the streak camera system. Measurements were carried out without a polarizer to decrease the acquisition time. Therefore the early decay range (few ns) may be disturbed by contributions from rotational diffusion. However, due to the relatively longer excited-state lifetimes, this is not an issue for lifetime determination. The lifetime values were obtained from monoexponential fits of the linear portion of the integrated decay profiles. The samples were prepared to yield an optical density of 0.1 at the excitation wavelength in a 1-cm quartz cuvette using air-equilibrated, spectroscopic grade solvents.

5.4. H_2 evolution experiments

All H_2 production experiments were evaluated in a Schlenk tube (21 mL) with a side visible light irradiation using two LED sticks (λ = 470 nm). The reactor was charged with 10 μM PS, 0.33 mM catalyst [Co(bpy)$_3$]Cl$_2$, and 0.19 M TEOA in an aqueous solution (10 mL; acetone/water: 4:1, v/v). The pH value was adjusted to approximately 8.0 by the addition of concentrated hydrochloric acid. Prior to light irradiation, the system was evacuated successively *via* freeze pump thaw method before being backfilled with argon. The hydrogen evolved was measured by headspace GC on a Bruker Scion GC/MS, with a thermal conductivity detector 15 (column: Mol. Sieve 5A 75 m × 0.53 mm I.D., oven temp. 70 °C, flow rate 25 mL min^{-1}, detector temp. 200 °C) with argon as carrier gas. The GC was calibrated by mixing different volumes of pure hydrogen together with argon into a schlenk vessel. The obtained signal was plotted against the calibration curve to receive the total produced hydrogen content in the headspace.

5.5. Synthesis of (ppy)$_2$Ir(tmBBI)Ru(tbbpy)$_2$ (Ir-BBI-Ru)

Route A: 50 mg [Ir(ppy)$_2$(tmBBI-H$_2$)][Cl] (**IrBBI**) (60.35 μmol, M = 828.42 g/mol) together with 4.1 mL triethylamine were dissolved in a mixture of degassed ethanol/water (3:1) and stirred for 1 h 26 mg Ru(tbbpy)$_2$Cl$_2$ **P$_{Ru}$** (59.00 μmol, M = 442.32 g/mol) were also dissolved in a mixture of degassed ethanol/water (3:1) and added dropwise to the solution of **IrBBI** over half an hour. Under constant stirring the solution was heated up to 100 °C for 24 h.

Route B: 38 mg (35.47 μmol, M = 1072.09 g/mol) [Ir(ppy)$_2$Cl]$_2$ and 86 mg [Ru(bpy)$_2$(tmBBI-H$_2$)][PF$_6$]$_2$ (70.68 μmol, M = 1218.15 g/mol) were dissolved in 17 mL degassed ethanol and 4 mL triethylamine und heated up to 100 °C for 24 h under constant stirring.

In both cases the heterodinuclear complex **Ir-BBI-Ru** was precipitated as its hexafluorophosphate salt by addition of aqueous NH_4PF_6 to the solution and the precipitate was collected by a frit, washed with water (3 × 30 mL), diethyl ether (3 × 30 mL) and cold ethanol (1 × 20 mL). The crude product was then purified by chromatography on a silica gel column (acetonitrile/water 4:1, *v/v*). A second purification step was performed using a sephadex column (LH-20, methanol). The fraction of the pure compound was collected, concentrated and again precipitated by aqueous NH_4PF_6 (88 mg, 540 μmol) to get a dark purple powder. Yield: 64.04 mg (44.76 μmol, 75.86%, route A), 67.01 mg (46.83 μmol, 66.26%, route B).

^{1}H-NMR (DCM-d$_2$, 400 MHz): δ = 8.25–8.20 (m, 3H), 8.15–8.13 (m, 3H), 8.04–8.02 (m, 1H), 7.97 (d, ^3J = 5.0 Hz, 1H), 7.92 (d, ^3J = 6.1 Hz, 1H), 7.87 (d, ^3J = 8.0 Hz, 1H), 7.83 (d, ^3J = 6.0 Hz, 1H), 7.77 (d, ^3J = 8.1 Hz, 1H), 7.70 (d, ^3J = 7.0 Hz, 1H), 7.65–7.62 (m, 3H), 7.57–7.53 (m, 1H), 7.39–7.36 (m, 2H), 7.27 (dd, ^4J = 6.0 Hz, ^3J = 2.0 Hz, 1H), 7.08–7.03 (m, 3H), 6.93–6.88 (m, 2H), 6.84–6.81 (m, 1H), 6.63–6.54 (m, 3H), 5.80 (d, ^3J = 7.9 Hz, 2H), 5.29 (d, ^3J = 9.7 Hz, 2H), 1.93 (d, ^3J = 2.2 Hz, 6H), 1.91 (d, ^3J = 2.6 Hz, 6H), 1.46 (m, 18H), 1.42 (s, 6H), 1.37 (s, 6H).

ESI-MS: m/z = 1427.524 (M^+), 713.762 (M^{2+}).

Crystal data for **Ru-BBI-Ir**: C_{76} H_{80} F_6 Ir N_{10} P Ru, M_r = 1571.74 g mol^{-1}, dark red prism, crystal size 0.1183 × 0.0589 × 0.0472 mm^3, triclinic, space group *P*–1, a = 15.4174(4) Å, b = 16.7904(4) Å, c = 17.0628(4) Å, α = 86.505(2)°, β = 68.364(2)°, γ = 85.356(2) V = 4089.97(18) Å^3, T = 180(2) K, Z = 2, $\rho_{calcd.}$ = 1.276 Mg/m^3, μ (Cu-K$_\alpha$) = 5.251 mm^{-1}, F(000) = 1592, altogether 46056 reflexes up to h(−19/19), k(−20/20), l(−15/21) measured in the range of 7.513° ≤ Θ ≤ 73.787°, completeness Θ_{max} = 99.7%, 16068 independent reflections, R_{int} = 0.0412, 13087 reflections with $F_0 > 4\ \sigma(F_0)$, 821 parameters, 1 restraint, $R1_{obs}$ = 0.0634, $wR2_{obs}$ = 0.1654, $R1_{all}$ = 0.0754, $wR2_{all}$ = 0.1719, GOOF = 1.102, largest difference peak and hole: 1.703/−0.965 e Å^{-3}. The DFIX restraint was used once to fix one of the tertiary butyl groups. The crystal contains two chiral pairs of isomers, that is ΛΔ and ΔΛ, ΔΔ and ΛΛ. Each unit cell contains either one isomer of the ruthenium complex in Λ and Δ configuration. The iridium complex in contrast appears to be unregularly distributed with a ΔΔ/ΛΛ *versus* ΛΔ/ΔΛ ratio of 3:1 which is reflected in the respective site occupation values for the disordered isomers. Due to the comparatively low intensity of the electron density maxima of the less occupied phenylpyridine ligands, the latter were calculated isotropically and the refinement was stabilized using the AFIX66 for these ligands. CCDC 1452843 contains the supplementary crystallographic data for this paper. These data can be obtained free of charge from The Cambridge Crystallographic Data Centre *via* www.ccdc.cam.ac.uk/data_request/cif.

Acknowledgments

Financial support by the Carl Zeiss Stiftung (D. S.), the Deutsche Bundesstiftung Umwelt (N. R.) and the German Science Foundation (DI 1517/3-1) is thankfully acknowledged. We thank the European Cooperation in Science and Technology (COST ACTION CM1202 PERSPECT-H2O).

Appendix A. Supplementary data

CCDC 1452843 contain the supplementary crystallographic data for this paper. These data can be obtained free of charge from The Cambridge Crystallographic Data Centre *via* www.ccdc.cam.ac.uk/data_request/cif.

Appendix B. Supplementary data

Supplementary data related to this article can be found at http://

Please cite this article in press as: S.A. Rommel, et al., Journal of Organometallic Chemistry (2016), http://dx.doi.org/10.1016/j.jorganchem.2016.04.002

ARTICLE IN PRESS

dx.doi.org/10.1016/j.jorganchem.2016.04.002.

References

[1] J.H. Alstrum-Acevedo, M.K. Brennaman, T.J. Meyer, Inorg. Chem. 44 (2005) 6802–6827.
[2] S.-S. Sun, A.J. Lees, Chem. Commun. (2000) 1687–1688.
[3] L. Sun, L. Hammarström, B. Åkermark, S. Styring, Chem. Soc. Rev. 30 (2001) 36–49.
[4] V. Amendola, D. Esteban-Gómez, L. Fabbrizzi, M. Licchelli, Acc. Chem. Res. 39 (2006) 343–353.
[5] V. Balzani, A. Credi, M. Venturi, Molecular Devices and Machines, Wiley-VCH, Weinheim, 2003.
[6] V. Balzani, F. Scandola, Supramolecular Photochemistry, Ellis Horwood, New York, 1991.
[7] R. Siebert, A. Winter, U.S. Schubert, B. Dietzek, J. Popp, Phys. Chem. Chem. Phys. 13 (2011) 1606–1617.
[8] R. Siebert, A. Winter, B. Dietzek, U.S. Schubert, J. Popp, Macromol. Rapid Commun. 31 (2010) 883–888.
[9] J. Cai, Z. Yu, Y. Yuan, F. Li, Z. Zou, ACS Catal. 4 (2014) 1953–1963.
[10] S.A. Rommel, D. Sorsche, N. Rockstroh, F.W. Heinemann, J. Kübel, M. Wächtler, B. Dietzek, S. Rau, Eur. J. Inorg. Chem. (2015) 3730–3739.
[11] L. Donato, C.E. McCusker, F.N. Castellano, E. Zysman-Colman, Inorg. Chem. 52 (2013) 8495–8504.
[12] S.W. Kaiser, R.B. Saillant, W.M. Butler, P.G. Rasmussen, Inorg. Chem. 15 (1976) 2681–2688.
[13] M. Haga, A.M. Bond, Inorg. Chem. 30 (1991) 475–480.
[14] E.A. Plummer, J.W. Hofstraat, L. De Cola, Dalton Trans. (2003) 2080.
[15] J. Kübel, A. Winter, U.S. Schubert, B. Dietzek, J. Phys. Chem. A 118 (2014) 12137–12148.
[16] M.B. Robin, P. Day, in: H.J. Emeléus, A.G. Sharpe (Eds.), Adv. Inorg. Chem. Radiochem, Academic Press, New York and London, 1967, pp. 247–422.
[17] A. Juris, V. Balzani, Coord. Chem. Rev. 84 (1988) 85–277.
[18] Y.-J. Yuan, Z.-T. Yu, H.-L. Gao, Z.-G. Zou, C. Zheng, W. Huang, Chem. Eur. J. 19 (2013) 6340–6349.
[19] D. Hanss, J.C. Freys, G. Bernardinelli, O.S. Wenger, Eur. J. Inorg. Chem. (2009) 4850–4859.
[20] A.B. Tamayo, B.D. Alleyne, P.I. Djurovich, S. Lamansky, I. Tsyba, N.N. Ho, R. Bau, M.E. Thompson, J. Am. Chem. Soc. (2003) 7377–7387.
[21] A. Tsuboyama, H. Iwawaki, M. Furugori, T. Mukaide, J. Kamatani, S. Igawa, T. Moriyama, S. Miura, T. Takiguchi, S. Okada, et al., J. Am. Chem. Soc. 125 (2003) 12971–12979.
[22] S. Lamansky, P. Djurovich, D. Murphy, F. Abdel-Razzaq, H. Lee, C. Adachi, P.E. Burrows, S.R. Forrest, M.E. Thompson, J. Am. Chem. Soc. 123 (2001) 4304–4312.
[23] F.O. Garces, K.A. King, R.J. Watts, Inorg. Chem. 27 (1988) 3464–3471.
[24] L. Flamigni, A. Barbieri, C. Sabatini, B. Ventura, F. Barigelletti, Top. Curr. Chem. 281 (2007) 143–203.
[25] S. Lamansky, P. Djurovich, D. Murphy, F. Abdel-Razzaq, R. Kwong, I. Tsyba, M. Bortz, B. Mui, R. Bau, M.E. Thompson, Inorg. Chem. 40 (2001) 1704–1711.
[26] M. Bräutigam, M. Wächtler, S. Rau, J. Popp, B. Dietzek, J. Phys. Chem. C 116 (2012) 1274–1281.
[27] J. Meyer-Ilse, S. Bauroth, M. Bräutigam, M. Schmitt, J. Popp, R. Beckert, N. Rockstroh, T.D. Pilz, K. Monczak, F.W. Heinemann, et al., Dalton Trans. 43 (2014) 17659–17665.
[28] S.A. Rommel, D. Sorsche, A. Dixit, S. Rau, Eur. J. Inorg. Chem. 2016 (2016) 40–48.
[29] S.A. Rommel, D. Sorsche, S. Rau, Dalton Trans. 45 (2016) 74–77.
[30] D. Sorsche, S.A. Rommel, S. Rau, Eur. J. Inorg. Chem. (2016) 1503–1513.
[31] B. Dietzek, W. Kiefer, J. Blumhoff, L. Böttcher, S. Rau, D. Walther, U. Uhlemann, M. Schmitt, J. Popp, Chem. – A Eur. J. 12 (2006) 5105–5115.
[32] F.O. Garces, K.A. King, R.J. Watts, Inorg. Chem. 27 (1988) 3464–3471.
[33] S. Rau, B. Schäfer, A. Grüßing, S. Schebesta, K. Lamm, J. Vieth, H. Görls, D. Walther, M. Rudolph, U.W. Grummt, et al., Inorg. Chim. Acta (2004) 4496–4503.
[34] S. Rau, M. Ruben, T. Büttner, C. Temme, S. Dautz, H. Görls, M. Rudolph, D. Walther, A. Brodkorb, M. Duati, et al., J. Chem. Soc. Dalton Trans. (2000) 3649–3657.
[35] D. Sorsche, S. Rau, Eur. J. Inorg. Chem. (2014) 4244–4249.
[36] S. Rau, T. Büttner, C. Temme, M. Ruben, H. Görls, D. Walther, M. Duati, S. Fanni, J.G. Vos, Inorg. Chem. 39 (2000) 1621–1624.
[37] N. Rockstroh, K. Peuntinger, H. Görls, D.M. Guldi, F.W. Heinemann, B. Schäfer, S. Rau, Z. Naturforsch. 65b (2010) 281–290.
[38] D. Walther, L. Böttcher, J. Blumhoff, S. Schebesta, H. Görls, K. Schmuck, S. Rau, M. Rudolph, Eur. J. Inorg. Chem. (2006) 2385–2392.
[39] J.C. Freys, G. Bernardinelli, O.S. Wenger, Chem. Commun. (2008) 4267–4269.
[40] K. Halbauer, A. Göbel, A. Sterzik, H. Görls, S. Rau, W. Imhof, Eur. J. Inorg. Chem. (2007) 1508–1514.
[41] A. Grüßing, S. Rau, S. Schebesta, A. Scholz, H. Görls, D. Walther, Z. Anorg. Allg. Chem. (2007) 961–970.
[42] R. Indumathy, P.S. Parameswaran, C.V. Aiswarya, B. Unni Nair, Polyhedron 75 (2014) 22–29.
[43] M. Haga, Inorg. Chim. Acta 45 (1980) L183–L184.
[44] M. Haga, T. Matsumura-Inoue, S. Yamabe, Inorg. Chem. 26 (1987) 4148–4154.
[45] S. Welter, F. Lafolet, E. Cecchetto, F. Vergeer, L. De Cola, ChemPhysChem 6 (2005) 2417–2427.
[46] K.J. Arm, J.A.G. Williams, Dalton Trans. (2006) 2172–2174.
[47] C. Sabatini, A. Barbieri, F. Barigelletti, K.J. Arm, J.A.G. Williams, Photochem. Photobiol. Sci. 6 (2007) 397–405.
[48] J. Osío Barcina, N. Herrero-García, F. Cucinotta, L. De Cola, P. Contreras-Carballada, R.M. Williams, A. Guerrero-Martínez, Chem. Eur. J. 16 (2010) 6033–6040.
[49] V.L. Whittle, J.A.G. Williams, Dalton Trans. (2009) 3929–3940.
[50] M. Cavazzini, P. Pastorelli, S. Quici, F. Loiseau, S. Campagna, Chem. Commun. (2005) 5266–5268.
[51] Y. Cui, Y. Niu, M. Cao, K. Wang, H. Mo, Y. Zhong, B. Ye, Inorg. Chem. 47 (2008) 5616–5624.
[52] R.D. Costa, G. Fernández, L. Sánchez, N. Martín, E. Ortí, H.J. Bolink, Chem. Eur. J. 16 (2010) 9855–9863.
[53] E.A. Plummer, J.W. Hofstraat, L. De Cola, Dalton Trans. (2003) 2080.
[54] A. Tsuboyama, T. Takiguchi, S. Okada, M. Osawa, M. Hoshino, K. Ueno, Dalton Trans. (2004) 1115–1116.
[55] M. Cavazzini, S. Quici, C. Scalera, F. Puntoriero, G. La Ganga, S. Campagna, Inorg. Chem. 48 (2009) 8578–8592.
[56] A.M. Bond, M. Haga, Inorg. Chem. 25 (1986) 4507–4514.
[57] M. Haga, Inorg. Chim. Acta 75 (1983) 29–35.
[58] K. Monczak, K. Peuntinger, D. Sorsche, F.W. Heinemann, D.M. Guldi, S. Rau, Chem. Eur. J. 20 (2014) 15426–15433.
[59] E. Müller, G. Bernardinelli, J. Reedijk, Inorg. Chem. 34 (1995) 5979–5988.
[60] B. Schmid, F.O. Garces, R.J. Watts, Inorg. Chem. 33 (1994) 9–14.
[61] G.M. Sheldrick, Acta Cryst. A64 (2008) 112–122.
[62] SADABS, 2008/1, Bruker AXS Inc., Madison, WI, U.S.A., 2008.

Please cite this article in press as: S.A. Rommel, et al., Journal of Organometallic Chemistry (2016), http://dx.doi.org/10.1016/j.jorganchem.2016.04.002

Electronic Supplementary Information

Visible-light sensitized photocatalytic hydrogen generation using a dual emissive heterodinuclear cyclometalated iridium(III)/ruthenium(II) complex

Sebastian A. Rommel[a]†, Dieter Sorsche[a]†, Stefanie Schönweiz[a], Joachim Kübel[b,c], Nils Rockstroh[a], Benjamin Dietzek[b,c], Carsten Streb[a] and Sven Rau[a]*

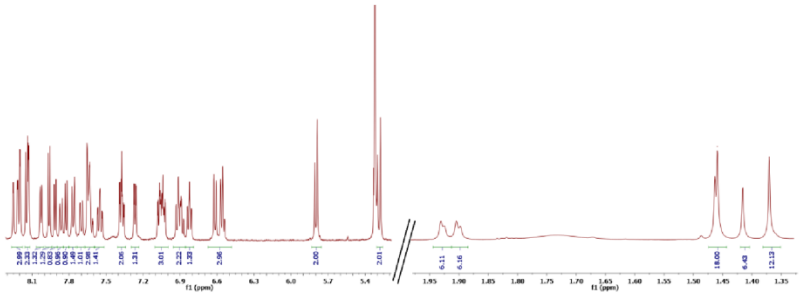

Figure S 1. ^{1}H NMR spectrum of **Ir-BBI-Ru** in deuterated dichloromethane.

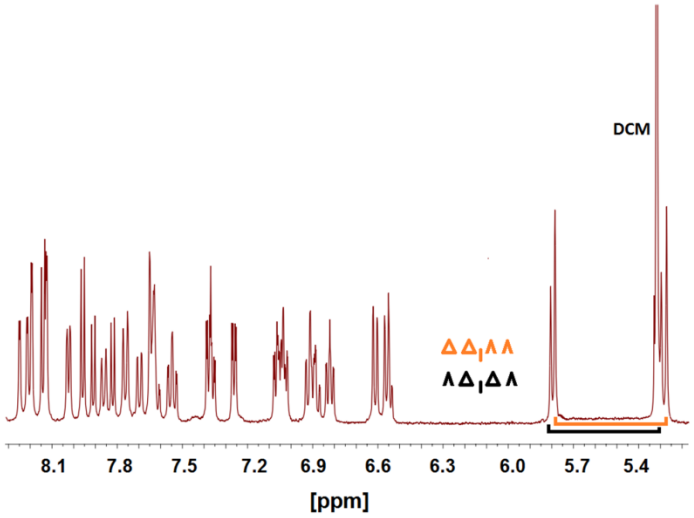

Figure S 2. Selected part of the ^{1}H NMR spectrum of **Ir-BBI-Ru** in deuterated dichloromethane.

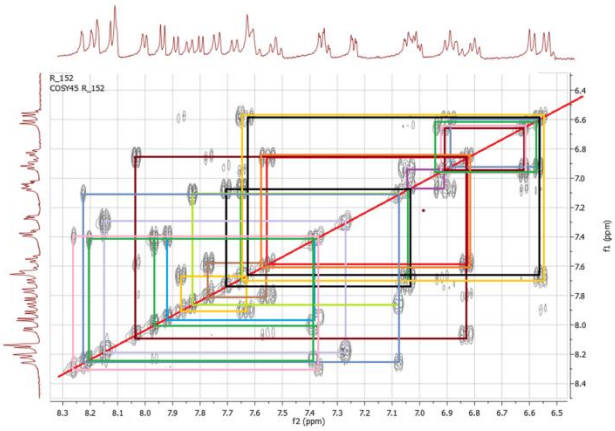

Figure S 3. ^{1}H-^{1}H COSY spectrum of **Ir-BBI-Ru** in deuterated dichloromethane.

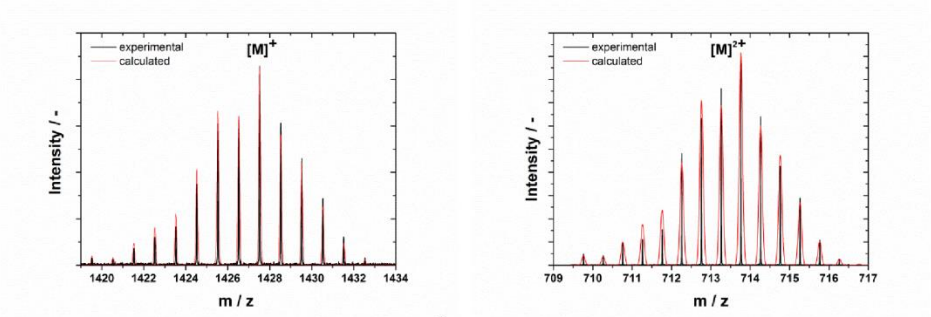

Figure S 4. ESI-MS peaks of $[Ir\text{-}BBI\text{-}Ru]^{+}$ and $[Ir\text{-}BBI\text{-}Ru]^{2+}$.

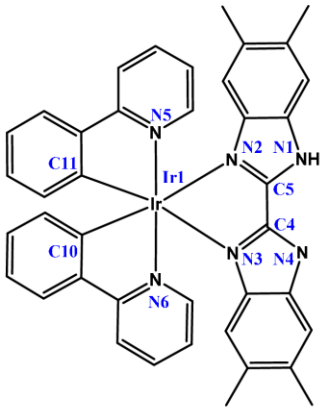

Scheme 1. Numbering scheme of the crystal structure of **Ir(tmBBI)**-H.

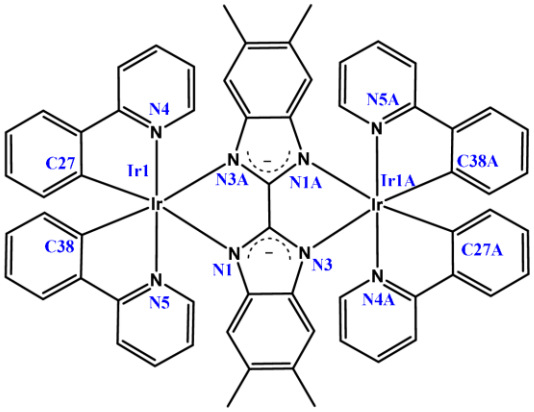

Scheme 2. Numbering scheme of the crystal structure of **Ir(tmBBI)Ir**.

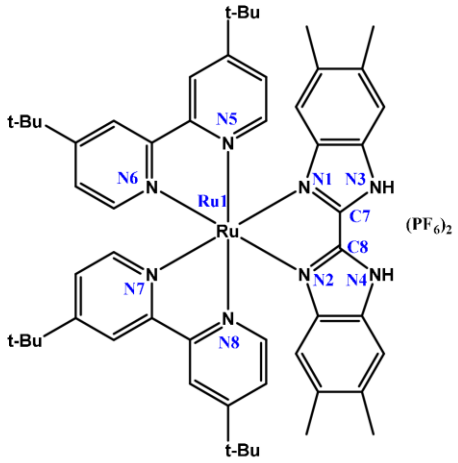

Scheme 3. Numbering scheme of the crystal structure of $[(tbbpy)_2Ru(tmBBI)][PF_6]_2$ (**R3**).

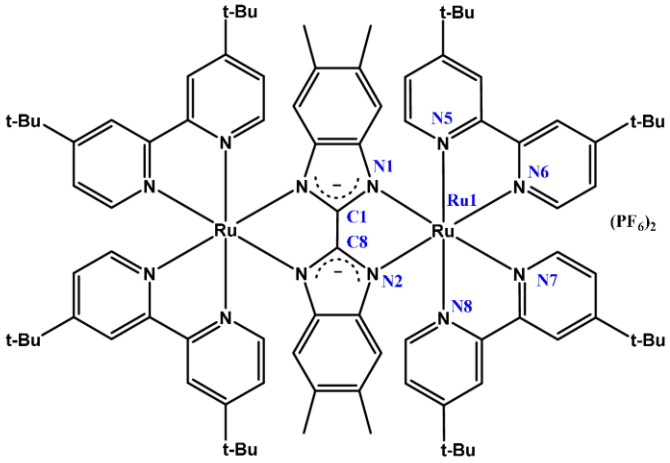

Scheme 4. Numbering scheme of the crystal structure of $[\{(tbbpy)_2Ru\}_2(\mu\text{-}tmBBI)][PF_6]_2$ (**R2**).

[{(tbbpy)$_2$Ru}$_2$(μ-tmBBI)][PF$_6$]$_2$ (**Ru-BBI-Ru**)	
Ru1-N1	2.124(3)
Ru1-N2	2.128(3)
Ru1-N5	2.032(3)
Ru1-N6	2.043(3)
Ru1-N8	2.051(3)
Ru1-N7	2.028(3)
N2-Ru1-N1	81.05(12)
N6-Ru1-N5	78.54(13)
N7-Ru1-N8	78.54(13)
N7-Ru1-N5	176.34(14)
N6-Ru1-N2	169.58(13)
N7-Ru1-N1	168.89(13)

Table 1 Selected bond lengths [Å] and angles [°] of **Ru-BBI-Ru**. The numbering scheme is according to that depicted in Scheme 4.[1]

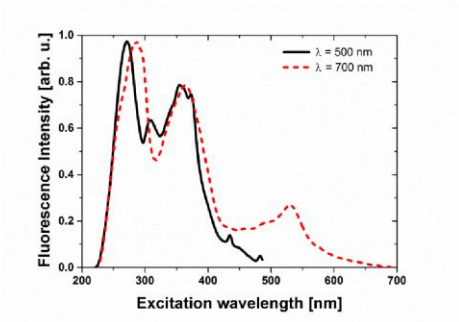

Figure S 5. Fluorescence excitation spectra of **Ir-BBI-Ru** of the emission at λ = 500 nm (black) and at λ = 700 nm (normalized).

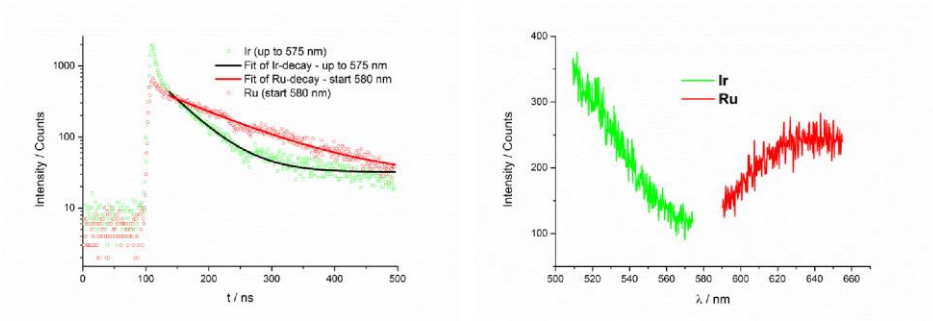

Figure S 6. Left: Emission decay curves (spectrally integrated streak camera data of the intervals marked in the spectrum on the right) of **Ir-BBI-Ru** in air- equilibrated chloroform. Red circles: Ruthenium core related emission, 580-660 nm; green: Iridium core related emission, 510-575 nm. The solid lines represent respective mono-exponential fit curves (black: 48 ns, red: 112 ns). Right: Temporally integrated data, i.e. emission spectra, with the respective intervals that were used for lifetime determination in green (Ir-based emission) or red (Ru-based emission).

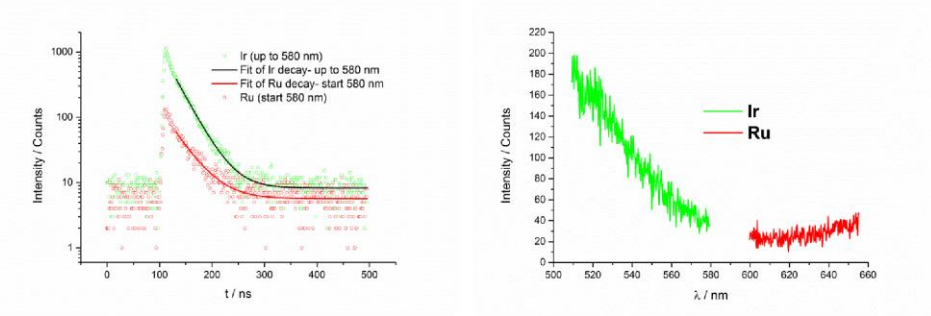

Figure S 7. Left: Emission decay curves (spectrally integrated streak camera data of the intervals marked in the spectrum on the right) of Ir-BBI-Ru in air- equilibrated acetonitrile. Red circles: Ruthenium core related emission, 580-660 nm; green: Iridium core related emission, 510-580 nm. The solid lines represent respective mono-exponential fit curves (black: 29 ns, red: 36 ns). Right: Temporally integrated data, i.e. emission spectra, with the respective intervals that were used for lifetime determination in green (Ir-based emission) or red (Ru-based emission).

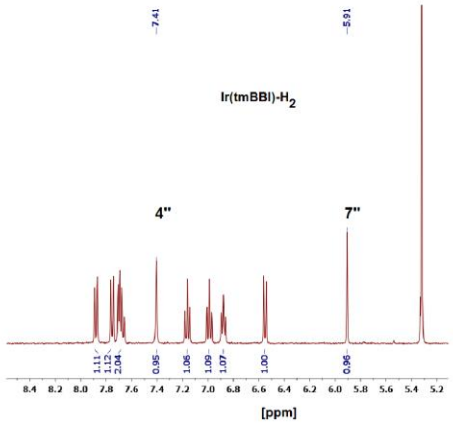

Figure S 8. ^{1}H-NMR of **Ir(tmBBI)**-H_2 in deuterated dichloromethane.

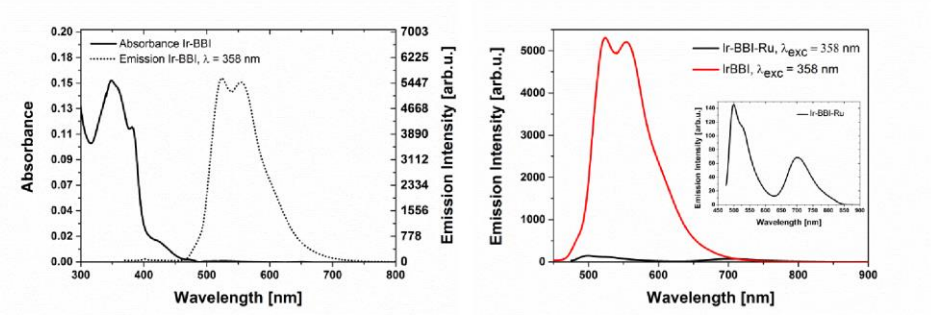

Figure S 9. Left: absorbance and emission spectrum of **IrBBI** in dichloromethane (c = 5 x 10^{-6} M); right: emission spectra of **IrBBI** (red) and **Ir-BBI-Ru** (black) in deuterated dichloromethane (c = 5 x 10^{-6} M).

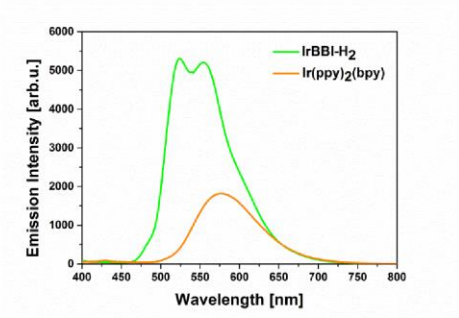

Figure S 10. Emission spectra of **IrBBI** and $[Ir(ppy)_2(bpy)]^+[PF_6]^-$ in dichloromethane (c = 5 x 10^{-6} M, λ_{exc} = 378 nm).

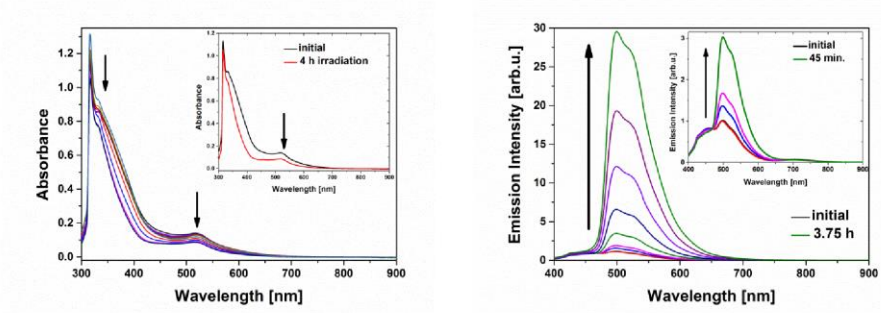

Figure S 11. Left: Absorption spectra of **Ir-BBI-Ru** under catalysis condition measured at different time intervals up to 4 h; right: Emission spectra of **Ir-BBI-Ru** under catalysis condition up to 3.75 h; inset: process within 45 min.

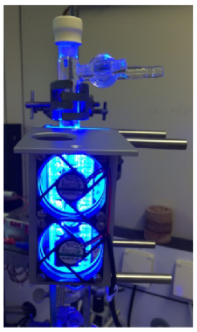

Figure S 12. Experimental set up for the irradiation test of samples.

Table 2. Crystal data and structure refinement for **Ru-BBI-Ir**.

Empirical formula	C76 H80 F6 Ir N10 P Ru	
Formula weight	1571.74	
Temperature	180(2) K	
Wavelength	1.54178 Å	
Crystal system	Triclinic	
Space group	*P* -1	
Unit cell dimensions	a = 15.4174(4) Å	α= 86.505(2)°.
	b = 16.7904(4) Å	β= 68.364(2)°.
	c = 17.0628(4) Å	γ = 85.356(2)°.
Volume	4089.97(18) $Å^3$	
Z	2	
Density (calculated)	1.276 Mg/m^3	
Absorption coefficient	5.251 mm^{-1}	
F(000)	1592	
Crystal size	0.1183 x 0.0589 x 0.0472 mm^3	
Theta range for data collection	7.513 to 73.787°.	
Index ranges	-19<=h<=19, -20<=k<=20, -15<=l<=21	
Reflections collected	46056	
Independent reflections	16068 [R(int) = 0.0412]	
Completeness to theta = 67.679°	99.7 %	
Refinement method	Full-matrix least-squares on F^2	
Data / restraints / parameters	16068 / 1 / 821	
Goodness-of-fit on F^2	1.102	
Final R indices [I>2sigma(I)]	R1 = 0.0634, wR2 = 0.1654	

R indices (all data)	R1 = 0.0754, wR2 = 0.1719
Largest diff. peak and hole	1.703 and -0.965 e·Å^{-3}

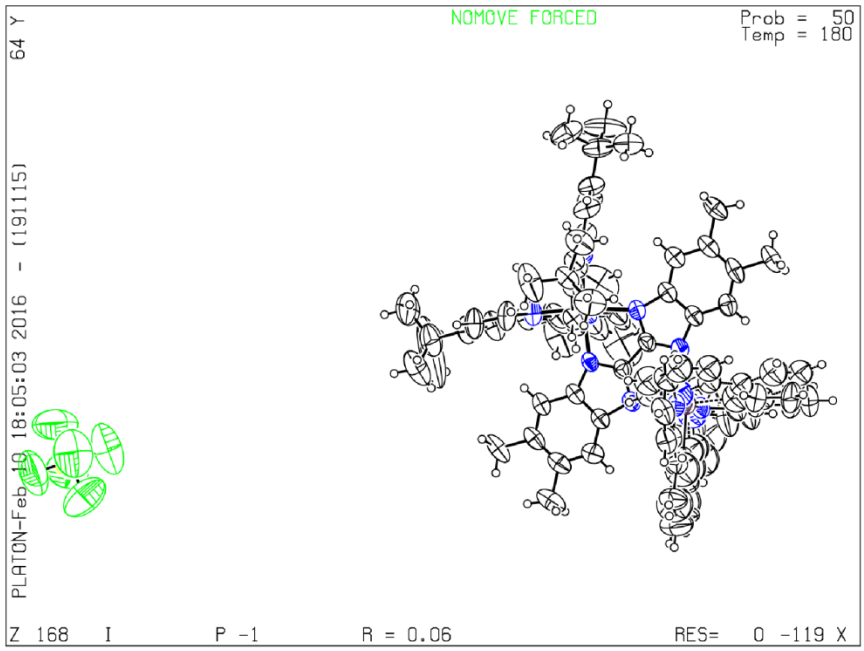

Figure S12: ORTEP ellipsoid representation of the asymmetric unit of Ir-BBI-Ru with 50% probability level

Literature

1 S. Rau, M. Ruben, T. Büttner, C. Temme, S. Dautz, H. Görls, M. Rudolph, D. Walther, A. Brodkorb, M. Duati, C. O'Connor and J. G. Vos, *J. Chem. Soc., Dalton Trans.*, **2000**, 3649–3657.

2 SADABS 2008/1, Bruker AXS Inc., **2008**, Madison, WI, U.S.A.

3 G. M. Sheldrick, *Acta Cryst.* **2008**, *A64*, 112–122.

7 Curriculum vitae

Personal information

Name:	Sebastian Andreas Rommel
Date of birth:	10/06/1987
Place of birth:	Augsburg
Nationality:	German

Education

02/2013 – 7/2016	PhD studies, University of Ulm (Ulm, Germany)
10/2010 - 12/2012	Master of Science in Chemistry and Management, University of Ulm (Ulm, Germany)
10/2007 – 10/2010	Bachelor of Science in Chemistry and Management, University of Ulm (Ulm, Germany)
09/1997 - 06/2006	Abitur, Rudolf Diesel Gymnasium (Augsburg, Germany)
09/1990 - 07/1994	Primary school, Volkshochschule Augsburg-Hochzoll-Nord, (Augsburg, Germany)

8 Publications and conference contributions

8.1 Publications in peer reviewed journals

8.1.1 S. A. Rommel, D. Sorsche, N. Rockstroh, F. W. Heinemann, J. Kübel, M. Wächtler, B. Dietzek, S. Rau, *Eur. J. Inorg. Chem.* **2015**, 3730–3739.
DOI: 10.1002/ejic.201500234.

8.1.2 D. Sorsche, C. Pehlken, C. Baur, S. Rommel, K. Kastner, C. Streb, S. Rau, *Dalton Trans.* **2015**, *44*, 15404–15407.
DOI: 10.1039/c5dt02383a.

8.1.3 S. A. Rommel, D. Sorsche, A. Dixit, S. Rau; *Eur. J. Inorg. Chem.* **2016**, 40–48
DOI: 10.1002/ejic.201501108.

8.1.4 S. A. Rommel, D. Sorsche, S. Rau, *Dalton Trans.* **2016**, *45*, 74–77.
DOI: 10.1039/c5dt04152j.

8.1.5 D. Sorsche, S. A. Rommel, S. Rau, *Eur. J. Inorg. Chem.* **2016**, 1503-1513.
DOI: 10.1002/ejic.201501472.

8.1.6 S. A. Rommel, D. Sorsche, S. Schönweiz, J. Kübel, N. Rockstroh, B. Dietzek, C. Streb, S. Rau, *Journal of Organomet. Chem.***, 2016**, in press.
DOI: 10.1016/j.jorganchem.2016.04.002.

8.1.7 S. Schönweiz, S.A. Rommel, J. Kübel, M. Micheel, B. Dietzek, S. Rau, C. Streb
Chem. Eur. J., **2016**, 22, 1-5.
DOI: 10.1002/chem.201602850

8.2 Conference proceedings

8.2.1 Poster contributions

07/2015 "Protonation dependent luminescence of an Iridium(III) bibenzimidazole chromophore", 21st International Symposium on the Photochemistry and Photophysics of Coordination Compounds, Krakow (Poland).

08-09/2014 "Development of photoactive bimetallic complexes with luminescent Iridium, Ruthenium und Osmium complex fragments", 5th EuChems Chemistry Congress, Istanbul (Turkey).

03/2014 ”Development of photoactive bimetallic complexes with luminescent Iridium, Ruthenium und Osmium complex fragments”, GdCH Frühjahrssymposium, Jungchemikerforum, Jena (Germany).

8.2.2 Travel grants

07/2015 **Gesellschaft Deutscher Chemiker e. V. (GDCh)**
Travel grant (21st International Symposium on the Photochemistry and Photophysics of Coordination Compounds, Krakow (Poland))

08/2014 **Gesellschaft Deutscher Chemiker e. V. (GDCh)**
Travel grant (5th EuChems Chemistry Congress, Istanbul (Turkey))

03/2014 **Gesellschaft Deutscher Chemiker e. V. (GDCh)**
Travel grant (GdCH Frühjahrssymposium, Jungchemikerforum, Jena (Germany))

9 Abbreviations

a.u. (also arb. u.)	arbitrary units
boc	tert-butyloxycarbonyl
bpy	2,2'-bipyridine
CT	charge transfer
dmBBI^{Anis}H$_2$	1,1’-bis(t-butoxycarbonyl)-4,4’-bis(4-methoxyphenyl)-6,6’-dimethyl-2,2’-bibenzimidazole
dmBBI^{dmAnis}H$_2$	1,1’-bis(t-butoxycarbonyl)-4,4’-bis(2,6-dimethyl-4-methoxylphenyl)-6,6’-dimethyl-2,2’-bibenzimidazole
DMSO	dimethyl sulfoxide
DNA	deoxyribonucleic acid
ESI	electrospray ionization
ET	energy transfer
eT	electron transfer
Fc/Fc$^+$	Ferrocene/Ferrocenium redox couple
HOMO	highest occupied molecular orbital
HSAB	Pearson's concept of hard and soft acids and bases
IC	internal conversion
Ir-K0	[(ppy)$_2$Ir(tmBBIH$_2$)]PF$_6$
Ir-tmBBI-Ir	[{(ppy)$_2$Ir}$_2$(μ-tmBBI)]
ISC	intersystem crossing
L1	*see* dmBBI^{Anis}H$_2$
L2	*see* dmBBI^{dmAnis}H$_2$
LC	ligand-centered (also referring to ligand-centered state)
LED	light emitting diode
LLCT	ligand-to-ligand charge transfer
LMCT	ligand-to-metal charge transfer
LUMO	lowest unoccupied molecular orbital
MALDI	matrix-assisted layer deposition ionization
MC	metal-centered (also referring to metal-centered state)
MLCT	metal-to-ligand charge transfer (also referring to metal-to-ligand charge transfer state

M^{n+}	generalized cationic species
MS	mass spectrometry
NMR	nuclear magnetic resonance (spectroscopy)
OLED	organic light emitting diode
ppy	2-phenylpyridine
PS	photosensitizer
rac	racemic pair of chiral isomers
Ru-K0	$[(tbbpy)_2Ru(tmBBIH_2)](PF_6)_2$
Ru-K1	$[(tbbpy)_2Ru(dmBBI^{Anis}H_2)](PF_6)_2$
Ru-tmBBI-Ir	$[(tbbpy)_2Ru(tmBBI)Ir(ppy)_2](PF_6)$
TBA	tetrabutylammonium
tbbpy	4,4'-di-*tert*-butyl-2,2'-bipyridine
TEA	triethylamine
THF	tetrahydrofuran
tmBBI(H_2)	5,5',6,6'-tetramethyl-2,2'-bibenzimidazole
TON	turn-over-number, generated equivalents of hydrogen with respect to the catalyst concentration
UV	ultraviolet
UV/vis	ultraviolet/visible light
XRD	X-ray diffractometry

10 Acknowledgements

An diesem Punkt möchte ich allen danken die zum Erfolg dieser Arbeit beigetragen haben.

Mein größter Dank gilt meinem Doktorvater Prof. Sven Rau für ein äußerst spannendes und herausforderndes Projekt und seine unermüdliche Unterstützung

.

Besonderer Dank gilt an dieser Stelle auch Prof. Carsten Streb für die Übernahme des Zweitgutachtens und die schnelle Bearbeitung des letzteren.

Ich danke den Kooperationspartnern in Jena, Erlangen und Ulm, insbesondere den Arbeitsgruppen um die Professoren Dietzek (Jena), Streb (Ulm) und Linden (Ulm) für die gute und freundliche Zusammenarbeit.

Ich danke meine Kollegen und Freunden am Institut ACI für die tolle Zeit zusammen, vielen Erfahrungen und natürlich die gute Zusammenarbeit.

Ein großes Dankeschön geht an meine Freunde Matze, Walter, Luxe, Stefan, Paule, Bene, Phil und meinen Bruder Stefan – für die zahlreichen Abende die wir miteinander verbracht haben, die tausenden Kaffeepausen und so viel mehr!

Ich danke meinem langjährigen Laborpartner Dieter Sorsche für die Einarbeitung während der Masterarbeit, die kontinuierliche Zusammenarbeit während der Promotion, seine Unterstützung und Freundschaft.

Mein abschließender Dank gilt meiner Familie; ganz besonders meinen Eltern. Danke für eure Unterstützung, euren Rat und vor allem dafür, dass ihr immer für mich da seid. Ohne Euch wäre all dies nicht möglich gewesen.

11 Declaration of honesty in academic work

Die vorliegende Arbeit entstand im Zeitraum von Februar 2013 bis Juli 2016 am Institut für Anorganische Chemie I (Materialien und Katalyse) der Universität Ulm in den Arbeitskreisen von Prof. Dr. Sven Rau und Prof. Dr. Carsten Streb.

Hiermit erkläre ich, dass ich die vorliegende Arbeit selbstständig angefertigt und keine anderen als die angegebenen Quellen und Hilfsmitteln benutzt sowie die wörtlich oder inhaltlich übernommenen Stellen als solche kenntlich gemacht und die Satzung der Universität Ulm zur Sicherung guter wissenschaftlicher Praxis in der aktuell gültigen Fassung vom 08.03.2012 beachtet habe.

_____ _____

Ort, Datum Sebastian Rommel